

The Pioneer Anomaly

Slava G. Turyshev

Jet Propulsion Laboratory, California Institute of Technology,
4800 Oak Grove Drive, Pasadena, CA 91109, USA

email: turyshev@jpl.nasa.gov

<http://science.jpl.nasa.gov/people/Turyshev/>

Viktor T. Toth

Ottawa, ON K1N 9H5, Canada

email: vttoth@vttoth.com

<http://www.vttoth.com/>

Abstract

Radio-metric Doppler tracking data received from the Pioneer 10 and 11 spacecraft from heliocentric distances of 20–70 AU has consistently indicated the presence of a small, anomalous, blue-shifted frequency drift uniformly changing with a rate of $\sim 6 \times 10^{-9}$ Hz/s. Ultimately, the drift was interpreted as a constant sunward deceleration of each particular spacecraft at the level of $a_P = (8.74 \pm 1.33) \times 10^{-10}$ m/s². This apparent violation of the Newton’s gravitational inverse-square law has become known as the Pioneer anomaly; the nature of this anomaly remains unexplained. In this review, we summarize the current knowledge of the physical properties of the anomaly and the conditions that led to its detection and characterization. We review various mechanisms proposed to explain the anomaly and discuss the current state of efforts to determine its nature. A comprehensive new investigation of the anomalous behavior of the two Pioneers has begun recently. The new efforts rely on the much-extended set of radio-metric Doppler data for both spacecraft in conjunction with the newly available complete record of their telemetry files and a large archive of original project documentation. As the new study is yet to report its findings, this review provides the necessary background for the new results to appear in the near future. In particular, we provide a significant amount of information on the design, operations and behavior of the two Pioneers during their entire missions, including descriptions of various data formats and techniques used for their navigation and radio-science data analysis. As most of this information was recovered relatively recently, it was not used in the previous studies of the Pioneer anomaly, but it is critical for the new investigation.

1 Introduction

For generations of researchers our solar system provided opportunities to establish and test fundamental laws of gravity. By studying the motion of planets, their moons, and comets, astronomers learned the basic rules that govern the dynamics of a system of gravitating bodies. Today we apply this knowledge to study the universe around us, expecting that the same laws of gravity govern the behavior of the universe on large scales, from planetary systems similar to our own to galaxies and to the entire cosmos as a whole.

Astronomers, however, do not normally discover new laws of nature. We are not yet able to manipulate the objects of our scrutiny. The telescopes and detectors we operate are simply passive probes that cannot order the cosmos what to do. Yet they *can* tell us when something isn't following established rules. For example, take the planet Uranus, whose discovery is credited to the English astronomer William Herschel and dated to 1781 (others had already noted its presence in the sky but misidentified it as a star). As observational data about its orbit accumulated over the following decades, people began to notice that Uranus's orbit deviated slightly from the dictates of Newton's gravity, which by then had withstood a century's worth of testing on the other planets and their moons. Some prominent astronomers suggested that perhaps Newton's laws begin to break down at such great distances from the Sun.

This led immediately to the question: What is there to do? Abandon or modify Newton's laws and come up with new rules of gravity? Or postulate a yet-to-be-discovered planet in the outer solar system, whose gravity was absent from the calculations for Uranus's orbit? The answer came in 1846, when astronomers discovered the planet Neptune just where a planet had to be for its gravity to perturb Uranus in just the ways measured. Newton's laws were safe... for the time being.

Then there is Mercury, the planet closest to the Sun. Its orbit, too, habitually disobeyed Newton's laws of gravity resulting in an anomalous precession of its perihelion. This anomaly was known for a long time; it amounts to 43 seconds of arc (") per century and cannot be explained within Newton's gravity, thereby presenting a challenge for physicists and astronomers. In 1855, the French astronomer Urbain Jean Joseph Le Verrier, who in 1846 predicted Neptune's position in the sky within one degree, wrote that the anomalous residue of the Mercurial precession would be accounted for if yet another as-yet undiscovered planet – call it Vulcan – revolves inside the Mercurial orbit so close to the Sun that it would be practically impossible to discover in the solar glare, or perhaps it was an entire uncatalogued belt of asteroids orbiting between Mercury and the Sun.

It turns out that Le Verrier was wrong on both counts. This time he really did need a new understanding of gravity. Within the limits of precision that our measuring tools impose, Newton's laws behave well in the outer solar system. However, they break down in the inner solar system, where the Sun's gravitational field is so powerful that it warps space. And that is where we cannot ignore the effects of general relativity. It took another 60 years to solve this puzzle. In 1915, before publishing the historical paper with the field equations of the general theory of relativity (e.g., [104, 105]), Albert Einstein computed the expected perihelion precession of Mercury's orbit. This was not the first time Einstein tackled this problem: indeed, earlier versions of his gravity theory were rejected, in part, because they predicted the wrong value (often with the wrong sign) for Mercury's perihelion advance [101]. However, when he obtained the famous 43"/century needed to account for the anomaly, he realized that a new era in gravitational physics had just begun.

The stories of these two planets, Mercury and Uranus, involve two similar-looking anomalies, yet two completely different solutions.

Ever since its original publication on November 25, 1915 [104, 105], Einstein's general theory of relativity continues to be an active area of both theoretical and experimental research [389, 390]. Even after nearly a century since its discovery, the theory successfully accounts for all solar system

observations gathered to date; it is remarkable that Einstein’s theory has survived every test [419]. In fact, both in the weak field limit evident in our solar system and with the stronger fields present in systems of binary pulsars the predictions of general relativity have been extremely well tested. Such longevity and success make general relativity the *de facto* “standard” theory of gravitation for all practical purposes involving spacecraft navigation, astronomy, astrophysics, cosmology and fundamental physics [392].

Remarkably, even after more than 300 years since the publication of Newton’s “Principia” and nearly 100 years after the discovery of Einstein’s general theory of relativity, our knowledge of gravitation is still incomplete. Many challenges remain, leading us to explore the physics beyond Einstein’s theory [389, 390]. In fact, growing observational evidence points to the need for new physics. Multiple dedicated efforts to discover new fundamental symmetries, investigations of the limits of established symmetries, tests of the general theory of relativity, searches for gravitational waves, and attempts to understand the nature of dark matter were among the topics that had been the focus of scientific research at the end of the last century. These efforts have further intensified with the unexpected discovery in the late 1990s of a small acceleration rate of our expanding Universe, which triggered many new activities aimed at answering important questions related to the most fundamental laws of Nature [390, 392].

Many modern theories of gravity that were proposed to address the challenges above, including string theory, supersymmetry, and brane-world theories, suggest that new physical interactions will appear at different ranges. For instance, this may happen because at sub-millimeter distances new dimensions can exist, thereby changing the gravitational inverse-square law [28, 29]. Similar forces that act at short distances are predicted in supersymmetric theories with weak scale compactifications [25], in some theories with very low energy supersymmetry breaking [93], and also in theories of very low quantum gravity scale [98, 306, 371].

Although much of the research effort was devoted to the study of the behavior of gravity at very short distances, notably on millimeter-to-micrometer ranges, it is possible that tiny deviations from the inverse-square law occur at much larger distances. In fact, there is a possibility that noncompact extra dimensions could produce such deviations at astronomical distances [99]. By far the most stringent constraints to date on deviations from the inverse-square law come from very precise measurements of the Moon’s orbit about the Earth. Analysis of lunar laser ranging data tests the gravitational inverse-square law on scales of the Earth-Moon distance [422], so far reporting no anomaly at the level of accuracy of 3×10^{-11} of the gravitational field strength.

While most of the modern experiments in the solar system do not show disagreements with general relativity, there are puzzles that require further investigation. One such puzzle was presented by the Pioneer 10 and 11 spacecraft. The radiometric tracking data received from these spacecraft while they were at heliocentric distances of 20–70 astronomical units (AU) have consistently indicated the presence of a small, anomalous, Doppler frequency drift. The drift was interpreted as a constant sunward acceleration of $a_P = (8.74 \pm 1.33) \times 10^{-10} \text{ m/s}^2$ experienced by both spacecraft [15, 18, 391]. This apparent violation of the inverse-square law has become known as the Pioneer anomaly; the nature of this anomaly remains unexplained.

Before Pioneer 10 and 11, Newtonian gravity was not measured with great precision over great distances and was therefore never confirmed. The unique “built-in” navigation capabilities of the two Pioneers allowed them to reach the levels of $\sim 10^{-10} \text{ m/s}^2$ in acceleration sensitivity. Such an exceptional sensitivity allowed researchers to use Pioneer 10 and 11 to test the gravitational inverse square law in the largest-scale gravity experiment ever conducted. However, the experiment failed to confirm the validity of this fundamental law of Newtonian gravity in the outer regions of the solar system. Thus, the nagging question remains: Just how well do we know gravity?

One can demonstrate that beyond 15 AU the difference between the predictions of Newton and Einstein are negligible. So, at the moment, two forces seem to be at play in deep space: Newton’s law of gravity and the Pioneer anomaly. Until the anomaly is thoroughly accounted

for by conventional causes, and can therefore be eliminated from consideration, the validity of Newton’s laws in the outer solar system will remain in doubt. This fact justifies the importance of the investigation of the nature of the Pioneer anomaly.

However, the Pioneer anomaly is not the only unresolved puzzle. Take the dark matter and dark energy problem. While extensive efforts to detect the dark matter that is believed to be responsible for the puzzling observations of galaxy rotation curves have not met with success so far, modifications of gravitational laws have also been proposed as a solution to this puzzle. We still do not know for sure whether or not the ultimate solution for the dark matter problem will require a modification of the Standard Model of cosmology, but some suggested that new gravitational laws are at play in the arms of spiral galaxies.

A similar solution was proposed to explain the cosmological observations that indicate that the expansion of the universe is accelerating. There is now a great deal of evidence indicating that over 70% of the critical density of the universe is in the form of a “negative-pressure” dark energy component; we have no understanding of its origin or nature. Given the profound challenge presented by the dark energy problem, a number of authors have considered the possibility that cosmic acceleration is not due to a particular substance, but rather that it arises from new gravitational physics (see discussion in [390]).

Many of the models that were proposed to explain the observed acceleration of the universe without dark energy or the observed deviation from Newtonian laws of gravity in the arms of spiral galaxies without dark matter may also produce measurable gravitational effects on the scale of the solar system. These effects could manifest themselves as a “dark force”, similar to the one detected by the Pioneer 10 and 11 spacecraft. Some believe that the Pioneer anomaly may be a critical piece of evidence as it may indicate a deviation from Einstein’s gravity theory on the scales of the solar system. But is it? Or can the Pioneer anomaly be explained by the mundane physics of a previously unaccounted-for on-board systematic effect? In this review we summarize the current knowledge of the anomaly and explore possible ways to answer this question.

The review is organized as follows. We begin with descriptions of the Pioneer 10 and 11 spacecraft and the strategies for obtaining and analyzing their data. In Section 2 we describe the Pioneer spacecraft. We provide a significant amount of information on the design, operations and behavior of Pioneer 10 and 11 during their entire missions, including information from original project documentation, descriptions of various data formats, and techniques used for their navigation. This information is critical to the ongoing investigation of the Pioneer anomaly.

In Section 3 we describe the techniques used for acquisition of the Pioneer data. In particular, we discuss the Deep Space Network (DSN), its history and current status, describe the DSN tracking stations and details of their operations in support of deep space missions. We present the available radiometric Doppler data and describe techniques for data preparation and analysis. We also discuss the Pioneer telemetry data and its value for the anomaly investigation.

In Section 4 we address the basic elements of the theoretical foundation for precision spacecraft navigation. In particular, we discuss the observational techniques and physical models that were used for precision tracking of the Pioneer spacecraft and analysis of their data. We describe models of gravitational forces and those that are of nongravitational nature.

In Section 5 we focus on the detection and initial characterization of the Pioneer anomaly. We describe how the anomalous acceleration was originally identified in the data. We continue by summarizing the current knowledge of the physical properties of the Pioneer anomaly. We briefly review the original efforts to understand the signal.

In Section 6 we review various mechanisms proposed to explain the anomaly that use unmodeled forces with origin either external to the spacecraft or those generated on-board. We discuss theoretical proposals that include modifications of general relativity, modified Newtonian gravity, cosmological theories, theories of dark matter and other similar activities. We review the efforts at independent confirmation with other spacecraft, planets, and other bodies in the solar system.

In Section 7, we describe the results of various independent studies of the Pioneer anomaly. We discuss new Pioneer 10 and 11 radiometric Doppler data that recently became available. This much extended set of Pioneer Doppler data is the primary source for the new investigation of the anomaly. A near complete record of the flight telemetry that was received from the two Pioneers is also available. Together with original project documentation and newly developed software tools, this additional information is now used to reconstruct the engineering history of both spacecraft, with special emphasis on the possible contribution to the anomalous acceleration by on-board systematic effects. We review the current status of these efforts to investigate the anomaly.

In Section 8, we present our summary and conclusions.

In Appendices A–D, we provide additional information on the geometry and design of Pioneer 10 and 11 spacecraft and describe various data formats used for mission operations.

2 The Pioneer 10 and 11 Project

NASA's Pioneer program began in 1958, in the earliest days of the space age, with experimental spacecraft that were designed to reach Earth escape velocity and perform explorations of the interplanetary space beyond the Earth's orbit. Several of these launch attempts ended in failure; the five spacecraft that reached space later became known as Pioneers 1–5. These were followed in the second half of the 1960s by Pioneers 6–9, a series of significantly more sophisticated spacecraft that were designed to be launched into solar orbit and make solar observations. These spacecraft proved extremely robust¹ and paved the way for the most ambitious projects yet in the unmanned space program: Pioneers 10 and 11.

The Pioneer 10 and 11 spacecraft were the first two man-made objects designed to explore the outer solar system (see details in [294, 291, 293, 290, 292, 289, 154, 297, 280, 358, 276, 116, 115, 132, 264, 354, 298, 370, 279, 295]). Their objectives were to conduct, during the 1972–73 Jovian opportunities, exploratory investigation beyond the orbit of Mars of the interplanetary medium, the nature of the asteroid belt, the environmental and atmospheric characteristics of Jupiter and Saturn (for Pioneer 11), and investigate the solar system beyond Jupiter's orbit.

In this section we review the Pioneer 10 and 11 missions. We present information about the spacecraft design. Our discussion focuses on subsystems that played important roles in the continued functioning of the vehicles and on subsystems that may have affected their dynamical behavior: specifically, we review the propulsion, attitude control, power, communication, and thermal subsystems. We also provide information about the history of these systems throughout the two spacecrafts' exceptionally lengthy missions.

2.1 The Pioneer 10 and 11 missions

The Pioneer missions were the first to cross the asteroid belt, perform in situ observations of the interplanetary medium in the outer solar system, and close-up observations of the gas giant Jupiter. Their mission design was characterized by simplicity: a powerful launch vehicle placed the spacecraft on an hyperbolic trajectory aimed directly at Jupiter, which the spacecraft were expected to reach approximately 21 months after launch.

At the distance of Jupiter, operating a spacecraft using solar panels is no longer practical (certainly not at the level of technology that was available to the designers of the Pioneer missions in the late 1960s.) For this reason, nuclear power was chosen as the means to provide electrical power to the spacecraft, in the form of ²³⁸Pu powered radioisotope thermoelectric generators (RTGs). As even this was relatively new technology at the time the missions were designed, the power subsystem was suitably over-engineered, the design requirement being a completely functional spacecraft capable of performing all planned science observations with only three (out of four) RTGs operating.

Such conservative engineering characterized the entire design of these spacecraft and their missions, and it was likely responsible for the two spacecrafts' exceptional longevity, and their ability to deliver science results that far exceeded the expectations of their designers. The original plan envisioned a primary mission of 600–900 days in duration. Nevertheless, following its encounter with Jupiter, Pioneer 10 remained functional for over 30 years; meanwhile Pioneer 11, though not as long lived as its sister craft, successfully navigated a path across the solar system for another encounter with Saturn, offering the first close-up observations of the ringed planet.

After the Jupiter and Saturn (for Pioneer 11) encounters (see Figure 2.1), the craft followed escape hyperbolic orbits near the plane of the ecliptic on opposite sides of the solar system, continuing their extended missions [115]. (See Figure 2.2.) The spacecraft explored the outer regions of

¹See details on the Pioneer missions at <http://www.nasa.gov/centers/ames/missions/archive/pioneer.html>. Note that Pioneer 6 remained operational for more than 35 years after launch.

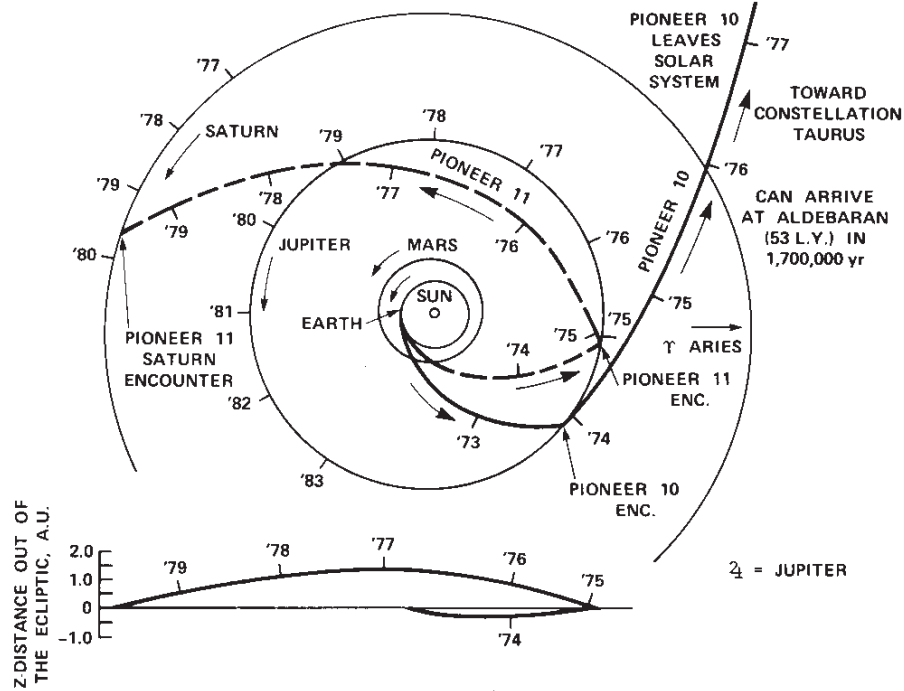


Figure 2.1: Trajectories of Pioneer 10 and 11 during their primary missions in the solar system (from [115]). The time ticks shown along the trajectories and planetary orbits represent the distance traveled during each year.

the solar system, studying energetic particles from the Sun (solar wind), and cosmic rays entering our portion of the Milky Way. Major milestones of the two Pioneer projects are shown in Table 2.1.

Table 2.1: Major milestones of the Pioneer 10 and 11 projects.

Event	Pioneer 10	Pioneer 11
Launch	March 3, 1972	March 6, 1973
Jupiter encounter	December 3, 1973	December 4, 1974
Saturn encounter	N/A	September 1, 1979
Last telemetry received	April 27, 2002	September 30, 1995

The Pioneers were excellent vehicles for the purposes of precision celestial mechanics experiments [15, 18, 23, 185, 247, 248, 249, 251, 252, 254, 255, 266, 391, 393, 394, 395]. This was due to a combination of many factors, including the presence of a coherent mode transceiver on board, their attitude control (spin-stabilized, with a minimum number of attitude correction maneuvers using thrusters), power design (the RTGs being on extended booms aided the stability of craft and also reduced thermal effects on the craft; see Figure 2.3), and precise Doppler tracking (with the accuracy of post-fit Doppler residuals at the level of mHz). The exceptional “built-in” acceleration sensitivity of the Pioneer 10 and 11 spacecraft naturally allowed them to reach a level of accuracy of $\sim 10^{-10}$ m/s². The result was one of the most precise spacecraft navigations in deep space to date [261].

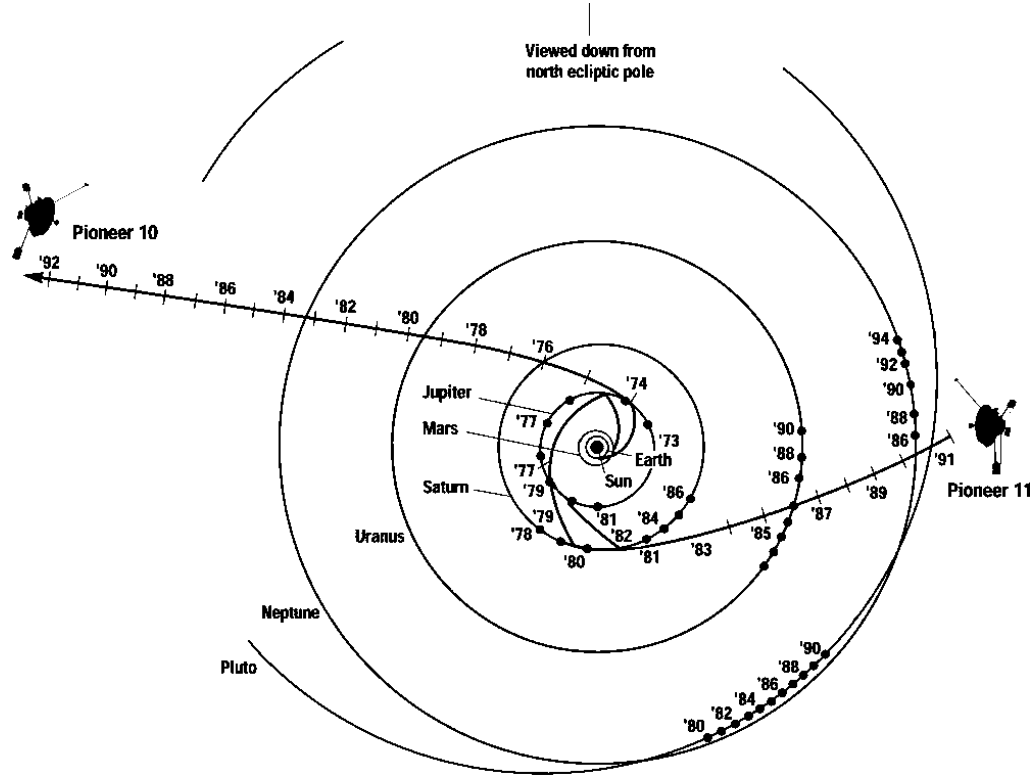


Figure 2.2: Ecliptic pole view of the Pioneer 10 and Pioneer 11 trajectories during major parts of their extended missions. Pioneer 10 is traveling in a direction almost opposite to the galactic center, while Pioneer 11 is heading approximately in the shortest direction to the heliopause. The direction of the solar system’s motion in the galaxy is approximately towards the top. (From [18].)

2.1.1 Pioneer 10 mission details

Pioneer 10 was launched on 2 March 1972 (3 March 1972 at 01:49 Universal Coordinated Time) from Cape Canaveral on top of an Atlas/Centaur/TE364-4 launch vehicle [238]. The launch marked the first use of the Atlas-Centaur as a three-stage launch vehicle.

The launch vehicle configuration was an Atlas launch vehicle equipped with a Centaur D upper stage and a TE364-4 solid-fuel third stage that provided additional thrust and also supplied the initial spin of the spacecraft. The third stage was required to accelerate Pioneer 10 to the speed of 14.39 km/s, needed for the flight to Jupiter.

After a powered flight of approximately 14 minutes, the spacecraft was separated from its launch vehicle; its initial spin ~ 60 revolutions per minute (rpm) was reduced by thrusters, and then reduced further when the magnetometer and RTG booms were extended [274, 134]. The spacecraft was then oriented to ensure that its high-gain antenna pointed towards the Earth. Thus, the initial cruise phase from the Earth to Jupiter began.

The first interplanetary cruise phase of Pioneer 10 took approximately 21 months. During this time, Pioneer 10 successfully crossed the asteroid belt, demonstrating for the first time that this region of the solar system is safe for spacecraft to travel through.

Pioneer 10 arrived at Jupiter in late November, 1973 [154]. Its closest approach to the red giant occurred on 4 December 1973, at 02:25 UTC. It performed the first ever close-up observations

of the gas giant, before continuing its journey out of the solar system on an hyperbolic escape trajectory (Figure 2.2). During the planetary encounter, Pioneer 10 took several photographs of the planet and its moons, measured Jupiter’s magnetic fields, and observed the planet’s radiation belts. Radiation in the Jovian environment, potentially damaging to the spacecraft’s electronics, was a concern to the mission designers. However, Pioneer 10 survived the planetary encounter without significant damage, although its star sensor became inoperative shortly afterwards [353], a likely result of excessive radiation exposure near Jupiter.

The encounter with Jupiter changed Pioneer 10’s trajectory as was planned by JPL navigators [405]. As a result, Pioneer 10 was now on an hyperbolic escape trajectory that took it to ever more distant parts of the solar system. Originally, signal loss was expected before Pioneer 10 reached twice the heliocentric distance of Jupiter (the downlink telecommunication power margin was 6 dB at the time of Jupiter encounter); however, continuing upgrades to the facilities of the Deep Space Network (DSN) permitted tracking of Pioneer 10 until the official termination of Pioneer 10’s science mission in 1997 and even beyond.

Pioneer 10 continued to make valuable scientific investigations until its science mission ended on March 31, 1997. After this date, Pioneer 10’s weak signal was tracked by the NASA’s DSN as part of an advanced concept study of communication technology in support of NASA’s future interstellar probe mission. Pioneer 10 eventually became the first man-made object to leave the solar system.

During one of the last attempts to contact Pioneer 10, in April 2001, at first no signal was detected; however, the spacecraft’s signal did appear once it detected a signal from the Earth and its radio system switched to coherent mode. From this, it was concluded that the on-board transmitter frequency reference (temperature controlled crystal oscillator) failed, possibly due to the combined effects of aging, the extreme cold environment of deep space, and a drop in the main bus voltage due to the depletion of the spacecraft’s RTG power source. This failure had no impact on the ability to obtain precision Doppler measurements from Pioneer 10.

On March 2, 2002 NASA’s DSN made another contact with Pioneer 10 and confirmed that the spacecraft was still operational thirty years after its launch on March 3, 1972 (UT). The uplink signal was transmitted on March 1 from the DSN’s Goldstone, California facility and a downlink response was received twenty-two hours later by the 70-meter antenna at Madrid, Spain. At this time the spacecraft was 11.9 billion kilometers from Earth at about 79.9 AU from the Sun and heading outward into interstellar space in the general direction of Aldebaran at a distance of about 68 light years from the Earth, and a travel time of two million years. The last telemetry data point was obtained from Pioneer 10 on 27 April 2002 when the craft was 80 AU from the Sun.

The last signal from Pioneer 10 was received on Earth on 23 January 2003, when NASA’s DSN received a very weak signal from the venerable spacecraft from the distance of ~ 82.1 AU from the Sun. The previous three contacts had very faint signals with no telemetry received. At that time, NASA engineers reported that Pioneer 10’s RTG has decayed to the point where it may not have enough power to send additional transmissions to Earth. Consequently, the DSN did not detect a signal during a contact attempt on 7 February 2003. Thus, after more than 30 years in space, the Pioneer 10 spacecraft sent its last signal to Earth.

The final attempt to contact Pioneer 10 took place on the 34th anniversary of its launch, on 3–5 March 2006 [399]. At that time, the spacecraft was 90.08 AU from the Sun, moving at 12.08 km/s. The round-trip light time (i.e., time needed for a DSN radio signal to reach Pioneer 10 and return back to the Earth) was approximately 24 h 56 m, so the same antenna, DSS-14 at Goldstone, CA, was used for the track. Unfortunately, no signal was received. Given the age of the spacecraft’s power source, it was clear that there was no longer sufficient electrical power on board to operate the transmitter [383].

2.1.2 Pioneer 11 mission details

Pioneer 11 followed its older sister approximately one year later. It was launched on 5 April 1973 (on April 6, 1973 at 02:11 UTC), also on top of an Atlas/Centaur/TE364-4 launch vehicle. The second stage used for Pioneer 11 was a Centaur D-1A, while the third stage was a TE364-4 solid fuel vehicle.

After safe passage through the asteroid belt on 19 April 1974, Pioneer 11's thrusters were fired to add another ~ 65 m/s to the spacecraft's velocity. This adjusted the aiming point at Jupiter to 43,000 km above the cloud tops. The close approach also allowed the spacecraft to be accelerated by Jupiter to a velocity of 48.06 km/s, so that it would be carried across the solar system some 2.4 billion km to Saturn.

Early in its mission, Pioneer 11 suffered a propulsion system anomaly that caused the spin rate of the spacecraft to increase significantly (see Figure 2.16). Fortunately, the spin rate was not high enough to endanger the spacecraft or compromise its mission objectives.

Pioneer 11's first interplanetary cruise phase lasted approximately 20 months. During this time, a major trajectory correction maneuver was performed, aiming Pioneer 11 for a precision encounter with Jupiter. Pioneer 11's closest approach to Jupiter occurred on 2 December 1974 at 17:22 UTC. This encounter provided the necessary gravity assist to alter Pioneer 11's trajectory for a planned encounter with Saturn (see Figure 2.1).

The second interplanetary cruise phase of Pioneer 11's mission took it across the solar system. Initially, Pioneer 11's heliocentric distance was actually decreasing as it followed an hyperbolic trajectory taking the spacecraft more than 1 AU above the plane of the ecliptic. This phase of the mission culminated in a successful encounter with Saturn. Pioneer 11's closest approach to the ringed planet occurred on 1 September 1979, at 16:31 UTC. Still fully operational, Pioneer 11 was able to make close-up observations of the ringed planet.

After this second planetary encounter, Pioneer 11 continued to escape the solar system on an hyperbolic escape trajectory, and remained operational for many years. Pioneer 11 explored the outer regions of our solar system, studying the solar wind and cosmic rays.

The spacecraft sent its last coherent Doppler data on October 1, 1990 while at 31.7 AU from the Sun². In October 1990 a microwave relay switch failed on board Pioneer 11, in its communications subsystem. The most notable consequence of this failure is that it was no longer possible to operate this spacecraft's radio system in coherent mode, which is required for precision Doppler observations. Therefore, after this event, precision Doppler data was no longer produced by the Pioneer 11 spacecraft.

The spacecraft continued to provide science observations until the end of its mission in 1995. In September 1995, Pioneer 11 was at a distance of 6.5 billion km from Earth. At that distance, it takes over 6 hours for the radio signal to reach Earth. However, by September 1995, Pioneer 11 could no longer make any scientific observations as its power supply was nearly depleted. On 30 September 1995, routine daily mission operations were stopped. Intermittent contact continued until November 1995, at which time the last communication with Pioneer 11 took place. There has been no communication with Pioneer 11 since. The Earth's motion has carried our planet out of the view of the spacecraft antenna.

2.1.3 Pioneer 10 and 11 project documentation

Up until 2005, very little documentation on the Pioneer spacecraft was available to researchers. Indeed, around this time much of the Pioneer archival material stored at NASA's Ames Research Center was scheduled for destruction due to budget constraints.

²To generate ephemerides for solar-system bodies, including many spacecraft, one can use JPL's HORIZONS system, which is located at: <http://ssd.jpl.nasa.gov/?horizons>.

The growing interest in the Pioneer anomaly helped to initiate an effort at the NASA Ames Research Center to recover the entire archive of the Pioneer Project documents for the period from 1966 to 2003 (see details in [384, 399]). This massive archive contains all Pioneer 10 and 11 project documents discussing the spacecraft and mission design, fabrication of various components, results of various tests performed during fabrication, assembly, pre-launch, as well as calibrations performed on the vehicles; and also administrative documents including quarterly reports, memoranda, etc. Most of the maneuver records, spin rate data, significant events of the craft, etc., have also been identified.

A complete set of Pioneer-related documentation is listed in the Bibliography. Here, we mention some of the more significant pieces of documentation that are essential to understanding the Pioneer 10 and 11 spacecraft and their anomalous accelerations:

- The first document to be mentioned is entitled “Pioneer F/G: Spacecraft Operational Characteristics” [292] (colloquially referred to by its identifier as “PC-202”), and contains a complete description of the Pioneer 10 and 11 spacecraft and their subsystems. The document was last revised in mid-1971, just months before the launch of Pioneer 10, indicating that it reflects accurately the configuration of the Pioneer 10 spacecraft as it flew.
- Valuable information was found in the TRW Systems Group’s document entitled “Pioneer Project Flights F and G Final Report” [295], which contained post-launch information about both spacecraft, including, among other things, detailed information about their exact launch configuration.
- Details about the SNAP-19 radioisotope thermoelectric generators can be found in Teledyne Isotopes Energy Systems Division’s “SNAP 19 Pioneer F & G Final Report” [354], which has been released for public distribution on 9 February 2006.
- Much additional detail about the thermal design of the spacecraft was obtained from TRW Systems Group’s “Pioneer F/G Thermal Control Subsystem Design Review Number 3” [279].
- The Master Data Record (MDR) file format is described in Alliedsignal Technical Services Corporation’s document [403]. Sensor calibration data for Pioneer 10 is provided by BENDIX Field Engineering Corporation [374]; for Pioneer 11, the same information was provided privately by L. Kellogg [159]. The data format used by scientific instruments in the MDRs is described in “Pioneer F/G: EGSE Computer Programming Specifications for Scientific Instruments” [289]; further information about both scientific and engineering data words is present in “Pioneer F/G: On-line Ground Data System Software Specification” [291]. Together, these resources make it possible to read and interpret the entire preserved telemetry record of Pioneer 10 and 11 using modern software [399].
- Operational details about the Pioneer 10 and 11 missions were recorded in meeting presentations, many of which have been preserved [288, 287, 282, 283, 284, 285, 296, 286]. Additional details are provided in [281, 110, 299, 300, 100, 404].
- Details about tracking and data acquisition were published in the *JPL Deep Space Network’s Technical Reports* series [5, 6, 7, 8, 9, 37, 38, 39, 40, 41, 58, 66, 67, 68, 136, 138, 139, 152, 176, 177, 206, 207, 208, 209, 210, 211, 212, 213, 214, 215, 216, 217, 218, 219, 240, 241, 242, 243, 267, 273, 309, 317, 318, 338, 339, 340, 341, 342, 343, 344, 345, 346, 347, 348, 349, 351, 366, 407, 409]. Further, relevant details can be found in [76, 96, 153, 174, 175, 227, 311, 410]. Details about orbit estimation procedures are provided in [50, 377, 120, 121, 122, 123, 125, 376, 426].

The on-going study of the Pioneer anomaly would not be possible without these resources, much of which was preserved only because of the labors of dedicated individuals.

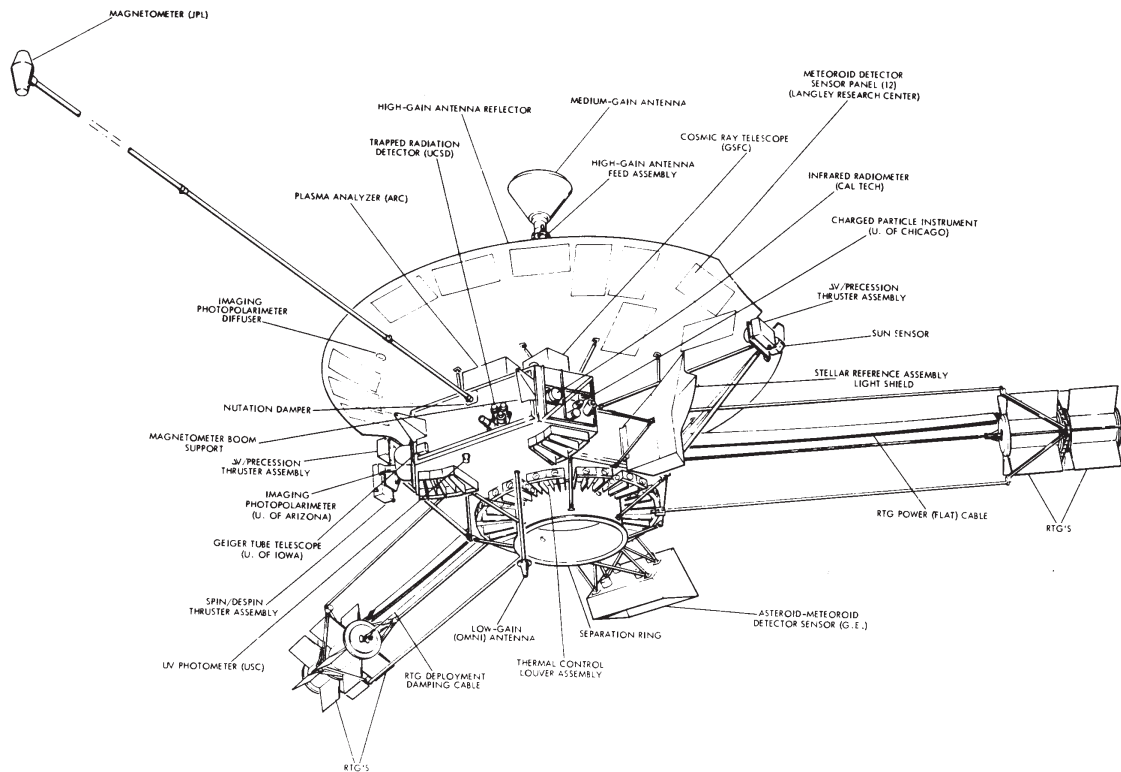


Figure 2.3: A drawing of the Pioneer spacecraft. (From [292].)

2.2 The Pioneer spacecraft

In this section we discuss the details of the Pioneer 10 and 11 spacecraft, focusing only on those most relevant to the study of the Pioneer anomaly.

2.2.1 General characteristics

Externally, the shape of the Pioneer 10 and 11 spacecraft was dominated by the large (2.74 m diameter) high-gain antenna (HGA)³, behind which most of the spacecraft's instrumentation was housed in two adjoining hexagonal compartments (Figure 2.3). The main compartment, in the shape of a regular hexagonal block, contained the fuel tank, electrical power supplies, and most control and navigation electronics. The adjoining compartment, shaped as an irregular hexagonal block, contained science instruments. Several openings were provided for science instrument sensors. The internal arrangement of spacecraft components is shown in Figure 2.4.

The main and science compartments collectively formed the spacecraft body, which was covered by multilayer thermal insulation on all sides except part of the aft side, where a passive thermal control louver system was situated.

For the purposes of attitude control, the entire spacecraft was designed to spin in the plane of the HGA.

³Customarily, the direction in which the high-gain antenna points is referred to as the “fore” (also, $+z$) direction, whereas the direction towards the “bottom” of the spacecraft is referred to as the “aft” (also $-z$) direction. Note that most of the time, the spacecraft is, in fact, traveling in the aft direction, as the HGA is pointing in the general direction towards the Earth, in a direction opposite to the direction of travel (especially in deep space).

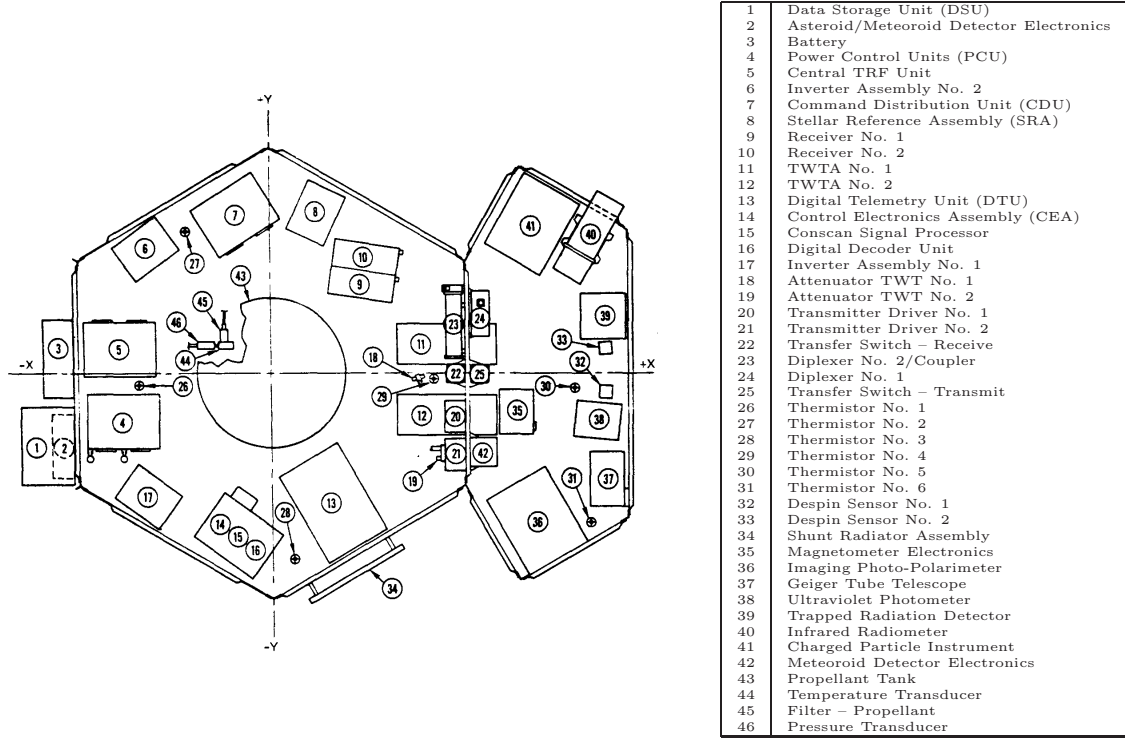


Figure 2.4: Pioneer 10 and 11 internal equipment arrangement. (From [292].)

Three extensible booms were attached to the main compartment, spaced at 120° . Two of these booms, both approximately 3 m long, each held two radioisotope thermoelectric generators (RTGs). This design was dictated mainly by concerns about the effects of radiation from the RTGs on the spacecrafts' instruments, but it also had the beneficial side effect of minimizing radiative heat exchange between the RTGs and the spacecraft body. The third boom, approximately 6 m in length, held the magnetometer sensor. The length of this boom ensured that the sensor was not responding to magnetic fields originating in the spacecraft itself.

The total mass of Pioneer 10 and 11 was approximately 260 kg at the time of launch, of which approximately 30 kg was propellant and pressurant. The masses of the spacecraft slowly varied throughout their missions primarily due to propellant usage (for details, see Section 2.3.2).

The propulsion system was designed to perform three types of maneuvers: spin/despin (setting the initial spin rate shortly after launch), precession (to keep the HGA pointing towards the Earth, and also to orient the spacecraft during orbit correction maneuvers) and velocity changes. Of the two spacecraft, Pioneer 11 used more of its propellant, in the course of velocity correction maneuvers that were used to adjust the spacecraft's trajectory for its eventual encounter with Saturn.

2.2.2 Science instruments

The Pioneer spacecraft carried an identical set of 11 science instruments, with a 12th instrument present only on Pioneer 11, namely:

1. JPL Helium Vector Magnetometer
2. ARC Plasma Analyzer

3. U/Chicago Charged Particle Experiment
4. U/Iowa Geiger Tube Telescope
5. GSFC Cosmic Ray Telescope
6. UCSD Trapped Radiation Detector
7. UCS Ultraviolet Photometer
8. U/Arizona Imaging Photopolarimeter
9. CIT Jovian Infrared Radiometer
10. GE Asteroid/Meteoroid Detector
11. LaRC Meteoroid Detector
12. Flux-Gate Magnetometer (Pioneer 11 only)

The power system of the Pioneer spacecraft was designed to ensure that a successful encounter with Jupiter (with all science instruments operating) can be carried out with only three (out of four) functioning radioisotope thermoelectric generators. Instruments could be commanded on or off by ground control; late in the extended mission, when sufficient power to operate all instruments simultaneously was no longer available, a power sharing plan was implemented to ensure that the power demand on board would not exceed available power levels.

At the end of its mission, only one instrument on board Pioneer 10 remained in operation; the University of Iowa Geiger Tube Telescope. An attempt was made to power down this instrument, in order to improve the available power margin. It is not known if this command was received or executed by the spacecraft.

2.2.3 Radioisotope thermoelectric generators (RTGs)

The primary electrical source on board Pioneer 10 and 11 was a set of four radioisotope thermoelectric generators [1, 124, 354, 278, 31]. Each of these RTGs contains 18 ^{238}Pu capsules, approximately two inches (5.08 cm) in diameter and 0.2 inches (0.51 cm) thick. The total thermal power of each RTG, when freshly fueled, was ~ 650 W. Each RTG contains two sets of 45 bimetallic thermocouples, connected in series. The thermocouples initially operated at $\sim 6\%$ efficiency; the nominal RTG output is ~ 4 V, 10 A. The total available power at launch on board each spacecraft was ~ 160 W (Figure 2.14).

Excess heat from each RTG is radiated into space by a set of six heat radiating fins. The fins provide the necessary radiating area to ensure that a sufficient temperature differential is present on the thermocouples, for efficient operation.

The thermal power of the RTGs is a function of the total power produced by the ^{238}Pu fuel, and the amount of power removed in the form of electrical energy by the thermocouples. The half-life of ^{238}Pu is 87.74 years. The efficiency of the thermocouples decreased over the years as a result of the decreasing temperature differential between the hot and cold ends, and also as a result of aging. At the time of last transmission, each RTG on board Pioneer 10 produced less than 15 W of electrical power.

The actual shape of the RTGs is shown in Figure 2.5. It is important to note that the RTGs on board Pioneer 10 and 11 were built with the large fins that are depicted in this figure. These enlarged fins are not shown in many drawings and photographs (including Figure 2.3).

2.2.4 The electrical subsystem

Electrical power from the RTGs reached the spacecraft body via a set of ribbon cables. There, raw power from the RTGs was fed into a series of electric power supplies that produced 28 VDC for the spacecraft's main bus, and also other voltages on secondary power buses.

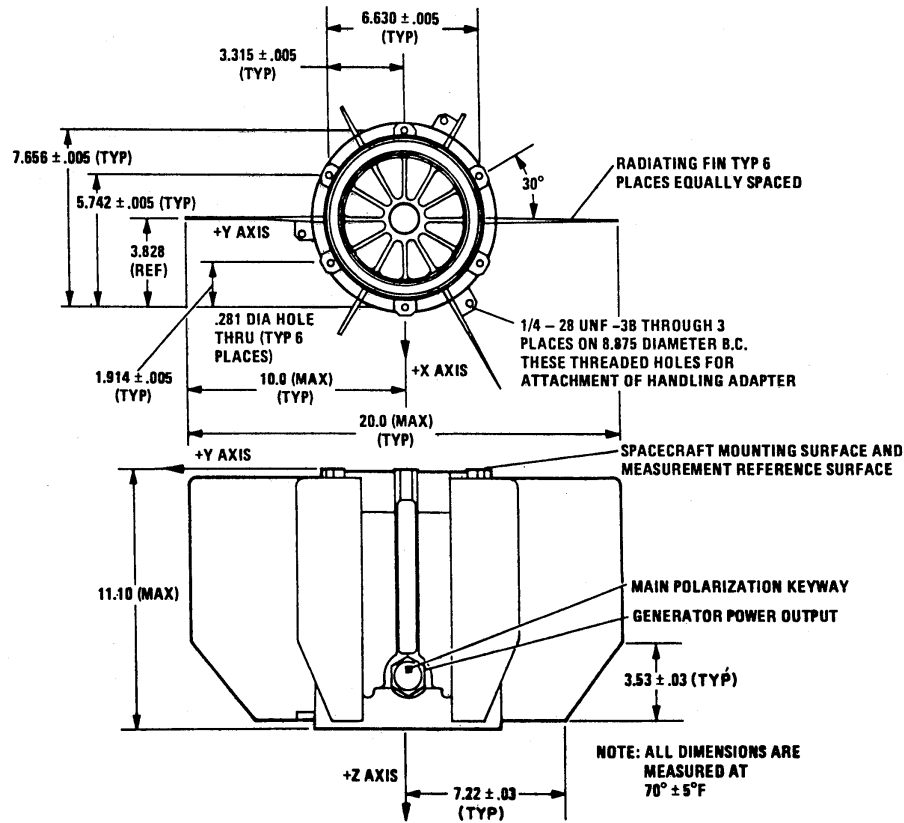


Figure 2.5: The SNAP-19 RTGs used on Pioneer 10 and 11 (from [354]). Note the enlarged fin structure. Dimensions are in inches (1" = 2.54 cm).

Electrical power consumption on board the spacecraft was regulated to ensure a constant voltage on the various power buses on the one hand, and an optimal current draw from the RTGs on the other hand. The electrical power subsystem was designed such that the spacecraft could perform its primary mission, namely close-up observations of the planet Jupiter approximately 21 months after launch, using only three RTGs, while operating a full complement of science instruments. Consequently, in the early years of their mission, significant amounts of excess electrical power were available on both spacecraft. The power regulation circuitry diverted this excess power to a shunt circuit, which dissipated some excess power internally, while routing the remaining excess power to an externally mounted shunt radiator.

The total power available on board at the time of launch was in excess of ~ 160 W. This figure decreased steadily throughout the missions, obeying an approximate negative exponential law. The actual amount of power available was a function of the decay of the radioisotope fuel, the decreasing temperature differential between the hot and cold ends of thermoelectric elements, and degradation of the elements themselves. At the end of its mission, the power available on board Pioneer 10 was less than 60 W. (Indeed, a drop in the main bus voltage is the most likely reason that Pioneer 10 eventually fell silent, as the reduced voltage was no longer sufficient to operate the spacecraft's transmitter.)

The RTGs generated electrical power at ~ 4 VDC (Figure 2.6). Power output from each RTG was fed to a separate inverter circuit, producing 61 VAC (peak-to-peak) at ~ 2.5 kHz. Output

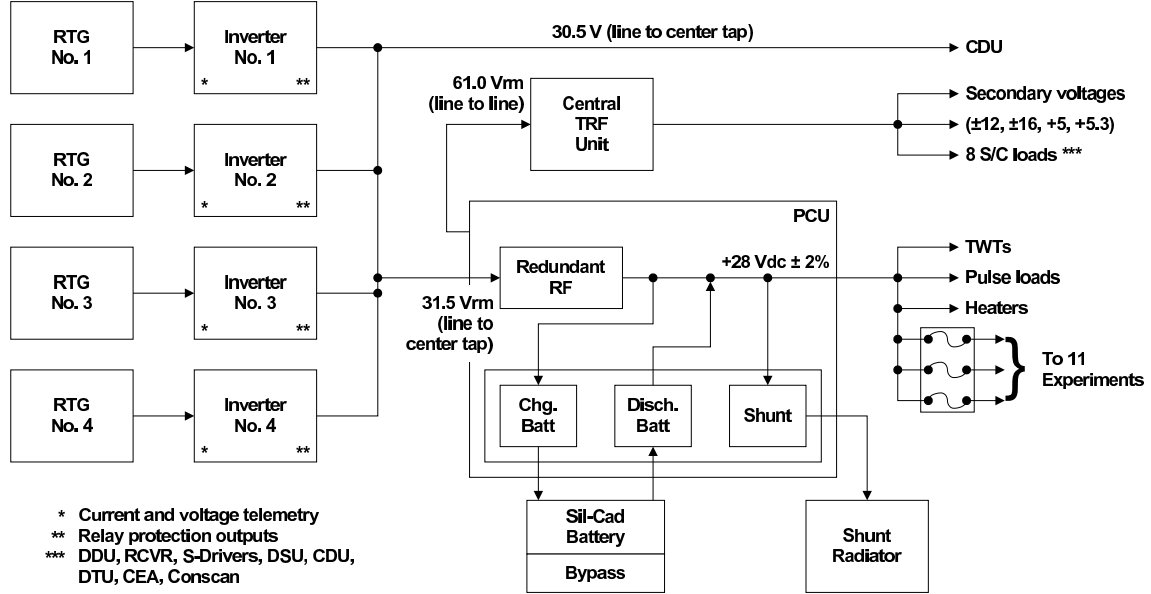


Figure 2.6: Overview of the Pioneer 10 and 11 electrical subsystem (from [292]).

from the four inverters was combined and fed to the Power Control Unit (PCU), which generated the 28 VDC main bus voltage, managed the on-board battery, controlled the dissipation of excess power via a shunt circuit, and also provided power to the Central Transformer Rectifier (CTRF) component, which, in turn, supplied power at various voltages (e.g., ± 16 VDC, ± 12 VDC, $+5$ VDC) to other subsystems and instruments.

The power budget at any given time was a function of available power vs. spacecraft load. For instance, Figure 2.7 shows Pioneer 10's power budget on July 25, 1981.

The on-board battery was designed to help with transient peak loads that temporarily exceeded the capabilities of the RTGs. The battery was composed of eight silver-cadmium cells, each of which had a capacity of 5 Ah and was equipped with an individual charge/discharge bypass circuitry.

2.2.5 Propulsion and attitude control

After separation from their respective launch vehicles, the orbits of Pioneer 10 and 11 were determined by the laws of celestial mechanics. The spacecraft had only a small amount of fuel on board, used by their propulsion system designed to control the spacecraft's spin and orientation, and execute minor course correction maneuvers.

The propulsion system consisted of three thruster cluster assemblies (see Figure 2.8), each comprising two 1 lb (~ 4.5 N) thrusters. All thruster cluster assemblies were mounted along the rim of the HGA. One pair of clusters was oriented tangentially along the antenna perimeter, and its two thrusters were intended to be used to increase or decrease the spin rate of the spacecraft. The remaining two pairs were oriented perpendicular to the antenna plane, on opposite sides of the antenna. These two thruster cluster assemblies were used in pairs. If two thrusters pointing in the same direction were fired simultaneously, this resulted in a net change in the spacecraft's velocity in a direction perpendicular to the antenna plane. If two clusters were fired in the opposite direction, this caused the spacecraft's spin axis to precess. This latter type of maneuver was used, in particular, to maintain an Earth-pointing orientation of the HGA to ensure good reception of radio signals.

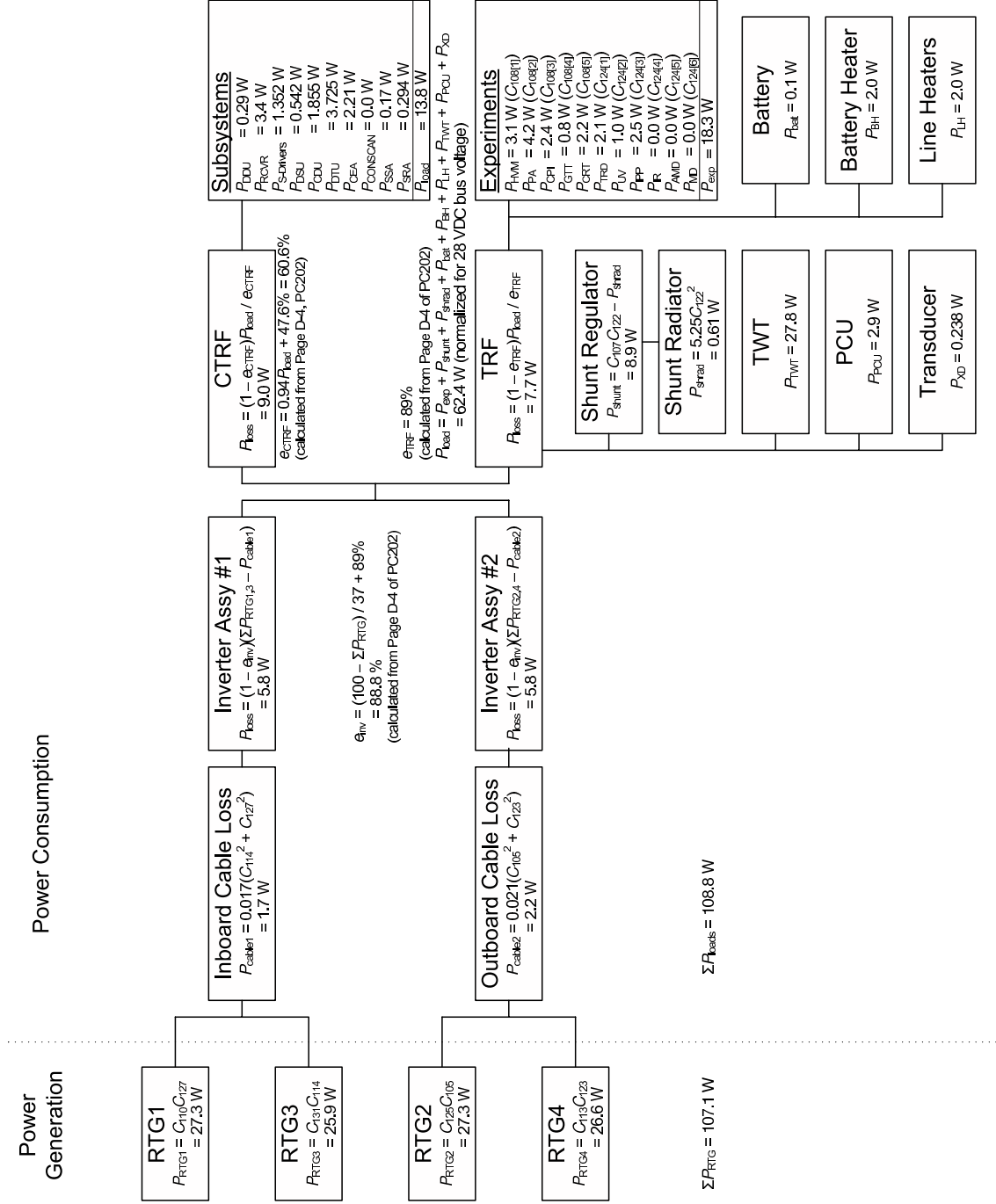


Figure 2.7: Pioneer 10 power budget on July 25, 1981, taken as an example. Power readings that were obtained from spacecraft telemetry are indicated by the telemetry word in the form C_{nnn} . The discrepancy between generated power and power consumption is due to rounding errors and uncertainties in the nominal vs. actual power consumption of various subsystems.

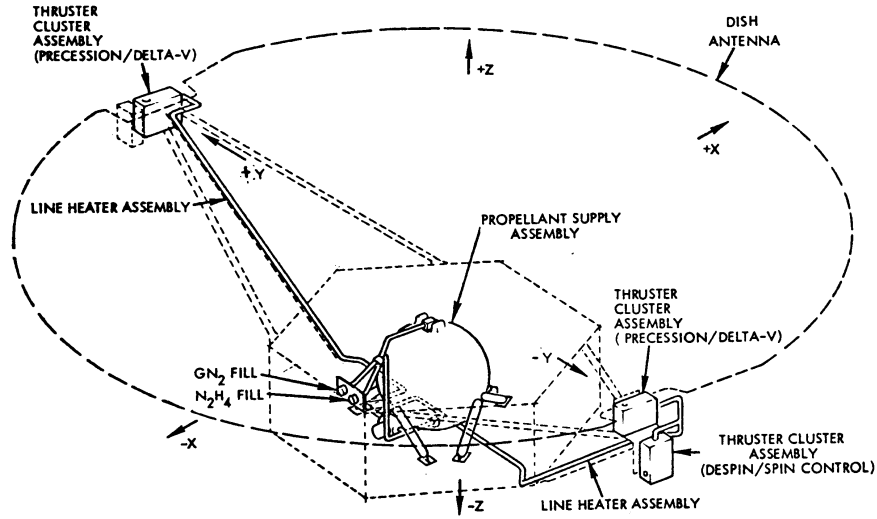


Figure 2.8: An overview of the Pioneer 10 and 11 propulsion subsystem (from [292]).

The thrusters were labeled VPT (velocity and precession thruster) and SCT (spin control thruster.) VPT 1 and VPT 3 were oriented in the same direction as the HGA (the $+z$ direction), while VPT 2 and VPT 4 were oriented in the opposite direction.

The propulsion system utilized hydrazine (N_2H_4) monopropellant fuel, of which ~ 27 kg was available on board, in a 38 liter tank that was pressurized with N_2 . The propellant and pressurant were separated by a flexible membrane, which prevented the mixing of the liquid propellant and gaseous pressurant in the weightless environment of space. The fuel tank was located at the center of the spacecraft, and was heated by the spacecraft's electrical equipment. Fuel lines leading to the thruster cluster assemblies were heated electrically, while the thruster cluster assemblies were equipped with small (1 W) radioisotope heating units (RHUs) containing ^{238}Pu fuel.

The capabilities of the propulsion system are summarized in Table 2.2.

Table 2.2: Capabilities of the Pioneer 10 and 11 propulsion system.

Maneuver	Thrusters	Max. capability
Despin	SCT 1 or 2	58 rpm
Spin control	SCT 1 or 2	14 rpm
Precession	VPT 1 and 4 or VPT 2 and 3	1250°
Delta- v	VPT 1 and 3 or VPT 2 and 4	250 m/s

The spacecraft's Earth-pointing attitude was maintained as the spacecraft were spinning in the plane of the HGA, at a nominal rate of 4.8 revolutions per minute (rpm). The propulsion system had the capability to adjust the spin rate of the spacecraft, and to precess the spin axis, in order to correct for orientation errors, and to ensure that the spacecraft followed the Earth's position in the sky as seen from on board.

The spin axis perpendicular to the plane of the HGA is one of the spacecraft's principal axis of inertia. A wobble damper mechanism [292] dampened rotations around any axis other than this principal axis of inertia, ensuring a stable attitude even after a precession maneuver.

2.2.6 Navigation

The Pioneer 10 and 11 spacecraft relied on standard methods of deep space navigation [226, 231] (see Section 4). The spacecraft’s position was determined using the spacecraft’s radio signal and the laws of celestial mechanics. The radio signal offered a precision Doppler observable, from which the spacecraft’s velocity relative to an Earth station along the line-of-sight could be computed. Repeated observations and knowledge of the spacecraft’s prior trajectory were sufficient to obtain highly accurate solutions of the spacecraft’s orbit.

The orientation of the spacecraft was estimated from the quality of the radio communication link (i.e., the spacecraft had to be approximately Earth-pointing in order for the Earth to fall within the HGA radiation pattern.) The rate and phase of the spacecraft’s rotation was established by a redundant pair of sun sensors and a star sensor on board. These sensors (selectable by ground command) provided a roll reference pulse that was used for navigation purposes (as explained in the next paragraph) as well as by on-board science instruments. The time between two subsequent roll reference pulses was measured and telemetered to the ground.

The spacecraft also had minimal autonomous (closed loop) navigation capability, designed to make it possible for the spacecraft to restore its orientation by “homing in” on an Earth-based signal. The maneuver, called a conical scan (CONSCAN) maneuver, utilized a piston mechanism [3] with electrically heated freon gas that displaced the feed horn located at the focal point of the high-gain antenna. Unless the Earth was exactly on the HGA centerline, this introduced a sinusoidal modulation in the amplitude of the signal received from the Earth. A simple integrator circuit, utilizing this sinusoidal modulation and the roll reference pulse, triggered firings of the precession thrusters, adjusting the spacecraft’s axis of rotation until it coincided with the direction of the Earth.

Frequently, instead of CONSCAN maneuvers, “open loop” attitude correction maneuvers were used, calculated to ensure that after the maneuver, the spacecraft was oriented to “lead” the Earth, allowing the Earth to move through the antenna pattern subsequently. This reduced the frequency of attitude correction maneuvers; further, open loop maneuvers generally consumed less propellant than autonomous CONSCAN maneuvers.

Early in the mission, attitude correction maneuvers had to be executed regularly, due to the combined motion of the Earth and the spacecraft. Late in the extended mission, only two attitude correction maneuvers were needed annually, to compensate for the Earth’s motion around the Sun, and for the spacecraft’s “sideways” motion along its hyperbolic escape trajectory.

2.2.7 Communication system

The spacecraft maintained its communication link with the Earth using a set of S-band transmitters and receivers on board, in combination with three antennae.

The main communication antenna of the spacecraft was the 2.74 m diameter high-gain antenna. The antenna’s narrow beamwidth (3.3° downlink, 3.5° uplink) ensured an effective radiated power of 70 dBm, allowing communication with the spacecraft over interplanetary distances. (The original mission design anticipated signal loss some time after Jupiter encounter, but still within the orbit of Saturn; increases in the sensitivity of Earth stations allowed communication with Pioneer 10 up until 2003, when the spacecraft was over 70 AU from the Earth.)

Mounted along the centerline of the HGA was the horn of a medium-gain antenna (MGA). On the opposite ($-z$) side of the spacecraft, at the bottom of the main compartment was mounted a third, low-gain omnidirectional antenna (LGA). This antenna was used during the initial mission phases, before the HGA was oriented towards the Earth.

The spacecraft had two receivers and two transmitters on board, switchable by ground command. While one receiver was connected to the HGA, the other was connected to the MGA/LGA.

The sensitivity of the receiver was -149 dBm; at the time of the last transmission, the spacecraft detected the Earth station's signal at a strength of -131.7 dBm.

The spacecraft utilized two traveling wave tube (TWT) transmitters for microwave transmission. The TWTs were selectable by ground command; it was possible to power off both TWTs to conserve power (such as when CONSCAN maneuvers were performed late in the mission, when the available electrical power on board was no longer sufficient to operate a TWT transmitter and the feed movement mechanism simultaneously.)

The radio systems operated in the S-band, utilizing a frequency of ~ 2.1 GHz for uplink, and ~ 2.3 GHz for downlink. The transmitter frequency was synthesized on board by an independent oscillator. However, the spacecraft's radio system could also operate in a *coherent mode*: in this mode, the downlink signal's carrier frequency was phase-coherently synchronized to the uplink frequency, at the exact frequency ratio of 240/221. In this mode, the precision and stability of the downlink signal's carrier frequency was not limited by the equipment on board. This mode allowed precision Doppler frequency measurements with millihertz accuracy.

The main function of the spacecraft's communication system was to provide two-way data communication between the ground and the spacecraft. Data communication was performed at a rate of 16–2048 bits per second (bps). Communication from the ground consisted of commands that were decoded by the spacecraft's radio communication subsystem. Communication to the ground consisted of measurement results from the spacecraft's suite of science instruments, and engineering telemetry.

2.2.8 Telemetry data and its interpretation

Communication between the spacecraft and a DSN antenna took place using a variety of data formats; the format selected depended on the type of experiment that the spacecraft was ordered to perform, but typically the format gave precedence to science results over telemetry. However, telemetry information was continuously transmitted to the Earth at all times, using a small portion of the available data bandwidth.

The telemetry data stream was assembled on board by the digital telemetry unit (DTU), which comprised some ~ 800 TTL⁴ integrated circuits, and was also equipped with 49,152 bits of ferrite core data memory. A total of 10 science data formats (of which 5 were utilized) and 4 engineering data formats, yielding a total number of 18 different valid format combinations, was selectable by ground command. The DTU could operate in three modes: realtime (passing through science measurements as received from instruments), store (storing measurements in the on-board memory) and readout (transmitting measurements previously stored in on-board memory.)

When one of the engineering data formats was selected, the spacecraft transmitted only engineering telemetry. These formats were utilized, for instance, during maneuvers or spacecraft troubleshooting.

Most of the time, a science data format was used, in which case most of the bits in the telemetry data stream contained science data. A small portion, called the subcommutator, was reserved for engineering data; this part of the telemetry record cycled through all telemetry data words in sequence.

The telemetry record size was 192 bits, divided into 36 6-bit words. Depending on the telemetry format chosen, either all 36 6-bit words contained engineering telemetry, or a single engineering telemetry word was transmitted in every (or every second) telemetry record.

There were 128 distinct engineering telemetry words. Depending on the science format used, the subcommutator was present either in every transmitted record or every second record. Therefore,

⁴Transistor-Transistor-Logic, or TTL integrated circuits are standardized logic circuits built using bipolar transistors that have been in widespread use since the 1960s in the form of small-scale integration (SSI) integrated circuits containing a small number of logic gates per chip.

it may have taken as many as 256 telemetry records before a particular engineering word was transmitted. At the lowest data rate of 16 bits per second, this meant that any given parameter was telemetered to the Earth once every 51.2 minutes.

An additional 64 telemetry words were used to transmit engineering information from science instruments. These parameters were only transmitted in the subcommutator, and at the lowest available data rate, a particular science instrument telemetry word was repeated every 25.6 minutes.

The 128 engineering telemetry words were organized into 4 groups of 32 words each; it is customary to denote them using the notation C_{mnn} , where $m = 1...4$ is the group number, and $nn = 01...32$ is the telemetry word. Similarly, science instrument telemetry words were labeled E_{mnn} , with $m = 1...2$ and $nn = 01...32$.

When a science or engineering telemetry word was used to convey the reading from an analog (temperature, voltage, current, pressure, etc.) sensor, the reading was digitized with 6-bit resolution [135, 403, 159], and the resulting 6-bit data word was transmitted. Associated with each telemetry word representing an analog measurement was a set of calibration coefficients that formed a 5th-order calibration polynomial. For each calibration polynomial, a range was also defined that established valid readings that could be decoded by that polynomial.

Appendix D lists selected engineering and science telemetry data words that may be relevant to the analysis of the Pioneer anomaly.

2.2.9 Thermal subsystem

The Pioneer spacecraft were equipped with a thermal control system comprising a variety of active and passive thermal control devices. The purpose of these devices was to maintain the required operating temperatures for all vital subsystems of the spacecraft.

The main spacecraft body was covered by multilayer insulating blankets [368, 369]. These blankets were designed to retain heat within the spacecraft when it was situated in deep space, far from the Sun.

To prevent overheating of the spacecraft interior near the Sun, a thermal louver system [292, 71, 301, 279] was utilized. The louvers were located at the bottom of the spacecraft, organized in a circular pattern, with additional louvers on the science compartment (Figure 2.10). These louvers were actuated by bimetallic springs that were thermally (radiatively) coupled to the main electronics platform behind the louvers. The louvers were designed to be fully open when the platform temperature exceeded 90° F, and fully close when the temperature fell below 40° F (Figure 2.11).

The louver system emits heat in two ways: through structural components (Figure 2.12), and through the louver blade assemblies (Figure 2.13). The total heat emitted by the louver system is the sum of the heat emitted via these two mechanisms.

The fuel lines extending from the spacecraft body to the thruster cluster assemblies located along the rim of the HGA were insulated by multilayer thermal blankets and were kept warm by electric heater lines. The thruster cluster assemblies contained radioisotope heater units (RHUs), designed to prevent the propellant from freezing. Additional RHUs heated the star sensor and the magnetometer assembly at the end of the magnetometer boom.

The spacecraft's battery was mounted on the outside of the main spacecraft body, and heated by an electrical heater.

Most heat produced by electrical equipment on board was released within the insulated interior of the spacecraft. The requirement for science instruments was to leak no more than the instrument's own power consumption plus 0.5 W to space.

Some excess electrical power was radiated away as heat by an externally mounted shunt radiator plate, which formed part of the spacecraft's electrical power subsystem.

Most heat on board was produced by the four radioisotope thermoelectric generators. Electrical power in these generators was produced by bimetallic thermocouples that relied on the temperature

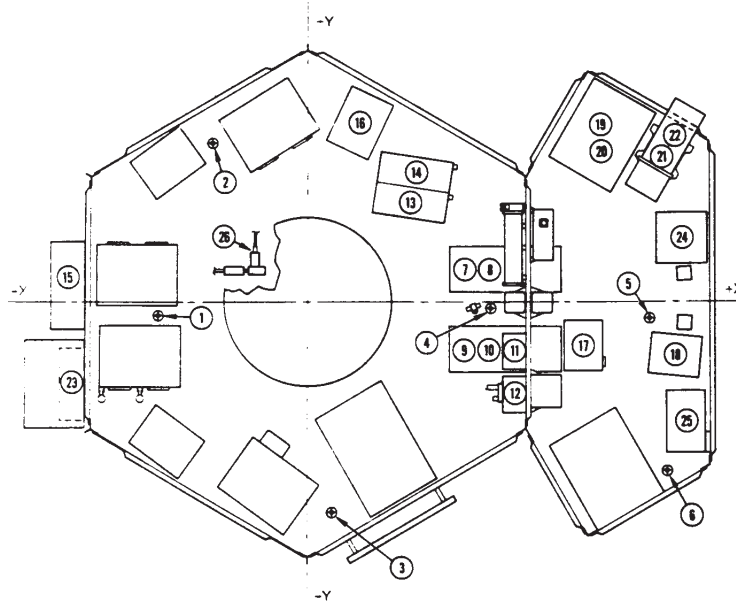


Figure 2.9: Location of thermal sensors in the instrument compartment of the Pioneer 10 and 11 spacecraft (from [292]). Platform temperature sensors are mounted at locations 1 to 6. Some locations (i.e., end of RTG booms, propellant tank interior, etc.) not shown.

difference between their hot and cold ends for power generation. Therefore, it was essential that the cold ends of the thermocouples were connected to RTG radiator fins that radiated heat into space with high efficiency.

Temperature readings from many locations throughout the spacecraft, including temperatures at six key locations on the main electronics platform, were telemetered to the ground (Figure 2.9).

With the exception of the louver system, the two adjacent hexagonal parts of the spacecraft body are covered by multilayer insulation. There is no insulation between the main and science compartments of the spacecraft body.

The surface materials and paints used to cover most major exterior surfaces are documented [292, 53, 103, 133, 197, 279]. In particular, the surfaces of the spacecraft body, HGA, and RTGs are well described, along with the thermal control louver system in terms of solar absorptance and infrared emittance (Table 2.3). Solar absorptance is characterized by a dimensionless number (usually denoted by α) between 0 and 1 representing the efficiency with which a particular material absorbs the radiant energy of the Sun when compared to an ideal black body. Infrared emittance is similarly characterized by a dimensionless number (usually denoted by ϵ) between 0 and 1 that represents the efficiency with which a material radiates heat at lower (typically, room) temperatures as compared to an ideal black body.

The exterior surfaces of the Pioneer 10 and 11 spacecraft are covered by a variety of materials and paints. Changes in the spacecraft properties can affect/induce forces that are both of on-board and of external origin. Therefore, it is of great importance to establish the extent to which any of the spacecraft's properties might have been changing over time.

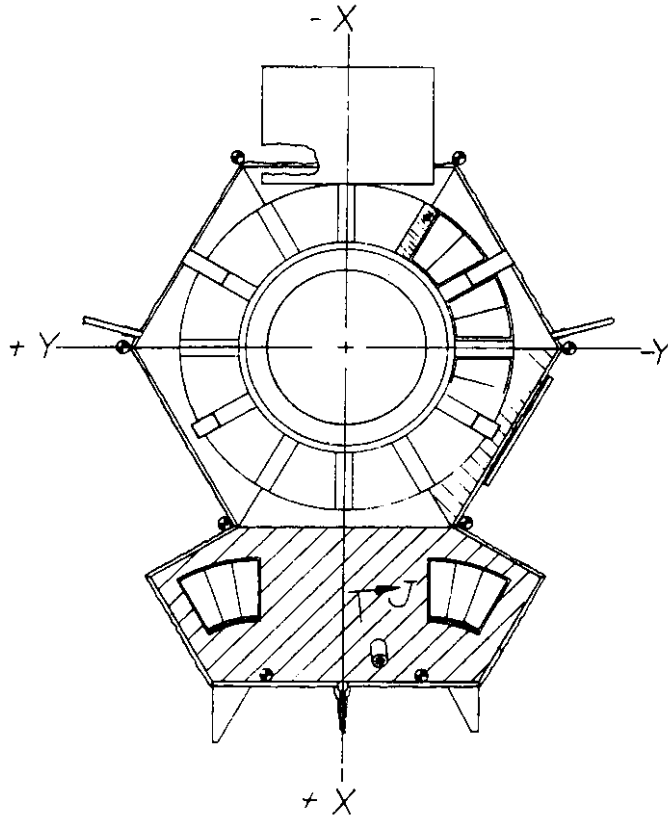


Figure 2.10: The Pioneer 10 and 11 thermal control louver system, as seen from the aft ($-z$) direction (from [292]).

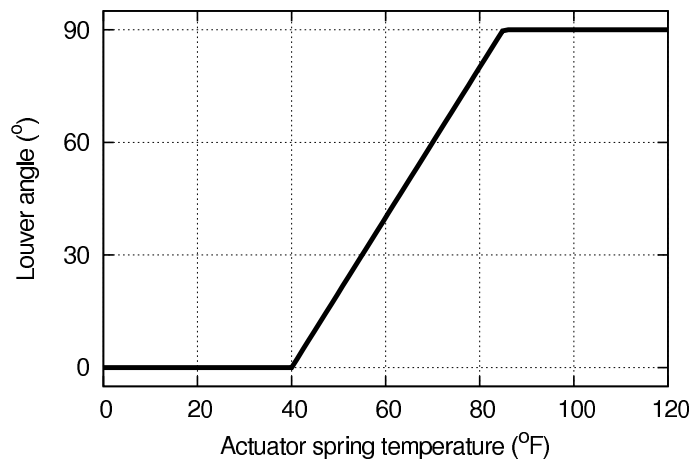


Figure 2.11: Louver blade angle as a function of platform temperature (from [279]). Temperatures in $^{\circ}\text{F}$ ($[^{\circ}\text{C}] = ([^{\circ}\text{F}] - 32) \times 5/9$).

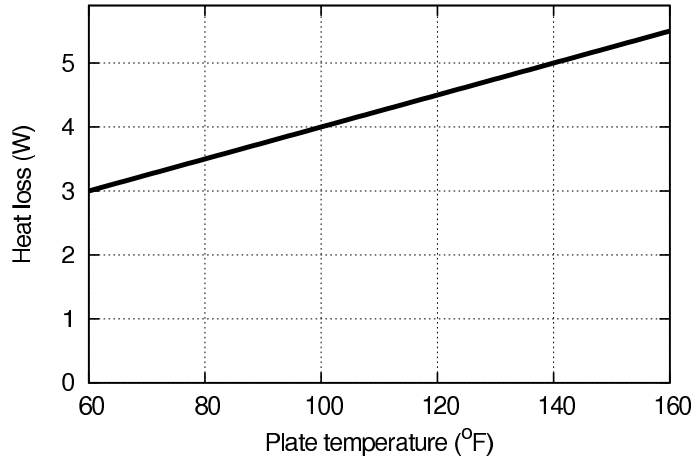


Figure 2.12: Louver structure heat loss as a function of platform temperature (from [279]). Temperatures in °F ($[^{\circ}\text{C}] = ([^{\circ}\text{F}] - 32) \times 5/9$).

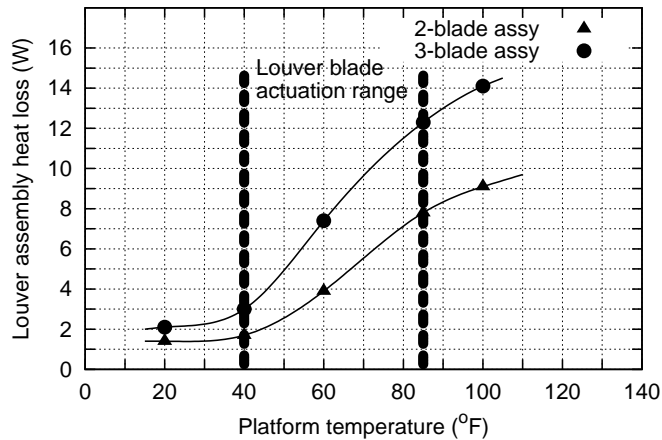


Figure 2.13: Louver assembly performance (from [279]). Temperatures in °F ($[^{\circ}\text{C}] = ([^{\circ}\text{F}] - 32) \times 5/9$).

2.3 Spacecraft operating history

The Pioneer 10 and 11 spacecraft spent about three decades in deep space. Most of what we know about the anomalous acceleration is based on data that was collected when the spacecraft were well into their second and third decades of operation. This raises an obvious question: what are the effects of aging and to what extent may aging be responsible for the anomalous acceleration?

In this section, we summarize our knowledge about the effects of aging on the spacecrafts' subsystems.

2.3.1 Spacecraft physical configuration

The overall shape of the Pioneer 10 and 11 spacecraft is not expected to change significantly with age. The spacecraft is fundamentally a rigid body; other than the constant centrifugal force that

Table 2.3: Radiometric properties of Pioneer 10 and 11 major exterior surfaces (at launch): solar absorptance (α) and infrared emittance (ϵ).

Surface	Area (m ²)	α	ϵ
HGA front (white paint)	5.91	0.21	0.85
HGA rear (bare aluminum)	5.91	0.17	0.04
Spacecraft body, front (2-mil aluminized Mylar)	1.55	0.17	0.70
Spacecraft body, rear (2-mil aluminized Kapton)	1.19	0.40	0.70
Spacecraft body, RTG sides (2-mil aluminized Kapton)	0.65	0.40	0.70
Spacecraft body, other sides (2-mil aluminized Mylar)	1.21	0.17	0.70
RTG fin surfaces (white paint)		0.20	0.83
Louver blades, closed (bare aluminum)	0.36	0.17	0.04

arises as a result of the spacecraft’s rotation, there are no forces stretching, bending, or otherwise acting on the spacecraft structurally.

The Pioneer spacecraft had few moving parts. After initial boom deployment, the spacecrafts’ physical configurations remained largely unchanging, with a few notable exceptions.

Consumption of the fuel load on board resulted in small changes in the spacecrafts’ mass distribution during the large course correction maneuvers early in the Pioneer 10 and 11 missions. As the amount of fuel on board was small, and the fuel tank was situated near the spacecraft’s center-of-gravity, the effects of later attitude correction maneuvers, which consumed minuscule amounts of fuel, were likely negligible.

Some instruments had moving parts: notably, the Imaging Photopolarimeter (IPP) instrument had a telescope that was mounted on a scan platform, allowing it to be used for Jupiter imaging. Operating this instrument’s small moving parts, however, would have introduced only minute changes in the spacecraft’s mass distribution and thermal properties.

More notable was the spacecraft’s passive louver system. As discussed in Section 2.4, the louver system was designed to vent excess heat radiatively from the interior of the spacecraft. The state of the louver system can be determined as a function of the electronics platform temperatures. The position of the louver blades can significantly alter the thermal behavior of the spacecraft, by allowing a higher proportion of interior heat to escape through the louver system.

At large heliocentric distances (beyond ~ 25 AU), the louver system is always closed, and the spacecraft’s physical configuration remains constant.

2.3.2 Changes in spacecraft mass

As we discussed in Section 2.2.1, the nominal launch mass of the Pioneer 10 and 11 spacecraft was ~ 260 kg, of which ~ 30 kg was propellant and pressurant.⁵ The spacecraft mass slowly decreased, primarily as a result of propellant usage. Additionally, small mass losses may occur due to fuel leaks, pressurant outgassing, He outgassing (α particles) from the RTGs and RHUs, and possibly, outgassing from the spacecraft batteries.

Pioneer 10 used only a moderate amount of propellant, as it performed no major trajectory correction maneuvers. If the propellant used amounted to one quarter of the propellant on board, this means that Pioneer 10’s mass would have decreased to ~ 250 kg late in its mission (the 2002 JPL study used the nominal value of 251.883 kg). Further, it should be noted that most propellant usage occurred prior to Jupiter encounter; afterwards, Pioneer 10 only used minimal amounts of propellant for precession maneuvers, needed to keep its antenna aimed at the Earth.

⁵Note that the acceleration due to nongravitational forces, regardless of their external or internal origin, is dependent on the actual mass of the spacecraft.

Pioneer 11 performed major trajectory correction maneuvers en route to Jupiter and Saturn. The maneuvers were in order to allow it to follow a precisely calculated orbit that utilized a gravitational assist from Jupiter that was needed to set up the spacecraft for its encounter with Saturn. As a result, Pioneer 11 is believed to have used significantly more propellant than its twin, perhaps three quarters of the total available on board. The spacecraft’s mass, therefore, may have decreased to ~ 232 kg following its encounter with Saturn (the mass used in the 2002 JPL study was somewhat higher, 239.73 kg [18]).

We note that these figures are crude estimates, as the actual amount of propellant on board is not telemetered. Sensors inside the propellant tank did offer temperature and pressure telemetry, but these sensors were not sufficiently reliable for a precise estimate of the remaining fuel on board.

The spacecraft can also lose mass due to outgassing. Two possible sources of outgassing are helium outgassing from the radioactive fuel on board in the radioisotope thermoelectric generators and radioisotope heater units, and chemical outgassing from the spacecraft’s battery. An upper limit of 18 g on helium outgassing can be established using the known physical properties of the ^{238}Pu fuel (see Section 4), which is not significant. Similarly, the amount of gas that can escape from the spacecraft’s batteries is small, especially in view of the fact that the batteries performed nominally far longer than anticipated: under no circumstances can it exceed the battery mass, but in all likelihood, and especially in view of the fact that the batteries performed nominally throughout the mission, any outgassing is necessarily limited to a very small fraction of the ~ 2.35 kg battery mass (see Section 4). Therefore, outgassing cannot have played a major role in the evolution of the spacecraft mass; furthermore, any mass loss due to outgassing is dwarfed by uncertainties in the mass of the remaining fuel inventory.

Could the spacecraft have gained mass, for instance, by collecting dust particles from the interplanetary medium? In situ measurements by the Pioneer spacecraft themselves provide an upper limit on the amount of dust encountered by the spacecraft. After passing Jupiter’s orbit, the dust flux measured by Pioneer 10 remained approximately constant, at $3 \times 10^{-6} \text{ m}^{-2}\text{s}^{-1}$ particles [170]. The upper limit on particle sizes is 10^{-4} kg. Even assuming that all particles had masses near this upper limit, the total amount of mass that could have accumulated on the spacecraft over the course of 20 years would be no more than ~ 1 kg. However, given that the spacecraft is moving through interplanetary space at a velocity of 10 km/s or higher, these assumptions on particle size would imply a dust density of $\sim 10^{-14} \text{ kg/m}^3$, which is many orders of magnitude higher than more realistic estimates (see Section 4.3.5). Therefore, the actual dust mass accumulated on the spacecraft cannot be more than a few grams at the most; consequently, this mechanism for mass increase can also be safely ignored.

2.3.3 Instrumentation

It is not known how on-board instrumentation (i.e., telemetry sensors) respond to aging. What we know is that many sensors stopped providing usable readings when measured values (e.g., temperatures) dropped outside calibrated ranges [383, 384, 397, 399]. Other sensors continued to provide consistent readings, with no indication of sensor failure.

However, there were a few sensor anomalies that may be due to age-related sensor defects. Most notable among these are the anomalous readings from the propellant tank of Pioneer 10 (described in Section 2.3.6).

It is also unknown how on-board instrumentation responds when their supply voltage drops below the nominal level. Late in its mission, the electrical power subsystem on board Pioneer 10 no longer had sufficient power to maintain the nominal main bus voltage of 28 VDC. As this coincides with changes in physical sensor readings (e.g., drops in temperature), the extent to which those readings are affected by the drop in voltage is not readily evident.

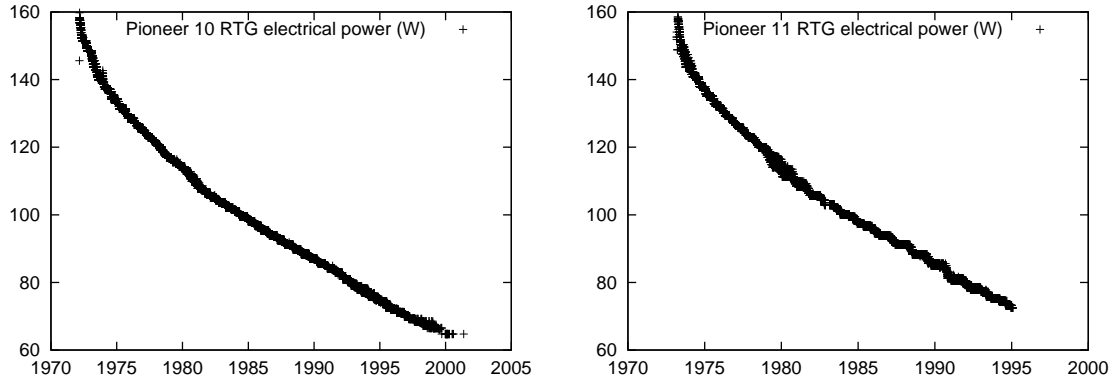


Figure 2.14: Changes in total RTG electrical output (in W) on board Pioneer 10 (left) and 11 (right), as computed using the missions’ on-board telemetry.

2.3.4 Electrical system

Insofar as we can determine from telemetry, the electrical subsystems on board Pioneer 10 and 11 performed nominally throughout the missions, so long as sufficient electrical power was available from the RTGs. The on-board chemical batteries remained functional for many years; eventually, due to irreversible chemical changes and decreasing temperatures, the batteries ceased functioning.

2.3.5 Radioisotope thermoelectrical generators

The effects of aging on the RTGs are complex. Internally, aging causes a degradation of the bimetallic thermocouples, contributing to their loss of efficiency and the decrease in RTG electrical power output. Externally, it has been conjectured [331] that the RTG exterior surfaces may have aged due to solar bleaching and impact by dust particles. The extent to which such degradation may have occurred (if at all) is unknown. The resulting fore-aft asymmetry may be a significant source of unaccounted-for acceleration in the approximately sunward direction.

2.3.6 Propulsion system

The propellant pressure sensor on board Pioneer 10 began to show anomalous behavior in June 1989. Propellant pressure, which remained steady up to this point, only decreasing slowly as a result of cooling and occasional propellant usage, suddenly began to show a sharp decay, dropping from over 300 psia down to about 150 psia by January 1992 (Figure 2.15). At this time, the propellant pressure instantaneously increased to its pre-1989 value of ~ 310 psia, after which it began dropping again. There were no corresponding changes or other anomalies in the observed propellant temperature and expellant temperature. Therefore, the most likely explanation for this anomaly is a sensor malfunction, not a real loss of fuel or propellant.

On December 18, 1975, subsequent to an attempted maneuver, and as a result of a stuck thruster valve, the spin of Pioneer 11 increased dramatically, from a spin rate of ~ 5.5 revolutions per minute (rpm) to ~ 7.7 rpm (Figure 2.16, right panel). Fortunately, the thruster ceased firing before the spin rate increased to a value that would have threatened the spacecraft’s structural integrity or compromised its ability to carry out its mission.

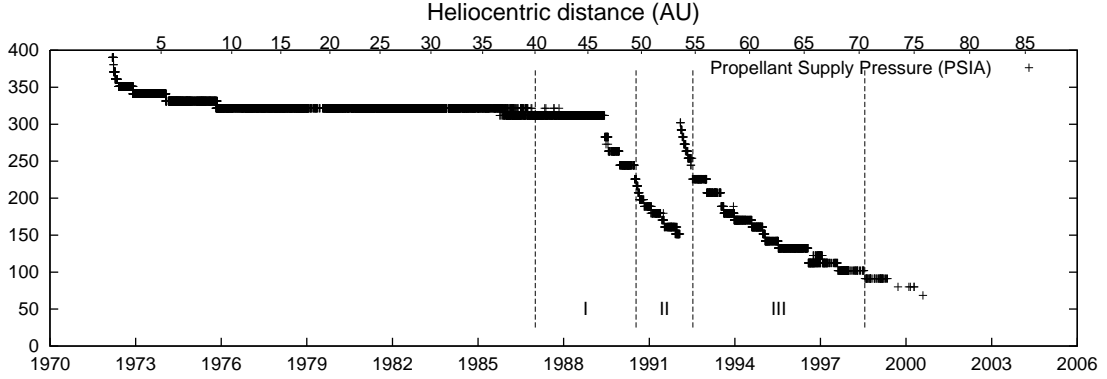


Figure 2.15: Propulsion tank pressure (in pounds per square inch absolute; 1 psia = 6.895 kPa) on board Pioneer 10. The three intervals studied in [18] are marked by roman numerals and separated by vertical lines.

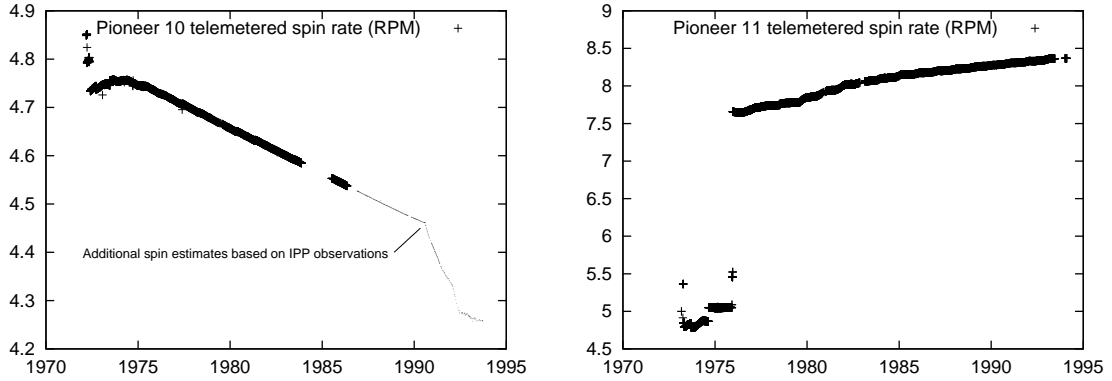


Figure 2.16: On-board spin rate measurements (in rpm) for Pioneer 10 (left) and Pioneer 11 (right). The sun sensor used on Pioneer 10 for spin determination was temporarily disabled between November 1983 and July 1985, and was turned off in May 1986, resulting in a ‘frozen’ value being telemetered that no longer reflected the actual spin rate of the spacecraft. Continuing spot measurements of the spin rate were made using the Imaging Photo-Polarimeter (IPP) until 1993. The anomalous increase in Pioneer 11’s spin rate early in the mission was due to a failed spin thruster. Continuing increases in the spin rate were due to maneuvers; when the spacecraft was undisturbed, its spin rate slowly decreased, as seen in Figure 2.17.

2.3.7 Attitude control and spin

Encounter with the intense radiation environment in the vicinity of Jupiter damaged the star sensor on board Pioneer 10. As the sun sensors operate only up to a distance of ~ 30 AU, Pioneer 10 had operated without a primary roll reference for many years before the end of its mission. (The rate of Pioneer 10’s spin was determined from measurements taken by its Imaging Photo-Polarimeter (IPP) instrument and other methods [353].)

The nominal spin rate of the Pioneer 10 and 11 spacecraft was 4.8 rpm. This spin rate was achieved by reducing the spacecraft’s initial rate of spin, provided by the launch vehicle, in successive stages, first by firing spin/despin thrusters, and then by extending the RTG and magnetometer

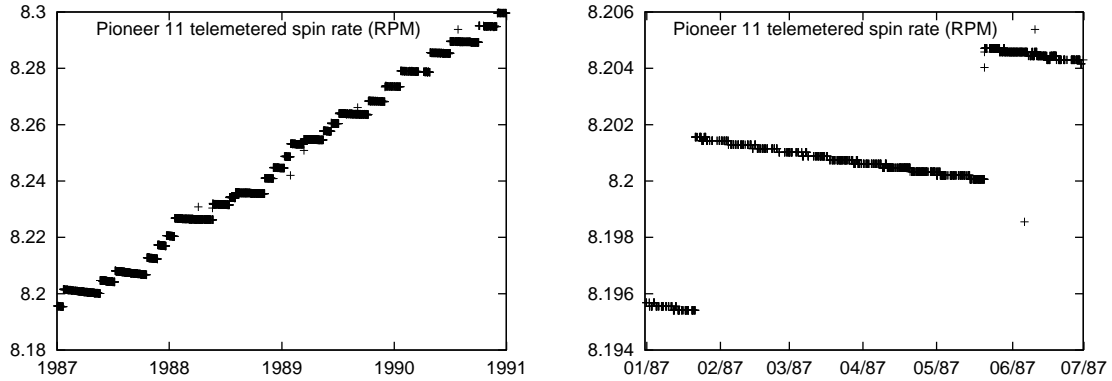


Figure 2.17: Zoomed plots of the spin rate of Pioneer 11. On the left, the interval examined in [18] is shown; maneuvers are clearly visible, resulting in discrete jumps in the spin rate. The figure on the right focuses on the first half of 1987; the decrease in the spin rate when the spacecraft was undisturbed is clearly evident.

booms. Later, spin could be precisely adjusted and corrected by the spin/despin thrusters.

On Pioneer 11, due to the spin thruster anomaly described in the previous section, the spacecraft’s spin remained at an abnormally high value. In fact, it further increased, presumably as a result of fuel leaks, all the way up to ~ 8.4 rpm at the time of the last available telemetry data point, on February 11, 1994.

Meanwhile, Pioneer 10’s spin slowly decreased over time, probably due to a combination of effects that may include fuel leaks as well as the thermal recoil force and associated change in angular momentum.

The spin rates of Pioneer 10 and 11 are shown in Figure 2.16. Spin was measured on board using one of several sensors, namely a star sensor and two sun sensors. The purpose of these sensors was to provide a roll reference pulse that could then be used to synchronize other equipment, including the IPP instrument and the navigational system.

The sun sensors required a minimum angle between the spacecraft’s spin axis and the spacecraft-Sun line. Further, they required that the spacecraft be within a certain distance of the Sun, in order for a reliable roll reference pulse to be generated. For these reasons, the sun sensors could not be used to provide a roll reference pulse once the spacecraft were more than ~ 30 AU from the Sun.

There were no such limitations on the star sensor; however, the star sensor on board Pioneer 10 ceased functioning shortly after Jupiter encounter, probably due to radiation damage suffered while the spacecraft traversed the intense radiation environment in the gas giant’s vicinity.

As a result, Pioneer 10 lost its roll reference source when its distance from the Sun increased beyond ~ 30 AU. Although the roll reference assembly continued to provide roll reference pulses at the last “frozen in” rate, this rate no longer matched the actual rate of revolution of the spacecraft.

Nevertheless, it was important to know the spin rate of the spacecraft with reasonable precision, in order to be able to carry out precession maneuvers reliably, and also because the spacecraft’s spin affected the spacecraft’s radio signal and the Doppler observable. For this reason, the IPP was reused as a surrogate star sensor, its images of the star field providing a reference that could then be used by the navigation team to compute the actual spin rate of the spacecraft on the Earth [353]. It was during the time when the IPP instrument was used to compute the rate of spin that a spin anomaly was detected. The spin-down rate of Pioneer 10 suddenly grew in 1990, and then eventually returned to its approximate previous value (Figure 2.16, left panel.)

Very late in Pioneer 10's mission, when the power on board was no longer sufficient to operate the IPP instrument, crude estimates of the spin rate were made using navigational data.

In contrast to the spin behavior of Pioneer 10, the spin rate of Pioneer 11 continued to increase after the initial jump following the thruster anomaly. However, a close look at detailed plots of the spin rate reveal a more intricate picture. It seems that Pioneer 11's spin rate was actually *decreasing* between maneuvers, when the spacecraft was undisturbed; however, each precession maneuver increased the spacecraft's spin rate by a notable amount. The rate of decrease between successive maneuvers was not constant, suggesting that fuel leaks played a more significant role in Pioneer 11's spin behavior than in Pioneer 10's.

2.4 Thermal control subsystem

A quick look at the Pioneer spacecraft (Figure 2.3) is sufficient to see that the spacecraft's thermal radiation pattern may be anisotropic: whereas one side is dominated by the high-gain antenna, the other side contains a thermal louver system designed to vent excess heat into space. The RTGs are also positioned slightly behind the HGA, making it likely that at least some of their heat is reflected in the $-z$ direction.

This leads to the conclusion that anisotropically rejected thermal radiation cannot be ignored when we evaluate the evolution of the Pioneer 10 and 11 trajectories, and must be accounted for with as much precision as possible.

Far from the Sun and planets, the only notable heat sources on board Pioneer 10 and 11 are internal to the spacecraft. We enumerate the following heat sources:

- Waste heat from the radioisotope thermoelectric generators;
- Heat produced by electrical equipment on board;
- Heat from small radioisotope heater units;
- Transient heating from the propulsion system.

While strictly speaking it is not a heat source, one must also consider microwave radiation from the spacecraft's radio transmitter and HGA, as this radiation also removes what would otherwise appear as thermal energy from within the spacecraft.

2.4.1 Waste heat from the RTGs

The RTGs are the most substantial sources of heat on board. Each of the four generators on board the spacecraft produced ~ 650 W of power at the time of launch, of which ~ 40 W was converted into electrical energy; the rest was radiated into space as waste heat. The radiation pattern of the RTGs is determined by the shape and composition of their radiating fins (see Figure 2.5), but, notwithstanding the possible effects of aging, it is believed to be fore-aft symmetrical.

The amount of power generated by the RTGs is determined by the radioactive decay of the ^{238}Pu fuel on board. The radioactive half-life of the fuel is precisely known (~ 87.74 years), and the total power output of each RTG was measured before launch (Table 2.4).

The amount of power removed from each RTG in the form of electrical energy is telemetered to the ground. (Specifically, the RTG output voltage and current for each individual RTG is telemetered.) The remainder of the RTG power is radiated in the form of waste heat.

For each RTG, two temperature measurements are also available. One sensor, internal to the RTG, measures the temperature at the hot end of the bimetallic thermocouples. The other sensor measures the temperature near the root of one of the RTG radiating fins.

Table 2.4: RTG total power measurements prior to launch [354]. The reported accuracy of these measurements is 0.1 W, but values are rounded to the nearest W. RTG numbering corresponds to the actual number of units built.

RTG#	Spacecraft	Location	Test date	Thermal power (W)
44	Pioneer 10	Outboard	Oct 1971	649
45	Pioneer 10	Inboard	Nov 1971	646
46	Pioneer 10	Outboard	Nov 1971	647
48	Pioneer 10	Inboard	Dec 1971	649
49	Pioneer 11	Outboard	Sep 1972	649
51	Pioneer 11	Inboard	Oct 1972	650
52	Pioneer 11	Outboard	Oct 1972	649
53	Pioneer 11	Inboard	Oct 1972	649

2.4.2 Electrical heat

Next to the RTGs, the second most significant source of thermal radiation on board is the set of electrical equipment operating on the spacecraft. (Figure 2.4 shows the internal arrangement of components.) From a thermal perspective, nearly all electrical systems on board perform only one function: they convert electrical energy into waste heat. The one exception is the spacecraft’s radio transmitter, converting some electrical energy into a directed beam of radio frequency energy.

Early in the missions, the RTGs produced more electrical power than what was needed on board. The main bus voltage on board was maintained at a constant value by a power supply circuit, while excess electrical power was converted into heat. The shunt regulator controlled a variable current, which flowed through the regulator itself and an external radiator plate. The external radiator plate acted as an ohmic resistor, and the power radiated by it can be easily computed from the shunt current telemetry (Figure 2.7). The shunt radiator is mounted such that its thermal radiation is primarily in a direction that is perpendicular to the spacecraft spin axis.

Some electrical heat is generated outside the spacecraft body: notable items include electrical heaters for the fuel lines that deliver fuel to the thruster cluster assemblies along the antenna rim, an electrical heater for the spacecraft battery, and some scientific instruments.

Most of the electrical power not radiated away by the spacecraft antenna or the shunt radiator is converted into heat inside the spacecraft body. As the spacecraft is very close to a thermal steady state, all the electrical heat produced internally must be radiated into space. This thermal radiation is likely to cause a measurable sunward acceleration, for several reasons. First, the spacecraft body is heavily insulated by multilayer thermal insulation; however, at the bottom of the spacecraft body is the thermal louver system designed to vent excess heat. Even in its closed state, the effective emissivity of this louver system is much higher than that of the multilayer insulation, so this is the preferred direction in which heat escapes the spacecraft. Second, the spacecraft body is situated behind the high-gain antenna; even if the thermal radiation pattern of the spacecraft body were isotropic, the back of the HGA would preferentially reflect a significant portion of this heat in the aft direction.

Figure 2.7 also indicates how the power consumption by various pieces of equipment on board can be computed from telemetry.

The thermal state of the interior of the spacecraft is characterized in a redundant manner. In addition to the thermal power of various components that can be computed from telemetry, there exist numerous temperature sensors on board, most notably among them six platform temperature sensors, which are the most likely to measure ambient temperatures (as opposed to sensors that, say, are designed to measure the temperature of a specific electrical component, such as a transistor

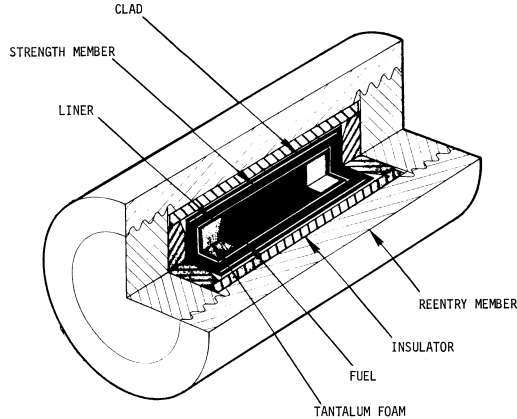


Figure 2.18: 1 W radioisotope heater unit (RHU). From [292].

amplifier.)

Much less is known about heat escaping the interior of the spacecraft through other routes. The spacecraft's science instruments utilize various holes and openings in the spacecraft body in order to collect information from the environment. Design documentation prescribes that no instrument can lose more heat through the opening than its own power consumption plus 0.5 W; however, the actually heat loss per instrument is not known.

2.4.3 Radioisotope heater units

A further source of continuous heat on board is the set of radioisotope heater units (RHUs) placed at strategic locations to maintain operating temperatures. These RHUs are capsules containing a small amount of ^{238}Pu fuel, generating ~ 1 W of heat (Figure 2.18).

Each thruster cluster assembly housed three RHUs that prevented the freezing of thruster valves. One RHU was located at the sun sensor, while an additional RHU was placed at the magnetometer. (Some reports suggest that a 12th RHU may also have been on board one or both spacecraft.)

The thruster cluster assemblies were designed to radiate heat in a direction perpendicular to the spin axis⁶. There are no known asymmetries of any thermal radiation from the magnetometer assembly at the end of the magnetometer boom. Therefore, it is unlikely that thermal radiation from the RHUs in general contributed much thermal recoil force in the fore-aft direction.

2.4.4 Waste heat from the propulsion system

The spacecraft's propulsion system, when operating, produced significant amounts of heat; as the hydrazine monopropellant underwent a chemical reaction in the presence of a catalyst in the spacecraft's thrusters, the thrusters and thruster cluster assemblies warmed up to several hundred degrees Centigrade. This heat was radiated into space as the assemblies cooled down to their pre-maneuver temperatures after a thruster firing event over the course of several hours.

However, the uncertainty in the magnitude of velocity change caused by the thruster event itself dwarfs any acceleration produced by the radiation of this residual heat. For this reason, heat from the propulsion system does not need to be considered when accounting for thermal recoil forces.

⁶Private communication in 2008 with Jim Moses, a TRW retiree.

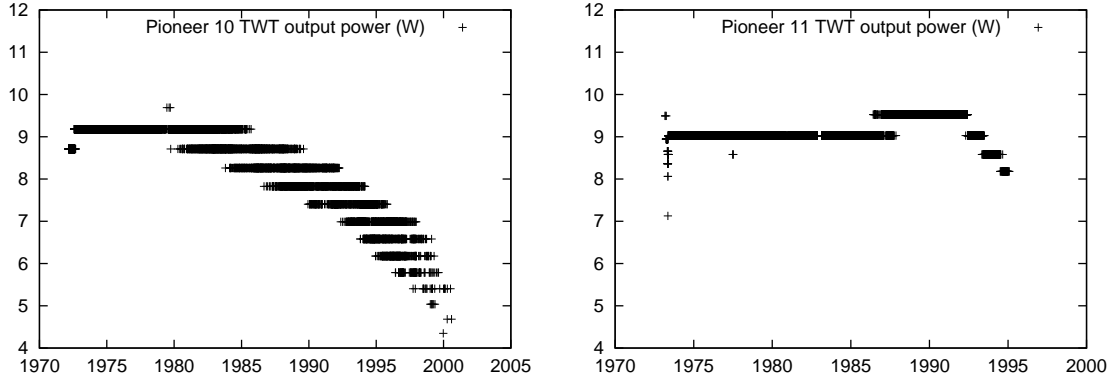


Figure 2.19: The emitted power (measured in dBm, converted to W) of the traveling wave tube transmitter throughout the mission, as measured by on-board telemetry. *Left:* Pioneer 10, which used TWT A (telemetry word C₂₃₁). *Right:* Pioneer 11, initially using TWT A but switching to TWT B (telemetry word C₂₁₄) early in its mission.

2.4.5 The energy radiated in the radio beam

To complete our discussion of thermal radiation emitted by the spacecraft, we must also consider the spacecraft's radio beam, for two reasons. First, any energy radiated by the radio beam is energy that is not converted into heat inside the spacecraft body. Second, the radio beam itself produces a recoil force that is similar in nature to the thermal recoil force.

The nominal power of the radio transmitter is 8 W, and the radio beam is highly collimated by the high gain antenna. Nevertheless, some loss occurs around the antenna fringes, and the beam itself also has a spread. Assuming that $\sim 10\%$ of the radio beam emitted by the feedhorn misses the antenna dish, at an approximate angle of 45° , we can calculate an efficiency of ~ 0.83 at which the antenna converts the emitted radio energy into momentum [331].

The actual power of the radio beam may not have been exactly 8 W. The output of the traveling wave tube oscillator that generated this microwave energy was measured on board and telemetered to the ground (Figure 2.19). Especially in the case of Pioneer 10, we note the variability of the TWT power near the end of mission. This corresponds to the drop in main bus voltage when the power available on board was no longer sufficient to maintain nominal voltages. It is unclear, therefore, if the measured drop in output power is an actual drop or a sensor artifact.

2.4.6 Thermal measurements in the telemetry

The thermal history of Pioneer 10 and 11 can be characterized accurately, and in detail, with the help of the recently recovered telemetry files and project documentation.

The telemetry data offer a redundant picture of the spacecrafts' thermal state. On the one hand, the amount of power available on board can be computed from electrical readings. On the other hand, a number of temperature sensors on board offer a coarse temperature map of the spacecraft.

The electrical state of Pioneer 10, when the spacecraft was at 25 AU from the Sun, is shown in Figure 2.7. While this figure represents a snapshot of the spacecraft's state at a particular moment in time, this information is available for the entire duration of both Pioneer missions.

The thermal state of the spacecraft body can be verified using the readings of six temperature sensors that were located at various points on the electronics platform: four in the main compartment, two in the adjacent compartment that housed science instruments (see locations 1–6

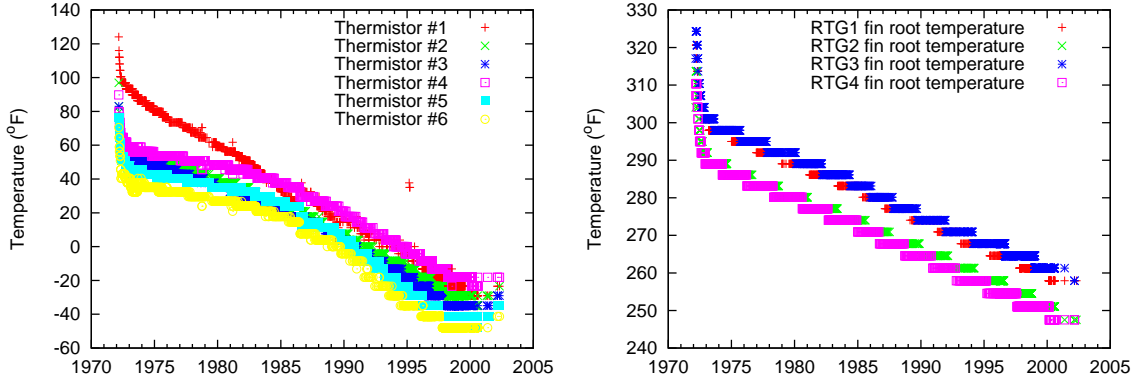


Figure 2.20: Platform temperatures (left) and RTG fin root temperatures (right) on board Pioneer 10. Temperatures in $^{\circ}\text{F}$ ($[^{\circ}\text{C}] = ([^{\circ}\text{F}] - 32) \times 5/9$).

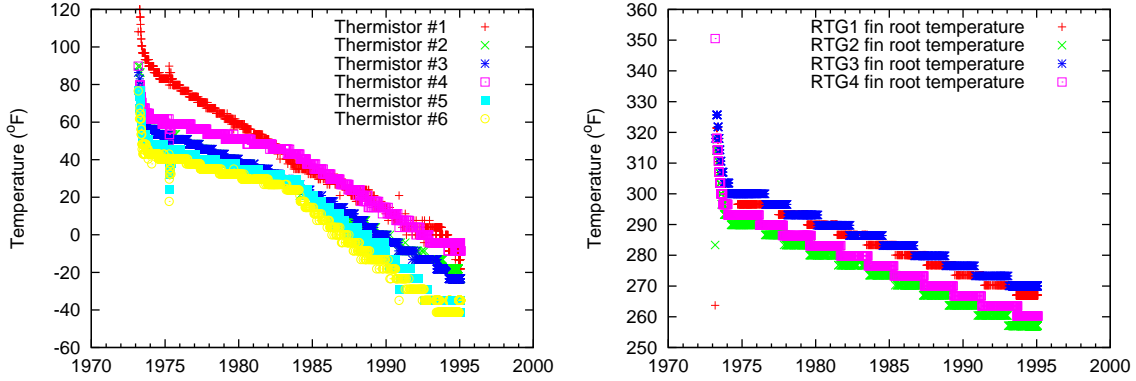


Figure 2.21: Platform temperatures (left) and RTG fin root temperatures (right) on board Pioneer 11. Temperatures in $^{\circ}\text{F}$ ($[^{\circ}\text{C}] = ([^{\circ}\text{F}] - 32) \times 5/9$).

in Figure 2.9). The temporal evolution of these temperature readings agrees with expectations: outlying sensors show consistently lower temperatures, and all temperatures are dropping steadily, as the distance between the spacecraft and the Sun increases while the amount of power available on board decreases (Figures 2.20 and 2.21).

There was a large number of additional temperature sensors on board (see Appendix D). However, these temperature sensors measured the internal temperatures of on-board equipment and science instruments. One example is the hot junction temperature sensor inside the RTGs, measuring the thermocouple temperature at its hot end. These readings may be of limited use when assessing the overall thermal state of the spacecraft. Nevertheless, they are also available in the telemetry.

The thermal behavior of the spacecraft was an important concern when Pioneer 10 and 11 were designed. Going beyond a general description [292], much of the work that was done to ensure proper thermal behavior is documented in a review document of the Pioneer 10 and 11 thermal control subsystem [279]. Specifically, this document provides detailed information about the thermal properties of components internal to the spacecraft, and about the anticipated maximum heat losses through various spacecraft structural and other components.

Detailed information about the SNAP-19 RTGs used on board Pioneer 10 and 11 is also available [354].

2.4.7 Surface radiometric properties and thermal behavior

It has been suggested (see, e.g., [331]) that the material properties of these surfaces may have changed over time, introducing a time-dependent anisotropy in the spacecraft’s thermal properties. For instance, solar bleaching may affect spacecraft surfaces facing the Sun [53], while surfaces facing the direction of motion may be affected by the impact of interplanetary dust particles.

Note that through most of their operating lives, the high-gain antennas of the Pioneer 10 and 11 spacecraft were always pointing in the approximate direction of the Sun. Therefore, the same side of the spacecraft: notably, the interior surfaces of their HGAs and one side of each RTG, were exposed to the effects of solar light, including ultraviolet radiation, and charged particles. It is not unreasonable to assume that this continuous exposure may have altered the visible light and infrared optical properties of these surfaces, introducing in particular, a fore-aft asymmetry in the thermal radiation pattern of the RTGs. On the other hand, any such effects would be mitigated by the fact that the spacecraft were receding from the Sun very rapidly, and spent most of their operating lives at several AUs or more from the Sun, receiving only a fraction of the solar radiation that is received, for instance, by Earth-orbiting satellites of comparable age.

Another possible effect may have altered the infrared radiometric properties of spacecraft surfaces facing in the direction of motion (which, most of the time, would be surfaces facing away from the Sun.) As the spacecraft travels through the interplanetary medium at speeds in excess of 12 km/s, impact by charged particles and dust may have corroded these surfaces. Once again, this may have introduced a fore-aft anisotropy in the infrared radiometric properties of the spacecraft, most notably their RTGs.

NASA conducted several experiments to investigate the effect of space exposure on the thermal and optical properties of various materials. One investigation, called the Thermal Control Surfaces (TCS) experiment [412], examined the long-term effects of exposure of different materials placed on an external palette on the International Space Station. Although results of this test are quite important, the near-Earth environment is quite different from that of deep space. Concerning solar bleaching, although the spacecraft spent decades in space, most of the time was spent far away from the Sun, resulting in a low number of “equivalent Sun hours” (ESH). The cumulative exposure to solar radiation of the Sun-facing surfaces of Pioneer 10 and 11 is less than the amount of solar radiation test surfaces were exposed to during the TCS experiment, in which test surfaces were also exposed to the atomic oxygen of the upper atmosphere, which is not a consideration in the case of the Pioneer spacecraft.

The most pronounced effect on coatings in the deep space environment is due to exposure to solar ultraviolet radiation [53]. The ESH for the Pioneer 10 and 11 spacecraft is approximately 3000 hours, most of which ($> 95\%$) were accumulated when the spacecraft were relatively close (< 15 AU) to the Sun. The exterior surfaces of the RTGs were covered by a zirconium coating in a sodium silicate binder [354]. For similar inorganic coatings, the most pronounced effect of prolonged solar exposure is an increase ($\Delta\alpha \sim 0.05$) in solar absorptance. No data suggest a noticeable change in infrared emittance.

The effects of exposure to dust and micrometeoroid impacts in the interplanetary environment do not result in significant optical damage, defined in terms of changes in solar absorptance or infrared emittance [53]. This is confirmed by the Voyager 1 and 2 spacecraft that had unprotected camera lenses that were facing the direction of motion, yet suffered no observable optical degradation. This fact suggests that the optical effects of exposure to the interplanetary medium on the spacecraft are negligible (see discussion in [18, 394]).

3 Pioneer Data Acquisition and Preparation

Discussions of radio science experiments with spacecraft in the solar system require a general knowledge of the sophisticated experimental techniques used by NASA’s Deep Space Network⁷ (DSN). Specifically, for the purposes of the Pioneer Doppler data analysis one needs a general knowledge of the methods and techniques implemented in the radio science subsystem of the DSN. One also needs an understanding of how spacecraft telemetry is collected at the DSN, distributed and used to assess the state of the spacecraft systems at a particular epoch.

Since its beginnings in 1958, the DSN underwent a number of major upgrades and additions. This was necessitated by the needs of particular space missions⁸. The history of the Pioneer 10 and 11 projects is inextricably connected to that of DSN. Due to the continuing improvements of the entire network, Pioneer 10 was able to communicate with the project team for over 30 years – far beyond the originally planned operational life of 3 years or less.

In this section, we discuss the history of the DSN, its current status, and describe the DSN antennas and operations in support of deep space missions. We also review the methods and techniques implemented in the radio science subsystem of the DSN that is used to obtain the radio tracking data, from which, after analysis, results are generated.

3.1 The Deep Space Network

Conceived at the dawn of the space era in the late 1950s, the DSN is a collection of radio tracking stations positioned around the globe [117, 141, 379], along with ground data transfer and data processing systems, designed to maintain continuous two-way communication, including commands and telemetry, with a variety of deep space vehicles located throughout the solar system.

The first DSN complex was constructed near the Jet Propulsion Laboratory (JPL), in Goldstone, California. It was here that the first large (26 m) DSN antenna, DSS-11 “Pioneer” (named after, unsurprisingly, the early Pioneer program) was constructed.

The first overseas DSN location was in Woomera, Australia, about 350 km north of Adelaide. DSS-41, another 26 m antenna, was constructed there in 1960. The second overseas DSN complex was built near Johannesburg, South Africa. The 26 m antenna of DSS-26 was constructed there in 1961. Together, Goldstone, Woomera and Johannesburg made it possible to initiate and maintain continuous communication with distant spacecraft at any time of the day⁹, marking the beginning of the DSN.

Today, three locations – Goldstone, California; Madrid, Spain; and Canberra, Australia – form the backbone of the DSN. Presently, each of the three DSN complexes hosts several tracking stations with different capabilities and antennas of different sizes [141, 232].

3.1.1 DSN tracking stations

The primary purpose of the DSN is to maintain two-way communication with distant spacecraft. The DSN can send, or uplink, command instructions and data, and it can receive, or downlink,

⁷A technical description, with a history and photographs, of NASA’s Deep Space Network can be found at <http://deepspace.jpl.nasa.gov/dsn/>. The document describing the radio science system can be found at <http://deepspace.jpl.nasa.gov/dsndocs/810-5/810-5.html>.

⁸The last such upgrade was conducted for the Cassini mission when the DSN capabilities were extended to cover the Ka radio frequency bandwidth. For more information on DSN methods, techniques, and present capabilities, see [30, 379].

⁹The station location in Johannesburg was a compromise; Spain would have been preferred for technical reasons. As a result of historical changes in South Africa and Spain, construction of a new DSN complex near Madrid began, and eventually, the Johannesburg facility was closed. In the meantime, there was a strong rationale to construct additional antennas in Australia at a more accessible location. The Woomera complex remained operational until Pioneer 10 was well on its way towards Jupiter, but eventually, it was superseded by a new DSN complex on Australian soil, in Tidbinbilla near Canberra.

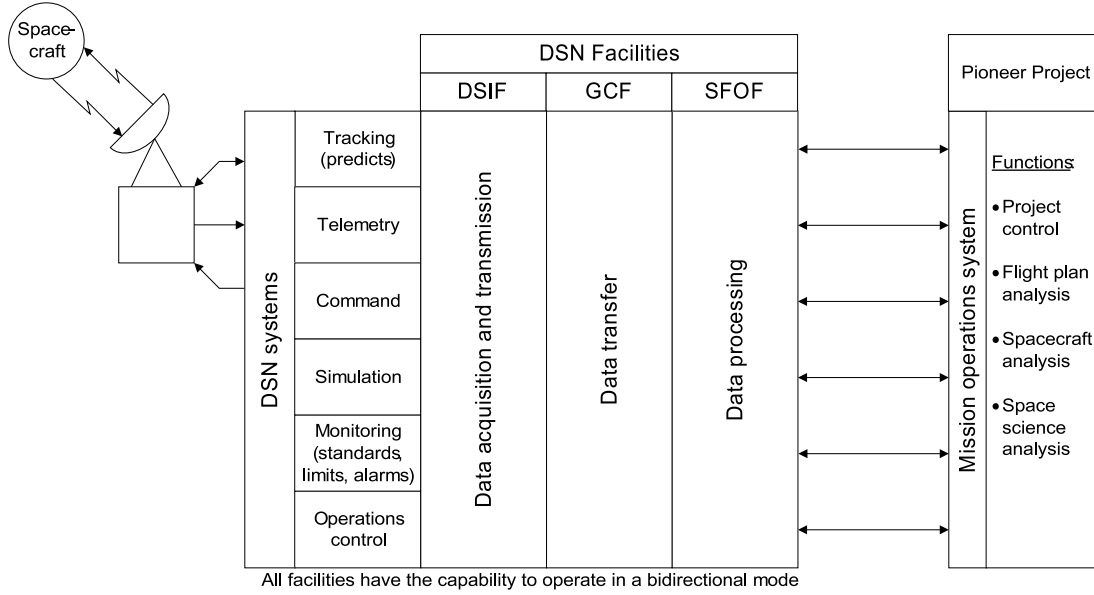


Figure 3.1: DSN facilities planned to be used by the Pioneer project in 1972 [338]. DSIF stands for Deep Space Instrumentation Facility, GCF is the abbreviation for Ground Communications Facility, while SFOF stands for the Space Flight Operations Facility.

engineering telemetry and scientific observations from instruments on board these spacecraft.

The DSN can also be used for precision radio science measurements, including measurements of a signal's frequency and timing observations. These capabilities allow the DSN to perform, for instance, Doppler measurements of line-of-sight velocity, ranging measurements to suitably equipped spacecraft, occultation experiments when a spacecraft flies behind a planetary body, and planetary radar observations [30].

The antennas of the DSN are capable of bidirectional communication using a variety of frequencies in the L-band (1–2 GHz), S-band (2–4 GHz), X-band (8–12 GHz) and, more recently, K-band (12–40 GHz). Early spacecraft used the L-band for communication [232] but within a few years, S-band replaced L-band as the preferred frequency band. The Pioneer 10 and 11 spacecraft used S-band transmitters and receivers. X-band and, more recently, K-band is used on more modern spacecraft.

In addition to the permanent DSN complexes that presently exist at Goldstone, California, Madrid, Spain, and Canberra, Australia, and the now defunct complexes in Woomera, Australia and Johannesburg, South Africa, occasionally, non-DSN facilities (e.g., the Parkes radio observatory in Australia) were also utilized for communication and navigation. During the long lifetime of the Pioneer project, nearly all the large antennas of DSN tracking stations and also some non-DSN facilities participated in the tracking of the Pioneer 10 and 11 spacecraft at one time or another.

The capabilities of the DSN evolved over the years. By the time of the launch of Pioneer 10, the DSN was a mature network comprising a number of 26 m tracking stations at four locations around the globe, a new 64 m tracking station in operation at Goldstone, California, and two more 64 m tracking stations under construction in Australia and Spain. The Goldstone facility was connected to the then new Space Flight Operations Facility (SFOF) built at the JPL via a pair of 16.2 kbps communication links (Figure 3.1), allowing for the real-time monitoring of spacecraft

Table 3.1: Pre-launch planned use of Deep Space Instrumentation Facilities in support of the Pioneer 10 and 11 projects (from [338]). Some stations only became operational in 1973. Several stations were decommissioned during the lifetime of the Pioneer project (DSS-11 and DSS-62 in 1981, DSS-12 in 1996, and DSS-42 and DSS-61 in 1999).

Station	Location	Size	Pioneer support function
DSS-11 “Pioneer”	Goldstone	26 m	Cruise
DSS-12 “Echo”	Goldstone	26 m	Cruise
DSS-14 “Mars”	Goldstone	64 m	Mission enhancement and Jupiter encounter
DSS-41	Woomera	26 m	Cruise
DSS-42	“Weemala”	26 m	Cruise
DSS-43*	“Ballima”	64 m	Mission enhancement and Jupiter encounter
DSS-51	Johannesburg	26 m	Launch and cruise
DSS-61	Robledo	26 m	Cruise
DSS-62	Cebreros	26 m	Cruise
DSS-63*	Robledo	64 m	Mission enhancement and Jupiter encounter

*After July 1973.

telemetry [232].

The most important characteristics of a DSN tracking station can be described using parameters such as antenna size, antenna (mechanical) stability, receiver sensitivity, and oscillator stability. These characteristics determine the accuracy with which the DSN can perform radio science investigations and, in particular with respect to the Pioneer 10 and 11 Doppler frequency measurements.

3.1.2 Antennas of the DSN

Large, precision-steerable parabolic dish antennas are the most recognizable feature of a DSN tracking station. In 1972, several 26 m antennas were in existence at the Goldstone, Madrid, Johannesburg and Woomera facilities. Additionally, the 64 m antenna at Goldstone was already operational, while two 64 m antennas at Madrid and Woomera were under construction (Figure 3.1).

To appreciate the impressive performance of the DSN in support of the Pioneer 10 and 11 missions in deep space, one needs to be able to evaluate the factors that contribute to the sensitivity of an antenna. The maximum strength of a signal received by a tracking station or spacecraft is a function of antenna area and distance between the transmitting and receiving stations. The gain G of a parabolic antenna of diameter d at wavelength λ is calculated as

$$G = \pi^2 \frac{d^2}{\lambda^2} = 4\pi \frac{A}{\lambda^2}, \quad (3.1)$$

where $A = \pi d^2/4$ is the antenna area. Space loss due to the distance R between a transmitting and a receiving antenna is calculated, in turn, as

$$L_{\text{spc}} = \frac{\lambda^2}{(4\pi R)^2}. \quad (3.2)$$

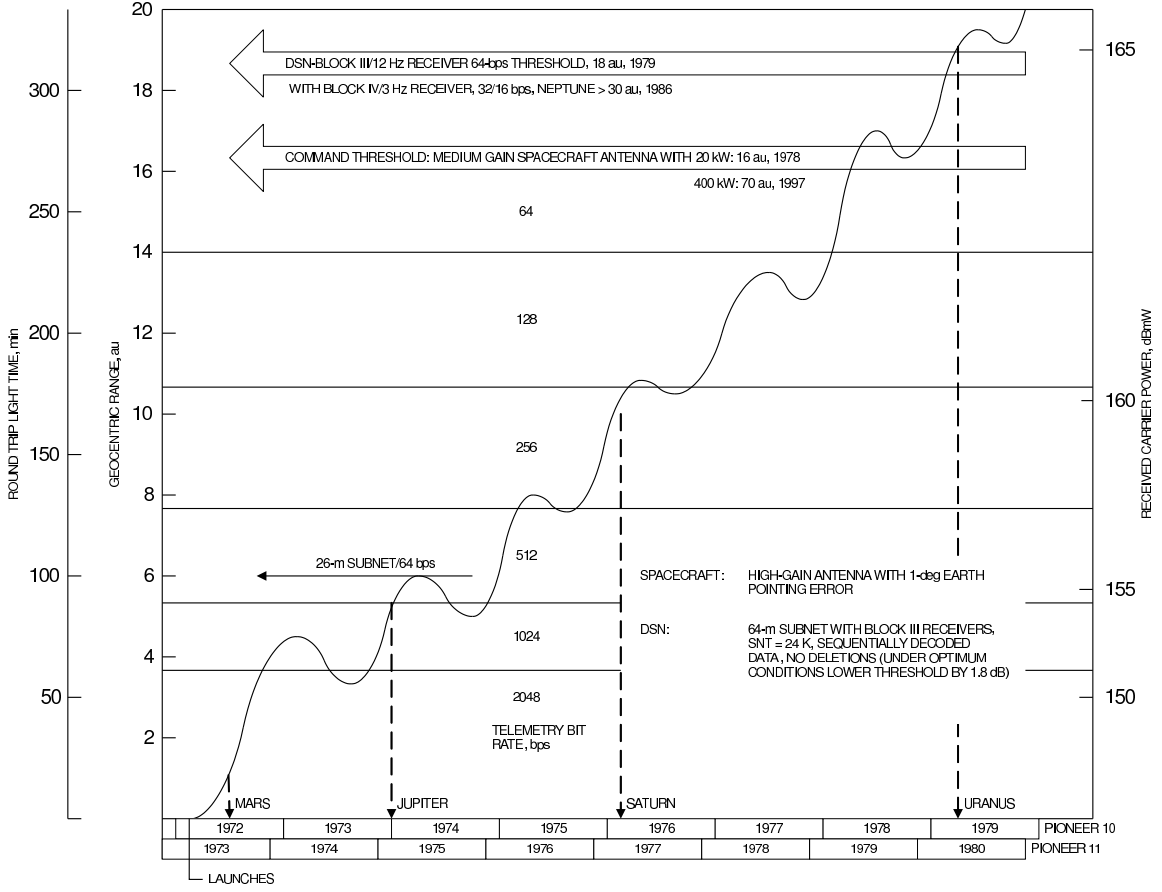


Figure 3.2: DSN performance estimate throughout the primary missions of Pioneer 10 and 11. Adapted from [343].

The thermal noise power N (also known as the Johnson–Nyquist noise) of a receiver is calculated from the receiver’s system noise temperature T_s using

$$N = kBT_s, \quad (3.3)$$

where B is the bandwidth (Hz) and $k = 1.381 \times 10^{-23} \text{ JK}^{-1}$ is Boltzmann’s constant. The S-band system noise temperature of a 64 m antenna (DSS-14) was 28 K in 1971 [339]. Later, with the installation of new receivers, for an antenna at 60° elevation, the system noise was reduced to 12.9 K [309]. The receiver bandwidth in 1971 was 12 Hz, reduced to 3 Hz for the Block IV receivers and then eventually to as low as 0.1 Hz for the Block V receivers (details are in Section 3.1.3).

Antenna sensitivity is measured by its signal-to-noise ratio, relating the power S of the received signal to the noise power N of the receiver. The strength of the received signal can be calculated as [141]:

$$\frac{S}{N} = G_T G_R L_{\text{spc}} \frac{P_T}{N} = \frac{P_T A_T A_R}{\lambda^2 R^2 N}, \quad (3.4)$$

where P_T is the transmitter power, A_T is the effective area of the transmitting antenna, and A_R is the effective area of the receiving antenna.

To calculate the actual signal-to-noise ratio, one must also take into account additional losses. The effective area of an antenna may be less than the area of the dish proper, for instance due

to obstructions in front of the antenna surface (e.g., struts, assemblies, other structural elements). For a 64 m DSN antenna, these losses amount to 2.7 dB [339], whereas for the 2.74 m parabolic dish antenna of Pioneer 10 and 11, these losses are about 3.7 dB.

Further (circuit, modulation, pointing) losses must also be considered. For the downlink from Pioneer 10 and 11 to the ground, the sum total of these losses is about 10.4 dB.

The signal-to-noise ratio also determines the bit error rate at various bit rates through the equation

$$\frac{S}{N} = \frac{E_b}{N_0} \frac{f_b}{B}, \quad (3.5)$$

where E_b is energy per bit, N_0 is the noise energy per Hz, and f_b is the bit rate. From this and Equation (3.3), the bit error rate p_e can be computed as [379]:

$$p_e = 0.5 \operatorname{erfc} \left(\sqrt{\frac{E_b}{N_0}} \right) = 0.5 \operatorname{erfc} \left(\sqrt{\frac{S}{k f_b T_s}} \right). \quad (3.6)$$

The discussion above allows one to present a typical downlink communications power budget for Pioneer 10, which is given in Table 3.2 (adapted from [340]).

Table 3.2: Pioneer 10 Jupiter downlink carrier power budget for tracking system [340].

Link	Carrier		Subcarrier	
Transmitter	38.9	dBm	38.9	dBm
Modulation loss	-7.3	dB	-27.8	dB
Circuit loss	-2.0	dB	-2.0	dB
2.75 m antenna gain	+32.7	dB	+32.7	dB
Space loss	-278.5	dB	-278.5	dB
Pointing loss	-1.0	dB	-1.0	dB
64 m antenna gain	+61.0	dB	+61.0	dB
Received signal level	-156.2	dBm	-176.7	dBm
Less: S/N Ratio	-17.1	dB	-6.9	dB
Detection efficiency	N/A		-0.5	dB
Noise level at receiver	-173.3	dBm	-184.1	dBm
Bit rate	N/A		512	bits
Error rate	N/A		10^{-3}	

Using the facilities in existence in 1973, the DSN would have been able to track Pioneer 10 and 11 up to a geocentric distance of ~ 22 AU, but not beyond. However, due to numerous improvements of the DSN it was in fact possible to track Pioneer 10 all the way to over ~ 83 AU from the Earth. Not the least of these improvements was an increase in antenna size, when the DSN's 64 m antennas were enlarged to 70 m, and many of the 26 m antennas (notably, DSS-12, DSS-42, and DSS-61 from Table 3.1) were enlarged to 34 m.

In addition to the stations used initially (see Table 3.1) for communication with Pioneer 10 and 11, over the years many other stations were utilized, which are listed in Table 3.3.

In order to perform precision tracking, the location of these radio stations must be known to high accuracy in the same coordinate frame (e.g., a solar system barycentric frame) in which spacecraft orbits are calculated.

This task is accomplished in two stages. First, station locations are given relative to a geocentric coordinate system, such as the International Terrestrial Reference Frame (ITRF). Second,

Table 3.3: Additional DSN stations in operation during the Pioneer mission lifetime that may have been used for tracking Pioneer 10 and 11.

Station	Location	Size
DSS-13 “Venus”	Goldstone	26/34 m
DSS-15 “Uranus”	Goldstone	34 m
DSS-16 “Apollo”	Goldstone	26 m
DSS-17	Goldstone	9 m
DSS-23	Goldstone	34 m
DSS-24	Goldstone	34 m
DSS-25	Goldstone	34 m
DSS-26	Goldstone	34 m
DSS-27	Goldstone	34 m
DSS-28	Goldstone	34 m
DSS-33	Tidbinbilla	11 m
DSS-34	Tidbinbilla	34 m
DSS-44	Honeysuckle Creek	26 m
DSS-45	Tidbinbilla	34 m
DSS-46	Tidbinbilla	26 m
DSS-49	Parkes	64 m
DSS-53	Madrid	11 m
DSS-54	Madrid	26 m
DSS-55	Madrid	34 m
DSS-65	Madrid	34 m
DSS-66	Madrid	26 m

a conversion from the geocentric coordinate system to the appropriate solar system barycentric reference frame is performed.

For operating DSN stations, station location information is readily available, e.g., from NASA’s Navigation and Ancillary Information Facility (NAIF¹⁰). Such information usually consists of station coordinates at a given epoch, and station drift (e.g., as a result of continental drift.) Higher precision station data (e.g., taking into account the effects of tide) is also available, but such precision is not required for the tracking of Pioneer 10 and 11.

Station data is harder to come by for stations that have been decommissioned or moved. Some decommissioned stations are listed in Table 3.4¹¹.

3.1.3 DSN receivers

Antenna size may have been the visually most apparent change at a DSN complex, but it was upgrades of DSN receiver hardware that resulted in a really significant improvement in a tracking station’s capabilities.

Receivers of the DSN have been improved on a continuous basis during the lifetime of Pioneer 10 and 11. These improvements were a result of other mission requirements, but the Pioneer project benefited: far beyond the predicted range of 22 AU, it was possible to maintain communication with Pioneer 10 when it was at an incredible 83 AU from the Sun. (The same DSN complex is

¹⁰See http://naif.jpl.nasa.gov/naif/data_generic.html.

¹¹Information on the location of DSN stations that are no longer in service was provided by W.M. Folkner of JPL via private communication. Relocation date for DSS-12 is from [232].

Table 3.4: Station location information for a set of decommissioned DSN stations. ITRF93 Cartesian coordinates (in km) and velocities (north, east, vertical, in cm/year) are shown. For DSS-12 and DSS-61, station information is for dates prior to July 1, 1978 and August 9, 1979, respectively.

ID	X	Y	Z	v_N	v_E	v_{vert}
DSS-11	-2351.429165	-4645.078818	3673.764161	-0.45	-1.90	-0.03
DSS-12	-2350.442882	-4651.978543	3665.629171	-0.45	-1.90	-0.03
DSS-41	-3978.720526	3724.850894	-3302.171112	4.74	2.08	-0.12
DSS-44	-4451.074302	2676.823855	-3691.346779	4.74	2.08	-0.12
DSS-51	5085.442790	2668.263555	-2768.696907	2.02	1.74	0.04
DSS-61	4849.242766	-360.277773	4114.882600	1.95	2.34	0.12
DSS-62	4846.700295	-370.1962103	4116.905713	1.95	2.34	0.12

now used to communicate with Voyager I spacecraft from heliocentric distances of over 110 AU.)

The receiver can contribute to a tracking station’s sensitivity in three different ways. First, the bandwidth of the receiver (loop bandwidth) can be reduced, increasing the signal-to-noise ratio. Two additional improvements, lowering the system noise temperature and eliminating other sources of signal attenuation, not only increase the signal-to-noise ratio but also decrease the bit error rate.

The “Block III” DSN receivers in use at the time of the launch of Pioneer 10 and 11 had an S-band system noise temperature of 28 K, and a receiver loop bandwidth of 12 Hz. These receivers were replaced in 1983–1985 by “Block IV” receivers in which the S-band system noise was reduced to 14.5 K in receive only mode, and the receiver loop bandwidth was reduced to 3 Hz. Further improvements came with the all-digital “Block V” receivers (also known as the Advanced Receivers [136]) installed in the early 1990s that had, under ideal circumstances, an S-band system noise of only 12.9 K, and a receiver loop bandwidth of 0.1 Hz.

Together with the enlarged 70 m antenna, these improved receivers made it possible to receive the signal of Pioneer 10 at 83 AU with a bit error rate of $\sim 1\%$. This error rate was reduced further by the convolutional code in use by Pioneer 10 and 11, which amounted to a 3.8 dB improvement in the signal-to-noise ratio, resulting in an error rate of about one in 10^4 bits.

During planetary encounters, the rapidly changing velocity of the spacecraft can result in a Doppler shift of its received frequency. During Pioneer 11’s close encounter with Jupiter, this rate could be as high as $df/dt = 0.52$ Hz/s [39]. Such a rapid change in received frequency can exceed the capabilities of the DSN closed loop receivers to remain “in lock”. To maintain continuous communication with such spacecraft, a “ramping” technique was implemented that allowed the tuned frequency of the DSN receiver to follow closely the predicted frequency of the spacecraft’s transmission [176]. This ramping technique was used successfully during the Pioneer 10 and 11 planetary encounters. Later it became routine operating procedure for the DSN. (As late as Pioneer 11’s 1979 encounter with Saturn, ramp frequencies at DSS-62 were tuned manually by relays of operators, as an automatic tuning capability was not yet available [232]).

3.1.4 DSN transmitters

To maintain continuous communication with distant spacecraft, the DSN must be able to transmit a signal to the spacecraft. The 70 m stations of the DSN are equipped with transmitters with a maximum transmitting power of 400 kW in the S-band¹². This is sufficient power to maintain

¹²The full 400-kW power of the DSN was used on March 3–5 2006, when the DSN attempted to contact Pioneer 10 for the last time. Unfortunately, the lack of sufficient power resources on-board the spacecraft prevented a successful two-way communication [383].

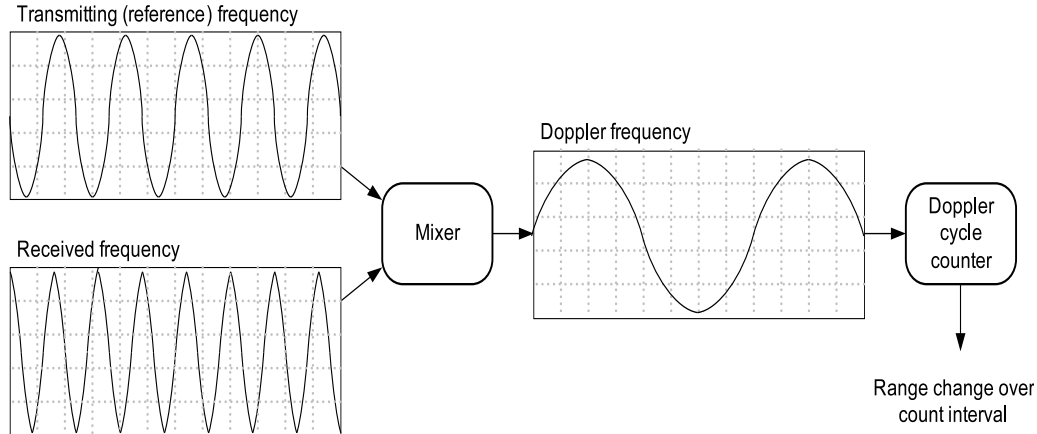


Figure 3.3: The Doppler extraction process. Adapted from [379].

continuous communication with distant spacecraft even when the spacecraft are not oriented favorably relative to the Earth, and must use a low-gain omnidirectional antenna to receive ground commands.

Just like its receivers, the DSN's transmitters are also capable of ramping. Ramped transmissions are necessary during planetary encounters in order to ensure that the spacecraft's closed loop receiver remains in lock even as its line-of-sight velocity relative to the Earth is changing rapidly¹³.

3.1.5 Data communication

Results of Pioneer radio observations were packaged in data files (see Figure 3.5). Initially, these data files were transcribed to magnetic tape and delivered physically to the project site where they were processed. The present-day DSN uses electronic ground communication networks for this purpose.

3.2 Acquisition of radiometric Doppler data

Radiometric observations are performed by the DSN stations located at several DSN sites around the world [226, 231]. Routine radiometric tracking and navigation of the Pioneer 10 and 11 spacecraft was performed using Doppler observations. The Doppler extraction process is schematically depicted in Figure 3.3. A reference signal of a known frequency (usually a frequency close to that of the original transmission) is mixed with the received signal. The resulting beat frequency is then measured by a frequency counter. The count over a given time interval is recorded as the Doppler observation.

Receiving stations of the DSN are equipped with ultra-stable oscillators, allowing very precise measurements of the frequency of a received signal. One way to accomplish this measurement is by comparing the frequency of the received signal against a reference signal of known frequency, and count the number of cycles of the resulting beat frequency for a set period of time. This Doppler count is then stored in a file for later analysis.

The operating principles of the DSN evolved over time, and modern receivers may not utilize a beat frequency. However, all Pioneer data was stored using a format that incorporates an actual

¹³Ramped transmissions were also used to compensate for a partial failure of the on-board receiver of Voyager 2.

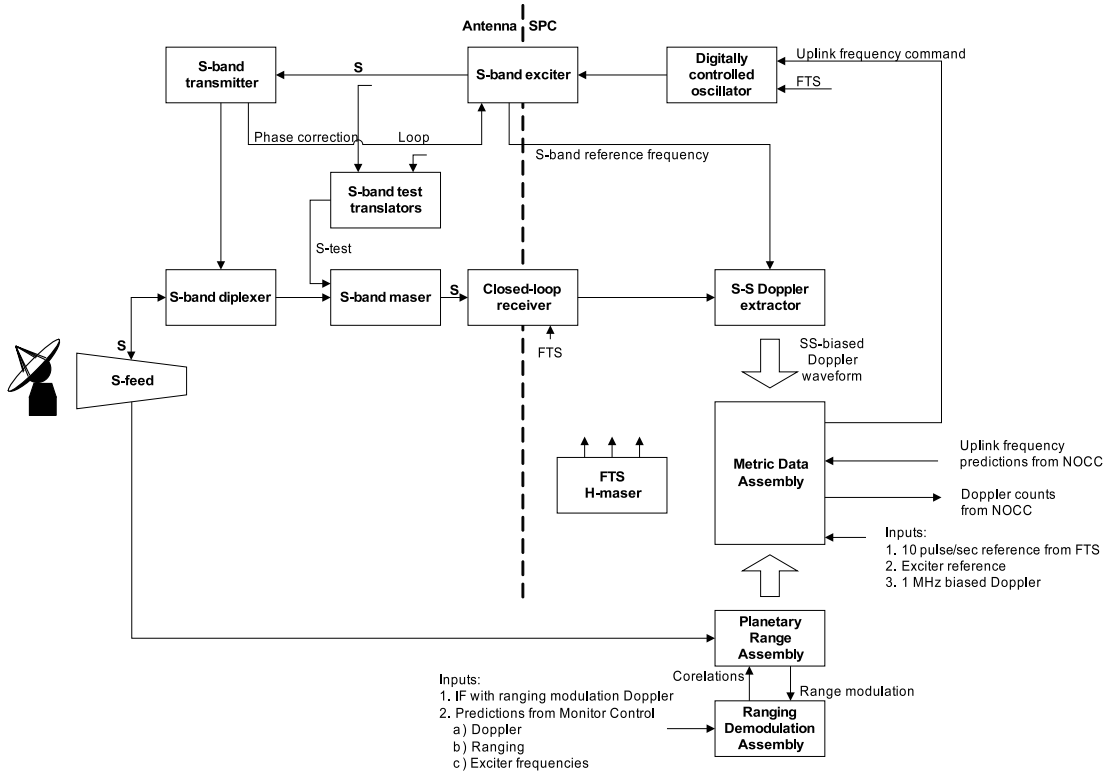


Figure 3.4: Block diagram of the DSN baseline configuration as used for radio Doppler tracking of the Pioneer 10 and 11 spacecraft. Adapted from [18, 277]. (IF stands for Intermediate Frequency.)

or simulated reference frequency.

Below we discuss the way Doppler observables are formed at the radio-science subsystem of the DSN. This description applies primarily to Block III and Block IV receivers, which were used for Pioneer radiometric observations throughout most of the Pioneer 10 and 11 missions.

3.2.1 DSN frequency and timing system¹⁴

Present day radiometric tracking of spacecraft requires highly accurate timing and frequency standards at tracking stations. For a two-way Doppler experiment, for instance, that involves transmitting a signal to a distant spacecraft and then receiving a response perhaps several hours later, long-term stability of tracking station oscillators is essential. Furthermore, if more than one tracking station is involved in an observation (e.g., “three-way” Doppler in which case one station is used to uplink a signal to the spacecraft, and another station receives the spacecraft’s response), frequency and clock synchronization between the participating tracking stations must be very precise [30].

Originally, the DSN used crystal oscillators. In the 1960s, these were replaced by rubidium or cesium oscillators that offered much improved frequency stability, and made precision radio-tracking of distant spacecraft possible. Rubidium and cesium oscillators offered a frequency stability of one

¹⁴We thank Craig G. Markwardt for helping us to improve this section significantly.

part in $\sim 10^{12}$ and one part in $\sim 10^{13}$, respectively [232], over typical Doppler counting intervals of $10^2 - 10^3$ seconds. (This is in agreement with the expected Allan deviation for the S-band signals.)

A further improvement occurred in the 1970s, when the rubidium and cesium oscillators were in turn replaced by hydrogen masers, which offered another order of magnitude improvement in frequency stability [232]. Today, the DSN's frequency and timing system (FTS) is the source for the high accuracy mentioned above (see Figure 3.4). At its center is a hydrogen maser that produces a precise and stable reference frequency. These devices have Allan deviations (see Section 5.3.6) of approximately 3×10^{-15} to 1×10^{-15} for integration times of 10^2 to 10^3 seconds, respectively [30, 379]. These masers are good enough that the quality of Doppler-measurement data is limited by thermal or plasma noise, and not by the inherent instability of the frequency references.

However, for two-way Doppler analysis, the relevant quantity is the stability of the station's frequency standard during the round-trip light travel time. During the 1980s, hydrogen maser frequency standards were required to have Allan deviations of less than 10^{-14} over time scales of 3–12 hours [72, 112]. This corresponds to a Doppler frequency noise of 2×10^{-5} Hz.

For three-way Doppler analysis, where the transmitting and receiving stations are different, the frequency offset between stations is the relevant quantity. During the 1980s, station frequencies were controlled to be the same, to a fractional error of 10^{-12} [312, 360]. This corresponds to a Doppler frequency bias of up to 2×10^{-3} Hz between station pairs. Station keepers did maintain frequency offset knowledge to a tighter level, but for the most part this knowledge is not available to analysts today.

Three-way Doppler analysis is weakly sensitive to clock offsets between stations. By 1968, the operational technique for time synchronization was the “Moon Bounce Time Synch” technique, in which a precision-timed X-band signal from DSS-13 (which served as master timekeeper) was transmitted to overseas stations by way of a lunar reflection, achieving a clock accuracy of $5 \mu\text{s}$ between stations [232]. Such timing offsets would produce Doppler errors of less than 10^{-6} Hz. Later, DSN stations were synchronized utilizing the Global Positioning Satellite (GPS) network, achieving a synchronization accuracy of $1 \mu\text{s}$ or better [379].

3.2.2 The digitally controlled oscillator and exciter

Using the highly stable output from the FTS, the digitally controlled oscillator (DCO), through digitally controlled frequency multipliers, generates the Track Synthesizer Frequency (TSF) of ~ 22 MHz. This is then sent to the Exciter Assembly. The Exciter Assembly multiplies the TSF by 96 to produce the S-band carrier signal at ~ 2.2 GHz. The signal power is amplified by Traveling Wave Tubes (TWT) for transmission. If ranging data are required, the Exciter Assembly adds the ranging modulation to the carrier. The DSN tracking system has undergone many upgrades during the 34 years of tracking Pioneer 10. During this period internal frequencies have changed (see Section 3.1.1).

This S-band frequency is sent to the antenna where it is amplified and transmitted to the spacecraft. The onboard receiver tracks the up-link carrier using a phase lock loop. To ensure that the reception signal does not interfere with the transmission, the spacecraft (e.g., Pioneer) has a turnaround transponder with a ratio of 240/221 in the S-band. The spacecraft transmitter's local oscillator is phase locked to the up-link carrier. It multiplies the received frequency by the above ratio and then re-transmits the signal to Earth.

3.2.3 Receiver and Doppler extractor

When the signal reaches the ground, the receiver locks on to the signal and tunes the Voltage Control Oscillator (VCO) to null out the phase error. The signal is sent to the Doppler Extractor. At the Doppler Extractor the current transmitter signal from the Exciter is multiplied by 240/221 (or 880/241 in the X-band) and a bias of 1 MHz for S-band or 5 MHz for X-band is added to

the Doppler. The Doppler data is no longer modulated at S-band but has been reduced as a consequence of the bias to an intermediate frequency of 1 or 5 MHz.

The transmitter frequency of the DSN is a function of time, due to ramping and other scheduled frequency changes. When a two-way or three-way (see Section 3.2.5) Doppler measurement is performed, it is necessary to know the precise frequency at which the uplink signal was transmitted. This, in turn, requires knowledge of the exact light travel time to and from the spacecraft, which is available only when the position of the spacecraft is determined with precision. For this reason, DSN transmitter frequencies are recorded separately so that they can be accounted for in the orbit determination programs that we discuss in Section 5.

3.2.4 Metric data assembly

The intermediate frequency (IF) of 1 or 5 MHz with a Doppler modulation is sent to the Metric Data Assembly (MDA). The MDA consists of computers and Doppler counters where continuous count Doppler data are generated. From the FTS a 10 pulse per second signal is also sent to the MDA for timing. At the MDA, the IF and the resulting Doppler pulses are counted at a rate of 10 pulses per second. At each tenth of a second, the number of Doppler pulses is recorded. A second counter begins at the instant the first counter stops. The result is continuously-counted Doppler data. (The Doppler data is a biased Doppler of 1 MHz, the bias later being removed by the analyst to obtain the true Doppler counts.) The range data (if present) together with the Doppler data are sent separately to the Ranging Demodulation Assembly. The accompanying Doppler data is used to “rate-aid” (i.e., to “freeze” the range signal) for demodulation and cross correlation.

3.2.5 Radiometric Doppler data

Doppler data is the measure of the cumulative number of cycles of a spacecraft’s carrier frequency received during a user-specified count interval. The exact precision to which these measurements can be carried out is a function of the received signal strength and station electronics, but it is a small fraction of a cycle. Raw Doppler data is generated at the tracking station and delivered via a DSN interface to customers.

When the measured signal originates on the spacecraft, the resulting Doppler data is called one-way or F1 data. In order for such data to be useful for precision navigation, the spacecraft must be equipped with a precision oscillator on board. The Pioneer 10 and 11 spacecraft had no such oscillator. Therefore, even though a notable amount of F1 Doppler data was collected from these spacecraft, these data are not usable for precision orbit determination.

An alternative to one-way Doppler involves a signal generated by a transmitter on the Earth, which is received and then returned by the spacecraft. The Pioneer 10 and 11 spacecraft were equipped with a radio communication subsystem that had the capability to operate in “coherent” mode, a mode of operation in which the return signal from the spacecraft is phase-locked to a signal received by the spacecraft from the Earth. In this mode of operation, the precision of the frequency measurement is not limited by the stability of equipment on board the spacecraft, only by the frequency stability of ground-based DSN stations.

When the signal is transmitted from, and received by, the same station, the measurement is referred to as a two-way or F2 Doppler measurement; if the transmitting and receiving stations differ, the measurement is a three-way (F3) Doppler measurement.

Knowing the frequency of a signal received at a precise time at a precisely known location is only half the story in the case of two-way or three-way Doppler data: information must also be known about the time and location of transmission and the frequency of the transmitted signal.

The frequency of the transmitter, or the frequency of the receiver’s reference oscillator may not be fixed. In order to achieve better quality communication with spacecraft the velocity of which varies with respect to ground stations, a technique called ramping has been implemented at the

DSN. When a frequency is ramped, it is varied linearly starting with a known initial frequency, at a known rate of frequency change over unit time.

Thus, a Doppler data point is completely characterized by the following:

- The location of the receiving station,
- The time of reception,
- The reference frequency of the receiver,
- Receiving station ramp information,
- The length of the Doppler count interval,
- The beat frequency (Doppler) count,
- Transmission frequency,

and, for two- and three-way signals only,

- The location of the transmitting station,
- Transmitting station amp information.

Below we discuss the radiometric Doppler data formats that were used to support navigation of the Pioneer 10 and 11 spacecraft.

3.2.6 Pioneer Doppler data formats

The Pioneer radiometric data was received by the DSN in “closed-loop” mode, i.e., it was tracked with phase lock loop hardware. (“Open loop” data is recorded to tape but not tracked by phase lock loop hardware.) There are basically two types of data: Doppler (frequency) and range (time of flight), recorded at the tracking sites of the DSN as a function of UT Ground Received Time [89]. During their missions, the raw radiometric tracking data from Pioneer 10 and 11 were received originally in the form of Intermediate Data Record (IDR) tapes, which were then processed into special binary files called Archival Tracking Data Files (ATDF, format TRK-2-25 [90]), containing Doppler data from the standard DSN tracking receivers (Figure 3.5)¹⁵. Note that the “closed-loop” data constitutes the ATDFs that were used in [18]. Figure 3.5 shows a typical tracking configuration for a Pioneer-class mission and corresponding data format flow.

ATDFs are files of radiometric data produced by the Network Operations Control Center (NOCC) Navigation Subsystem (NAV) (see Figure 3.4). They are derived from Intermediate Data Records by NAV and contain all radiometric measurements received from the DSN station including signal levels (AGC = automatic gain control in dB), antenna pointing angles, frequency (often referred to simply as “Doppler”), range, and residuals. Each ATDF consists of all tracking data types used to navigate a particular spacecraft (Pioneers had only Doppler data type) and typically include Doppler, range and angular types (in S-, X-, and L-frequency bands), differenced range versus integrated Doppler, programmed frequency data, pseudo-residuals, and validation data. (Unfortunately there was no range capability implemented on Pioneer 10 and 11 [15, 18]. Early in the mission, JPL successfully simulated range data using the “ramped-range” technique [176]. In this method, the transmitter frequency is ramped up and down with a known pattern. One round trip light time later, this same pattern appears at the DSN receiver, and can be used to solve for the round trip light travel time. Later in the mission, this technique became unusable because the carrier tracking loop bandwidth required to detect the carrier became too narrow to track the

¹⁵After the installation of Block V receivers, there is high time resolution Doppler data available, called “open loop” data. This data is stored in files called ODRs (Original Data Records), which became available only at the very end of the Pioneer missions and were not used as a standard format for navigating these missions in deep space [139].

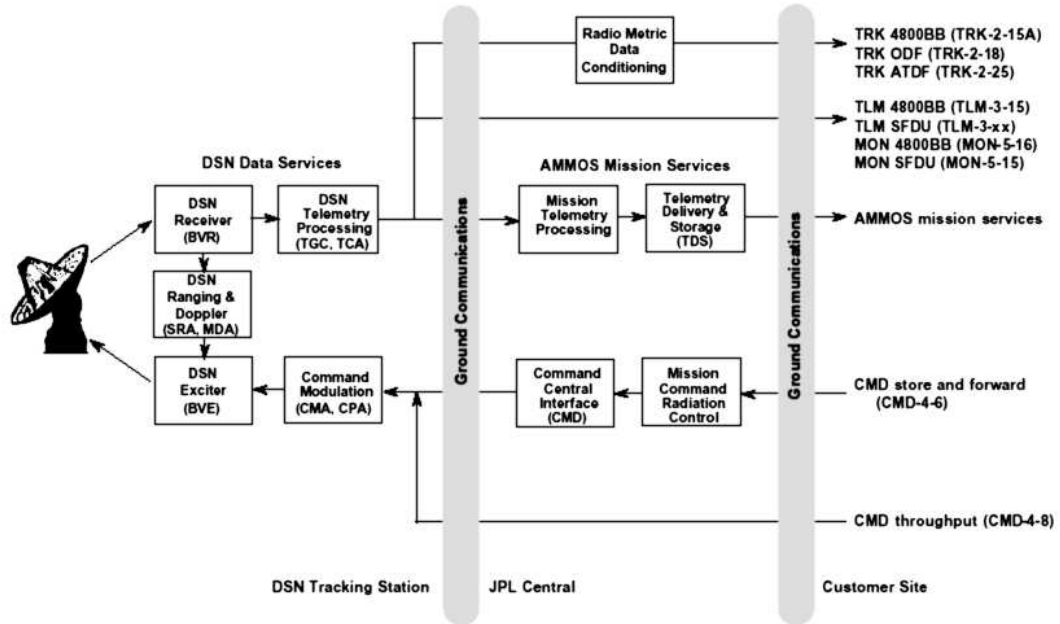


Figure 3.5: Typical tracking configuration for a Pioneer-class mission and corresponding data format flow [399].

ramped frequency changes.) Also, ATDFs contain data for a single spacecraft, for one or more ground receiving stations, and for one or more tracking passes or days.

After a standard processing at the Radio Metric Data Conditioning group (RMDC) of JPL's Navigation and Mission Design Section, ATDFs are transformed into Orbit Data Files (ODF, format TRK-2-18 [91]). A program called **STRIPPER** is used to produce the ODFs that are, at this point, the main product that is distributed to the end users for their orbit determination needs (see more discussion on the conversion process in [18]). At JPL, after yet additional processing, these ODFs are used to produce sequentially formatted input/output files in NAVIO format that is used by navigators while working with the JPL Orbit Determination Program. (Note that the NAVIO input/output file format is used only at JPL; other orbit determination programs convert ODFs to their particular formats.)

Each ODF physical record is 2016 32-bit words in length and consists of 224 9-word logical records per data block. The ODF records are arranged in a sequence that consists of one file label record, one file identifier logical record, orbit data logical records in time order, ramp data logical records in time order, clock offset data logical records in time order, data summary logical records in time order and software/hardware end-of-file markers. Bit lengths of data fields are variable and cross word boundaries. An ODF usually contains most types of records, but may not have them all. The first record in each of the 7 primary groups is a header record; depending on the group, there may be from zero to many data records following each header. For further details, see Appendix B.

3.3 Available Doppler data

The Pioneer 10 and 11 spacecraft were in space for more than three decades. The original 2002 study [18] of the Pioneer anomaly (see Section 5) used approximately 11.5 years of Pioneer 10 and 3.5 years of Pioneer 11 Doppler data. These data points were obtained from the late phases of the respective missions, when the spacecraft were far from the Earth and the Sun.

An effort was launched at JPL in June 2005 to recover more Pioneer Doppler data, preferably the entire Doppler mission records, if possible: almost 30 years of Pioneer 10 and 20 years of Pioneer 11 Doppler data, most of which was never used previously in the investigation of the anomalous acceleration. This task proved much harder than anticipated, due to antiquated file formats, missing data, and corrupted files (see discussion below and [399]).

Below we discuss these two sets of Pioneer 10 and 11 Doppler data.

3.3.1 Pioneer Doppler data available in 2002

The anomalous acceleration of the Pioneer spacecraft was first reported in 1998 [15]. This effort utilized Pioneer 10 data from 1987 to 1995, and a shorter span of Pioneer 11 data to obtain accelerations of $a_{P10} = (8.09 \pm 0.20) \times 10^{-10} \text{ m/s}^2$, and $a_{P11} = (8.56 \pm 0.11) \times 10^{-10} \text{ m/s}^2$, respectively, using JPL’s Orbit Determination Program (ODP). The Pioneer 10 result was also verified by the Aerospace Corporation’s Compact High Accuracy Satellite Motion Program (CHASMP), which yielded $a_{P10} = (8.65 \pm 0.03) \times 10^{-10} \text{ m/s}^2$. The errors quoted are the statistical formal errors produced by the fitting procedure.

In 2002, JPL published the results of a study that, to this date, remains the definitive result on the Pioneer anomaly [18] (see Section 5). In this study, a significantly expanded set of Doppler data was utilized. For Pioneer 10, the data set covered the period between January 3, 1987 and July 22, 1998. This corresponds to heliocentric distances between 40 and 70.5 AU. The data set contained 19,403 Doppler data points. For Pioneer 11, the data set was smaller: the trajectory of the spacecraft between January 5, 1987 and October 1, 1990 was covered, corresponding to heliocentric distances between 22.42 and 31.7 AU, with 10,252 Doppler data points.

The 2002 JPL study was also the first to combine Pioneer 10 and Pioneer 11 results. The study attempted to estimate realistic errors, e.g., errors due to physical or computational systematic effects. This approach resulted in the value of $a_P = (8.74 \pm 1.33) \times 10^{-10} \text{ m/s}^2$, which is now the widely quoted “canonical” value of the anomalous acceleration of Pioneer 10 and 11.

3.3.2 The extended Pioneer Doppler data set

The recovery of radiometric Doppler data for a mission with such a long duration was never attempted before. It presents unique challenges, as a result of changing data formats, changes in navigational software and supporting hardware, changes in the configuration of the DSN (new stations built, old ones demolished, relocated, or upgraded), and the loss of people [399]. Even physically locating the data proved to be a difficult task, as incomplete holdings were scattered among various archives. Nonetheless, as of November 2009, the transfer of the available Pioneer Doppler data to modern media formats has been completed.

Initially, the following sources for Doppler data were considered:

- Archived tracking files at JPL and the Deep Space Network;
- Files archived by JPL researchers at the NSSDC (i.e., National Space Science Data Center);
- Data segments available from individual researchers at JPL.

During these data collection efforts, multiple serious problems were encountered (see details in [399]), including

- The files were in several different formats, including old (e.g., “Type 66” [402]) formats that are no longer used, nor very well documented, and for which no data conversion tools exist;
- The files were often missing critical information; for instance, tracking data may have been recorded for the spacecraft, but critically important ramp (see Section 3.1.3 and also [176]) data for the corresponding transmitting stations may have been lost;
- The files were not processed with a consistent strategy; for instance, some files contained Doppler frequency data that was corrected for the spacecraft’s spin, whereas other files did not include such corrections;
- Some files were corrupted but recoverable; for instance, writing fixed size records using inappropriate software tools may have introduced spurious bytes into the data in a manner that can be corrected;
- Some files were corrupted in an unrecognizable manner and had to be discarded.

Despite the unanticipated complexities, as of late 2009 the transfer of the available Pioneer Doppler data to modern media formats has been completed. Initial analysis of these data is under way, and it appears that while Pioneer 10 data prior to February 1980 is not usable, coverage is nearly continuous from that data until the end of mission. Similarly, for Pioneer 11, good data is available from mid-1978 until the loss of coherent mode in late 1990. Further details will be reported as appropriate upon the conclusion of this initial data analysis.

To summarize, there exists more than 20 years of Pioneer 10 and more than 10 years of Pioneer 11 data, a significant fraction of which had never been well studied for the purposes of anomaly investigation. This new, expanded data set may make it possible to answer questions concerning the constancy and direction of the anomalous acceleration.

3.4 Doppler observables and data preparation

The Doppler observable can be predicted if the spacecraft’s orbit is known. Given known initial conditions and the ephemerides of gravitating sources, a dynamic model can be constructed that yields predictions of the spacecraft’s position as a function of time. An observational model can account for the propagation of the signal, allowing a computation of the received signal frequency at a ground station of known terrestrial location. The difference between the calculated and observed values of the received frequency is known as the Doppler residual. If this residual exceeds acceptable limits, the dynamic model or observational model must be adjusted to account for the discrepancy. Once the model is found to be sufficiently accurate, it can also be used to plan the spacecraft’s future trajectory (see Figure 4.1 and relevant discussion in Section 4).

Various radio tracking strategies are available for determining the trajectory parameters of interplanetary spacecraft. However, radio tracking Doppler and range techniques are the most commonly used methods for navigational purposes. (Note that Pioneers did not have a range observable; all the navigational data is in the form of Doppler observations.) The position and velocities of the DSN tracking stations must be known to high accuracy. The transformation from a Earth fixed coordinate system to the International Earth Rotation Service (IERS) Celestial System is a complex series of rotations that includes precession, nutation, variations in the Earth’s rotation (UT1-UTC) and polar motion.

Calculations of the motion of a spacecraft are made on the basis of the range time-delay and/or the Doppler shift in the signals. This type of data was used to determine the positions, the velocities, and the magnitudes of the orientation maneuvers for the Pioneer spacecraft.

Theoretical modeling of the group delays and phase delay rates are done with the orbit determination software we describe in Section 4.

3.4.1 Doppler experimental techniques and strategy

In Doppler experiments a radio signal transmitted from the Earth to the spacecraft is coherently transponded and sent back to the Earth. Its frequency change is measured with great precision, using the hydrogen masers at the DSN stations. The observable is the DSN frequency shift¹⁶

$$\Delta\nu(t) = \nu_0 \frac{1}{c} \frac{d\ell}{dt}, \quad (3.7)$$

where ℓ is the overall optical distance (including diffraction effects) traversed by a photon in both directions. (In the Pioneer Doppler experiments, the stability of the fractional drift at the S-band is on the order of $\Delta\nu/\nu_0 \simeq 10^{-12}$, for integration times on the order of 10^3 s.) Doppler measurements provide the “range rate” of the spacecraft and therefore are affected by all the dynamical phenomena in the volume between the Earth and the spacecraft.

Expanding upon what was discussed in Section 3.2, the received signal and the transmitter frequency (both are at S-band) as well as a 10 pulse per second timing reference from the FTS are fed to the Metric Data Assembly (MDA). There the Doppler phase (difference between transmitted and received phases plus an added bias) is counted. That is, digital counters at the MDA record the zero crossings of the difference (i.e., Doppler, or alternatively the beat frequency of the received frequency and the exciter frequency). After counting, the bias is removed so that the true phase is produced.

The system produces “continuous count Doppler” and it uses two counters. Every tenth of a second, a Doppler phase count is recorded from one of the counters. The other counter continues the counts. The recording alternates between the two counters to maintain a continuous unbroken count. The Doppler counts are at 1 MHz for S-band or 5 MHz for X-band. The wavelength of each S-band cycle is about 13 cm. Dividers or “time resolvers” further subdivide the cycle into 256 parts, so that fractional cycles are measured with a resolution of 0.5 mm. This accuracy can only be maintained if the Doppler is continuously counted (no breaks in the count) and coherent frequency standards are kept throughout the pass. It should be noted that no error is accumulated in the phase count as long as lock is not lost. The only errors are the stability of the hydrogen maser and the resolution of the “resolver.”

Consequently, the JPL Doppler records are not frequency measurements. Rather, they are digitally counted measurements of the Doppler phase difference between the transmitted and received S-band frequencies, divided by the count time.

Therefore, the Doppler observables to which we will refer have units of cycles per second or Hz. Since total count phase observables are Doppler observables multiplied by the count interval T_c , they have units of cycles. The Doppler integration time refers to the total counting of the elapsed periods of the wave with the reference frequency of the hydrogen maser. The usual Doppler integrating times for the Pioneer Doppler signals refers to the data sampled over intervals of 10 s, 60 s, 600 s, 660 s, or 1980 s.

In order to acquire Doppler data, the user must provide a reference trajectory and information concerning the spacecraft’s RF system to JPL’s Deep Space Mission System (DSMS), to allow for the generation of pointing and frequency predictions. The user specified count interval can vary from 0.1 s to tens of minutes. Absent any systematic errors, the precision improves as the square root of the count interval. Count times of 10 to 60 seconds are typical [88], as well as intervals of ~ 2000 s, which is an averaging interval located at the minimum of the Allan variance curve for hydrogen masers. The average rate of change of the cycle count over the count interval

¹⁶The JPL and DSN convention for Doppler frequency shift is $(\Delta\nu)_{\text{DSN}} = \nu_0 - \nu$, where ν is the measured frequency and ν_0 is the reference frequency. It is positive for a spacecraft receding from the tracking station (red shift), and negative for a spacecraft approaching the station (blue shift), just the opposite of the usual convention, $(\Delta\nu)_{\text{usual}} = \nu - \nu_0$. In consequence, the velocity shift, $\Delta v = v - v_0$, has the same sign as $(\Delta\nu)_{\text{DSN}}$ but the opposite sign to $(\Delta\nu)_{\text{usual}}$. Unless otherwise stated, we use the DSN frequency shift convention in this document.

expresses a measurement of the average velocity of the spacecraft in the line between the antenna and the spacecraft. The accuracy of Doppler data is quoted in terms of how accurate this velocity measurement is over a 60 second count.

It is also possible to infer the position in the sky of a spacecraft from the Doppler data. This is accomplished by examining the diurnal variation imparted to the Doppler shift by the Earth's rotation. As the ground station rotates underneath a spacecraft, the Doppler shift is modulated by a sinusoid. The sinusoid's amplitude depends on the declination angle of the spacecraft and its phase depends upon the right ascension. These angles can therefore be estimated from a record of the Doppler shift that is (at least) of several days duration. This allows for a determination of the distance to the spacecraft through the dynamics of spacecraft motion using standard orbit theory contained in the orbit determination programs.

3.4.2 Data preparation

In an ideal system, all scheduled observations would be used in determining parameters of physical interest. However, there are inevitable problems that occur in data collection and processing that corrupt the data. So, at various stages of the signal processing one must remove or "edit" corrupted data. Thus, the need arises for objective editing criteria. Procedures have been developed, which attempt to excise corrupted data on the basis of objective criteria. There is always a temptation to eliminate data that is not well explained by existing models, to thereby "improve" the agreement between theory and experiment. Such an approach may, of course, eliminate the very data that would indicate deficiencies in the *a priori* model. This would preclude the discovery of improved models.

In the processing stage that fits the Doppler samples, checks are made to ensure that there are no integer cycle slips in the data stream that would corrupt the phase. This is done by considering the difference of the phase observations taken at a high rate (10 times a second) to produce Doppler. Cycle slips often are dependent on tracking loop bandwidths, the signal-to-noise ratios, and predictions of frequencies. Blunders due to out-of-lock can be determined by looking at the original tracking data. In particular, cycle slips due to loss-of-lock stand out as a 1 Hz blunder point for each cycle slipped.

If a blunder point is observed, the count is stopped and a Doppler point is generated by summing the preceding points. Otherwise the count is continued until a specified maximum duration is reached. Cases where this procedure detected the need for cycle corrections were flagged in the database and often individually examined by an analyst. Sometimes the data was corrected, but nominally the blunder point was just eliminated. This ensures that the data is consistent over a pass. However, it does not guarantee that the pass is good, because other errors can affect the whole pass and remain undetected until the orbit determination is done.

To produce an input data file for an orbit determination program, JPL has a software package known as the Radio Metric Data Selection, Translation, Revision, Intercalation, Processing and Performance Evaluation Reporting (RMD-STRIPPER) program. As we discussed in Section 3.4.1, this input file has data that can be integrated over intervals with different durations: 10 s, 60 s, 600 s, 660 s, and 1980 s. This input orbit determination file obtained from the RMDC group is the data set that can be used for analysis. Therefore, the initial data file already contained some common data editing that the RMDC group had implemented through program flags, etc. The data set we started with had already been compressed to 60 s. So, perhaps there were some blunders that had already been removed using the initial STRIPPER program.

The orbit analyst manually edits the remaining corrupted data points. Editing is done either by plotting the data residuals and deleting them from the fit or plotting weighted data residuals. That is, the residuals are divided by the standard deviation assigned to each data point and plotted. This gives the analyst a realistic view of the data noise during those times when the data was obtained

while looking through the solar plasma. Applying an “ N - σ ” (σ is the standard deviation) test, where N is the choice of the analyst (usually 4–10) the analyst can delete those points that lie outside the N - σ rejection criterion without being biased in his selection.

A careful analysis edits only very corrupted data; e.g., a blunder due to a phase lock loss, data with bad spin calibration, etc. If needed or desired, the orbit analyst can choose to perform an additional data compression of the original navigation data.

3.4.3 Data weighting

The Pioneers used S-band (~ 2.2 GHz) radio signals to communicate with the DSN. The S-band data is available from 26 m, 70 m, and some 34 m antennas of the DSN complex (see baseline DSN configuration in the Figure 3.4). The dominant systematic error that can affect S-band tracking data is ionospheric transmission delays. When the spacecraft is located angularly close to the Sun, with Sun-Earth-spacecraft angles of less than 10 degrees, degradation of the data accuracy will occur. S-band data is generally unusable for Sun-Earth-spacecraft angles of less than 5 degrees.

Therefore, considerable effort has gone into accurately estimating measurement errors in the observations. These errors provide the data weights necessary to accurately estimate the parameter adjustments and their associated uncertainties. To the extent that measurement errors are accurately modeled, the parameters extracted from the data will be unbiased and will have accurate sigmas assigned to them. Typically, for S-band Doppler data one assigns a standard 1- σ uncertainty of 1 mm/s over a 60 s count time after calibration for transmission media effects.

A change in the DSN antenna elevation angle also directly affects the Doppler observables due to tropospheric refraction. Therefore, to correct for the influence of the Earth’s troposphere the data can also be deweighted for low elevation angles. The phenomenological range correction used in JPL’s analysis technique is given as

$$\sigma = \sigma_{\text{nominal}} \left(1 + \frac{18}{(1 + \theta_E)^2} \right), \quad (3.8)$$

where σ_{nominal} is the basic standard deviation (in Hz) and θ_E is the elevation angle in degrees. Each leg is computed separately and summed. For Doppler the same procedure is used. First, Equation (3.8) is multiplied by $\sqrt{60 \text{ s}/T_c}$, where T_c is the count time. Then a numerical time differentiation of Equation (3.8) is performed. That is, Equation (3.8) is differenced and divided by the count time, T_c . (For more details on this standard technique see [228, 231].)

There is also the problem of data weighting for data influenced by the solar corona. This is discussed in Section 4.5.1.

3.4.4 Spin calibration of the data

The radio signals used by DSN to communicate with spacecraft are circularly polarized. When these signals are reflected from spinning spacecraft antennas a Doppler bias is introduced that is a function of the spacecraft spin rate. Each revolution of the spacecraft adds one cycle of phase to the up-link and the down-link. The up-link cycle is multiplied by the turn around ratio 240/221 so that the bias equals $(1+240/221)$ cycles per revolution of the spacecraft.

For the Pioneer 10 and 11 spacecraft, high-accuracy spin data is available from the spacecraft telemetry. Due to the star sensor failure on board Pioneer 10 (see Section 2), once the spacecraft was more than ~ 30 AU from the Sun, no on-board roll reference was available. Until mid-1993, a science instrument (the Infrared Photo-Polarimeter) was used as a surrogate star sensor, which allowed the accurate determination of the spacecraft spin rate; however, due to the lack of available electrical power on board, this instrument could not be used after 1993. However, analysts still could get a rough spin determination approximately every six months using information obtained

from the conscan maneuvers. No spin determinations were made after 1995. However, the archived conscan data could still yield spin data at every maneuver time if such work was approved. Further, as the phase center of the main antenna is slightly offset from the spin axis, a very small (but detectable) sine-wave signal appears in the high-rate Doppler data. In principle, this could be used to determine the spin rate for passes taken after 1993, but it has not been attempted.

The changing spin rates of Pioneer 10 and 11 can be an indication of gas leaks, which can also be a source of unmodeled accelerations. We discussed this topic in more detail in Section 2.3.7.

3.5 Pioneer telemetry data

Telemetry received from the Pioneer 10 and 11 spacecraft was supplied to the Pioneer project by the DSN in the form of Master Data Records (MDRs). MDRs contained all information sent by the spacecraft to the ground, and some information about the DSN station that received the data. The information in the MDRs that was sent by the spacecraft included engineering telemetry as well as scientific observations.

The Pioneer project used engineering data extracted from the MDRs to monitor and control the spacecraft, while scientific data, also extracted from the MDRs, was converted into formats specific to each experiment and supplied to the experimenter groups.

Far beyond the original expectations¹⁷, telemetry is now seen to be of value for the investigation of the Pioneer anomaly, as the MDRs, specifically the telemetry data contained therein, are helpful in the construction of an accurate model of the spacecraft during their decades long journey, including a precise thermal profile, the time history of propulsion system activation and usage, and many other potential sources of on-board disturbances. After recent recovery efforts [399], this data is available for investigation.

3.5.1 MDR data integrity and completeness

The total amount of data stored in these MDR files is approximately 40 GB [399]. According to the original log sheets that record the transcription from tape to magneto-optical media, only a few days worth of data is missing, some due to magnetic tape damage. One notable exception is the Jupiter encounter period of Pioneer 10. According to the transcription log sheets, DOY 332–341 from 1973 were not available at the time when the magnetic tapes on which the MDRs were originally stored were transcribed to more durable magneto-optical media.

Other significant periods of missing data are listed in Table 3.5. It is not known why these records are not present, except that we know that very few days are missing due to unreadable media (i.e., the cause is missing, not damaged, tapes.)

So, the record is fairly complete. But how good is the data? Over forty billion bytes were received by the DSN, processed, copied to tape, copied from tape to magneto-optical disks, then again copied over a network connection to a personal computer. It is not inconceivable that the occasional byte was corrupted by a transmission or storage error. There are records that contain what is apparently bogus data, especially from the later years of operation. This, plus the fact that the record structure (e.g., headers, synchronization sequences) is intact suggests reception errors as the spacecraft’s signal got weaker due to increasing distance, and not copying and/or storage errors.

¹⁷Normally, MDRs are seen to be of little use once the relevant information is extracted from them. Scientific measurements are extracted, packaged in the appropriate form, and sent to the corresponding experimenters for further processing and evaluation. Engineering telemetry is used by the spacecraft operations team to control and guide the spacecraft. MDRs are not necessarily considered worth preserving once the scientific data has been extracted, and the engineering telemetry is no longer needed for spacecraft operations. Indeed, the MDR retention schedule prescribed that the tapes be destroyed after 7 years. Fortunately, most of the MDRs for the Pioneer 10 and 11 projects have been preserved nevertheless (see discussion in [399]).

Table 3.5: Pioneer 10 and 11 missing MDRs (periods of missing data shorter than 1–2 days not shown.)

Spacecraft	Year	Days of the Year (DOY)
Pioneer-10	1972	133–149
	1973	004–008, 060–067, 332–341
	1974	034–054
	1979	025–032, 125–128, 137–157, 171–200
	1980	173–182, 187–199, 248–257
	1983	329–348
	1984	346–359
Pioneer-11	1973	056–064, 067–080, 082–086, 088–094
	1980	309–330, 337–365
	1982	318–365
	1983	001–050
	1984	343–357
	1990	081–096

The MDRs contain no error detection or error correction code, so it is not possible to estimate the error rate. However, it is likely to be reasonably low, since the equipment used for storage and copying is generally considered very reliable. Furthermore, any errors would likely show up as random noise, and not as a systemic bias. In this regard, the data should generally be viewed to be of good quality insofar as the goal of constructing an engineering profile of the spacecraft is considered.

3.5.2 Interpreting the data

MDRs are a useless collection of bits unless information is available about their structure and content. Fortunately, this is the case in the case of the Pioneer 10 and Pioneer 11 MDRs.

The structure of an MDR is shown in Appendix C (see also [403]). The frame at the beginning and at the end of each 1344-bit record contained information about the DSN station that received the data, and included a timestamp, data quality and error indicators, and the strength of the received signal. The middle of the record was occupied by as many as four consecutive data frames received by the spacecraft.

The MDR header is followed by four data frames (not all four frames may be used, but they are all present) of 192 bits each. Lastly, an additional 8 words of DSN information completes the record. The total length of an MDR is thus 42 words of 32 bits each.

The 192-bit data frames are usually interpreted as 64 3-bit words or, alternatively, as 32 6-bit words. The Pioneer project used many different data frame formats during the course of the mission. Some formats were dedicated to engineering telemetry (accelerated formats). Other formats are science data formats, but still contain engineering telemetry in the form of a subcommutator: a different engineering telemetry value is transmitted in each frame, and eventually, all telemetry values are cycled through.

The Pioneer spacecraft had a total of 128 6-bit words reserved for engineering telemetry. Almost all these values are, in fact, used. A complete specification of the engineering telemetry values can be found in Section 3.5 (“Data Handling Subsystem”) of [292]. When engineering telemetry was accelerated to the main frame rate, four different record formats (C-1 through C-4) were used to transmit telemetry information. When the science data formats were in use, an area of the record was reserved for a subcommutator identifier and value.

The formats are further complicated by the fact that some engineering telemetry values appear only in subcommutators, whereas others only appear at the accelerated (main frame) rate.

In the various documentation packages, engineering data words are identified either by mnemonic, by the letter 'C' followed by a three-digit number that runs from 1 through 128, or most commonly, by the letter 'C' followed by a digit indicating which 'C' record (C-1 through C-4) the value appears in, and a two-digit number between 1 and 32: for instance, C-201 means the first engineering word in the C-2 record.

3.5.3 Available telemetry information

Pioneer 10 and 11 telemetry data is very relevant for a study of on-board systematics. The initial studies of the Pioneer anomaly [15, 18, 185, 391] and several subsequent papers [19, 393, 394, 395] had emphasized the need for a very detailed investigation of the on-board systematics. Other researchers also focused their work on the study of several on-board generated mechanisms that could contribute to an anomalous acceleration of the spacecraft [156, 236, 331]. Most of these investigations of on-board systematics were not very precise. This was due to a set of several reasons, one of them is insufficient amount of actual telemetry data from the vehicles. In 2005, this picture changed dramatically when this critical information became available.

Table 3.6 summarizes all available telemetry values in the C (engineering) and E (science) telemetry formats. The MDRs also contain a complete set of science readings that were telemetered in the A, B, and D formats.

As this table demonstrates, telemetry readings can be broadly categorized as temperature, voltage, current readings; other analog readings; various binary counters, values, and bit fields; and readings from science instruments. Temperature and electrical readings are of the greatest use, as they help to establish a detailed thermal profile of the spacecrafts' major components. Some binary readings are useful; for instance, thruster pulse count readings help to understand maneuvers and their impact on the spacecrafts' trajectories. It is important to note, however, that some readings may not be available and others may not be trusted. For example, thruster pulse count readings are only telemetered when the spacecraft is commanded to send readings in accelerated engineering formats; since these formats were rarely used late in the mission, we may not have pulse count readings for many maneuvers. Regarding reliability, we know from mission status reports about the failure of the sun and star sensors; these failures invalidate many readings from that point onward. Thus it is important to view telemetry readings in context before utilizing them as source data for our investigation.

On-board telemetry not only gives a detailed picture of the spacecraft and its subsystems, but this picture is redundant: electrical, thermal, logic state and other readings provide means to examine the same event from a multitude of perspectives.

In addition to telemetry, there exists an entire archive of the Pioneer Project documents for the period from 1966 to 2003. This archive contains all Pioneer 10 and 11 project documents discussing the spacecraft and mission design, fabrication of various components, results of various tests performed during fabrication, assembly, pre-launch, as well as calibrations performed on the vehicles; and also administrative documents including quarterly reports, memoranda, etc. Information on most of the maneuver records, spin rate data, significant events of the craft, etc. is also available.

Table 3.6: Available parameter set that may be useful for the Pioneer anomaly investigation.

Parameters	Subsystem	Telemetry words
TEMPERATURES		
RTG fin root temps	Thermal	C ₂₀₁ , C ₂₀₂ , C ₂₀₃ , C ₂₀₄
RTG hot junction temps	Thermal	C ₂₂₀ , C ₂₁₉ , C ₂₁₈ , C ₂₁₇
TWT temperatures	Communications	C ₂₀₅ , C ₂₀₆ , C ₂₀₇ , C ₂₂₈ , C ₂₂₃ , C ₂₂₁
Receiver temperatures	Communications	C ₂₂₂ , C ₂₂₇
Platform temperatures	Thermal	C ₃₀₁ , C ₃₀₂ , C ₃₀₄ , C ₃₁₈ , C ₃₁₉ , C ₃₂₀
PSA temperatures	Thermal	C ₂₂₅ , C ₂₂₆
Thruster cluster temps	Propulsion	C ₃₀₉ , C ₃₂₆ , C ₃₁₀ , C ₃₁₁ , C ₃₁₂ , C ₃₂₈ , C ₃₂₅
SRA/SSA temperatures	ACS	C ₃₀₃ , C ₃₁₇
Battery temperature	Power	C ₁₁₅
Propellant temperature	Propulsion	C ₃₂₇
N2 tank temperature	Propulsion	C ₁₃₀
Science instr temps	Science	E ₁₀₁ , E ₁₀₂ , E ₁₀₉ , E ₁₁₀ , E ₁₁₇ , E ₁₁₈ , E ₁₂₅ , E ₁₂₈ , E ₂₀₁ , E ₂₀₉ , E ₂₁₃ , E ₂₂₁
VOLTAGES		
Calibration voltages	Data handling	C ₁₀₁ , C ₁₀₂ , C ₁₀₃
RTG voltages	Power	C ₁₁₀ , C ₁₂₅ , C ₁₃₁ , C ₁₁₃
Battery/Bus voltages	Power	C ₁₀₆ , C ₁₀₇ , C ₁₁₇ , C ₁₁₈ , C ₁₁₉
TWT voltages	Communications	C ₂₂₄ , C ₂₃₀
Science instr voltages	Science	E ₁₁₉ , E ₁₂₉ , E ₂₁₀ , E ₂₁₁ , E ₂₁₇ , E ₂₂₀
CURRENTS		
RTG currents	Power	C ₁₂₇ , C ₁₀₅ , C ₁₁₄ , C ₁₂₃
Battery/Bus currents	Power	C ₁₀₉ , C ₁₂₆ , C ₁₂₉
Shunt current	Power	C ₁₂₂ , C ₂₀₉
TWT currents	Communications	C ₂₀₈ , C ₂₁₁ , C ₂₁₅ , C ₂₁₆
Science instr currents	Science	E ₁₁₁ , E ₁₁₂ , E ₁₁₃
PRESSURE		
Propellant pressure	Propulsion	C ₂₁₀
OTHER ANALOG		
TWT power readings	Communications	C ₂₃₁ , C ₂₁₄
Receiver readings	Communications	C ₁₁₁ , C ₂₁₂ , C ₂₃₂ , C ₁₂₁ , C ₂₂₉ , C ₂₁₃
BINARY/BIT FIELDS		
Conscan	Communications	C ₃₁₃ , C ₃₁₄ , C ₃₁₅ , C ₃₁₆
Stored commands	Electrical	C ₃₀₅ , C ₃₀₆ , C ₃₀₇
Thruster pulse counts	Propulsion	C ₃₂₉ , C ₃₂₁ , C ₃₂₂ , C ₃₃₀
Status bits	Data handling	C ₁₀₄
	Power	C ₁₂₈
	Electrical	C ₁₂₀ , C ₁₃₂ , C ₃₂₄ , C ₃₃₂
	Communications	C ₃₀₈
Power switches	Electrical	C ₁₀₈ , C ₁₂₄
Roll attitude	Data handling	C ₁₁₂ , C ₁₁₆
Precession	ACS	C ₄₀₃ , C ₄₁₁ , C ₄₁₂ , C ₄₁₅ , C ₄₁₆ , C ₄₂₂ , C ₄₂₃ , C ₄₂₄ , C ₄₂₅ , C ₄₂₈ , C ₄₂₉ , C ₄₃₀
Spin/roll	Data handling	C ₄₀₅ , C ₄₀₆ , C ₄₀₇ , C ₄₀₈ , C ₄₁₇
Delta v	ACS	C ₄₁₃ , C ₄₁₄ , C ₄₂₆
ACS status	Propulsion	C ₄₀₉
	ACS	C ₄₁₀ , C ₄₂₇ , C ₄₃₁ , C ₄₃₂
Star sensor	ACS	C ₄₀₄ , C ₄₁₉ , C ₄₂₀ , C ₄₂₁
SCIENCE INSTRUMENTS		
Status/housekeeping	Science	E ₁₀₈ , E ₁₂₄ , E ₁₃₀ , E ₂₀₂ , E ₂₂₄ , E ₁₃₁ , E ₁₃₂ , E ₂₀₈
JPL/HVM readings	Science	E ₁₀₃ , E ₁₀₄ , E ₁₀₅ , E ₁₀₆ , E ₁₀₇ , E ₂₀₃ , E ₂₀₄ , E ₂₀₅
UC/CPI readings	Science	E ₁₁₄ , E ₁₁₅ , E ₁₁₆ , E ₂₀₆ , E ₂₁₂ , E ₂₁₄ , E ₂₁₅ , E ₂₁₆
GE/AMD readings	Science	E ₁₂₂ , E ₁₂₃ , E ₂₂₂ , E ₂₂₃
GSFC/CRT readings	Science	E ₁₂₆ , E ₁₂₇
LaRC/MD readings	Science	E ₂₀₇

4 Navigation of the Pioneer Spacecraft

Modern radio tracking techniques made it possible to explore the gravitational environment in the solar system up to a level of accuracy never before possible. The two principal forms of celestial mechanics experiments that were used involve planets (e.g., passive radar ranging) and Doppler and range measurements with interplanetary spacecraft [11, 20]. This work was motivated by the desire to improve the ephemerides of solar system bodies and knowledge of solar system dynamics.

The main objective of spacecraft navigation is to determine the present position and velocity of a spacecraft and to predict its future trajectory. This is usually done by measuring changes in the spacecraft's radio signal and then, using those measurements, correcting (fitting and adjusting) the predicted spacecraft trajectory.

In this section we discuss the theoretical foundations that are used for the analysis of tracking data from interplanetary spacecraft. We describe the basic physical models used to determine a trajectory.

4.1 Models for gravitational forces acting on a spacecraft

The primary force acting on a spacecraft in deep space is the force of gravity, specifically, the gravitational attraction of the Sun and, to a lesser extent, planetary bodies. When the spacecraft is in deep space, far from the Sun and not in the vicinity of any planet, these sources of gravity can be treated as Newtonian point sources. However, when the spacecraft is in the vicinity of a massive body, corrections due to general relativity as well as the finite extent and mass distribution of the body in question must be considered.

Of particular interest is the possibility that a celestial mechanics experiment might help distinguish between different theories of gravity. There exists a method, the parametrized post-Newtonian (PPN) formalism, that allows one to describe various metric theories of gravity up to $\mathcal{O}(c^{-5})$ using a common parameterized metric. As this formalism forms the basis of modern spacecraft navigational codes, in the following, we provide a brief summary.

4.1.1 The parametrized post-Newtonian formalism

In 1922, Eddington [102] developed the first parameterized generalization of Einstein's theory, expressing components of the metric tensor in the form of a power series of the Newtonian potential. This phenomenological parameterization has since been developed into what is known as the parametrized post-Newtonian (PPN) formalism [221, 256, 257, 258, 259, 378, 413, 414, 415, 416, 417, 418, 420]. This formalism represents the metric tensor for slowly moving bodies and weak gravitational fields. The formalism is valid for a broad class of metric theories, including general relativity as a unique case. The parameters that appear in the PPN formalism are individually associated with various symmetries and invariance properties of the underlying theory (see [418] for details).

The full PPN formalism has 10 parameters [419]. However, if one assumes that Lorentz invariance, local position invariance and total momentum conservation hold, the metric tensor for a system of N point-like gravitational sources in four dimensions at the spacetime position of body i may be written as (see [390])

$$\begin{aligned}
g_{00} = & 1 - \frac{2}{c^2} \sum_{j \neq i} \frac{\mu_j}{r_{ij}} + \frac{2\beta}{c^4} \left[\sum_{j \neq i} \frac{\mu_j}{r_{ij}} \right]^2 - \frac{1+2\gamma}{c^4} \sum_{j \neq i} \frac{\mu_j \dot{r}_j^2}{r_{ij}} \\
& + \frac{2(2\beta-1)}{c^4} \sum_{j \neq i} \frac{\mu_j}{r_{ij}} \sum_{k \neq j} \frac{\mu_k}{r_{jk}} - \frac{1}{c^4} \sum_{j \neq i} \mu_j \frac{\partial^2 r_{ij}}{\partial t^2} + \mathcal{O}(c^{-5}),
\end{aligned}$$

$$\begin{aligned}
g_{0\alpha} &= \frac{2(\gamma+1)}{c^3} \sum_{j \neq i} \frac{\mu_j \dot{\mathbf{r}}_j^\alpha}{r_{ij}} + \mathcal{O}(c^{-5}), \quad (\alpha = 1 \dots 3) \\
g_{\alpha\beta} &= -\delta_{\alpha\beta} \left(1 + \frac{2\gamma}{c^2} \sum_{j \neq i} \frac{\mu_j}{r_{ij}} \right) + \mathcal{O}(c^{-5}), \quad (\alpha, \beta = 1 \dots 3)
\end{aligned} \tag{4.1}$$

where the indices $1 \leq i, j \leq N$ refer to the N bodies, r_{ij} is the distance between bodies i and j (calculated as $|\mathbf{r}_j - \mathbf{r}_i|$ where \mathbf{r}_i is the spatial position vector of body i), μ_i is the gravitational constant for body i given as $\mu_i = Gm_i$, where G is the Newtonian gravitational constant and m_i is the body's rest mass. The Eddington-parameters β and γ have, in this special case, clear physical meaning: β represents a measure of the nonlinearity of the law of superposition of the gravitational fields, while γ represents the measure of the curvature of the spacetime created by a unit rest mass.

The Newtonian scalar gravitational potential in Equation (4.1) is given by the $1/c^2$ term in g_{00} . Corrections of order $1/c^4$, parameterized by β and γ , are post-Newtonian terms. In the case of general relativity, $\beta = \gamma = 1$. One of the simplest generalizations of general relativity is the theory of Brans and Dicke [52] that contains, in addition to the metric tensor, a scalar field and an undetermined dimensionless coupling constant ω . Brans–Dicke theory yields the values $\beta = 1$, $\gamma = (1 + \omega)/(2 + \omega)$ for the Eddington parameters. The value of β may be different for other scalar-tensor theories [80, 79, 390].

The PPN formalism is widely used in studies of relativistic gravitation [55, 56, 229, 230, 363, 388, 418]. The relativistic equations of motion for an N -body system are derived from the PPN metric using a Lagrangian formalism [388, 418], discussed below.

4.1.2 Relativistic equations of motion

Navigation of spacecraft in deep space requires computing a spacecraft's trajectory and the compilation of spacecraft ephemeris: a file containing the position and velocity of the spacecraft as functions of time [390]. Spacecraft ephemerides are computed by orbit determination codes that utilize a numerical integrator in conjunction with various input parameters. These include an estimate of the spacecraft's initial state vector (comprising its position and velocity vector), adopted constants (c , G , planetary mass ratios, etc.) and parameters that are estimated from fits to observational data (e.g., corrections to the ephemerides of solar system bodies).

The principal equations of motion used by orbit determination codes describe the relativistic gravitational acceleration in the presence of the gravitational field of multiple point sources that include the Sun, planets, major moons and larger asteroids [364]. These equations are derived from the metric Equation (4.1) using a Lagrangian formalism. The point source model is adequate in deep space when a spacecraft is traveling far from those sources. When the spacecraft is in the vicinity of a planet, ephemeris programs also compute corrections due to deviations from spherical symmetry in the planetary body, as well as the gravitational influences from the planet's moons, if any.

The acceleration of body i due to the gravitational field of point sources, including Newtonian and relativistic perturbative accelerations [106, 388, 418], can be derived in the solar system

barycentric frame in the form [18, 108, 228, 229, 231, 244]:

$$\begin{aligned}\ddot{\mathbf{r}}_i = & \sum_{j \neq i} \frac{\mu_j (\mathbf{r}_j - \mathbf{r}_i)}{r_{ij}^3} \left\{ 1 - \frac{2(\beta + \gamma)}{c^2} \sum_{l \neq i} \frac{\mu_l}{r_{il}} - \frac{2\beta - 1}{c^2} \sum_{k \neq j} \frac{\mu_k}{r_{jk}} + \gamma \left(\frac{\dot{r}_i}{c} \right)^2 + (1 + \gamma) \left(\frac{\dot{r}_j}{c} \right)^2 \right. \\ & - \frac{2(1 + \gamma)}{c^2} \dot{\mathbf{r}}_i \dot{\mathbf{r}}_j - \frac{3}{2c^2} \left[\frac{(\mathbf{r}_i - \mathbf{r}_j) \dot{\mathbf{r}}_j}{r_{ij}} \right]^2 + \frac{1}{2c^2} (\mathbf{r}_j - \mathbf{r}_i) \ddot{\mathbf{r}}_j \left. \right\} + \frac{3 + 4\gamma}{2c^2} \sum_{j \neq i} \frac{\mu_j \ddot{\mathbf{r}}_j}{r_{ij}} \\ & + \frac{1}{c^2} \sum_{j \neq i} \frac{\mu_j}{r_{ij}^3} \left\{ [\mathbf{r}_i - \mathbf{r}_j] \cdot [(2 + 2\gamma) \dot{\mathbf{r}}_i - (1 + 2\gamma) \dot{\mathbf{r}}_j] \right\} (\dot{\mathbf{r}}_i - \dot{\mathbf{r}}_j) + \mathcal{O}(c^{-4}),\end{aligned}\quad (4.2)$$

where the indices $1 \leq j, k, l \leq N$ refer to the N bodies and where k includes body i , whose motion is being investigated.

These equations can be integrated numerically to very high precision using standard techniques in numerical codes that are used to construct solar system ephemerides, for spacecraft orbit determination [231, 363, 388], and for the analysis of gravitational experiments in the solar system [389, 400, 418, 419, 421].

In the vicinity of a celestial body, one must also take into account that a celestial body is not spherically symmetric. Its gravitational potential can be modeled in terms of spherical harmonics. As Pioneers 10 and 11 both flew by Jupiter and Pioneer 11 visited Saturn, of specific interest to the navigation of these spacecraft is the gravitational potential due to the oblateness of a planet, notably a gas giant. The gravitational potential due to the oblateness of planetary body i can be expressed using zonal harmonics in the form [231]:

$$U_{\text{obl}} = -\frac{\mu_i}{|\mathbf{r}_i - \mathbf{r}|} \sum_{k=1}^{\infty} \frac{J_k^{(i)} a_i^k P_k(\sin \theta)}{|\mathbf{r}_i - \mathbf{r}|^k}, \quad (4.3)$$

where $P_k(x)$ is the k -th Legendre polynomial in x , a_i is the equatorial radius of planet i , θ is the latitude of the spacecraft relative to the planet's equator, and $J_k^{(i)}$ is the k -th spherical harmonic coefficient of planet i .

In order to put Equation (4.3) to use, first it must be translated into an expression for force by calculating its gradient. Second, it is also necessary to express the position of the spacecraft in a coordinate system that is fixed to the planet's center and equator.

4.2 Light times and time scales

The complex gravitational environment of the solar system manifests itself not just through its effects on the trajectory of a spacecraft or celestial body: the propagation of electromagnetic signals to or from an observing station on the Earth must also be considered. Additionally, proper timekeeping becomes an issue of significance: clocks that are in relative motion do not tick at the same rate, and changing gravitational potentials may also affect them.

4.2.1 Light time solution

The time it takes for a signal to travel between two locations in space in the gravitational environment of a massive point source with gravitational constant μ can be derived from the PPN metric Equation (4.1) in the form [231]:

$$t_2 - t_1 = \frac{r_{12}}{c} + (1 + \gamma) \frac{\mu}{c^3} \ln \frac{r_1 + r_2 + r_{12} + (1 + \gamma)\mu/c^2}{r_1 + r_2 - r_{12} + (1 + \gamma)\mu/c^2} + \mathcal{O}(c^{-5}), \quad (4.4)$$

where t_1 refers to the signal transmission time, and t_2 refers to the reception time, $r_{1,2}$ represent the distance of the point of transmission and point of reception, respectively, from the massive body, and r_{12} is the spatial separation of the points of transmission and reception. The terms proportional to μ/c^2 are important only for the Sun and are negligible for all other bodies in the solar system.

4.2.2 Standard time scales

The equations of motion Equation (4.2) and the light time solution Equation (4.4) are both written in terms of an independent time variable, which is called the ephemeris time, or ET. Ephemeris time is simply coordinate time in the chosen coordinate frame, such as a solar system barycentric frame. As such, the ephemeris time differs from the standard International Atomic Time (TAI, Temps Atomique International), measured in SI (Système International) seconds relative to a given epoch, namely the beginning of the year 1958.

When a solar system barycentric frame of reference is used to integrate the equations of motion, the relationship between ET and TAI can be expressed, to an accuracy that is sufficient for the purposes of the Pioneer project¹⁸, as

$$\text{ET} - \text{TAI} = (32.184 + 1.657 \times 10^{-3} \sin E) \text{ seconds}, \quad (4.5)$$

where

$$E = M + 0.01671 \sin M, \quad (4.6)$$

$$M = 6.239996 + 1.99096871 \times 10^{-7} t, \quad (4.7)$$

and t is ET in seconds since the J2000 epoch (noon, January 1, 2000). For further details, including higher accuracy time conversion formulae, see the relevant literature [81, 82, 83, 84, 226, 231] (in particular, see Eqs. (2–26) through (2–28) in [231].)

There exist alternate expressions with up to several hundred additional periodic terms, which provide greater accuracies. The use of these extended expressions provide transformations of $\text{ET} - \text{TAI}$ to accuracies of 1 ns [231].

For the purposes of the investigation of the Pioneer anomaly, the Station Time (ST) is especially significant. The station time is the time kept by the ultrastable oscillators of DSN stations, and it is measured in Universal Coordinated Time (UTC). All data records generated by DSN stations are timestamped using ST, that is, UTC as measured by the station’s clock.

UTC is a discontinuous time scale; it is similar to TAI, except for the regular insertion of leap seconds, which are used to account for minute variations in the Earth’s rate of rotation. Converting from UTC to international atomic time (TAI) requires the addition or subtraction of the appropriate number of leap seconds (ranging between 10 and 32 during the lifetime of the Pioneer missions.) For more details see [231, 335].

4.3 Nongravitational forces external to the spacecraft

Even in the vacuum of interplanetary space, the motion of a spacecraft is governed by more than just gravity. There are several nongravitational forces acting on a spacecraft, many of which must be taken into account in order to achieve an orbit determination accuracy at the level of the Pioneer anomaly. (For a general introduction to nongravitational forces acting on spacecraft, consult [178] and p. 125 in [201].) To determine the Pioneer orbits to sufficient precision, orbit determination

¹⁸JPL’s Orbit Determination Program, ODP, uses a higher precision conversion algorithm, not the simplified formula presented here.

programs must take into account these nongravitational accelerations unless a particular force can be demonstrated to be too small in magnitude to have a detectable effect on the spacecraft’s orbit.

In the presentation below of the standard modeling of small nongravitational forces, we generally follow the discussion in [18], starting with nongravitational forces that originate from sources external to the spacecraft, and followed by a review of forces of on-board origin. We also discuss effects acting on the radio signal sent to, or received from, the spacecraft.

4.3.1 Solar radiation pressure

Most notable among the sources for the forces external to the Pioneer spacecraft is the solar pressure. This force is a result of the exchange of momentum between solar photons and the spacecraft, as solar photons are absorbed or reflected by the spacecraft. This force can be significant in magnitude in the vicinity of the Earth, at ~ 1 AU from the Sun, especially when considering spacecraft with a large surface area, such as those with large solar panels or antennas. For this reason, solar pressure models are usually developed before a spacecraft is launched. These models take into account the effective surface areas of the portions of the spacecraft exposed to sunlight, and their thermal and optical properties. These models offer a computation of the acceleration of the spacecraft due to solar pressure as a function of solar distance and spacecraft orientation.

The simplest way of modeling solar pressure is by using a “flat plate” model. In this case, the spacecraft is treated as a flat surface, oriented at same angle with respect to incoming solar rays. The surface absorbs some solar heat, while it reflects the rest; reflection can be specular or diffuse. A flat plate model is fully characterized by three numbers: the area of the plate, its specular and its diffuse reflectivities. This model is particularly applicable to Pioneer 10 and 11 throughout most of their mission, as the spacecraft were oriented such that their large parabolic dish antennas were aimed only a few degrees away from the Sun, and most of the spacecraft body was behind the antenna, not exposed to sunlight.

In the case of a flat plate model, the force produced by the solar pressure can be described using a combination of several force vectors. One vector, the direction of which coincides with the direction of incoming solar radiation, represents the force due to photons from solar radiation intercepted by the spacecraft. The magnitude of this vector $\mathbf{F}_{\text{intcpt}}$ is proportional to the solar constant at the spacecraft’s distance from the Sun, multiplied by the projected area of the flat plate surface:

$$\mathbf{F}_{\text{intcpt}} = \frac{f_{\odot} A}{c r^2} (\mathbf{n} \cdot \mathbf{k}) \mathbf{n}, \quad (4.8)$$

where \mathbf{r} is the Sun-spacecraft vector, $\mathbf{n} = \mathbf{r}/r$ is the unit vector in this direction with $r = |\mathbf{r}|$, A is the effective area of the spacecraft (i.e., flat plate), \mathbf{k} is a unit normal vector to the flat plate, f_{\odot} is the solar radiation constant at 1 AU from the Sun and c is the speed of light. The standard value of the solar radiation constant is $f_{\odot} \simeq 1367 \text{ AU}^2 \text{ Wm}^{-2}$ when A is measured in units of m^2 and \mathbf{r} , in units of AU. According to Equation (4.8), approximately 65 W of intercepted sunlight can produce a force comparable in magnitude to that of the Pioneer anomaly; in contrast, in the vicinity of the Earth, the Pioneer 10 and 11 spacecraft intercepted ~ 7 kW of sunlight, indicating that solar pressure is truly significant, even as far away from the Sun as Saturn, for precision orbit determination.

Equation (4.8) reflects the amount of momentum carried by solar photons that are intercepted by the spacecraft body. However, one must also account for the amount of momentum carried away by photons that are reflected or re-emitted by the spacecraft body. These momenta depend on the material properties of the spacecraft exterior surfaces. The absorptance coefficient α determines the amount of sunlight absorbed (i.e., not reflected) by spacecraft materials. The emittance coefficient ϵ determines the efficiency with which the spacecraft radiates (absorbed or internally generated) heat relative to an idealized black body. Finally, the specularity coefficient σ determines the direction in

which sunlight is reflected: a fully specular surface reflects sunlight like a mirror, whereas a diffuse (Lambertian) surface reflects light in the direction of its normal. Together, these coefficients can be used in conjunction with basic vector algebra to calculate the force acting on the spacecraft due to specular reflection:

$$\mathbf{F}_{\text{spec}} = (1 - \alpha)\sigma[\mathbf{F}_{\text{intcpt}} - 2(\mathbf{F}_{\text{intcpt}} \cdot \mathbf{k})\mathbf{k}], \quad (4.9)$$

and the force due to diffuse reflection:

$$\mathbf{F}_{\text{diffuse}} = (1 - \alpha)(1 - \sigma)|\mathbf{F}_{\text{intcpt}}|\mathbf{k}. \quad (4.10)$$

Lastly, the force due to solar heating (i.e., re-emission of absorbed solar heat) can be computed in conjunction with the recoil force due to internally generated heat, which is discussed later in this section.

4.3.2 Solar wind

The solar wind is a stream of charged particles, primarily protons and electrons with energies of ~ 1 keV, ejected from the upper atmosphere of the Sun. Solar wind particles intercepted by a spacecraft transfer their momentum to the spacecraft. The acceleration caused by the solar wind has the same form as Equation (4.8), with f_{\odot} replaced by $m_p v^3 n$, where $n \approx 5 \text{ cm}^{-3}$ is the proton density at 1 AU and $v \approx 400 \text{ km/s}$ is the speed of the wind (electrons in the solar wind travel faster, but due to their smaller mass, their momenta are much smaller than the momenta of the protons). Thus,

$$\mathbf{F}_{\text{solar wind}} = \frac{m_p v^3 n A}{c r^2} (\mathbf{n} \cdot \mathbf{k}) \mathbf{n} \simeq 7 \times 10^{-4} \frac{A}{r^2} (\mathbf{n} \cdot \mathbf{k}) \mathbf{n}. \quad (4.11)$$

Because the density can change by as much as 100%, the exact acceleration is unpredictable. Nonetheless, as confirmed by actual measurement¹⁹, the magnitude of Equation (4.11) is at least 10^5 times smaller than the direct solar radiation pressure. This contribution is completely negligible [18], and therefore, it can be safely ignored.

4.3.3 Interaction with planetary environments

When a spacecraft is in the vicinity of a planetary body, it interacts with that body in a variety of ways. In addition to the planet's gravity, the spacecraft may be subjected to radiation pressure from the planet, be slowed by drag in the planet's extended atmosphere, and it may interact with the planet's magnetosphere.

For instance, for Earth orbiting satellites, the Earth's optical albedo of [226]:

$$\alpha_{\text{Earth}} \simeq 0.34 \quad (4.12)$$

yields typical albedo accelerations of 10–35% of the acceleration due to solar radiation pressure. On the other hand, when the spacecraft is in the planetary shadow, it does not receive direct sunlight.

Atmospheric drag can be modeled as follows [226]:

$$\ddot{\mathbf{r}} = -\frac{1}{2} C_D \frac{A}{m} \rho |\dot{\mathbf{r}}| \dot{\mathbf{r}}, \quad (4.13)$$

where \mathbf{r} is the spacecraft's position, $\dot{\mathbf{r}}$ its velocity, A is its cross-sectional area, m its mass, ρ is the atmospheric density, and the coefficient C_D has typical values between 1.5 and 3.

¹⁹See <http://www.ngdc.noaa.gov/stp/SOLAR/IRRADIANCE/irrad.html>.

The Lorentz force acting on a charged object with charge q traveling through a magnetic field with field strength \mathbf{B} at a velocity \mathbf{v} is given by

$$\mathbf{F} = q(\mathbf{v} \times \mathbf{B}). \quad (4.14)$$

Considering the velocity of the Pioneer spacecraft relative to a planetary magnetic field during a planetary encounter (up to 60 km/s during Pioneer 11's encounter with Jupiter) and a strong planetary magnetic field (up to 1 mT for Jupiter near the poles), if the spacecraft carries a net electric charge, the resulting force can be significant: up to 60 N per Coulomb of charge. In actuality, the maximum measured magnetic field by the two Pioneers at Jupiter was $113.5 \mu\text{T}$ [261]. An upper bound of $0.1 \mu\text{C}$ exists for any positive charge carried by the spacecraft [261], but a possible negative charge cannot be excluded [261] and a negative charge as high as 10^{-4} C cannot be ruled out [261].

The long-term accelerations of Pioneer 10 and 11, however, remain unaffected by planetary effects, due to the fact that except for brief encounters with Jupiter and Saturn, the two spacecraft traveled in deep space, far from any planetary bodies.

4.3.4 Interplanetary magnetic fields

The interplanetary magnetic field strength is less than 1 nT [18]. Considering a spacecraft velocity of 10^4 m/s and a charge of 10^{-4} C , Equation (4.14) gives a force of 10^{-9} N or less, with a corresponding acceleration (assuming a spacecraft mass of $\sim 250 \text{ kg}$) of $4 \times 10^{-12} \text{ m/s}^2$ or less. This value is two orders of magnitude smaller than the anomalous Pioneer acceleration of $a_P = (8.74 \pm 1.33) \times 10^{-10} \text{ m/s}^2$ (see Section 5.6).

4.3.5 Drag forces

While there have been attempts to explain the anomalous acceleration as a result of a drag force induced by exotic forms of matter (see Section 6.2), no known form of matter (e.g., gas, dust particles) in interplanetary space produces a drag force of significance.

The drag force on a sail was estimated as [253]:

$$\mathbf{F}_{\text{sail}} = -\mathcal{K}_d \rho A v^2, \quad (4.15)$$

where v is the spacecraft's velocity relative to the interplanetary medium, A its cross sectional area, ρ is the density of the interplanetary medium, and \mathcal{K}_d is a dimensionless coefficient that characterizes the absorptance, emittance, and transmittance of the spacecraft with respect to the interplanetary medium.

Using the Pioneer spacecraft's 2.74 m high-gain antenna as a sail and an approximate velocity of 10^{-4} m/s relative to the interplanetary medium, and assuming \mathcal{K}_d to be of order unity, we can estimate a drag force of

$$\mathbf{F}_{\text{sail}} \simeq -5.9 \times 10^8 \rho, \quad (4.16)$$

with \mathbf{F} and ρ measured in SI units. According to this result, a density of $\rho \sim 3 \times 10^{-16} \text{ kg/m}^3$ or higher can produce accelerations that are comparable in magnitude to the Pioneer anomaly [186].

The density ρ_{ISD} of dust of interstellar origin has been measured by the Ulysses probe [181, 254] at $\rho_{\text{ISD}} \lesssim 3 \times 10^{-23} \text{ kg/m}^3$. The average interplanetary dust density, which also contains orbiting dust, is believed to be almost two orders of magnitude higher according to the consensus view [254]. However, higher dust densities are conceivable.

On the other hand, if one *presumes* a model density, the constancy of the observed anomalous acceleration of the Pioneer spacecraft puts upper limits on the dust density. For instance, an isothermal density model $\rho_{\text{isoth}} \propto r^{-2}$ yields the limit $\rho_{\text{isoth}} \lesssim 5 \times 10^{-17} (20 \text{ AU}/r)^2 \text{ kg/m}^3$.

4.4 Nongravitational forces of on-board origin

Perhaps the most fundamental question concerning the anomalous acceleration of Pioneer 10 and 11 is whether or not the acceleration is due to an on-board effect: i.e., is the “anomalous” acceleration simply a result of our incomplete understanding of the engineering details of the two spacecraft? Therefore, it is essential to analyze systematically any possible on-board source of acceleration that may be present.

In the broadest terms, momentum conservation dictates that in order for an on-board effect to accelerate the spacecraft, the spacecraft must eject mass or emit radiation. As no significant anomaly occurred in the Pioneer 10 and 11 missions, it is unlikely that either spacecraft lost a major component during their cruise. In any case, such an occurrence would have resulted in a one time change in the spacecraft’s velocity, not any long-term acceleration. Therefore, it is safe to consider only the emission of volatiles as a means of mass ejection. Such emissions can be intentional (as during maneuvers) or due to unintended leaks of propellant or other volatiles on board. Radiation emitted as radiative energy is produced by on-board processes.

The spin of the Pioneer spacecraft makes it possible to apply a simplified treatment of forces of on-board origin that change slowly with time. Let us denote the unit vector normal to the spacecraft’s plane of rotation (i.e., the spin axis, which we assume to remain constant in time) by \mathbf{s} . Then, considering a force \mathbf{F} that is a linear function of time in a co-rotating reference frame that is attached to the spacecraft, it can be described in a co-moving (nonrotating) inertial frame as

$$\mathbf{F}(t) = \mathbf{F}_{\parallel}(t) + \mathbf{F}_{\perp}(t) = \mathbf{F}_{\parallel}(t) + \mathbb{R}(\omega t) \cdot [\mathbf{F}_{\perp}(t_0) + \dot{\mathbf{F}}_{\perp} \cdot (t - t_0)], \quad (4.17)$$

where $\mathbf{F}_{\parallel}(t) = [\mathbf{F}(t) \cdot \mathbf{s}]\mathbf{s}$ is the component of $\mathbf{F}(t)$ parallel with the spin axis and $\mathbf{F}_{\perp}(t) = \mathbf{F}(t) - \mathbf{F}_{\parallel}(t)$ is the perpendicular component of $\mathbf{F}(t)$. The component \mathbf{F}_{\parallel} accelerates the spacecraft in the spin axis direction. The displacement due to the perpendicular component can be obtained by double integration with integration limits of $t = t_0$ and $t = t_0 + 2\pi n/\omega$:

$$\Delta \mathbf{x}_{\perp} = \frac{1}{\omega^2 m} \mathbb{R}(\omega t_0 - \pi) \cdot \dot{\mathbf{F}}_{\perp} \Delta t, \quad (4.18)$$

describing an arithmetic spiral around the spin axis. This spiral vanishes (i.e., the displacement of the spacecraft remains confined along the spin axis) if $\dot{\mathbf{F}} = 0$, and even for nonzero $\dot{\mathbf{F}}$ its radius increases only linearly with time, and thus in most cases, it can be ignored safely.

4.4.1 Modeling of maneuvers

There were several hundred²⁰ Pioneer 10 and Pioneer 11 maneuvers during their entire missions. The modeling of maneuvers entails significant uncertainty due to several reasons. First, the duration of a thruster firing is known only approximately and may vary between maneuvers due to thermal and mechanical conditions, aging, manufacturing deficiencies in the thruster assembly, and other factors. Second, the thrust can vary as a result of changing fuel temperature and pressure. Third, imperfections in the mechanical mounting of a thruster introduce uncertainties in the thrust direction. Lastly, after a thruster has fired, leakage may occur, producing an additional, small amount of slowly decaying thrust. When combined, these effects result in a velocity change of several mm/s.

By the time Pioneer 11 reached Saturn, the behavior of its thrusters was believed to be well understood [18]. The effectively instantaneous velocity change caused by the firing of a thruster was followed by several days of decaying acceleration due to gas leakage. This acceleration was large enough to be observable in the Doppler data [262].

²⁰The exact number of maneuvers is unknown due to incomplete records, although most maneuvers can be reconstructed from the preserved telemetry.

The Jet Propulsion Laboratory’s analysis of Pioneer orbits included either an instantaneous velocity increment at the beginning of each maneuver (instantaneous burn model) or a constant acceleration over the duration of the maneuver (finite burn model) [18]. In both cases, the burn is characterized by a single unknown parameter. The gas leak following the burn was modeled by fitting to the post-maneuver residuals a two-parameter exponential model in the form of

$$\Delta v(t) = v_0 \exp(-t/\tau), \quad (4.19)$$

with v_0 and τ being the unknown parameters. The typical magnitude of v_0 is several mm/s, while the time constant τ is of order ~ 10 days. Due to the spin of the spacecraft, only acceleration in the direction of the spin axis needs to be accounted for, as accelerations perpendicular to the spin axis are averaged out over several resolutions [18, 385].

4.4.2 Other sources of outgassing

Regardless of the source of a leak, the effects of outgassing on the spacecraft are governed by the rocket equation [18]:

$$a = -v_e \frac{\dot{m}}{m}, \quad (4.20)$$

where the dot denotes differentiation with respect to time, and v_e is the exhaust velocity. The Pioneer spacecraft mass is approximately $m \simeq 250$ kg. For comparison, the anomalous acceleration, $a_P = 8.74 \times 10^{-10} \text{ m/s}^2$, requires an outgassing rate of $\sim 6.89 \text{ g/yr}$ at an exhaust velocity of 1 km/s.

The exhaust velocity v_e of a hot gas, according to the rocket engine nozzle equation, can be calculated as [372]²¹:

$$v_e^2 = \frac{2kRT}{(k-1)M_{\text{mol}}} \left[1 - \left(\frac{P_e}{P_i} \right)^{(k-1)/k} \right], \quad (4.21)$$

where k is the isentropic expansion factor (or heat capacity ratio, $k = C_p/C_v$ where C_p and C_v are the heat capacities at constant pressure and constant volume, respectively) of the exhaust gas, T is its temperature, $R = 8314 \text{ JK}^{-1} \text{ kmol}^{-1}$ is the gas constant, m_{mol} is the molecular weight of the exhaust gas in kg/kmol, P_i is its pressure at the nozzle intake, and P_e is the exhaust pressure. At room temperature, $k = 1.41$ for H_2 , $k = 1.66$ for He , and $k = 1.40$ for O_2 . Typical values for liquid monopropellants are $1.7 \text{ km/s} < v_e < 2.9 \text{ km/s}$.

A review of the Pioneer 10 and 11 spacecraft design reveals only three possible sources of outgassing: the propulsion system (fuel leaks), the radioisotope thermoelectric generators, and the battery.

The propulsion system carried ~ 30 kg of hydrazine propellant and N_2 pressurant. Loss of either due to a leak could produce a constant or slowly changing acceleration term. Propellant and pressurant can be lost due to a malfunction in the propulsion system, and also due to the regular operation of thruster valves, which are known to have small, persistent leaks lasting days or even weeks after each thruster firing event, as described above in Section 4.4.1. While the possibility of additional propellant leaks cannot be ruled out, in order for such leaks to be responsible for a constant acceleration like the anomalous acceleration of Pioneer 10 and 11, they would have had to be i) constant in time; ii) the same on both spacecraft; iii) not inducing any detectable changes in the spin rate or precession. Given these considerations, Anderson et al. *conservatively* estimate that undetected gas leaks introduce an uncertainty not greater than

$$\sigma_{\text{gl}} = \pm 0.56 \times 10^{-10} \text{ m/s}^2. \quad (4.22)$$

Outgassing can also occur in the radioisotope thermoelectric generators as a result of alpha decay. Each kg of ^{238}Pu produces $\sim 0.132 \text{ g}$ of helium annually; the total amount of helium

²¹See also http://en.wikipedia.org/wiki/Rocket_engine_nozzles

produced by the approx. 4.6 kg of radioisotope fuel on board²² is, therefore, 0.6 g/year. Exterior temperatures of the RTGs at no point exceeded 320 ° F=433 K. According to Equation (4.21), the corresponding exhaust velocity is 2.13 km/s, resulting in an acceleration of $1.62 \times 10^{-10} \text{ m/s}^2$. (This is slightly larger than the corresponding estimate in [18], where the authors adopted the figures of $\dot{m} = 0.77 \text{ g/year}$ and $v_e = 1.16 \text{ km/s}$.) However, the circumstances required to achieve this acceleration are highly unrealistic, requiring all the helium to be expelled at maximum efficiency and in the spin axis direction. Using a more realistic (but still conservative) scenario, Anderson et al. estimate the bias and error in acceleration due to He-outgassing as

$$a_{\text{He}} = (0.15 \pm 0.16) \times 10^{-10} \text{ m/s}^2. \quad (4.23)$$

Another source of possible outgassing not previously considered may be the spacecraft's battery. According to Equation (4.21), H₂ gas leaving the battery system at a temperature of 300 K can acquire an exhaust velocity of 92.6 m/s. For O₂ at 300 K, the exhaust velocity is 23.2 m/s. At these velocities, an outgassing of $\sim 74 \text{ g/year}$ of H₂ or 298 g/year of O₂ can produce an acceleration equal to a_P , so the battery cannot be ruled out in principle as a source of a near constant acceleration term. However, no realistic construction [75] for a 5 A, 11.3 V AgCd battery would provide near enough volatile electrolytes for such outgassing to occur, and in any case, the nominal performance of the battery system for a far longer time period than designed indicates that no significant loss of volatiles from the battery has taken place. A conservative (but still generous) estimate using a battery of maximum weight, 2.35 kg, assuming a loss of 10% of its mass over 30 years, and a thrust efficiency of 50% yields

$$\sigma_{\text{bat}} = \pm 0.14 \times 10^{-10} \text{ m/s}^2. \quad (4.24)$$

4.4.3 Thermal recoil forces

The spacecraft carried several on-board energy sources that produced waste heat (see Section 2.4). Most notably among these are the RTGs; additional heat was produced by electrical instrumentation. Further heat sources include Radioisotope Heater Units and the propulsion system.

As the spacecraft is in an approximate thermal steady state, heat generated on board must be removed from the spacecraft [385]. In deep space, the only mechanism of heat removal is thermal radiation: the spacecraft can be said to be radiatively coupled to the cosmic background, which can be modeled by surrounding the spacecraft with a large, hollow spherical black body at the temperature of $\sim 2.7 \text{ K}$.

As the spacecraft emits heat in the form of thermal photons, these also carry momentum p_γ , in accordance with the well known law of $p_\gamma = h\nu/c$, where ν is the photon's frequency, h is Planck's constant, and c is the velocity of light. This results in a recoil force in the direction opposite to that of the path of the photon. For a spherically symmetric body, the net recoil force is zero. However, if the pattern of radiation is not symmetrical, the resulting anisotropy in the radiation pattern yields a net recoil force.

The magnitude of this recoil force is a subject of many factors, including the location and thermal power of heat sources, the geometry, physical configuration, and thermal properties of the spacecraft's materials, and the radiometric properties of its external (radiating) surfaces.

Key questions concerning the thermal recoil force that have been raised during the study of the Pioneer anomaly include [156, 236, 331]:

- How much heat from the RTGs is reflected by the spacecraft, notably the rear of its high-gain antenna, and in what direction?

²²The fuel inventory quoted in [18] is 5.8 kg. This much ²³⁸Pu would produce significantly more heat at the rate of 0.57 W/g than the known thermal power of the Pioneer RTGs. Likely, 5.8 kg was the total mass of the plutonium-molybdenum cermet pucks on board, which contained approximately 4.6 kg plutonium metal.

- Was there a fore-aft asymmetry in the radiation pattern of the RTGs due to differential aging?
- How much electrical heat generated on-board was radiated through the spacecraft's louver system?

The recoil force due to on-board generated heat that was emitted anisotropically was recognized early as a possible origin of the Pioneer anomaly. The total thermal inventory on board the Pioneer spacecraft exceeded 2 kW throughout most of their mission durations. The spacecraft were in an approximate steady state: the amount of heat generated on-board was equal to the amount of heat radiated by the spacecraft.

The mass of the Pioneer spacecraft was ~ 250 kg. An acceleration of $8.74 \times 10^{-10} \text{ m/s}^2$ is equivalent to a force of $\sim 0.22 \mu\text{N}$ acting on a ~ 250 kg object. This is the amount of recoil force produced by a 65 W collimated beam of photons. In comparison with the available thermal inventory of 2500 W, a fore-aft anisotropy of less than 3% can account for the anomalous acceleration in its entirety. Given the complex shape of the Pioneer spacecraft, it is certainly conceivable that an anisotropy of this magnitude is present in the spacecrafts' thermal radiation pattern.

The issue of the thermal recoil force remains a subject of on-going study, as estimates of the actual magnitude of this force may require significant revision in the light of new data and new investigations [383, 384, 385, 399].

4.4.4 The radio beam recoil force

Throughout most of their missions, the Pioneer 10 and 11 spacecraft were transmitting continuously in the direction of the Earth using a highly focused microwave radio beam that was emitted by the high gain antenna (HGA; see Section 2.4.5). The recoil force due to the radio beam can be readily calculated.

A naive calculation uses the nominal value of the radio beam's power (8 W), multiplied by the reciprocal of the velocity of light, c^{-1} , to obtain the radio beam recoil force. This is a useful way to estimate the recoil force, but it may need refinement.

The spacecraft's radio transmission is concentrated into a very narrow beam: signal attenuation exceeds 20 dB at only 3.75° deviation from the antenna centerline (see Figure 3.6-13 in [292]). The projected transmitter power P_0 in the beam direction can be computed using the integral $P_0 = \int d\theta \sin\theta \mathcal{P}(\theta)$ where $\mathcal{P}(\theta)$ is the angular power distribution of the antenna. Given the antenna power distribution, we find that $P_0 = P$, where P is the total power radiated by the antenna, to an accuracy much better than 1%. For this reason, the shape of the transmission beam needs not be taken into account when computing the recoil force.

However, as discussed in Section 2.4.5, the power of the spacecraft's transmitter was not constant in time: if the telemetry readings are accepted as reliable, transmitter power may have decreased by as much as 3 W or more near the end of Pioneer 10's mission. Furthermore, some (estimated $\sim 10\%$) of the radio beam may have missed the antenna dish altogether, resulting in a reduced efficiency with which the energy of the spacecraft's transmitter is converted into momentum.

Note that the navigational model that was used to navigate the Pioneers did not include this effect. It became clear only recently leading to the need to include this model as a part of the on-going efforts to re-analyze the Pioneer data.

4.5 Effects on the radio signal

The radio signal to or from the Pioneer spacecraft travels several billion kilometers in interplanetary space. Unsurprisingly, the interplanetary environment, notably charged particles emitted by the

Sun and the gravitational fields in the solar system all affect the length of the path that the radio signal travels and its frequency.

The communication antennas of the DSN complex that are used to exchange data with the Pioneer spacecraft are located on the Earth's surface. This introduces many corrections to the modeling of the uplinked or downlinked radio signal due to the orbital motion, rotation, internal dynamics and atmosphere of our home planet.

4.5.1 Plasma in the solar corona and weighting

The interplanetary medium in the solar system is dominated by the solar wind, i.e., charged particles originating from the Sun. Although their density is low, the presence of these particles has a noticeable effect on a radio frequency signal, especially when the signal passes relatively close to the Sun.

Delay due to solar plasma is a function of the electron density in the plasma. Although this can vary significantly as a result of solar activity, the propagation delay Δt (in microseconds) can be approximated using the formula [137]:

$$\Delta t = -\frac{1}{2cn_{\text{crit}}(f)} \int_{\oplus}^{SC} d\ell n_e(t, \mathbf{r}), \quad (4.25)$$

where f is the signal frequency, $n_{\text{crit}}(f)$ is the critical plasma density for frequency f that is given by

$$n_{\text{crit}}(f) = 1.240 \times 10^4 \left(\frac{f}{1 \text{ MHz}} \right)^2 \text{ cm}^{-3}, \quad (4.26)$$

and n_e is the electron density as a function of time t and position \mathbf{r} , which is integrated along the propagation path ℓ between the spacecraft and the Earth.

We write the electron density as a sum of a static, steady-state part, $n_e(\mathbf{r})$ and fluctuation $\delta n_e(t, \mathbf{r})$ [394]:

$$n_e(t, \mathbf{r}) = n_e(\mathbf{r}) + \delta n_e(t, \mathbf{r}). \quad (4.27)$$

The second term, which is difficult to quantify, has only a small effect on the Doppler observable [394], except at conjunction, when noise due to the solar corona dominates the Doppler observable. In contrast, the steady-state behavior of the solar corona is well known and can be approximated using the formula [11, 137, 233, 234]:

$$n_e(t, \mathbf{r}) = A \left(\frac{R_{\odot}}{r} \right)^2 + B \left(\frac{R_{\odot}}{r} \right)^{2.7} e^{-\left[\frac{\phi}{\phi_0} \right]^2} + C \left(\frac{R_{\odot}}{r} \right)^6. \quad (4.28)$$

where $R_0 = 6.96 \times 10^8$ m is the solar radius, and r is the distance from the Sun along the propagation path.

Using Equation (4.28) in Equation (4.25), we obtain the range model [18]:

$$\Delta \text{range} = \pm \left(\frac{f_0}{f} \right)^2 \left[A \left(\frac{R_{\odot}}{\rho} \right) F + B \left(\frac{R_{\odot}}{\rho} \right)^{1.7} e^{-\left[\frac{\phi}{\phi_0} \right]^2} + C \left(\frac{R_{\odot}}{\rho} \right)^5 \right], \quad (4.29)$$

where $f_0 = 2295$ MHz is the reference frequency used for the analysis of Pioneer 10, ρ is the impact parameter with respect to the Sun, and F is a light-time correction factor, which is given for distant spacecraft as

$$F = F(\rho, r_T, r_E) = \frac{1}{\pi} \left[\arctan \left(\frac{\sqrt{r_T^2 - \rho^2}}{\rho} \right) + \arctan \left(\frac{\sqrt{r_E^2 - \rho^2}}{\rho} \right) \right], \quad (4.30)$$

where r_T and r_E are the heliocentric radial distances to the target and to the Earth, respectively. The sign of the solar corona range correction is negative for Doppler measurements (positive for range).

The values of the parameters A , B , and C are: $A = 6.0 \times 10^3$, $B = 2.0 \times 10^4$, $C = 0.6 \times 10^6$, all in meters [18].

4.5.2 Effects of the ionosphere

As the radio signal to or from the spacecraft travels through the Earth's ionosphere, it suffers an additional propagation delay due to the presence of charged particles. This delay Δt can be modeled as [199, 328]

$$\Delta t_{\text{iono}} = -\frac{1}{cN \sin \theta} \int_0^{h_{\max}} N_{\text{iono}} dh, \quad (4.31)$$

where θ is the antenna elevation, N is the atmospheric refractivity index, N_{iono} is the ionospheric refractivity index, and h_{\max} is the height of the ionosphere. N can be approximated at 10^6 , while N_{iono} is well approximated by the formula

$$N_{\text{iono}} = -40.28 \times 10^6 \frac{n_e}{f^2}, \quad (4.32)$$

where n_e is the electron density and f is the signal frequency in Hz. We introduce the total electron content,

$$N_e = \int_0^{h_{\max}} n_e dh, \quad (4.33)$$

, which allows us to express the propagation delay in the form,

$$\Delta t_{\text{iono}} = \frac{40.28}{cf^2} N_e, \quad (4.34)$$

with $c = 3 \times 10^8$ m/s. For European latitudes, the total electron content may vary from very few electrons at night to $(20-100) \times 10^{16}$ electrons during the day at various stages during the solar cycle.

4.5.3 Effects of the troposphere

Chao ([357]; see also [109, 387, 158, 196, 334]) estimates the delay due to signal propagation through the troposphere using the following formula:

$$\Delta l_{\text{tropo}} = \frac{1}{\sin \theta + A/(\tan \theta + B)}, \quad (4.35)$$

where Δl_{tropo} is the additional propagation path, θ is the elevation angle, and $A = A_{\text{dry}} + A_{\text{wet}}$ and $B = B_{\text{dry}} + B_{\text{wet}}$ are coefficients defined as

$$A_{\text{dry}} = 0.00143, \quad (4.36)$$

$$A_{\text{wet}} = 0.00035, \quad (4.37)$$

$$B_{\text{dry}} = 0.0445, \quad (4.38)$$

$$B_{\text{wet}} = 0.017. \quad (4.39)$$

Unfortunately, historical weather data going back over 30 years may not be available for most DSN stations. In the absence of such data, C.B. Markwardt suggests that seasonal weather data or historical weather data from nearby weather stations can be used to achieve good modeling accuracy.²³

²³C.B. Markwardt, private communication.

4.5.4 The effect of spin

The radio signal emitted by the DSN and the radio signal returned by the Pioneer 10 and 11 spacecraft are circularly polarized. The spacecraft themselves are spinning, and the spin axis coincides with the axis of the HGA. Therefore, every revolution of the spacecraft adds a cycle to both the radio signal received by, and that transmitted by the spacecraft.

At a nominal rate of 4.8 revolutions per minute, the spacecraft spin adds 0.08 Hz to the radio signal frequency in each direction.

The sign of the spin contribution to the spacecraft frequency depends on whether or not the radio signal is left or right circularly polarized, and the direction of the spacecraft's rotation.

The rotation of the spacecraft is clockwise [292] as viewed from a direction behind the spacecraft, facing towards the Earth. This implies that the spacecraft spin would contribute to the frequency of a right circularly polarized (as seen from the transmitter) signal's frequency with a positive sign. The assumption that the DSN signal is right circularly polarized is consistent with the explanation provided in [231]. This interpretation of the spacecraft's spin in relation to the radio signal agrees with what one finds when comparing orbit data files with or without previously applied spin correction.

The total amount of spin correction, therefore, must be written as

$$\Delta_{\text{spin}}f = \left(1 + \frac{240}{221}\right) \frac{\omega}{2\pi}, \quad (4.40)$$

where ω is the angular velocity of the spacecraft, and we accounted for the Pioneer communication system turnaround ratio of 240/221.

4.5.5 Station locations

Accurate estimation of the amount of time it takes for a signal to travel between a DSN station and a distant spacecraft, and the frequency shift due to the relative motion of these, requires precise knowledge of the position and velocity of not just the spacecraft itself, but also of any ground stations participating in the communication.

DSN transmitting and receiving stations are located on the surface of the Earth. Therefore, their coordinates in a solar system barycentric frame of reference are determined primarily by the orbital motion, rotation, precession and nutation of the Earth.

In addition to these motions of the Earth, station locations also change relative to a geocentric frame of reference due to tidal effects and continental drift.

Information about station locations is readily available for stations presently in operation; however, for stations that are no longer operating, or for stations that have been relocated, it is somewhat more difficult to obtain (see Section 3.1.2).

The transformation of station coordinates from a terrestrial reference frame, such as ITRF93, to a celestial (solar system barycentric) reference frame can be readily accomplished using publicly available algorithms or software libraries, such as NASA's SPICE library²⁴ [4].

4.6 Modeling the radiometric Doppler observable

The Pioneer spacecraft were navigated using radiometric Doppler data²⁵. The Doppler observable is defined as the difference between the number of cycles received by a receiving station and the number of cycles produced by a (fixed or ramped) known reference frequency, during a specific count interval.

²⁴See also <http://naif.jpl.nasa.gov/>.

²⁵Some ranging observations were also performed for the Pioneer spacecraft, by varying the frequency of the transmitted signal and observing the corresponding changes in the signal received from the spacecraft.

The expected value of the Doppler observable can be calculated accurately if the trajectory of the transmitting station (e.g., a spacecraft) and receiving station (e.g., a ground-based tracking station) are known accurately, along with information about the transmission medium along the route of the received signal.

The trajectory of the spacecraft is determined using the spacecraft’s initial position and velocity according to Section 4.1, in conjunction with a model of nongravitational forces, as detailed in Section 4.4.

The signal propagation delay due to the gravitational field of solar system can be calculated using Equation (4.4). Afterwards, from the known arrival times of the first and last cycle during a Doppler count interval, the times of their transmission can be obtained. Given the known frequency of the transmitter, one can then calculate the actual number of cycles that were transmitted during this interval. Comparing the two figures gives the difference known as the Doppler residual.

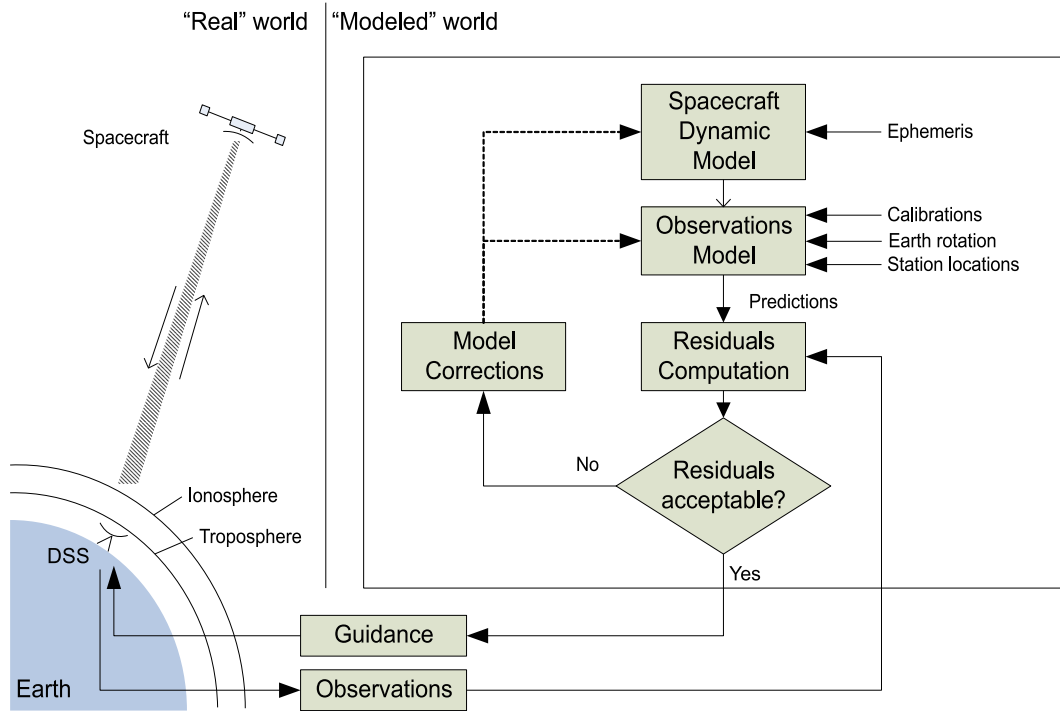


Figure 4.1: Schematic overview of the radio navigation process. Adapted from [379].

The model parameters, which include an estimate of the spacecraft’s initial state vector and other factors, can be adjusted to achieve a “best fit” between model and observation. A commonly used method to achieve a best fit is the use of a least squares estimator. The “solve-for” parameters can include orbital parameters of solar system bodies; the visible light and infrared radiometric properties of the spacecraft; or properties of the Earth’s atmosphere or the interplanetary medium.

While a spacecraft is in flight, the revised model can be used to make navigational predictions and provide guidance, as depicted in Figure 4.1. In the case of the historical Doppler data of Pioneer 10 and 11, the purpose is not to navigate a live spacecraft, but to provide a model of as large a segment of the spacecraft’s trajectory as possible, using a consistent set of parameters and minimizing the model residual. Several, independent efforts to analyze the trajectories of the two

spacecraft have demonstrated that this can be accomplished using multi-year spans of data with a root-mean-square model residual of no more than a few mHz.

4.7 Orbit determination and parameter estimation

The Pioneer anomaly has been verified using a variety of independent orbit determination codes. The code that was used for the initial discovery of the anomaly, JPL’s Orbit Determination Program (ODP), is probably also the most comprehensive and best tested among these, as it is the primary code that is being used to navigate US and many international spacecraft anywhere in the solar system, especially in very deep space. ODP is a complex engineering achievement that includes many thousands of lines of code that were built during the last 50 years of space exploration. The physical models in ODP draw on fundamental principles and practices developed during decades of deep space exploration (see [127, 195, 226, 231, 352, 379]). In its core, ODP relies on a program called “**Regress**” that calculates the computed values of Doppler (and other) observables obtained at the tracking stations of the DSN. **Regress** also calculates media corrections and partial derivatives of the computed values of the observables with respect to the solve-for-parameter vector-state.

An orbit determination procedure first determines the spacecraft’s initial position and velocity in a data interval. For each data interval, we then estimate the magnitudes of the orientation maneuvers, if any. The analysis uses models that include the effects of planetary perturbations, radiation pressure, the interplanetary media, general relativity, and bias and drift in the Doppler and range (if available). Planetary coordinates and solar system masses are obtained using JPL’s Export Planetary Ephemeris DE nnn , where DE stands for the Development Ephemeris and nnn is the current number. (Earlier in the study, DE200 and DE405 were used, presently DE412 is available.)

Current versions of ODP implement computations in the J2000.0 epoch. Past versions used B1950.0. (See [365] for details on the conversion of positions and proper motions between these two epochs.)

Standard ODP modeling includes a number of solid-Earth effects, namely precession, nutation, sidereal rotation, polar motion, tidal effects, and tectonic plates drift (see discussion in [18]). Model values of the tidal deceleration, nonuniformity of rotation, polar motion, Love numbers, and Chandler wobble are obtained observationally, by means of lunar and satellite laser ranging (LLR, SLR) techniques and very long baseline interferometry (VLBI). Currently this information is provided by way of the International Celestial Reference Frame (ICRF). JPL’s Earth Orientation Parameters (EOP) is a major source contributor to the ICRF.

Since the previous analysis [15, 18], physical models for the Earth’s interior and the planetary ephemeris have greatly improved. This is due to progress in GPS, SLR, LLR and VLBI techniques, Doppler spacecraft tracking, and new radio science data processing algorithms. ODP models have been updated using these latest Earth models (adopted by the IERS) and also are using the latest planetary ephemeris. This allows for a better characterization of not only the constant part of any anomalous acceleration, but also of the annual and diurnal terms detected in the Pioneer 10 and 11 Doppler residuals [18, 266, 391].

During the last few decades, the algorithms of orbital analysis have been extended to incorporate a Kalman-filter estimation procedure that is based on the concept of “process noise” (i.e., random, nonsystematic forces, or random-walk effects). This was motivated by the need to respond to the significant improvement in observational accuracy and, therefore, to the increasing sensitivity to numerous small perturbing factors of a stochastic nature that are responsible for observational noise. This approach is well justified when one needs to make accurate predictions of the spacecraft’s future behavior using only the spacecraft’s past hardware and electronics state history as well as the dynamic environmental conditions in the distant craft’s vicinity. Modern

navigational software often uses Kalman-filter estimation since it more easily allows determination of the temporal noise history than does the weighted least-squares estimation.

ODP also enables the use of batch-sequential filtering and a smoothing algorithm with process noise [18]. Though the name may imply otherwise, batch-sequential processing does not involve processing the data in batches. Instead, in this approach any small anomalous forces may be treated as stochastic parameters affecting the spacecraft trajectory. As such, these parameters are also responsible for the stochastic noise in the observational data. To characterize these noise sources, we split the data interval into a number of constant or variable size batches with respect to the stochastic parameters, and make assumptions on the possible statistical properties of the noise factors. We then estimate the mean values of the unknown parameters within the batch and their second statistical moments. (More details on this “batch-sequential algorithm with smoothing filter” in [127, 231]). ODP is permanently being updated to suit the needs of precision navigation; the progress in the estimation algorithms, programming languages, models of small forces and new navigation methods have strongly supported its recent upgrades.

There have been a number of new models developed that are needed for the analysis of tracking data from interplanetary spacecraft that are now an integral part of the latest generation of the JPL’s ODP. These include an update to the relativistic formulation of the planetary and spacecraft motion, relativistic light propagation and relevant radiometric observables (i.e., Doppler, range, VLBI, and Delta Differential One-way Ranging or Δ DOR), coordinate transformation between relativistic reference frames, and several models for nongravitational forces. Details on other models and their application for the analysis of the Pioneer anomaly are in [18, 394].

5 The Original 1995 – 2002 Study of the Pioneer Anomaly

The Pioneer 10 and 11 spacecraft have been described informally as the most precisely navigated deep space vehicles to date. Such precise navigation [15, 18, 252, 254, 391, 393, 394, 395] was made possible by many factors, including a conservative design (see Figure 2.3 for a design drawing of the spacecraft) that placed the spacecraft’s RTGs at the end of extended booms, providing added stability and reducing thermal effects. For attitude control, the spacecraft were spin-stabilized, requiring a minimum number of attitude correction maneuvers, further reducing navigation noise. As a result, precision navigation of the Pioneer spacecraft was possible across multi-year stretches spanning a decade or more [261].

Due in part to these excellent navigational capabilities, NASA supported a proposal to extend the Pioneer 10 and 11 missions beyond the originally planned mission durations, and use the spacecraft in an attempt to perform deep space celestial mechanics experiments, as proposed by J.D. Anderson from the Jet Propulsion Laboratory (JPL). Starting in 1979, the team led by Anderson began a systematic search for unmodeled accelerations in the trajectories of the two spacecraft. The principal aim of this investigation was the search for a hypothetical tenth planet, Planet X. Later, Pioneer 10 and 11 were used to search for trans-Neptunian objects; the superior quality of their Doppler tracking results also yielded the first ever limits on low frequency gravitational radiation [18].

The acceleration sensitivity of the Pioneer 10 and 11 spacecraft was at the level of $\sim 10^{-10}$ m/s². At this level of sensitivity, however, a small, anomalous, apparently constant Doppler frequency drift was detected [15, 18, 391].

5.1 The early evidence for the anomaly and the original study

By 1980, when Pioneer 10 had already passed a distance of ~ 20 AU from the Sun and the acceleration contribution from solar radiation pressure on the spacecraft had decreased to less than 4×10^{-10} m/s², the radiometric data started to show the presence of the anomalous sunward acceleration. Figure 5.1 shows these early unmodeled accelerations of Pioneer 10 (from about 1981 to 1989) and Pioneer 11 (from 1977 to 1989).

The JPL team continued to monitor the unexpected anomalous accelerations of Pioneer 10 and 11. Eventually, a proposal was made to NASA to initiate a formal study. The proposal argued that the anomaly is evident in the data of both spacecraft; that no physical model available can explain the puzzling behavior; and that, perhaps, an investigation with two independent software codes is needed to exclude the possibility of a systematic error in the navigational software. NASA supported the proposed investigation and, in 1995, the formal study was initiated at JPL and, independently, at the Aerospace Corporation, focusing solely on the acceleration anomaly detected in the radiometric Doppler data of both spacecraft Pioneer 10 and 11.

Acceleration estimates for Pioneer 10 and 11 were developed at the JPL using the Orbit Determination Program (ODP). The independent analysis performed by The Aerospace Corporation utilized a different software package called Compact High Accuracy Satellite Motion Program (CHASMP). This effort confirmed the presence of the anomalous acceleration, excluded computational systematics as a likely cause, and also indicated a possible detection of a sunward acceleration anomaly in the Galileo and Ulysses spacecrafts’ signals.

Standard navigational models account for a number of post-Newtonian perturbations in the dynamics of the planets, the Moon, and spacecraft. Models for light propagation are correct to order $(v/c)^2$. The equations of motion of extended celestial bodies are valid to order $(v/c)^4$. Non-gravitational effects, such as solar radiation pressure and precessional attitude-control maneuvers, make small contributions to the apparent acceleration we have observed. The solar radiation pressure decreases as r^{-2} ; at distances > 10 – 15 AU it produces an acceleration in the case of the

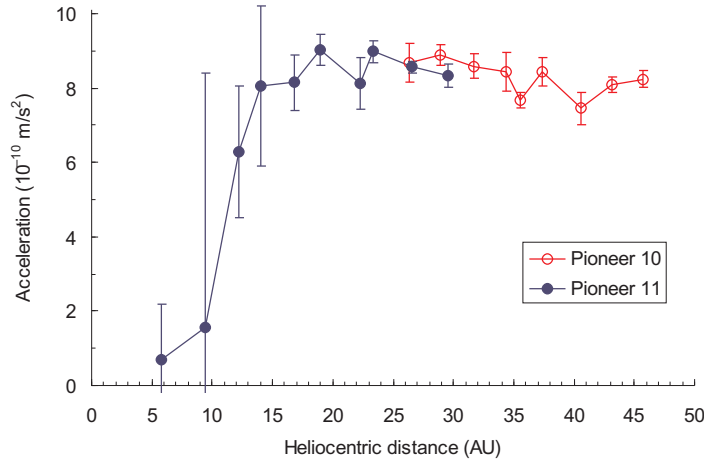


Figure 5.1: Early unmodeled sunward accelerations of Pioneer 10 (from about 1981 to 1989) and Pioneer 11 (from 1977 to 1989). Adapted from [18], which contained this important footnote: “Since both the gravitational and radiation pressure forces become so large close to the Sun, the anomalous contribution close to the Sun in [this figure] is meant to represent only what anomaly can be gleaned from the data, not a measurement.”

Pioneer 10 and 11 spacecraft that is much less than $8 \times 10^{-10} \text{ m/s}^2$, directed *away* from the Sun. (The acceleration due to the solar wind is roughly a hundred times smaller than this.)

The initial results of both teams (JPL and The Aerospace Corporation) were published in 1998 [15]. The JPL group concluded that there is indeed an unmodeled acceleration, a_P , towards the Sun, the magnitude of which is $(8.09 \pm 0.20) \times 10^{-10} \text{ m/s}^2$ for Pioneer 10 and $(8.56 \pm 0.15) \times 10^{-10} \text{ m/s}^2$ for Pioneer 11. The formal error is determined by the use of a five-day batch sequential filter with radial acceleration as a stochastic parameter, subject to white Gaussian noise (~ 500 independent five-day samples of radial acceleration). No magnitude variation of a_P with distance was found, within a sensitivity of $2 \times 10^{-10} \text{ m/s}^2$ over a range of 40 to 60 AU.

To determine whether or not the anomalous acceleration is specific to the spacecraft, an attempt was made to detect any anomalous acceleration signal in the tracking data of the Galileo and Ulysses spacecraft. It soon became clear that in the case of Galileo, the effects of solar radiation and an anomalous acceleration component cannot be separated. For Ulysses, however, a possible sunward anomalous acceleration was seen in the data, at $(12 \pm 3) \times 10^{-10} \text{ m/s}^2$. Thus, the data from the Galileo and Ulysses spacecraft yielded ambiguous results for the anomalous acceleration. Nevertheless, the analysis of data from these two additional spacecraft was useful in that it ruled out the possibility of a systematic error in the DSN Doppler system that could easily have been mistaken as a spacecraft acceleration.

The systematic error found in the Pioneer 10/11 post-fit residuals could not be eliminated by taking into account all known gravitational and nongravitational forces, both internal and external to the spacecraft. A number of potential causes have been ruled out. Continuing the search for an explanation, the authors considered the following forces and effects:

- gravity from the Kuiper belt (see Section 5.3.5);
- gravity from the galaxy (see Section 6.6.2);
- spacecraft gas leaks (see Section 4.4.2);
- errors in planetary ephemerides (see Section 6.7.1);

- errors in accepted values of the Earth’s orientation, precession and nutation (see Section 6.7.1);
- solar radiation pressure (see Section 4.3.1);
- precession attitude control maneuvers (see Section 6.5.2);
- radio beam recoil force (see Section 4.4.4);
- anisotropic thermal radiation (see Section 4.4.3).

Other possible sources of error were considered but none found to be able to explain the puzzling behavior of the two Pioneer spacecraft.

The availability of further data (the data spanned January 1987 to July 1998) from the then-still-active Pioneer 10 spacecraft allowed the collaboration to publish a revised solution for a_P . In 1999, based partially on this extended data set, they published a new estimate of the average Pioneer 10 acceleration directed towards the Sun, which was found to be $\sim 7.5 \times 10^{-10} \text{ m/s}^2$ [391]. The analyses used JPL’s Export Planetary Ephemeris DE200, and modeled planetary perturbations, general relativistic corrections, the Earth’s nonuniform rotation and polar rotation, and effects of radiation pressure and the interplanetary medium.

A possible systematic explanation of the anomalous residuals is nonisotropic thermal radiation. The thermal power of the spacecrafts’ radioisotope thermoelectric generators was in excess of 2500 W at launch with a half-life for the ^{238}Pu fuel of 87.74 years, and most of this power was thermally radiated into space. The power needed to explain the anomalous acceleration is $\sim 65 \text{ W}$. Nonetheless, anisotropically emitted thermal radiation was not seen as a likely explanation, for two reasons: first, it was assumed, after an initial analysis of the spacecraft’s geometry, that the thermal radiation would be largely isotropic, and further, the observed acceleration did not appear to be consistent with the decay rate of the radioactive fuel.

As a result of this work, it became clear that a detailed investigation of the Pioneer anomaly was needed.

5.2 The 2002 formal solution for the anomalous acceleration

The most definitive study to date of the Pioneer anomaly [18] used Pioneer 10 data from January 3, 1987 to July 22, 1998, and Pioneer 11 data from January 5, 1987 to October 1, 1990 (at this time, Pioneer 11 lost coherent mode capability, as described in Section 2.2.7). The data were again analyzed with two independently developed software packages, JPL’s ODP and The Aerospace Corporation’s CHASMP.

Following an analysis of the anomalous spin behavior of Pioneer 10 (see Section 2.3.7, and also Figure 2.16), the Pioneer 10 data set was further divided into three intervals. Interval I contained data January 3, 1987 to July 17, 1990; Interval II, from July 17, 1990 to July 12, 1992; and Interval III, from July 12, 1992 to July 22, 1998 (Table 5.1).

Analysis of results shown in Table 5.1 let the collaboration develop their estimate for the baseline “experimental” values for Pioneer 10 and 11 [18]. They found the optimally weighted least-squares solution “experimental” number for Pioneer 10:

$$a_{\text{exp}}^{\text{Pio10}} = (7.84 \pm 0.01) \times 10^{-10} \text{ m/s}^2. \quad (5.1)$$

Similarly, the experimental value for Pioneer 11 was found to be:

$$a_{\text{exp}}^{\text{Pio11}} = (8.55 \pm 0.02) \times 10^{-10} \text{ m/s}^2. \quad (5.2)$$

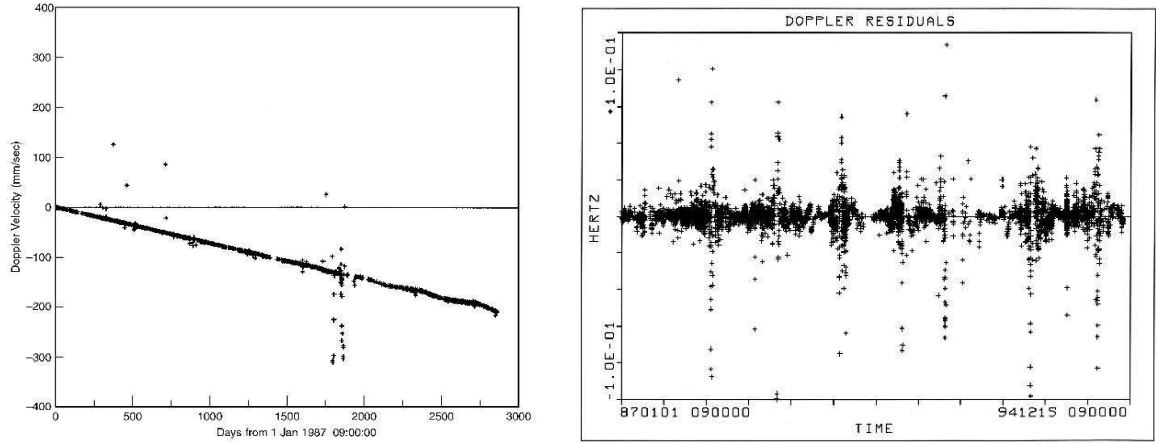


Figure 5.2: *Left*: Two-way Doppler residuals (observed Doppler velocity minus model Doppler velocity) for Pioneer 10. On the vertical axis, 1 Hz is equal to 65 mm/s range change per second. *Right*: The best fit for the Pioneer 10 Doppler residuals with the anomalous acceleration taken out. After adding one more parameter to the model (a constant radial acceleration of $a_P = (8.74 \pm 1.33) \times 10^{-10} \text{ m/s}^2$) the residuals are distributed about zero Doppler velocity with a systematic variation $\sim 3.0 \text{ mm/s}$ on a time scale of $\sim 3 \text{ months}$ [18].

Table 5.1: Acceleration estimates (in units of 10^{-10} m/s^2) published in [18]. Two programs (JPL’s ODP and The Aerospace Corporation’s CHASMP) were used to obtain weighted least squares (WLS) and batch-sequential filtering (BSF, 1-day batch) estimates. CHASMP could also incorporate corrections based on 10.7 cm solar flux observations, called F10.7 corrections.

Program	Method	Corona	P10 (I)	P10 (II)	P10 (III)	P11
ODP	WLS	no	8.02 ± 0.01	8.65 ± 0.01	7.83 ± 0.01	8.64 ± 0.04
ODP	WLS	yes	8.00 ± 0.01	8.66 ± 0.01	7.84 ± 0.01	8.44 ± 0.04
ODP	BSF	yes	7.82 ± 0.29	8.16 ± 0.40	7.59 ± 0.22	8.49 ± 0.33
CHASMP	WLS	no	8.25 ± 0.02	8.86 ± 0.02	7.85 ± 0.01	8.71 ± 0.03
CHASMP	WLS	yes	8.22 ± 0.02	8.89 ± 0.02	7.92 ± 0.01	8.69 ± 0.03
CHASMP	WLS+F10.7	yes	8.25 ± 0.03	8.90 ± 0.03	7.91 ± 0.01	8.91 ± 0.04

The main conclusions of the 2002 study [18] can be summarized as follows:

- The tracking data of Pioneer 10 and 11 are consistent with constant sunward acceleration;
- The magnitude of acceleration is several times noise level;
- No known source of error or systematic bias can account for the anomalous acceleration.

Initial announcement of the anomalous acceleration (e.g., [15, 391]) triggered many proposals that invoked various conventional physics mechanisms, all aimed at explaining the origin of the anomaly. Finding a systematic origin of the proper magnitude and behavior was the main focus of these proposals. Although the most obvious explanation would be that there is a systematic origin to the effect, perhaps generated by the spacecraft themselves from anisotropic heat rejection or propulsive gas leaks, the analysis did not find evidence for either mechanism: That is, no unambiguous, on-board systematic has been discovered.

This initial search was summarized in [18, 19], where possible contributions of various mechanisms to the final solution for a_P were given. The entire error budget was subdivided in three main types of effects, namely i) effects due to sources external to the spacecraft; ii) the contribution of on-board systematics; and iii) computational systematic errors (see Table 5.2.) These three categories are detailed in the following sections.

5.3 Sources of systematic error external to the spacecraft

External forces can contribute to all three vector components of spacecraft acceleration (in contrast, as detailed in Section 6, forces generated on board contribute primarily along the axis of rotation). However, nonradial spacecraft accelerations are difficult to observe by the Doppler technique, which measures the velocity along the Earth-spacecraft line of sight, which approximately coincides with the spacecraft spin axis.

Following [15, 18, 391], we first consider forces that affect the spacecraft motion, such as those due to i) solar-radiation pressure, and ii) solar wind pressure. We then discuss the effects on the propagation of the radio signal that are from iii) the solar corona and its mismodeling, iv) electromagnetic Lorentz forces, v) the influence of the Kuiper belt, vi) the phase stability of the reference atomic clocks, and vii) the mechanical and phase stability of the DSN antennae, together with influence of the station locations and troposphere and ionosphere contributions. Although some of the mechanisms detailed below are near the limit for contributing to the final error budget, it was found that none of them could explain the behavior of the detected signal. Moreover, some were three orders of magnitude or more too small.

5.3.1 Direct solar radiation pressure and mass

[18] estimated the systematic error from solar radiation pressure on the Pioneer 10 spacecraft over the interval from 40 to 70.5 AU, and for Pioneer 11 from 22.4 to 31.7 AU. Using Equation (4.8) they estimated that when the spacecraft reached 10 AU, the solar radiation acceleration was $18.9 \times 10^{-10} \text{ m/s}^2$ decreasing to $0.39 \times 10^{-10} \text{ m/s}^2$ at 70 AU. Because this contribution falls off with the inverse square of the spacecraft's heliocentric distance, it can bias the Doppler determination of a constant acceleration. By taking the average of the inverse square acceleration curve over the Pioneer distance, [18] estimated the error in the acceleration of the spacecraft due to solar radiation pressure. This error, in units of 10^{-10} m/s^2 , is $\sigma_{\text{sp}} = 0.001$ for Pioneer 10 over the interval from 40 to 70.5 AU, and six times this amount for Pioneer 11 over the interval from 22.4 to 31.7 AU. In addition the uncertainty in the spacecraft's mass for the studied data interval also introduced a bias of $b_{\text{sp}} = 0.03 \times 10^{-10} \text{ m/s}^2$ in the acceleration value. These estimates resulted in the error estimates

$$\delta a_{\text{sp}}^{\text{Pio10}} = b_{\text{sp}} \pm \sigma_{\text{sp}}^{\text{Pio10}} = (0.03 \pm 0.001) \times 10^{-10} \text{ m/s}^2, \quad (5.3)$$

$$\delta a_{\text{sp}}^{\text{Pio11}} = b_{\text{sp}} \pm \sigma_{\text{sp}}^{\text{Pio11}} = (0.03 \pm 0.006) \times 10^{-10} \text{ m/s}^2. \quad (5.4)$$

5.3.2 The solar wind

The acceleration caused by solar wind particles intercepted by the spacecraft can be estimated, as discussed in Section 4.3.2. Due to variations with a magnitude of up to 100%, the exact acceleration is unpredictable, but its magnitude is small, therefore its contribution to the Pioneer acceleration is completely negligible. Based on these arguments, the authors of [18] concluded that the total uncertainty in a_P due to solar wind can be limited as

$$\sigma_{\text{sw}} \leq 10^{-15} \text{ m/s}^2. \quad (5.5)$$

5.3.3 The effects of the solar corona

Given Equation (4.30) derived in Section 4.5.1 and the values of the parameters $(A, B, C) = (6.0 \times 10^3, 2.0 \times 10^4, 0.6 \times 10^6)$, all in meters, [18] estimated the acceleration error due to the effect of the solar corona on the propagation of radio waves between the Earth and the spacecraft.

The correction to the Doppler frequency shift is obtained from Equation (4.30) by simple time differentiation. (The impact parameter depends on time as $\rho = \rho(t)$ and may be expressed in terms of the relative velocity of the spacecraft with respect to the Earth, $v \approx 30$ km/s).

The effect of the solar corona is expected to be small on the Doppler frequency shift, which is our main observable. This is due to the fact that most of the data used for the Pioneer analysis were taken with large Sun-Earth-spacecraft angles. Further, the solar corona effect on the Doppler observable has a periodic signature, corresponding to the Earth's orbital motion, resulting in variations in the Sun-Earth-spacecraft angle. The time-averaged effect of the corona on the propagation of the Pioneers' radio-signals is of order

$$\sigma_{\text{corona}} = \pm 0.02 \times 10^{-10} \text{ m/s}^2. \quad (5.6)$$

5.3.4 Electro-magnetic Lorentz forces

The authors of [394] considered the possibility that the Pioneer spacecraft can hold a charge and be deflected in its trajectory by Lorentz forces. They noted that this was a concern during planetary flybys due to the strength of Jupiter's and Saturn's magnetic fields (see Figure 2.1). The magnetic field strength in the outer solar system, $\leq 10^{-5}$ Gauss, is five orders of magnitude smaller than the magnetic field strengths measured by the spacecraft at their nearest approaches to Jupiter: 0.185 Gauss for Pioneer 10 and 1.135 Gauss for Pioneer 11. Data from the Pioneer 10 plasma analyzer can be interpreted as placing an upper bound of $0.1\mu\text{C}$ on the positive charge during its Jupiter encounter [261].

These bounds allow us to estimate the upper limit of the contribution of the electromotive force on the motion of the Pioneer spacecraft in the outer solar system. This was accomplished in [18] using the standard formula for the Lorentz-force, $\mathbf{F} = q\mathbf{v} \times \mathbf{B}$, and found that the greatest force would be on Pioneer 11 during its closest approach to Jupiter, $< 20 \times 10^{-10} \text{ m/s}^2$. However, once the spacecraft reached the interplanetary medium, this force would decrease to

$$\sigma_{\text{Lorentz}} \lesssim 2 \times 10^{-14} \text{ m/s}^2, \quad (5.7)$$

, which is negligible.

5.3.5 The Kuiper belt's gravity

[18] specifically studied three distributions of matter in the Kuiper belt, including a uniform distribution and resonance distributions that were hypothesized in [180]. The authors assumed a total mass of one Earth mass, which is significantly larger than standard estimates. Even so, the resulting accelerations are only on the order of 10^{-11} m/s^2 , two orders of magnitude less than the observed effect. The calculated accelerations vary with time, increasing as Pioneer 10 approaches the Kuiper belt, even with a uniform density model. For these reasons, [18] excluded the dust belt as a source for the Pioneer effect.

More recent infrared observations established an upper limit of 0.3 Earth masses of Kuiper Belt dust in the trans-Neptunian region [32, 367, 375]. Therefore, for the contribution of Kuiper belt gravity, the authors of [18] placed a limit of

$$\sigma_{\text{KB}} = 0.03 \times 10^{-10} \text{ m/s}^2. \quad (5.8)$$

5.3.6 Stability of the frequency references

Reliable detection of a precision Doppler observable requires a very stable frequency reference at the observing stations. High precision Pioneer 10 and 11 Doppler measurements were made using 2-way and 3-way Doppler observations. In this mode, there was no on-board frequency reference at the spacecraft; the received frequency was converted to a downlink frequency using a fixed frequency ratio (240/221), and this signal was returned to the Earth. As the round-trip light time was many hours, the stability of the frequency reference over such timescales is essential. Further, in the case of 3-way Doppler measurements when the transmitting and receiving stations were not the same, it was essential to have stable frequency references that were synchronized between ground stations of the DSN.

The stability of a clock or frequency reference is usually measured by its Allan deviation. The Allan deviation $\sigma_y(\tau)$, or its square, the Allan-variance, are defined as the variance of the frequency departure $y_n = \langle \delta\nu/\nu \rangle_n$ (where ν is the frequency and $\delta\nu$ is its variance during the measurement period) over a measurement period τ :

$$\sigma_y^2(\tau) = \frac{1}{2} \langle (y_{n+1} - y_n)^2 \rangle, \quad (5.9)$$

where angle brackets indicate averaging.

The S-band communication systems of the DSN that were used for communicating with the Pioneer spacecraft had Allan deviations that are of order $\sigma_y \sim 1.3 \times 10^{-12}$ or less for $\sim 10^3$ s integration times [394]. Using the Pioneer S-band transmission frequency as $\nu \simeq 2.295$ GHz, we obtain

$$\delta\nu = \sigma_y \nu \simeq 2.98 \text{ mHz} \quad (5.10)$$

over a Doppler integration time of $\sim 10^3$ s. Applying this figure to the case of a steady frequency drift, the corresponding acceleration error over the course of a year was estimated [18] as

$$\sigma_{\text{freq}} = 0.0003 \times 10^{-10} \text{ m/s}^2. \quad (5.11)$$

5.3.7 Stability of DSN antenna complexes

The measurement of the frequency of a radio signal is affected by the stability of physical antenna structures. The large antennas of the DSN complexes are not perfectly stable. Short term effects include thermal expansion, wind loading, tides and ocean loading. Long term effects are introduced by continental drift, gravity loads and the aging of structures.

All these effects are well understood and routinely accounted for as part of DSN operations. DSN personnel regularly assess the performance of the DSN complex to ensure that operational limits are maintained [356, 357].

The authors of [18] found that none of these effects can produce a constant drift comparable to the observed Pioneer Doppler acceleration. Their analysis, which included errors due to imperfect knowledge of DSN station locations, to troposphere and ionosphere models at different stations, and to Faraday rotation effects of the atmosphere, shows a negligible contribution to the observed acceleration:

$$\sigma_{\text{DSN}} \leq 10^{-14} \text{ m/s}^2. \quad (5.12)$$

5.4 Sources of systematic error internal to the spacecraft

There exist several on-board mechanisms that can contribute to the acceleration of the Pioneer spacecraft. For spinning spacecraft, like Pioneer 10 and 11, the contribution of these forces to the spacecraft's acceleration will be primarily in the direction of the spin axis. The reason for

this is that for any force that is constant in a co-rotating coordinate system, the force component that is perpendicular to the spin axis will average to zero over the course of a full revolution. Consequently, for an arbitrary force, its contribution to lateral accelerations will be limited to its time-varying component (see Section 4.4).

There are several known forces of on-board origin that can result in unmodeled accelerations. These forces, in fact, represent the most likely sources of the anomaly, in particular because previously published magnitudes of several of the considered effects are subject to revision, in view of the recently recovered telemetry data and newly developed thermal models.

On-board mechanisms that we consider in this section include: i) thruster gas leaks, ii) non-isotropic radiative cooling of the spacecraft body, iii) heat from the RTGs, iv) the radio beam reaction force, and v) the expelled helium produced within the RTG and other gas emissions.

We also review the differences in experimental results between the two spacecraft.

5.4.1 Propulsive mass expulsion

The attitude control subsystems on board Pioneer 10 and 11 were used frequently to ensure that the spacecrafts' antennas remained oriented in the direction of the Earth. This raises the possibility that the observed anomalous acceleration is due to mismodeling of these attitude control maneuvers, or inadequate modeling of the inevitable gas leaks that occur after thruster firings.

The characteristics of propulsive gas leaks are well understood and routinely modeled by trajectory estimation software. Typical gas leaks vary in magnitude after each thruster firing, and usually decrease in time, until they become negligible.

The placement of thrusters (see Section 2.2.5) makes it highly likely that any leak would also induce unaccounted-for changes in the spacecraft's spin and attitude.

In contrast, to produce the observed acceleration, any propulsion system leaks would have had to be i) constant in time; ii) the same on both spacecraft; iii) not inducing any detectable changes in the spin rate or precession. Given these considerations, [18] *conservatively* estimates that undetected gas leaks introduce an uncertainty no greater than

$$\sigma_{gl} = \pm 0.56 \times 10^{-10} \text{ m/s}^2. \quad (5.13)$$

5.4.2 Heat from the RTGs

The radioisotope thermoelectric generators of the Pioneer 10 and 11 spacecraft emitted up to ~ 2500 W of heat at the beginning of the mission, slowly decreasing to ~ 2000 W near the end. Even a small anisotropy ($< 2\%$) in the thermal radiation pattern of the RTGs can account, in principle, for the observed anomalous acceleration. Therefore, the possibility that the observed acceleration is due to anisotropically emitted RTG heat has been considered [18, 394].

The cylindrical RTG packages (see Section 2.2.3) have geometries that are fore-aft symmetrical. Two mechanisms were considered that would nonetheless lead to a pattern of thermal radiation with a fore-aft asymmetry.

According to one argument, heat emitted by the RTGs would be reflected anisotropically by the spacecraft itself, notably by the rear of the HGA.

[18] used the spacecraft geometry and the resultant RTG radiation pattern to estimate the contribution of the RTG heat reflecting off the spacecraft to the Pioneer anomaly. The solid angle covered by the antenna as seen from the RTG packages was estimated at $\sim 2\%$ of 4π steradians. The equivalent fraction of RTG heat is ~ 40 W. This estimate was further reduced after the shape of the RTGs (cylindrical with large radiating fins) and the resulting anisotropic radiation pattern of the RTGs was considered. Thus, [18] estimated that this mechanism could produce only 4 W of directed power.

The force from 4 W of directed power suggests a systematic bias of $\approx 0.55 \times 10^{-10} \text{ m/s}^2$. The authors also add an uncertainty of the same size, to obtain a contribution from heat reflection of

$$a_{\text{hr}} = (-0.55 \pm 0.55) \times 10^{-10} \text{ m/s}^2. \quad (5.14)$$

Another mechanism may also have contributed to a fore-aft asymmetry in the thermal radiation pattern of the RTGs. Especially during the early part of the missions, one side of the RTGs was exposed to continuous intense solar radiation, while the other side was in permanent darkness. Furthermore this side, facing deep space, was sweeping through the dust contained within the solar system. These two processes may have led to different modes of surface degradation, resulting in changing emissivities [198].

To obtain an estimate of the uncertainty, [18] considered the case when one side (fore or aft) of the RTGs has its emissivity changed by only 1% with respect to the other side.²⁶ In a simple cylindrical model of the RTGs, with 2000 W power (only radial emission is assumed with no loss out of the sides), the ratio of the power emitted by the two sides would be $995/1005 = 0.99$, or a differential emission between the half cylinders of 10 W. Therefore, the fore/aft asymmetry toward the normal would be $10 \text{ W} \times \frac{1}{\pi} \int_0^\pi d\phi \sin \phi \approx 6.37 \text{ W}$. A more sophisticated model of the fin structure resulted in the slightly smaller estimate of 6.12 W, which the authors of [18] took as the uncertainty from the differential emissivity of the RTGs, to obtain an acceleration uncertainty of

$$\sigma_{\text{de}} = 0.85 \times 10^{-10} \text{ m/s}^2. \quad (5.15)$$

5.4.3 Nonisotropic radiative cooling of the spacecraft

It has also been suggested that the anomalous acceleration seen in the Pioneer 10/11 spacecraft can be, “explained, at least in part, by nonisotropic radiative cooling of the spacecraft [236].” Later this idea was modified, suggesting that “most, if not all, of the unmodeled acceleration” of Pioneer 10 and 11 is due to an essentially constant supply of heat coming from the central compartment, directed out the front of the craft through the closed louvers [330].

To address the original proposal [236] and several later modifications [330, 331], [16, 19, 329] developed a bound on the constancy of a_P . This bound came from first noting the 11.5 year 1-day batch-sequential result, sensitive to time variation: $a_P = (7.77 \pm 0.16) \times 10^{-10} \text{ m/s}^2$. It is conservative to take three times this error to be our systematic uncertainty for radiative cooling of the craft,

$$\sigma_{\text{rc}} = \pm 0.48 \times 10^{-10} \text{ m/s}^2. \quad (5.16)$$

5.4.4 Radio beam reaction force

The emitted radio-power from the spacecraft’s HGA produces a recoil force, which is responsible for an acceleration bias, b_{rp} , on the spacecraft away from the Earth. If the spacecraft were equipped with ideal antennas, the total emitted power of the spacecrafts’ radio transmitters would be in the form of a collimated beam aimed in the direction of the Earth. In reality, the antenna is less than 100% efficient: some of the radio frequency energy from the transmitter may miss the antenna altogether, the radio beam may not be perfectly collimated, and it may not be aimed precisely in the direction of the Earth.

Therefore, using β to denote the efficiency of the antenna, we can compute an acceleration bias as

$$b_{\text{rp}} = \frac{1}{mc} \beta P_{\text{rp}}, \quad (5.17)$$

²⁶A fore-aft difference of 1% is possible, but not supported by any available data.

where P_{rp} is the transmitter's power. The nominal transmitted power of the spacecraft is 8 W. Given the $m = 241$ kg as the mass of a spacecraft with half its fuel gone, and using the 0.4 dB antenna error as a means to estimate the uncertainty, we obtain the acceleration figure of

$$a_{\text{rp}} = b_{\text{rp}} \pm \sigma_{\text{rp}} = -(1.10 \pm 0.10) \times 10^{-10} \text{ m/s}^2, \quad (5.18)$$

where the negative sign indicates that this acceleration is in the direction *away* from the Earth (and thus from the Sun), i.e., this correction actually *increases* the amount of anomalous acceleration required to account for the Pioneer Doppler observations [18].

5.4.5 Expelled helium produced within the RTGs

Another possible on-board systematic error is from the expulsion of the He being created in the RTGs from the α -decay of ^{238}Pu . According to the discussion presented in Section 4.4.2, Anderson et al. estimate the bias and error in acceleration due to He-outgassing as

$$a_{\text{He}} = (0.15 \pm 0.16) \times 10^{-10} \text{ m/s}^2. \quad (5.19)$$

5.4.6 Variation between determinations from the two spacecraft

Section 5.2 presented two experimental results for the Pioneer anomaly from the two spacecraft: $7.84 \times 10^{-10} \text{ m/s}^2$ (Pioneer 10) and $8.55 \times 10^{-10} \text{ m/s}^2$ (Pioneer 11). The first result represents the entire 11.5 year data period for Pioneer 10; Pioneer 11's result represents a 3.75 year data period.

The difference between the two craft could be due to differences in gas leakage. It also could be due to heat emitted from the RTGs. In particular, the two sets of RTGs have had different histories and so might have different emissivities. Pioneer 11 spent more time in the inner solar system (absorbing radiation). Pioneer 10 has swept out more dust in deep space. Further, Pioneer 11 experienced about twice as much Jupiter/Saturn radiation as Pioneer 10.

[18] estimated the value for the Pioneer anomaly based on the two independent determinations derived from the two spacecraft, Pioneer 10 and 11. They calculated the time-weighted average of the experimental results from the two craft: $[(11.5)(7.84) + (3.75)(8.55)]/(15.25) = 8.01$ in units of 10^{-10} m/s^2 . This result implies a bias of $b_{2 \text{ craft}} = 0.17 \times 10^{-10} \text{ m/s}^2$ with respect to the Pioneer 10 experimental result $a_{P(\text{exp})}$ (see Equation (5.1)). We can take this number to be a measure of the uncertainty from the separate spacecraft measurements, so the overall quantitative measure is

$$a_{2 \text{ craft}} = b_{2 \text{ craft}} \pm \sigma_{2 \text{ craft}} = (0.17 \pm 0.17) \times 10^{-10} \text{ m/s}^2. \quad (5.20)$$

5.5 Computational systematics

The third group of effects was composed of contributions from computational errors (see Table 5.2). The effects in this group dealt with i) the numerical stability of least-squares estimations, ii) accuracy of consistency/model tests, iii) mismodeling of maneuvers, and that of iv) the solar corona model used to describe the propagation of radio waves. It has also been demonstrated that the influence of v) annual/diurnal terms seen in the data on the accuracy of the estimates was small.

5.5.1 Numerical stability of least-squares estimation

The authors of [18] looked at the numerical stability of the least squares estimation algorithms and the derived solutions.

Common precision orbit determination algorithms use double precision arithmetic. The representation uses a 53-bit mantissa, equivalent to more than 15 decimal digits of precision [140]. Is

this accuracy sufficient for precision orbit determination within the solar system? At solar system barycentric distances between 1 and 10 billion kilometers (10^{12} – 10^{13} m), 15 decimal digits of accuracy translates into a positional error of 1 cm or less. Therefore, we can conclude that double precision arithmetic is adequate in principle for modeling the orbits of Pioneer 10 and 11 in the outer solar system in a solar system barycentric reference frame. However, one must still be concerned about cumulative errors and the stability of the employed numerical algorithms.

The leading source for computational errors in finite precision arithmetic is the addition of quantities of different magnitudes, causing a loss of least significant digits in the smaller quantity. In extreme cases, this can lead to serious instabilities in numerical algorithms. Software codes that perform matrix operations are especially vulnerable to such stability issues, as are algorithms that use finite differences for solving systems of differential equations numerically.

While it is difficult to prove that a particular solution is not a result of a numerical instability, it is extremely unlikely that two independently-developed programs could produce compatible results that are nevertheless incorrect, as a result of computational error. Therefore, verifying a result using independently-developed software codes is a reliable way to exclude numerical instabilities as a possible error source, and also to put a limit on any numerical errors.

In view of the above, given the excellent agreement in various implementations of the modeling software, the authors of [18] concluded that differences in analyst choices (parameterization of clocks, data editing, modeling options, etc.) give rise to coordinate discrepancies only at the level of 0.3 cm. This number corresponds to an uncertainty in estimating the anomalous acceleration on the order of 8×10^{-14} m/s², which was found to be negligible for the investigation.

Analysis identified, however, a slightly larger error to contend with. After processing, Doppler residuals at JPL were rounded to 15 and later to 14 significant figures. When the Block 5 receivers came online in 1995, Doppler output was further rounded to 13 significant digits. According to [18], this roundoff results in the estimate for the numerical uncertainty of

$$\sigma_{\text{num}} = \pm 0.02 \times 10^{-10} \text{ m/s}^2. \quad (5.21)$$

5.5.2 Model consistency

The accuracy of navigational codes that are used to model the motion of spacecraft is limited by the accuracy of the mathematical models employed by the programs to model the solar system. The two programs used in the investigation – JPL’s ODP/*Sigma* modeling software and The Aerospace Corporation’s POEAS/CHASMP software package – used different parameter estimation procedures, employed different realizations of the Earth’s orientation parameters, used different planetary ephemerides, and different data editing strategies. While it is possible that some of the differences were partially masked by maneuver estimations, internal consistency checks indicated that the two solutions were consistent at the level of one part in 10^{15} , implying an acceleration error $\leq 10^{-4} a_P$ [18].

The consistency of the models was verified by comparing separately the Pioneer 11 results and the Pioneer 10 results for the three intervals studied in [18]. The models differed, respectively, by (0.25, 0.21, 0.23, 0.02) m/s². Assuming that these errors are uncorrelated, [18] computed the combined effect on anomalous acceleration a_P as

$$\sigma_{\text{consist/model}} = \pm 0.13 \times 10^{-10} \text{ m/s}^2. \quad (5.22)$$

5.5.3 Error due to mismodeling of maneuvers

The velocity change that results from a propulsion maneuver cannot be modeled exactly. Mechanical uncertainties, fuel properties and impurities, valve performance, and other factors all contribute uncertainties. The authors of [18] found that for a typical maneuver, the standard error

in the residuals is $\sigma_0 \sim 0.095$ mm/s. Given 28 maneuvers during the Pioneer 10 study period of 11.5 years, a mismodeling of this magnitude would contribute an error to the acceleration solution with a magnitude of $\delta a_{\text{man}} = \sigma_0/\tau = 0.07 \times 10^{-10}$ m/s². Assuming a normal distribution around zero with a standard deviation of δa_{man} for each single maneuver, a total of $N = 28$ maneuvers yields a total error of

$$\sigma_{\text{man}} = \frac{\delta a_{\text{man}}}{\sqrt{N}} = 0.01 \times 10^{-10} \text{ m/s}^2, \quad (5.23)$$

due to maneuver mismodeling.

5.5.4 Annual/diurnal mismodeling uncertainty

In addition to the constant anomalous acceleration term, an annual sinusoid has been reported [18, 391]. The peaks of the sinusoid occur when the spacecraft is nearest to the Sun in the celestial sphere, as seen from the Earth, at times when the Doppler noise due to the solar plasma is at a maximum. A parametric fit to this oscillatory term [18, 394] modeled this sinusoid with amplitude $v_{\text{at}} = (0.1053 \pm 0.0107)$ mm/s, angular velocity $\omega_{\text{at}} = (0.0177 \pm 0.0001)$ rad/day, and bias $b_{\text{at}} = (0.0720 \pm 0.0082)$ mm/s, resulting in post-fit residuals of $\sigma_T = 0.1$ mm/s, averaged over the data interval T .

The obtained amplitude and angular velocity can be combined to form an acceleration amplitude: $a_{\text{at}} = v_{\text{at}}\omega_{\text{at}} = (0.215 \pm 0.022) \times 10^{-10}$ m/s². The likely cause of this apparent acceleration is a mismodeling of the orbital inclination of the spacecraft to the ecliptic plane [18, 394].

[18] estimated the annual contribution to the error budget for a_P . Combining σ_T and the magnitude of the annual sinusoidal term for the entire Pioneer 10 data span, they calculated

$$\sigma_{\text{at}} = 0.32 \times 10^{-10} \text{ m/s}^2. \quad (5.24)$$

This number is assumed to be the systematic error from the annual term.

[18] also indicated the presence of a significant diurnal term, with a period that is approximately equal to the sidereal rotation period of the Earth, 23^h56^m04^s.0989. The magnitude of the diurnal term is comparable to that of the annual term, but the corresponding angular velocity is much larger, resulting in large apparent accelerations relative to a_P . These large accelerations, however, average out over long observational intervals, to less than 0.03×10^{-10} m/s² over a year. The origin of the annual and diurnal terms is likely the same modeling problem [18].

These small periodic modeling errors are effectively masked by maneuvers and plasma noise. However, as they are uncorrelated with the observed anomalous acceleration (characterized by an essentially linear drift, not annual/diurnal sinusoidal signatures), they do not represent a source of systematic error.

5.6 Error budget and the final 2002 result

The results of the 2002 study [18] are summarized in Table 5.2. Sources that contribute to the overall bias and error budget are grouped depending on their origin: external to the spacecraft, generated on-board, or computational in nature. Sources of error are treated as uncorrelated; the combined error is the root sum square of the individual error values.

The contribution of effects in the first group in Table 5.2, that is, effects external to the spacecraft to the overall error budget is negligible: $\sigma_{\text{external}} \sim 0.04 \times 10^{-10}$ m/s². The second group (on-board effects) yields the largest error contribution: $\sigma_{\text{on-board}} \sim 1.29 \times 10^{-10}$ m/s². Lastly, computational systematics amount to $\sigma_{\text{comp}} \sim 0.35 \times 10^{-10}$ m/s².

Similarly, the largest contribution to bias comes from on-board effects: $b_{\text{on-board}} \sim 0.87$ m/s², a value that is dominated by the radio beam reaction force. External effects contribute a bias of $b_{\text{external}} \sim 0.03$ m/s², while computational systematics contribute no bias.

Table 5.2: Error budget: a summary of biases and uncertainties as known in 2002 [18]. Values that are the subject of on-going study are marked by an asterisk.

Item	Description of error budget constituents	Bias 10^{-10} m/s^2	Uncertainty 10^{-10} m/s^2
1	Systematics generated external to the spacecraft:		
	a) Solar radiation pressure and mass	+0.03	± 0.01
	b) Solar wind		$\pm < 10^{-5}$
	c) Solar corona		± 0.02
	d) Electro-magnetic Lorentz forces		$\pm < 10^{-4}$
	e) Influence of the Kuiper belt's gravity		± 0.03
	f) Influence of the Earth's orientation		± 0.001
	g) Mechanical and phase stability of DSN antennae		$\pm < 0.001$
	h) Phase stability and clocks		$\pm < 0.001$
	i) DSN station location		$\pm < 10^{-5}$
	j) Troposphere and ionosphere		$\pm < 0.001$
2	On-board generated systematics:		
	a) Radio beam reaction force	+1.10*	± 0.11
	b) RTG heat reflected off the craft	-0.55*	± 0.55
	c) Differential emissivity of the RTGs		± 0.85
	d) Nonisotropic radiative cooling of the spacecraft	0.00*	± 0.48
	e) Expelled Helium produced within the RTGs	+0.15	± 0.16
	f) Gas leakage		± 0.56
	g) Variation between spacecraft determinations	+0.17	± 0.17
3	Computational systematics:		
	a) Numerical stability of least-squares estimation		± 0.02
	b) Accuracy of consistency/model tests		± 0.13
	c) Mismodeling of maneuvers		± 0.01
	d) Mismodeling of the solar corona		± 0.02
	e) Annual/diurnal terms		± 0.32
Estimate of total bias/error		+0.90	± 1.33

Note that several items in Table 5.2 are marked with an asterisk, indicating that these items are the subject of an on-going new investigation of the Pioneer anomaly (discussed in Section 7).

The bias (third column) and error (fourth column) in Table 5.2 give the final acceleration result in the form

$$a_P = a_{P(\text{exp})} + b_P \pm \sigma_P, \quad (5.25)$$

where

$$a_{P(\text{exp})} = (7.84 \pm 0.01) \times 10^{-10} \text{ m/s}^2 \quad (5.26)$$

is the reported formal solution for the Pioneer anomaly that was obtained with the data set available prior to 2002 [18]. Specifically, after accounting for the systematics listed in Table 5.2 and using Equations (5.25) and (5.26), the authors of [18] presented the final result of their study as

$$a_P = (8.74 \pm 1.33) \times 10^{-10} \text{ m/s}^2. \quad (5.27)$$

This 6- σ effect is clearly significant and, as of 2009, still remains unexplained.

The 2002 analysis demonstrated that after accounting for the gravitational and other large forces included in standard orbit determination programs [15, 18, 394], the anomaly in the Doppler frequency blue shift drift is uniformly changing with a rate of $\dot{f}_P = (5.99 \pm 0.01) \times 10^{-9} \text{ Hz/s}$ [393]

(see Figure 5.2). Let us denote the frequency of the signal observed by a DSN antenna as f_{obs} , and the predicted frequency of that signal after modeling conventional forces and other signal propagation effects as f_{model} . Then, for a one-way signal, the observed anomalous effect to first order in v/c is given by $f_{\text{obs}} - f_{\text{model}} = -\dot{f}_P t$. This translates to

$$[f_{\text{obs}}(t) - f_{\text{model}}(t)]_{\text{DSN}} = -f_0 \frac{a_P t}{c}, \quad (5.28)$$

where f_0 is the DSN reference frequency [18, 393, 395] (for a discussion of the DSN sign conventions, see Endnote 38 of [18]).

Since the publication of the 2002 study [18], many proposals have been put forth offering theoretical explanations of the anomaly. These are reviewed in the next section (Section 6). On the other hand, our knowledge of the anomaly also improved. The existence and magnitude of the anomalous acceleration has been confirmed by several independent researchers. Others have attempted to model the thermal behavior of the spacecraft, arguing that the magnitude of thermal recoil forces might have been underestimated by the 2002 study. The recovery of essentially all Pioneer 10 and 11 telemetry, as well as large quantities of archived project documentation, raised hope that it might be possible to construct a sufficiently accurate thermal model of the spacecraft using modeling software, and properly estimate the magnitude of the thermal recoil force. This remains one of several open, unresolved questions that, hopefully, will be answered in the near future as a result of on-going study, as detailed in Section 7.

6 Efforts to Explain and Study the Anomaly

Since the initial announcement of the anomalous acceleration of the Pioneer 10 and 11 spacecraft, a significant number of proposals have been made in an attempt to explain the nature of the discovered effect. The explanations targeted the effect with the properties presented in [15, 18, 391] and summarized in Section 5.6. These key properties include i) the magnitude and the apparent constancy of the anomalous acceleration, ii) its nearly Sun-pointing direction, and iii) the apparent “onset” of the anomaly. This set of “known” properties was used to analyze the mechanisms that were put forward in numerous attempts to identify the origin of the effect. Although the proposals are all very different and include conventional and new physics ideas, it is possible to place them into several broad categories. In this section we review some of these proposed mechanisms.

First, there are attempts to explain the anomaly using unmodeled conventional forces with an origin external to the spacecraft (Section 6.1), which may be both gravitational or nongravitational in nature. Some authors considered the possibility that the anomalous effect may be due to a new physics mechanism indicating, for instance, modification of gravity (Section 6.2), or may have a cosmological origin (Section 6.3). On the other hand, the fact that the Pioneer anomaly was observed in the radiometric Doppler signal opens up the possibility that the anomaly is not a dynamical effect on the trajectories of the probes but instead is due to an unmodeled effect on their radio signal (Section 6.4). We also consider proposals that attempt to explain the anomaly using unmodeled forces of on-board origin (Section 6.5). Lastly, we review miscellaneous mechanisms (Section 6.6) and some common misconceptions before moving on to a discussion of independent observational confirmations (Section 6.7) and proposals for dedicated space experiments (Section 6.8).

6.1 Unmodeled forces external to the spacecraft

The trajectory of the Pioneer spacecraft, while governed primarily by the gravity of the solar system, is nevertheless a result of a complex combination of gravitational and nongravitational forces, all of which must be taken into account for a precision orbit determination. What if some of those forces were not properly accounted for in the model, resulting in an unmodeled acceleration of the observed magnitude? Several authors considered this possibility.

6.1.1 Gravitational forces due to unknown mass distributions and the Kuiper belt

Of course, one of the most natural mechanisms to generate a putative physical force is the gravitational attraction due to a known mass distribution in the outer solar system; for instance, due to Kuiper belt objects or interplanetary dust. Anderson et al. [18] have considered such a possibility by studying various known density distributions for the Kuiper belt and concluded these density distributions are incompatible with the discovered properties of the anomaly. Even worse, these distributions cannot circumvent the constraint from the undisturbed orbits of Mars and Jupiter.

The possibility of a gravitational perturbation on the Pioneer paths has also been considered by the authors of [48, 86, 144, 245], who studied the possible effects produced by different Kuiper Belt mass distributions, and concluded that the Kuiper Belt cannot produce the observed acceleration.

Nieto [245] studied several models for 3-dimensional rings and wedges whose densities are either constant or vary as the inverse of the distance, as the inverse-squared distance, or according to the Boss–Peale model. It was demonstrated that physically viable models of this type can produce neither the magnitude nor the constancy of the Pioneer anomaly. In fact, the results emphasized the difficulty in achieving a constant acceleration within a finite cylindrically-symmetric distribution of matter. The difficulties are even stronger if one considers the amount of mass that would be needed to mimic the Pioneer anomaly.

The density of dust is not large enough to produce a gravitational acceleration on the order of a_P [18, 48, 245] and also it varies greatly within the Kuiper belt, precluding any constant

acceleration. In particular, Bertolami and Vieira [48] obtained the largest acceleration when the Kuiper belt was represented by a two-ring model. In this case, the following magnitude of a radial acceleration a_{rad} could be obtained (using spherical coordinates (r, θ, ϕ)):

$$a_{\text{rad}}(r, \theta) = -\frac{GM}{2\pi(R_1 + R_2)} \int_0^{2\pi} \sum_{i=1}^2 R_i \frac{r - R_i \cos \theta \cos \phi}{(r^2 + R_i^2 - 2rR_i \cos \theta \cos \phi)^{3/2}} d\phi, \quad (6.1)$$

where $R_1 = 39.4$ AU (3:2 resonance) and $R_2 = 47.8$ AU (2:1 resonance) are the radii of the two rings, M is the total mass of the Kuiper belt, and G is the gravitational constant. Equation (6.1) can be evaluated numerically, yielding a nonuniform acceleration that is at least an order of magnitude smaller than the Pioneer anomaly. Other dust distributions, such as those represented by a uniform disk model, a nonuniform disk model, or a toroidal model yield even smaller values. Hence, a gravitational attraction by the Kuiper belt can, to a large extent, be ruled out.

6.1.2 Drag forces due to interplanetary dust

Several nongravitational, conventional forces have been proposed by different authors to explain the anomaly. In particular, the drag force due to interplanetary dust has been investigated by the authors of [48, 245]. The acceleration a_{drag} due to drag can be modeled as

$$a_{\text{drag}} = -\frac{\kappa \rho v^2 A}{m}, \quad (6.2)$$

where ρ is the density of the interplanetary medium, v is the velocity of the spacecraft, A its effective cross section, m its mass, while κ is a dimensionless coefficient the value of which is 2 for reflection, 1 for absorption, and 0 for transmission of the dust particles through the spacecraft.

Using Equation (6.2) as an *in situ* measurement of the “apparent” density of the interplanetary medium, one obtains $\rho \simeq 2.5 \times 10^{-16}$ kg/m³. This is several orders of magnitude larger than the interplanetary dust density ($\sim 10^{-21}$ kg/m³) reported by other spacecraft (see discussion in [254]).

The analysis of data from the inner parts of the solar system taken by the Pioneer 10 and 11 dust detectors strongly favors a spherical distribution of dust over a disk. Ulysses and Galileo measurements in the inner solar system find very few dust grains in the $10^{-18} - 10^{-12}$ kg range [254]. The density of dust is not large enough to produce a gravitational acceleration on the order of a_P [18]. The resistance caused by the interplanetary dust is too small to provide support for the anomaly [254], so is the dust-induced frequency shift of the carrier signal.

The mechanism of drag forces due to interplanetary dust as the origin of the anomaly was discussed in detail in [254]. In particular, the authors considered this idea by taking into account the known properties of dust in the solar system, which is composed of thinly scattered matter with two main contributions:

- i) *Interplanetary Dust (IPD)*: a hot-wind plasma (mainly p and e^-) within the Kuiper Belt, from 30 to 100 AU with a modeled density of $\rho_{\text{IPD}} \lesssim 10^{-21}$ kg/m³; and
- ii) *Interstellar Dust (ISD)*: composed of fractions of interstellar dust (characterized by greater impact velocity). The density of ISD was directly measured by the Ulysses spacecraft, yielding $\rho_{\text{ISD}} \lesssim 3 \times 10^{-23}$ kg/m³.

In [254] these properties were used to estimate the effect of dust on Pioneer 10 and 11 and it was found that one needs an axially-symmetric dust distribution within 20–70 AU with a constant, uniform, and unreasonably high density of $\sim 3 \times 10^{-16}$ kg/m³ $\simeq 3 \cdot 10^5 (\rho_{\text{IPD}} + \rho_{\text{ISD}})$. Therefore, interplanetary dust cannot explain the Pioneer anomaly.

One may argue that higher densities are present within the Kuiper belt. IR observations rule out more than 0.3 Earth mass from Kuiper Belt dust in the trans-Neptunian region. Using this figure, the authors of [48] have noted that the Pioneer measurement of the interplanetary dust density is comparable to the density of various Kuiper belt models. Nonetheless, the density varies greatly within the Kuiper belt, precluding any constant acceleration.

6.2 Possibility for new physics? Modified gravity theories

Many authors investigated the possibility that the origin of the anomalous signal is “new physics” [15, 18]. This is an interesting conjecture, even though the probability is that some standard physics or some as-yet-unknown systematic will be found to explain this acceleration. Being more specific, one may ask the question, “Is it dark matter or a modification of gravity?” Unfortunately, as we discuss below, it is not easy for either of these solutions to provide a satisfactory answer.

6.2.1 Dark matter

Various distributions of dark matter in the solar system have been proposed to explain the anomaly, e.g., dark matter distributed in the form of a disk in the outer solar system with a density of $\sim 4 \times 10^{-16} \text{ kg/m}^3$, yielding the wanted effect. However, it would have to be a special kind of dark matter that was not seen in other nongravitational processes. Dark matter in the form of a spherical halo of a degenerate gas of heavy neutrinos around the Sun [235] and a hypothetical class of dark matter that would restore the parity symmetry, called the *mirror matter* [119], have also been discussed. However, it would have to be a special smooth distribution of dark matter that is not gravitationally modulated as normal matter so obviously is.

It was suggested that the observed deceleration in the Pioneer probes can be explained by the gravitational pull of a distribution of undetected dark matter in the solar system [86]. Explanations of the Pioneer anomaly involving dark matter depend on the small scale structure of Navarro–Frenk–White (NFW) haloes, which are not known. N -body simulations to investigate solar system size subhalos would require on the order of 10^{12} particles [237], while the largest current simulations involve around 10^8 particles [92]. As a consequence of this lack of knowledge about the small scale structure of dark matter, the existence of a dark matter halo around the Sun is still an open question.

It has been proposed that dark matter could become trapped in the Sun’s gravitational potential after experiencing multiple scatterings [302], perhaps combined with perturbations due to planets [78]. Moreover, the birth of the solar system itself may be a consequence of the existence of a local halo. The existence of dark matter streams crossing the solar system, perhaps forming ring-shaped caustics analogous to the dark matter ring postulated in [86], has also been considered by Sikivie [350]. Considering an NFW dark matter distribution [239], de Diego et al. [86] show that there should be several hundreds of earth masses of dark matter available in the solar system.

Gor’kavyi et al. [128] have shown that the solar system dust distributes in two dust systems and four resonant belts associated with the orbits of the giant planets. The density profile of these belts approximately follows an inverse heliocentric distance dependence law $[\rho \propto (R - k)^{-1}]$, where k is a constant. As in the case of dark matter, dust is usually modeled as a collisionless fluid as pressure, stresses, and internal friction are considered negligible. Although dust is subjected to radiation pressure, this effect is very small in the outer solar system. Gravitational pull by dark matter has also recently been considered also by Nieto [246], who also mentioned the possibility of searching for the Pioneer anomaly using the New Horizons spacecraft when the probe crosses the orbit of Saturn.

6.2.2 Modified Newtonian Dynamics (MOND)

The anomalous behavior of galaxy rotational curves led to an extensive search for dark matter particles. Some authors considered the possibility that a modification of gravity is needed to address this challenge. Consequently, there were many attempts made at constructing a theory that modifies Newton’s laws of gravity in the regime of weak gravitational fields. Presently, these efforts aim at constructing a consistent and stable theory that would also be able to account for a range of puzzling phenomena – such as flat galaxy rotational curves, gravitational lensing observations, and recent cosmological data – without postulating the existence of nonbaryonic dark matter or dark energy of yet unknown origin. Some of these novel theories were used to provide a cause of the Pioneer anomaly.

One approach to modify gravity, called Modified Newtonian Dynamics (MOND), is particularly well studied in the literature. MOND is a phenomenological modification that was proposed by Milgrom [33, 203, 202, 204, 325] to explain the “flat” rotation curves of galaxies by inducing a long-range modification of gravity. In this approach, the Newtonian force law for a test particle with mass m and acceleration \mathbf{a} is modified as follows:

$$m\mathbf{a} = \mathbf{F} \rightarrow \mu(|\mathbf{a}|/a_0)m\mathbf{a} = \mathbf{F}, \quad \text{with} \quad \mu(x) \simeq \begin{cases} 1 & \text{if } |x| \gg 1, \\ x & \text{if } |x| \ll 1, \end{cases} \quad (6.3)$$

where $\mu(x)$ is an unspecified function (a frequent, particularly simple choice is $\mu(x) = x/(x+1)$; other forms of μ are also used) and a_0 is some constant acceleration.

It follows from Equation (6.3) that a test particle separated by $\mathbf{r} = \mathbf{n}r$ from a large mass M , instead of the standard Newtonian expression $\mathbf{a} = -GM\mathbf{n}/r^2$ (which still holds when $|\mathbf{a}| \gg a_0$), is subject to an acceleration that is given phenomenologically by the rule

$$|\mathbf{a}| \rightarrow \mu(|\mathbf{a}|/a_0)|\mathbf{a}| \simeq \begin{cases} GM/r^2 \propto 1/r^2 & \text{if } a \gg a_0 \text{ (or large forces),} \\ \sqrt{a_0 GM}/r \propto 1/r & \text{if } a \ll a_0 \text{ (or small forces).} \end{cases} \quad (6.4)$$

Such a modification of Newtonian law produces a very distinct modification of galactic rotational curves. The velocities of circular orbits are modified by Equation (6.4) as

$$a_{\text{centrifugal}} = \frac{v^2}{r} \simeq \begin{cases} GM/r^2 & \text{if } a \gg a_0 \text{ (or small distances),} \\ \sqrt{a_0 GM}/r & \text{if } a \ll a_0 \text{ (or large distances).} \end{cases} \Rightarrow v^2 \simeq \begin{cases} GM/r & \text{if } a \gg a_0 \text{ (or small distances),} \\ \sqrt{a_0 GM} & \text{if } a \ll a_0 \text{ (or large distances).} \end{cases} \quad (6.5)$$

With a value of $a_0 \simeq 1.2 \times 10^{-10} \text{ m/s}^2$. MOND reproduces many galactic rotation curves.

Clearly, the original MOND formulation is purely phenomenological, which drew some criticism toward the approach. However, recently a relativistic theory of gravitation that reduces to MOND in the weak-field approximation was proposed by Bekenstein in the form of the tensor-vector-scalar (TeVeS) gravity theory [34]. As the exact form of $\mu(x)$ remains unspecified in both MOND and TeVeS, it is conceivable that an appropriately chosen $\mu(x)$ might reproduce the Pioneer anomaly even as the theory’s main result, its ability to account for galaxy rotation curves, is not affected.

As far as the Pioneer anomaly is concerned, considering the strong Newtonian regime (i.e., $a_0 \ll GM/r^2$) and choosing $\mu(x) = 1 + \xi x^{-1}$, one obtains a modification of Newtonian acceleration in the form $a = -GM/r^2 - \xi a_0$, which reproduces the qualitative behavior implied by the observed anomalous acceleration of the Pioneers. However, Sanders [327] concludes that if the effects of a MONDian modification of gravity are not observed in the motion of the outer planets in the solar system (see Section 6.7.1 for discussion), the acceleration cannot be due to MOND. On the other hand, Bruneton and Esposito-Farèse [57] demonstrate that while it may require model choices that are not justified by underlying symmetry principles, it is possible to simultaneously account for the

Pioneer anomalous acceleration and for the tests of general relativity in the solar system within a consistent field theory.

Laboratory experiments have recently reached new levels of precision in testing the proportionality of force and acceleration in Newton's second law, $\mathbf{F} = m\mathbf{a}$, in the limit of small forces and accelerations [2, 129]. The tests were motivated to explore the acceleration scales implied by several astrophysical puzzles, such as the observed flatness of galactic rotation curves (with MOND-implied acceleration of $a_0 = 1.2 \times 10^{-10} \text{ m/s}^2$), the Pioneer anomaly (with $a_P \sim 9 \times 10^{-10} \text{ m/s}^2$) and the natural scale set by the Hubble acceleration ($a_H = cH \simeq 7 \times 10^{-10} \text{ m/s}^2$). Gundlach et al. [129] reported no violation of Newton's second law at accelerations as small as $5 \times 10^{-14} \text{ m/s}^2$. The obtained result does not invalidate MOND directly as the formalism requires that the measurement must be carried out in the absence of any other large accelerations (i.e., those due to the Earth and our solar system). However, the test constrains theoretical formalisms that seek to derive MOND from fundamental principles by requiring that formalism to reproduce $\mathbf{F} = m\mathbf{a}$ under laboratory conditions similar to those used in the experiment.

Finally, there were suggestions that rather than modifying laws of gravity in order to explain the Pioneer effect, perhaps we need to modify laws of inertia instead [205]. To that extent, modified-inertia as a reaction to Unruh radiation has been considered in [192].

6.2.3 Large distance modifications of Newton's potential

Motivated by the puzzle of the anomalous galactic rotation curves, many phenomenological models of modified Newtonian potential (leading to the changes in the gravitational inverse-square law) were considered, a Yukawa-like modification being one of the most popular scenario. Following Sanders [326], consider the ansatz:

$$U(r) = U_{\text{Newton}}(r) \left(1 + \alpha e^{-r/\lambda} \right), \quad (6.6)$$

which, as was shown in [326], is able to successfully explain many galactic rotation curves. The same expression may also be used to study the physics of the Pioneer anomaly [220]. Indeed, Equation (6.6) implies that a body moving in the gravitational field of the Sun is subject to the acceleration law:

$$a(r) = -G_0 \frac{M_\odot}{r^2} + \frac{\alpha}{1+\alpha} G_0 \frac{M_\odot}{2\lambda^2} - \frac{\alpha}{1+\alpha} G_0 \frac{M_\odot}{3\lambda^2} \frac{r}{\lambda} + \dots, \quad (6.7)$$

where $G_0 = (1+\alpha)G$ is the observed gravitational constant in the limit $r \rightarrow 0$. Identifying the second term in Equation (6.7) with the Pioneer acceleration one can solve, for instance, for the parameter $\alpha = \alpha(a_P, \lambda)$, and obtain:

$$a_P = \frac{\alpha}{1+\alpha} G_0 \frac{M_\odot}{2\lambda^2} \quad \Rightarrow \quad \alpha = \frac{2\lambda^2 a_P}{G_0 M_\odot - 2\lambda^2 a_P}. \quad (6.8)$$

The denominator in Equation (6.8) implies that $\lambda > \sqrt{GM_\odot/(2a_P)}$, or $\lambda \geq 2.8 \times 10^{14} \text{ m}$.

A combination of $\log \lambda > 16$ with $\log |\alpha| \approx 0$ is compatible with the existing solar system data and the Yukawa modification in the form of Equation (6.6) may provide a viable model for the Pioneer anomaly [168]. Furthermore, after rearranging the terms in Equation (6.7) as

$$a(r) = -G_0 \frac{M_\odot}{r^2} + a_P - \frac{2}{3} a_P \frac{r}{\lambda} + \dots, \quad (6.9)$$

one can note that the third term in Equation (6.9) is smaller than a_P by a factor of $\frac{2}{3} \frac{r}{\lambda} \leq 0.06$ and may account for the small decrease in the observed acceleration. The values for the parameters α and λ obtained for the Pioneer anomaly are also compatible with the analysis of the galactic

rotation curves. Indeed, for the case of $\log \lambda > 16$ the Pioneer anomalous acceleration implies $\alpha + 1 \leq 10^{-5}$ while the galactic curves data yields a weaker limit of $\alpha + 1 \leq 10^{-1}$.

A modification of the gravitational field equations for a metric theory of gravity, by introducing a momentum-dependent linear relation between the Einstein tensor and the energy-momentum tensor, has been developed by Jaekel and Reynaud [147, 148, 149, 150, 151] and was shown to be able to account for a_P . The authors identify two sectors, characterized by the two potentials

$$g_{00} \simeq 1 + 2\Phi_N, \quad g_{00}g_{rr} \simeq 1 + 2\Phi_P, \quad (6.10)$$

where g_{00} and g_{rr} are components of the metric written in Eddington isotropic coordinates. The Pioneer anomaly could be accounted for by an anomaly in the Newtonian potential, $\delta\Phi_N \simeq (r - r_1)/\ell_P$ with a characteristic length scale given by $\ell_P^{-1} \equiv a_P/c^2$. However, this model is likely excluded by measurements such as Viking Mars radio ranging. On the other hand, an anomaly due to the potential in the second sector in the form

$$\delta\Phi_P \simeq -\frac{(r - r_1)^2 + \mu_P(r - r_1)}{3\kappa\ell_P}, \quad (6.11)$$

with κ given by $1/3\kappa\ell_P \simeq 4 \times 10^8 \text{ AU}^{-2}$ and μ_P being a further characteristic length representing the radial derivative of the metric anomaly at the Earth's orbit, could account for the Pioneer anomaly, and the conflict with Viking ranging data can be resolved [150].

Other related proposals include Yukawa-like or higher-order corrections to the Newtonian potential [18] and Newtonian gravity as a long wavelength excitation of a scalar condensate inducing electroweak symmetry breaking [73].

6.2.4 Scalar-tensor extensions of general relativity

There are many proposals that attempt to explain the Pioneer anomaly by invoking scalar fields. In scalar-tensor theories of gravity, the gravitational coupling strength exhibits a dependence on a scalar field φ . A general action for these theories can be written as

$$S = \frac{c^3}{4\pi G} \int d^4x \sqrt{-g} \left[\frac{1}{4} f(\varphi) R - \frac{1}{2} g(\varphi) \partial_\mu \varphi \partial^\mu \varphi + V(\varphi) \right] + \sum_i q_i(\varphi) \mathcal{L}_i, \quad (6.12)$$

where $f(\varphi)$, $g(\varphi)$, and $V(\varphi)$ are generic functions, $q_i(\varphi)$ are coupling functions, and \mathcal{L}_i is the Lagrangian density of matter fields, as prescribed by the Standard Model of particles and fields.

Effective scalar fields are prevalent in supersymmetric field theories and string/M-theory. For example, string theory predicts that the vacuum expectation value of a scalar field, the dilaton, determines the relationship between the gauge and gravitational couplings. A general, low energy effective action for the massless modes of the dilaton can be cast as a scalar-tensor theory (as in Equation (6.12)) with a vanishing potential, where $f(\varphi)$, $g(\varphi)$, and $q_i(\varphi)$ are the dilaton couplings to gravity, the scalar kinetic term, and the gauge and matter fields, respectively, which encode the effects of loop effects and potentially nonperturbative corrections.

Brans–Dicke theory [52] is the best known alternative scalar theory of gravity. It corresponds to the choice

$$f(\varphi) = \varphi, \quad g(\varphi) = \frac{\omega}{\varphi}, \quad V(\varphi) = 0. \quad (6.13)$$

In Brans–Dicke theory, the kinetic energy term of the field φ is noncanonical and the latter has a dimension of energy squared. In this theory, the constant ω marks observational deviations from general relativity, which is recovered in the limit $\omega \rightarrow \infty$. In the context of Brans–Dicke theory, one can operationally introduce Mach's principle, which states that the inertia of bodies is due to their interaction with the matter distribution in the Universe. Indeed, in this theory the gravitational

coupling is proportional to φ^{-1} , which depends on the energy-momentum tensor of matter through the field equation $\square^2 \varphi = 8\pi/(3 + 2\omega)T$ where T is the trace of the matter stress-energy tensor defined as the variation of \mathcal{L}_i with respect to the metric tensor.

The ω parameter can be directly related to the Eddington–Robertson (PPN) parameter γ by the relation [419]: $\gamma = (\omega + 1)/(\omega + 2)$. The stringent observational bound resulting from the 2003 experiment with the Cassini spacecraft require that $|\omega| \gtrsim 40\,000$ [49, 419]. On the other hand, $\omega = -3/2$ may be favored by cosmological observations and also offer a resolution of the Pioneer anomaly [77]. A possible resolution can be obtained by incorporating a Gauss–Bonnet term in the form of $\mathcal{L}_{\text{GB}} = R_{\mu\nu\rho\sigma}R^{\mu\nu\rho\sigma} - 4R_{\mu\nu}R^{\mu\nu} + R^2$ into the Brans–Dicke version of the Lagrangian Equation (6.12) with the choice of Equation (6.13), which may allow the Eddington parameter γ to be arbitrarily close to 1, while choosing an arbitrary value for ω [10]. Another scalar-tensor model, proposed by Novati et al. [60], was also motivated in part by the observed anomalous acceleration of the two Pioneer spacecraft.

Other scalar-tensor approaches using different forms of the Lagrangian Equation (6.12) were used to investigate the anomaly. Capozziello et al. [62] developed a proposal based on flavor oscillations of neutrinos in Brans–Dicke theory; Wood [427] proposed a theory of conformal gravity with dynamical mass generation, including the Higgs scalar. Cadoni [59] studied the coupling of gravity with a scalar field with an exponential potential, while Bertolami and Páramos [45] also applied a scalar field in the context of the braneworld scenarios. In particular, Bertolami and Páramos [45] have shown that a generic scalar field cannot explain a_P ; on the other hand, a non-uniformly-coupled scalar could produce the wanted effect. In addition, although braneworld models with large extra dimensions may offer a richer phenomenology than standard scalar-tensor theories, it seems difficult to find a convincing explanation for the Pioneer anomaly [46].

6.2.5 Scalar-tensor-vector modified gravity theory (MOG)

Moffat [224] attempted to explain the anomaly in the framework of Scalar-Tensor-Vector Gravity (STVG) theory. The theory originates from investigations of a nonsymmetric generalization of the metric tensor, which gives rise to a skew-symmetric field. Endowing this field with a mass led to the Metric-Skew-Tensor Gravity (MSTG) theory, while the further step of replacing the skew-symmetric field with the curl of a vector field yields STVG. The theory successfully accounts for observed galactic rotation curves, galaxy cluster mass profiles, gravitational lensing in the Bullet Cluster (1E0657-558), and cosmological observations.

The STVG Lagrangian takes the form,

$$\mathcal{L} = \sqrt{-g} \left\{ -\frac{1}{16\pi G} (R + 2\Lambda) - \frac{1}{4\pi} \omega \left[\frac{1}{4} B^{\mu\nu} B_{\mu\nu} - \frac{1}{2} \mu^2 \phi_\mu \phi^\mu + V_\phi(\phi) \right] - \frac{1}{G} \left[\frac{1}{2} g^{\mu\nu} \left(\frac{\nabla_\mu G \nabla_\nu G}{G^2} + \frac{\nabla_\mu \mu \nabla_\nu \mu}{\mu^2} - \nabla_\mu \omega \nabla_\nu \omega \right) + \frac{V_G(G)}{G^2} + \frac{V_\mu(\mu)}{\mu^2} + V_\omega(\omega) \right] \right\}, \quad (6.14)$$

where g is the determinant of the metric tensor, R is the Ricci-scalar, Λ is the cosmological constant, ϕ_ν is a massive vector field with (running) mass μ , $B_{\mu\nu} = \partial_\mu \phi_\nu - \partial_\nu \phi_\mu$, G is the (running) gravitational constant, ω is the (running) vector field coupling constant, and V_ϕ , V_G , V_μ and V_ω are the potentials associated with the vector field and the three running scalar fields.

The spherically symmetric, static vacuum solution of Equation (6.14) yields, in the weak field limit, an effective gravitational potential that is a combination of a Newtonian and a Yukawa-like term, and can be written as

$$G_{\text{eff}} = G_N \left(1 + \alpha - \alpha(1 + \mu r) e^{-\mu r} \right). \quad (6.15)$$

In earlier papers, the values of α and μ were treated as fitted parameters. This allowed Brownstein and Moffat [54, 223] to reproduce an anomalous acceleration of the correct magnitude and also

account for the anomaly’s apparent “onset” at a distance of ~ 10 AU from the Sun. More recently, the values of α and μ were derived successfully as functions of the gravitational source mass [225]. This later approach results in the prediction of Newtonian behavior within the solar system, indeed within all self-gravitating systems with a mass below several times $10^6 M_\odot$.

6.3 Cosmologically-motivated mechanisms

There have been many attempts to explain the anomaly in terms of the expansion of the Universe, motivated by the numerical coincidence $a_P \simeq cH_0$, where c the speed of light and H_0 is the Hubble constant at the present time (see Section 6.6.2 for details). These attempts were also stimulated by the fact that the initial announcement of the anomaly [15] came almost immediately after reports on the luminosity distances of type Ia supernovae [272, 314] that were followed by measurements of the angular structure of the cosmic microwave background (CMB) [85], measurements of the cosmological mass densities of large-scale structures [271] that have placed stringent constraints on the cosmological constant Λ and led to a revolutionary conclusion: The expansion of the universe is accelerating. These intriguing numerical and temporal coincidences led to heated discussion (see, e.g., [167, 265] for contrarian views) of the possible cosmological origin of the Pioneer anomaly.

Below we discuss cosmologically-motivated mechanisms used to explain the Pioneer anomaly.

6.3.1 Cosmological constant as the origin of the Pioneer anomaly

An inverse time dependence for the gravitational constant G produces effects similar to that of an expanding universe. So does a length or momentum scale-dependent cosmological term in the gravitational action functional [222, 321]. It was claimed that the anomalous acceleration could be explained in the frame of a quasi-metric theory of relativity [268]. The possible influence of the cosmological constant on the motion of inertial systems leading to an additional acceleration has been discussed [321]. Gravitational coupling resulting in an increase of the constant G with scale is analyzed by Bertolami and García-Bellido [44]. A 5-dimensional cosmological model with a variable extra dimensional scale factor in a static external space [35, 36] was also proposed. It was suggested that the coupling of a cosmological “constant” to matter [188] may provide a connection with the Pioneer anomaly.

Kagramanova et al. [155] (see also [160, 336]) have studied the effect of the cosmological constant on the outcome of the various gravitational experiments in the solar system by taking the metric of the Schwarzschild–de Sitter spacetime:

$$ds^2 = \alpha(r)dt^2 - \alpha(r)^{-1}dr^2 - r^2(d\theta^2 + \sin^2\theta d\phi^2), \quad (6.16)$$

where

$$\alpha(r) = 1 - \frac{2M}{r} - \frac{1}{3}\Lambda r^2 \quad (6.17)$$

with Λ being the cosmological constant and M the mass of the source. (Note that $\Lambda < 0$ would result in attraction, while $\Lambda > 0$ will lead to repulsion.)

The authors of [18] have shown that if the cosmological expansion would be at the origin of the Pioneer anomaly, such a mechanism would produce an opposite sign for the effect. Taken at face value, the anomaly would imply a negative cosmological constant of $\Lambda \sim -3 \times 10^{-37} \text{ m}^{-2}$, which contradicts both the solar system data and the data on cosmological expansion. Indeed, the highest limit on Λ allowable by the solar system tests is set by the data on the perihelion advance, which limit the value of the cosmological constant to $\Lambda \leq 3 \times 10^{-42} \text{ m}^{-2}$ [336]. However, the data on the cosmological accelerated expansion yields the value of $\Lambda \approx 10^{-52} \text{ m}^{-2}$, leading Kerr et al. [160] to conclude that the cosmological effects are too small to be measured in the solar system dynamical experiments.

Hackmann and Lämmerzahl [130, 131] developed the analytic solution of the geodesic equation in Schwarzschild–(anti-)de Sitter spacetimes and show that the influence of the cosmological constant on the orbits of test masses is negligible. They concluded that the cosmological constant cannot be held responsible for the Pioneer anomaly.

Thus, there is now a consensus that the Pioneer anomaly cannot be of a cosmological origin and, specifically, Λ cannot be responsible for the observed anomalous acceleration of the Pioneer 10 and 11 spacecraft. However, the discussion is still ongoing.

6.3.2 The effect of cosmological expansion on local systems

The effect of cosmological expansion on local systems had been studied by a number of authors [24, 74, 107, 126, 193], (for reviews, see [65, 113, 169, 423]). To study the behavior of small isolated mass in expanding universe, one starts with the weak field ansatz [65, 169]:

$$g_{\mu\nu} = b_{\mu\nu} + h_{\mu\nu}, \quad h_{\mu\nu} \ll b_{\mu\nu}, \quad (6.18)$$

and derives the linearized Einstein equations for $h_{\mu\nu}$:

$$b^{\rho\sigma} D_\rho D_\sigma \bar{h}_{\mu\nu} + b^{\rho\sigma} R_{\mu\rho\nu}^\kappa \bar{h}_{\kappa\sigma} = 16G\pi T_{\mu\nu}. \quad (6.19)$$

The relevant solution with modified Newtonian potential is given below

$$h_{00} = \frac{2GM}{R} \frac{\cos(\sqrt{6}|\dot{R}|r)}{r} = \frac{2GM}{Rr} \left(1 - 3H^2(Rr)^2 + \dots\right). \quad (6.20)$$

The first part in Equation (6.20) is the standard Newtonian potential with the measured distance $R(t)r$ in the denominator. Lämmerzahl et al. [169] observed that the additional acceleration towards the gravitating body is of the second order in the Hubble constant H . As such, this potential practically does not participate in the cosmic expansion; thus, there is no support for the cosmological origin of a_P .

Oliveira [265] conjectured that the solar system has escaped the gravity of the Galaxy, as evidenced by its orbital speed and radial distance and by the visible mass within the solar system radius. Spacecraft unbound to the solar system would also be unbound to the galaxy and subject to the Hubble law. However, this hypothesis produces practically unnoticeable effects.

6.3.3 The cosmological effects on planetary orbits

The cosmological effects on the planetary orbits has been addressed in many papers recently (for instance, [113]). To study the effect of cosmological modification of planetary orbit, one considers the action

$$S = -mc^2 \int \left(1 - 2\frac{U(x)}{c^2} - R^2(t)\frac{\dot{x}^2}{c^2}\right)^{\frac{1}{2}} dt \approx \int \left(-mc^2 + mU(r) + \frac{m}{2}R^2(t)(\dot{r}^2 + r^2\dot{\varphi}^2)\right) dt. \quad (6.21)$$

In the case of weak time dependence of $R(t)$ the action above has two adiabatic invariants:

$$I_\varphi = L, \quad I_r = -L + \frac{GmM}{R} \sqrt{\frac{m}{2|E|}}, \quad (6.22)$$

which determine the energy, E , momentum, p and the eccentricity, e , of an orbit:

$$E = -\frac{m^3 G^2 M^2}{2(I_r + I_\varphi)}, \quad p = \frac{I_\varphi^2}{m^2 M R(t)}, \quad e^2 = 1 - \left[\frac{I_\varphi}{I_r + I_\varphi}\right]^2. \quad (6.23)$$

Lämmerzahl [168] noted that in this scenario E , e and $R(t)p$ stay nearly constant. In addition, $R(t)p$ and e of the planetary orbits practically do not participate in cosmic expansion. Remember that the stability of adiabatic invariants is governed by the factor of $e^{-\tau/T}$, where τ is the characteristics time of change of external parameter (here: $\tau = 1/H$) and T is the characteristic time of the periodic motion (here: $T = \text{periods of planets}$). In the case of periodic bound orbits $\tau/T \sim 10^{10}$, thus, any change of the adiabatic invariants is truly negligible.

6.3.4 Gravitationally bound systems in an expanding universe

The question of whether or not the cosmic expansion has an influence on the size of the Solar system was addressed in conjunction to the study of the Pioneer anomaly. In particular, is there a difference between locally bound and escape orbits? If the former are proven to be practically immune to cosmic expansion, what about the latter? In fact, the properties of bound (either electrically or gravitationally) systems in an expanding universe have been discussed controversially in many papers, notably by [24, 194].

Effects of cosmological expansion on local systems were addressed by a number of authors (for reviews see [65, 168]). Gautreau [126] studied the behavior of a spherical mass with the energy-stress tensor taken in the form of an ideal fluid. The obtained results show that the outer planets would tend to out-spiral away from the solar system. Anderson [24] has studied the behavior of local systems in the cosmologically-curved background. He obtained cosmological modifications of local gravitational fields with an additional drag term for escape orbits and demonstrated that $Rr = \text{const}$ for bound orbits. Cooperstock et al. [74] used the Einstein-de Sitter universe $ds^2 = c^2 dt^2 - R^2(t)(dr^2 + d\Omega^2)$ and derived a geodesic deviation equation in Fermi normal coordinates $\ddot{x} - (\ddot{R}/R)x = 0$. Clearly, the additional terms are too small to be observed in the solar system.

As far as the Pioneer anomaly is concerned, the papers above are consistent in saying that planetary orbits in the solar system should see the effects of the anomaly and a_P may not be of gravitational origin. However, Anderson [24] found an interesting result that suggests that the expansion couples to escape orbits, while it does not couple to bound orbits.

To study this possibility Lämmerzahl [168] used a PPN-inspired spacetime metric:

$$g_{00} = 1 - 2\alpha \frac{U}{c^2} + 2\beta \frac{U^2}{c^4}, \quad g_{ij} = -\left(1 + 2\gamma \frac{U}{c^2}\right) R^2(t) \delta_{ij}, \quad (6.24)$$

that led to the following equation of motion (written in terms of measured distances and times):

$$\frac{d^2 X^i}{dT^2} = \frac{\partial U}{\partial X^i} \left[\alpha + \gamma \frac{1}{c^2} \left(\frac{dX}{dT} \right)^2 + (2\alpha^2 - \gamma\alpha - 2\beta) \frac{U}{c^2} \right] - \left[(\alpha + \gamma) \frac{1}{c^2} \frac{\partial U}{\partial X^j} \frac{dX^j}{dT} + \frac{\dot{R}}{R} \right] \frac{dX^i}{dT}. \quad (6.25)$$

Using Equation (6.25) Lämmerzahl [168] concludes that in cosmological context the behavior of bound orbits is different from that of unbound ones. However, cosmological expansion results in a decelerating drag term, which is a factor v/c too small to account for the Pioneer effect.

6.3.5 Dark-energy-inspired $f(R)$ gravity models

The idea that the cosmic acceleration of the Universe may be caused by a modification of gravity at very large distances, and not by a dark energy source, has recently received a great deal of attention (see [323, 355]). Such a modification could be triggered by extra space dimensions, to which gravity spreads over cosmic distances. Recently, models involving inverse powers of the curvature or other invariants have been proposed as an alternative to dark energy. Although such theories can lead to late-time acceleration, they typically result in one of two problems: either they are in conflict with tests of general relativity in the solar system, due to the existence of additional

dynamical degrees of freedom [69], or they contain ghost-like degrees of freedom that seem difficult to reconcile with fundamental theories.

Gravity theories that supplement the Einstein–Hilbert Lagrangian with a nonlinear function $f(R)$ of the curvature scalar have attracted interest in the context of inflationary cosmological scenarios, and because these theories may explain the accelerated expansion of the universe without the need to postulate scalar fields or a cosmological constant (for a review, see [355]).

As an upshot of these efforts, Bertolami et al. [42] explored a particular family of $f(R)$ Lagrangians that gives rise to an extra acceleration in the form

$$a_E = \frac{f^2 r^2}{GM} + 2f. \quad (6.26)$$

Assuming that $f \sim \alpha GM/r$ where α is a constant leads to $a_E \propto \alpha^2 = \text{const}$ in the limit of large r . For a galaxy, a_E is naturally associated with the MOND acceleration a_0 , while in the solar system, it may acquire the Pioneer acceleration value, a_P .

A similar result was obtained by Saffari and Rahvar [324] who used a metric formalism in $f(R)$ modified gravity to study the dynamics of various systems from the solar system to the cosmological scales. Replacing $f(R)$ with $F(R) = df/dR$, the authors postulated the ansatz $F(r) = (1 + r/d)^{-\alpha}$ where $\alpha \ll 1$ is a dimensionless constant and $\alpha r/d \ll 1$. They obtained an anomalous acceleration term of $-\alpha/2d$, which agrees with the Pioneer anomaly for $\alpha/d \simeq 10^{-26} \text{ m}^{-1}$.

On the other hand, Exirifard [111] demonstrated that a correction to the Einstein–Hilbert Lagrangian in the form of $\Delta\mathcal{L} = R_{\kappa\lambda\mu\nu}R^{\kappa\lambda\mu\nu}$ cannot offer a covariant resolution to the Pioneer anomaly.

Capozziello et al., [64] developed a general analytic procedure to investigate the Newtonian limit of $f(R)$ gravity. The authors discussed the Newtonian and the post-Newtonian limits of these gravity models, including the investigation of their possible relevance to the Pioneer anomaly. Capozziello et al. [61] mention that, by treating the Pioneer anomaly as a correction to the Newtonian potential, it could be studied in the general theoretical scheme of $f(R)$ gravity theories.

6.4 Effects on the radio signal

It has been argued [303] that the cosmic expansion influences the measurement process via a change in the frequency of the traveling electromagnetic signals. However, one expects that taking all effects of the cosmic expansion on the frequency as well as on the Pioneer motion into account, the resulting acceleration is $-vH_0$ and, thus, has the correct sign but is too small by a factor v/c [169]. The ways in which the cosmic expansion might be responsible for a_P vary considerably between the approaches. It is known [15, 18] that the very presence of the Pioneer anomalous acceleration contradicts the accurately known motion of the inner planets of our solar system. This motivated focusing on the effect of cosmic acceleration on the radio communication signal rather than on the spacecraft themselves. This mechanism might be able to overcome the apparent conflict that a_P presents to modern solar system planetary ephemerides [15, 18].

6.4.1 Helicity-rotation coupling

The radio signal used for communicating with Pioneer 10 and 11 (and indeed, used routinely with other spacecraft) is circularly polarized. Therefore, the question naturally arises as to whether the coupling between the helicity of the radio signal and the rotation of either the transmitter or the receiver could contribute to the observed Doppler anomaly in the Pioneer radio signal [187]. To first order, this coupling can increase or decrease the frequency of a radio signal by the rotational frequency of the transmitter (or receiver):

$$\omega' = \omega \mp \Omega, \quad (6.27)$$

where ω is the signal frequency that would be observed in the absence of rotation, Ω is the rotational frequency, while ω' is the observed frequency. The sign is positive for a negative helicity wave, and vice versa, and the formula must be applied to each leg of the communication separately (e.g., to the uplink and downlink leg in the case of two-way or three-way Doppler data.)

For the Pioneer spacecraft, $\Omega \simeq 0.076$ Hz (Pioneer 10) and $\Omega \simeq 0.13$ Hz (Pioneer 11). However, Anderson and Mashhoon [21] note that this effect cannot account for the Pioneer anomaly. The effect of rotation on the radio signal is already phenomenologically incorporated into the Doppler data analysis (see Section 4.5.4).

6.4.2 Clock acceleration

The fact that the anomaly was discovered using Doppler techniques leaves duality in the nature of the detected signal – it is either true physical acceleration a_P or a time acceleration a_t that is connected with the former by the relationship $a_P = c a_t$. This fact motivated Anderson et al. [18] to try to look for purely phenomenological “time” distortions that might fit the Pioneer data. The question was “is there any evidence that some kind of ‘time acceleration’ is being seen?”

A number of models were investigated and discarded for various reasons (see [18] for discussion), but there was one model that was especially interesting. This model adds a term that is quadratic in time to the light time, as seen by the DSN station as $t \rightarrow t + \frac{1}{2}a_t t^2$. In particular, let any labeled time t_a be given as

$$t_a - t_0 \rightarrow t_a - t_0 + \frac{1}{2}a_t (t_a^2 - t_0^2), \quad (6.28)$$

then the light time is

$$\Delta t = t_{\text{received}} - t_{\text{sent}} \rightarrow \Delta t + \frac{1}{2}a_t (t_{\text{received}}^2 - t_{\text{sent}}^2). \quad (6.29)$$

Expression (6.29) mimics a line of sight acceleration of the spacecraft, and could be thought of as an *expanding space* model. Note that a_t affects only the data, not the trajectory. It was pointed out by Anderson et al. that this model fits both Doppler and range very well for several spacecraft used in their study [18]. This fact motivated the discussion on the nature of the implied numerical relationship between the Hubble constant and a_P (Section 6.6.2). To investigate further the nature of this relation one would need to check the data of other spacecraft, compare modern clocks with accuracy much higher than that used in the navigation of the Pioneers, as well as the data on millisecond binary pulsars. Presently, not all of these venues are yet properly explored.

Rañada [304] investigated the effect of a background gravitational potential that pervades the universe and is increasing because of the expansion, provoking a drift of clocks [18]; however, such an effect should also be observed in the radio signals from pulsars [189, 411], which is not the case. Further refining their argument, Rañada and Tiemblo [305] investigated the nonequivalence of atomic and astronomical times and concluded that these times could be accelerating adiabatically with respect to one another.

Ostvang [268] proposes that cosmic expansion applies directly to gravitationally bound systems according to the *quasi-metric* framework. According to [319, 320], the scale factor of the spacetime background would cause an anomaly in the frequency. The cosmological constant has also been invoked to produce acceleration [260] or a gravitational frequency shift [190, 191].

6.4.3 Cosmological effects on radio signals

Lämmerzahl [168] considered the possibility that an expanding universe may have an effect on the Doppler microwave signals traveling in the solar system. The basic question is whether or not, if it exists, the coupling of the expansion of the universe to light has an observable effect. It was

shown that for a spacecraft moving with velocity v , the cosmologically-induced acceleration a_H would have the following form:

$$a_H = vH = \frac{v}{c}cH. \quad (6.30)$$

Clearly, this acceleration is a factor of v/c smaller than the observed Pioneer acceleration, for which $a_P \simeq cH$. Therefore, Doppler tracking in an expanding universe cannot account for the observed Pioneer anomaly [65, 168].

6.5 Unmodeled forces of on-board origin

The trajectory of the Pioneer 10 and 11 spacecraft may be affected by an unmodeled force of on-board origin. The Pioneer spacecraft can accelerate as a result of ejecting mass or radiation. Here we consider these mechanisms as the possible sources for the anomaly.

6.5.1 Thermal recoil forces

Immediately after publication of the initial report on the Pioneer anomaly [15], independent researchers raised questions concerning the estimated magnitude of the thermal recoil force due to internally generated heat. These ideas are summarized below.

Katz [17, 156] pointed out that although the electrical power generated on board Pioneer 10 and 11 was less than 100 W during the period that was investigated, the waste heat produced by each spacecraft's four RTGs amounted to ~ 2.5 kW. Therefore, even a small anisotropy in the spacecraft's thermal radiation pattern may be sufficient to produce the observed acceleration. Further, the amount of heat generated on-board decreased slowly, consistent with the quoted error bounds of the acceleration. In their reply, Anderson et al. [17] reasoned that due to the geometrical features of the Pioneer spacecraft such a mechanism would produce an acceleration much smaller than that observed in the Pioneer Doppler data.

Murphy [16, 236] brought attention to the fact that the louver system on the back of the Pioneer spacecraft is not a Lambertian emitter, and the electrical heat produced on-board may not have been declining steadily with time, as the spacecraft body contained mostly components that had to be powered at all times. In their reply, Anderson et al. [16] argued that by the time Pioneer 10 reached the distances of ~ 40 AU (i.e., the beginning of the data interval used in [18]), all louvers on the spacecraft were closed, thus forcing the remaining and decreasing heat to escape nonpreferentially.

Scheffer [329, 331] asserted that the 2002 study may have seriously underestimated the role of the thermal recoil force, and that up to 70 W of collimated thermal radiation, corresponding to an acceleration of 9.3×10^{-10} m/s², may have been present on board the two Pioneer spacecraft. Using the data on the electrical status of the Pioneer 10 spacecraft available prior to 2002, Anderson et al. [16] argued that such a mechanism would produce a significant decrease in the magnitude of the anomalous acceleration as a response to the decreasing supply of the radio-isotopic fuel. In fact, for the Pioneer 10 data interval used in the 2002 study, the amount of electrical energy decreased by nearly 30%, implying a similar decrease in the magnitude of the anomalous acceleration. Such a decrease was not observed in the data.

Given the later recovery of i) the telemetry records of Pioneers 10 and 11 for the entire duration of their respective missions and ii) documentation detailing the design of the Pioneer F/G spacecraft (both completed in 2005 [399]), further investigation into the contribution of the thermal recoil force as the source of the Pioneer anomaly is well founded. Indeed, the recoil force due to on-board generated thermal radiation is the subject of on-going study, discussed in Section 7.4.

6.5.2 Propulsive gas maneuvers

Among the possible mechanisms for the anomaly Anderson et al. [18] emphasized that propulsive gas maneuvers could contribute to the anomalous acceleration (see discussion in Sections 4.4.1 and 5.4.1). (The topic of fuel leaks was addressed in Section 4.4.2.) The errors associated with mismodeling of the maneuvers could be large enough to seriously affect the acceleration estimates. The number of maneuvers, their magnitude and the details of the trajectories of both Pioneers make it unlikely that similar acceleration estimates for both spacecraft would result, thus undermining this idea. Recently this mechanism was again put forward by Tortora et al. [380]. The recovered telemetry record, however, shows no indication of a loss of fuel or propulsion system activity that would support this notion [399].

6.6 Miscellaneous mechanisms

Some proposed mechanisms do not easily fit into the preceding categories, yet represent potentially promising avenues of research. In contrast, several proposed solutions to the Pioneer anomaly are based on simple misconceptions and numerical coincidences.

6.6.1 Other proposed mechanisms

Cherubini and Mashhoon [51] discuss the possibility of nongravitational acceleration of the Sun, orthogonal to the ecliptic plane, but they found that it is necessary for the Sun to emit all electromagnetic radiation in the opposite direction.

The possibility of an unknown interaction of the Pioneer radio signals with the solar wind was considered in [15]. In addition, there were ideas to invoke a model for superstrong interaction of photons or massive bodies with the graviton background [146].

Wilson and Blome [423] derived the equations of motion for an accelerated, rotating observer in a Gödel universe, and calculated the contribution of the universal cosmic rotation or vorticity. However, they found that this term cannot account for the observed Pioneer acceleration.

Trencevski [386] considered a time-dependent gravitational potential that could explain the Pioneer anomaly without causing planetary perihelion precessions that are in conflict with observation. Mansouri, Naseri, and Khorrami [182] argued in favor of an effective time variation of the gravitational constant; a similar analysis was performed by Sidharth [337].

Kowalski-Glikman and Smolin [166] proposed triply special relativity: a generalization of Einstein's theory of special relativity with three invariant scales, the speed of light c , a mass κ , and a length R , as a means to address several observational puzzles, including the Pioneer anomaly.

Wiltshire [424] considered the effects of decoupling bound systems from the global expansion of the universe. While he found that this cannot be responsible for the Pioneer effect, he also proposed an intriguing test case: a cosmic microwave background imager flown on a trajectory similar to that of Pioneer 10 and 11, with sufficient sensitivity to determine if an anomaly, if observed, is due to a clock effect related to gravitational energy.

Capozziello and Lambiase [63] argued that neutrino oscillations in Brans–Dicke theory could produce a phase shift with observable effects on astronomical or cosmological time scales.

6.6.2 Common misconceptions and numerical coincidences

Attempting to make sense of the Pioneer anomaly, one can easily discover several numerical coincidences that could mislead the discussion. We review some common misconceptions in the hope that this helps researchers navigate more easily through a formidable volume of literature.

The numerical value of the anomalous acceleration gave rise to much speculation. First, it was noticed that $a_P \simeq cH_0$ where c is the speed of light and H_0 is Hubble's constant at the present

epoch. However, an anomalous acceleration that is somehow connected to the cosmic *expansion* rate would necessarily point away from, not toward, the Sun. Furthermore, an acceleration with the magnitude cH_0 would only be observed for distant objects at a cosmic redshift of $z = 1$. Additionally, the numerical coincidence is only approximate, not exact; good agreement with the observed value of a_P requires $H_0 \simeq 95 \pm 14$ km/s/Mpc, well above the presently accepted value of $H_0 \simeq 73.2$ km/s/Mpc [359].

Then there were suggestions that the Pioneer anomaly may be related to galactic gravity. This claim is not true. The Milky Way, as most spiral galaxies, if approximated as a point mass using a nominal value of $r_{\text{gal}} \simeq 8,000$ pc as the distance from the Earth to the galactic bulge, and a nominal mass of $M_{\text{gal}} \simeq 4 \times 10^{11} M_{\odot}$, yields an acceleration of 8.75×10^{-10} m/s², a number that is almost identical to a_P . Yet this coincidence is misleading. Galactic gravity acts on all bodies in the solar system, including the Sun, the Earth, and flying spacecraft. The observed value of a_P is an acceleration relative to the Sun, so if it is caused by galactic gravity, it would have to be a result of a difference between the galactic gravitational force on the Sun vs. the spacecraft, i.e., a tidal force. Even at $d = 100$ AU, this tidal acceleration amounts to only $2GM_{\text{gal}}d/r_{\text{gal}}^3 \simeq 10^{-16}$ m/s², which is about seven orders of magnitude less than a_P .

Another numerical coincidence exploited in some proposals that have been communicated to the authors concerns the value v^4/c^3 or some variation thereof, where v is the heliocentric velocity of the Pioneer spacecraft. Evaluated numerically using the heliocentric velocity $v \simeq 12$ km/s of Pioneer 10, we obtain $v^4/c^3 \simeq 7.68 \times 10^{-10}$ m/s. While this value is very close numerically to a_P , it has the dimensions of a velocity, not acceleration, and the numerical coincidence is valid only so long as seconds are used as the unit of time.

Mäkelä [179] notes that $(\ln 2/16\pi)a_P \simeq Gm_P/l_P^2 \simeq 8.83 \times 10^{-10}$ m/s², where $m_P \simeq 1.67 \times 10^{-27}$ kg is the proton mass and $l_P = 2\pi\hbar/cm_P$ is the proton's Compton wavelength, is very close in value to the Pioneer acceleration. The factor of $\ln 2/16\pi$ may arise as the result of an unspecified quantum field theoretical calculation.

As described in Section 5, early data indicates that there was an “onset” of the anomalous acceleration of Pioneer 11 at around the time of its encounter with Saturn, which also marks this spacecraft's transition from an elliptic orbit to an hyperbolic escape trajectory. Some authors [246, 250] attempted to draw far reaching conclusions based solely on this fact. However, this observation cannot be used to draw any firm conclusions, as analysis of the early data is highly suspect: it was not developed using consistent methods and instead is an amalgamation of results derived by different analysts who used to work on Pioneer navigation at a particular time. So at best, it is only an indication of the temporal dependence of the anomaly, and quite likely, the “onset” is simply an artifact that will vanish when data is re-analyzed using a consistent strategy.

Lastly, the *flyby anomaly* [13, 26] must be mentioned, as it has been related to the Pioneer anomaly by some authors [13, 14]. Several spacecraft, including Galileo, NEAR and Rosetta, demonstrated a small, unexplained change in kinetic energy during a gravity-assist Earth flyby. The origin of this flyby anomaly remains unknown, although the possibility of a systematic origin cannot be excluded [398].

6.7 Search for independent confirmation

So far, the Pioneer anomaly has been observed unambiguously using two spacecraft of nearly identical design. The question naturally arises whether the anomalous acceleration is observed in the motion of solar system bodies or in the motion of other spacecraft.

6.7.1 Solar-system planetary data analysis

The biggest challenge to the mechanisms that use to explain the anomaly either the unseen matter distribution in the outer solar system or modifications of gravitational theory (see in Section 6.2) is the existence of a large volume of high-precision solar system data. Any naive modification of gravitational theory, for instance, that is designed to account for the anomalous acceleration of the Pioneer spacecraft would also likely induce changes in the predicted orbits of the outer planets.

A gravitational source in the solar system as a possible origin for the anomaly has been considered by [18]. According to the equivalence principle, such a gravitational source would also affect the orbits of the planets. In the case of the inner planets, which have orbits determined with great accuracy, they show no evidence of the expected anomalous motion if the source of the anomaly were located in the inner solar system. In fact, the anomalous acceleration is too large to have gone undetected in planetary orbits, particularly for Earth and Mars. Indeed, the authors of [18] observed that if a planet experiences a small, anomalous, radial acceleration, a_A , its orbital radius r is perturbed by

$$\Delta r = -\frac{l^6 a_A}{(GM_\odot)^4} \rightarrow -\frac{r a_A}{a_N}, \quad (6.31)$$

where l is the orbital angular momentum per unit mass and a_N is the Newtonian acceleration at distance r .

For Earth and Mars, Δr is about -21 km and -76 km. Take the orbit of Mars, for example, for which range data provided by the Mars Global Surveyor and Mars Odyssey missions have yielded measurements of the Mars system center-of-mass relative to the Earth to an accuracy of one meter [165]. However, the anomaly has been detected beyond 20 AU (i.e., beyond Uranus, 19 AU), and the orbits of the outer planets have been determined only by optical methods, resulting in much less accurate planet ephemerides.

The idea of looking at the impact of a Pioneer-like acceleration on the orbital dynamics of the solar system bodies was originally put forth in [15, 18]. These papers, however, considered the motion of the Earth and Mars finding no evidence of any effect induced by an extra acceleration like the Pioneer anomaly. In particular, a perturbation in r produces a perturbation to the orbital angular velocity of

$$\Delta\omega = \frac{2la_A}{GM_\odot} \rightarrow \frac{2\dot{\theta} a_A}{a_N}. \quad (6.32)$$

The determination of the synodic angular velocity ($\omega_E - \omega_M$) is accurate to 7 parts in 10^{11} , or to about 5 ms accuracy in synodic period. The only parameter that could possibly mask the spacecraft-determined a_R is (GM_\odot) . But a large error here would cause inconsistencies with the overall planetary ephemeris [18].

More interestingly, the authors of [22] have investigated the effect of an ever-present, uniform Pioneer-like force on the long-period comets. The authors of [270] proposed to use comets and asteroids to assess the gravitational field in the outer regions of the solar system and thereby investigate the Pioneer anomaly.

Furthermore, [18] concluded that available planetary ranging data limit any unmodeled radial acceleration acting on Earth and Mars to less than $0.1 \times 10^{-10} \text{ m/s}^2$. Consequently, if the anomalous radial acceleration acting on spinning spacecraft is gravitational in origin, it is *not* universal. That is, it must affect bodies in the 1000 kg range more than bodies of planetary size by a factor of 100 or more. As the authors of [18] said: “This would be a strange violation of the Principle of Equivalence”.

Attempts to detect observable evidence of unexpected gravitational effects acting on the orbits of the outer planets have not yielded any positive results yet. Hence, the authors of [308] used parametric constraints to the orbits of Uranus and Neptune and found that the reduced solar mass

to account for the Pioneer anomaly would not be compatible with the measurements. A similar result was obtained in [145] based on the Gauss equations to estimate the effect of a gravitational perturbation in terms of the time rate of change on the osculating orbital elements. These authors argue that the perturbation would produce long-period, secular rates on the perihelion and the mean anomaly, and short-period effects on the semimajor axis, the eccentricity, the perihelion and the mean anomaly large enough to be detected. [373] also considers the effect on the path of the outer planets of a disturbance on a spherically-symmetric spacetime metric, and rules out any model of the anomaly that implies that the Pioneer spacecraft move geodesically in a perturbed spacetime metric. A recent test of the orbits of 24 Trans-Neptunian Objects using bootstrap analysis also failed to find evidence of the anomaly in these objects [408].

Nevertheless, the absence of support for a perturbation of the planetary orbits in the outer solar system is weak and inconclusive (primarily due to the lack of precision range measurements). For example, the authors of [269] conclude that such anomalous gravitational disturbances would not be detected in the orbits of the outer planets. Therefore, efforts to find a gravitational explanation continue, as in the case of a recent paper [263] that proposes an azimuthally symmetric solution to Poisson’s equation for empty space to explain qualitatively the Pioneer anomaly. This solution results in a gravitational potential dependent on the distance and the polar angle, and it also has implications for the planetary orbits, albeit not yet tested with ephemeris data yet.

Many of these considerations are based on simplified models. As such, they must be contrasted with efforts that incorporate a radial acceleration into computations of planetary ephemerides.

Using the planetary ephemerides, Standish [362, 361] investigated modifications to the laws of gravitation that can explain the anomaly and still be compatible with the known motion of the planets from Saturn and outward. Out of five different acceleration models, four were shown to be not viable.

Using radiometric tracking data from the Cassini spacecraft, Folkner [118] established an upper bound on Saturn’s radial acceleration as less than 10^{-14} m/s². This is around just one tenth the anomalous acceleration of Pioneer 10 and 11.

Using the latest INPOP08 planetary ephemerides, Fienga et al [114] determined that a radial acceleration greater than 1/4 times the observed Pioneer anomaly at distances beyond 20 AU is not consistent with planetary orbits.

These investigations represent serious challenges to any attempt to explain the Pioneer anomaly using unseen mass distributions in the solar system or modifications of the theory of gravity. Such attempts, in addition to accounting for the anomalous acceleration of the two spacecraft, must also be able to explain why an acceleration of the same magnitude is *not* readily seen in the orbit of Saturn and in the known ephemerides of the outer planets.

6.7.2 Attempts to confirm the anomaly using other spacecraft

One reason that the Pioneer anomaly generated so much interest is that two spacecraft on very different trajectories yielded similar anomalous acceleration values. However, the two spacecraft are nearly identical in design, and although their trajectories are different, they both follow hyperbolic escape trajectories. This raises the obvious question: is it possible to confirm the presence of an anomalous acceleration using i) different spacecraft, or ii) spacecraft on different trajectories?

The Pioneer 10 and 11 spacecraft are sensitive to such a small, anomalous acceleration term because they are very far from the Sun, and therefore, the effects of solar radiation pressure are much smaller than the anomalous acceleration. For spacecraft located in the inner parts of the solar system (e.g., within the orbit of Jupiter), solar radiation pressure is significant; for Pioneer 10 and 11 at 5 AU, solar radiation results in an acceleration that exceeds the anomalous acceleration by nearly a full order of magnitude. This is a clear indication that the only candidates for investigating accelerations as small as the Pioneer anomaly are spacecraft in deep space, preferably at or beyond

the orbit of Jupiter.

The most obvious choice that comes to mind are the twin Voyagers. Voyager 1 and 2, like Pioneer 10 and 11 before them, are traveling on hyperbolic escape trajectories after encounters with the gas giants in the outer solar system. Unfortunately, unlike Pioneer 10 and 11, Voyager 1 and 2 are not spin stabilized. The three-axis stabilization employed by these spacecraft requires the use of small attitude stabilization thrusters several times a day. The noise produced by unmodeled small accelerations that arise as a result of uncertainties in the magnitude and exact duration of thruster firings and possible leakage afterwards reduce the sensitivity of these spacecraft to small accelerations such that an anomalous acceleration of order 10^{-9} m/s^2 is completely undetectable.

Next on the list was Galileo. This spacecraft, designed to orbit Jupiter, featured an innovative design comprising a spinning and a nonspinning section. However, due to mechanical problems between the two sections, the spacecraft was often configured to use the all-spinning mode. The malfunction of Galileo's high gain antenna opening mechanism put this antenna out of commission, and therefore, Galileo communicated with the Earth using an omnidirectional low-gain antenna at much lower than planned data rates, at a very low signal-to-noise ratio. Despite these difficulties, navigational data was obtained from this spacecraft with sufficient accuracy for precision orbit estimation. A combined analysis of Doppler and ranging data by The Aerospace Corporation from a 113-day period beginning shortly before Galileo's second Earth encounter (Galileo flew a complicated series of flyby orbits before it achieved a transfer orbit that took it to Jupiter) does show the presence of a possible acceleration term of the correct magnitude [18].

Ulysses, a joint project between NASA and the European Space Agency (ESA), flew on a highly elliptical heliocentric orbit tilted about 80° from the plane of the elliptic. Although Ulysses flew relatively close to the Sun and therefore, solar radiation had a significant effect on its trajectory, its varying distance from the Sun, combined with variations in the Earth-spacecraft-Sun angle make it possible in principle to separate the effects of solar radiation from any anomalous acceleration. This is how an estimate of $(12 \pm 3) \times 10^{-10} \text{ m/s}^2$ was obtained using JPL's ODP software. Although this value remains highly correlated with solar radiation pressure [18], it is compatible with the value of a_P measured for Pioneer 10 and 11.

Yet another deep-space craft, Cassini, is three-axis stabilized like Voyager 1 and 2. Nevertheless, the sophisticated tracking capabilities of this spacecraft could offer a potential contribution to the research of the anomalous acceleration [18].

The recently (2006) launched New Horizons mission to Pluto is potentially a better candidate for researching the anomalous acceleration. Like Pioneer 10 and 11, New Horizons is spin stabilized, using only infrequent thruster maneuvers for attitude stabilization. Unfortunately, current mission plans call for New Horizons to spend much of the time between Jupiter and Pluto in "hibernation" mode, with only infrequent communications with the Earth. Therefore, during the flight to Pluto, little or no precision Doppler data may be collected [246, 385, 393].

As a result, attempts to verify the anomaly using other spacecraft have proven disappointing [18, 19, 23, 252], because the Voyager, Galileo, Ulysses, and Cassini spacecraft navigation data all have their own individual difficulties for use as an independent test of the anomaly. In addition, many of the deep space missions that are currently being planned will not provide the needed navigational accuracy and trajectory stability of under 10^{-10} m/s^2 .

6.7.3 Possible future spacecraft searches

The acceleration regime in which the anomaly was observed diminishes the value of using modern disturbance compensation systems for a test. For example, the systems that are currently being developed for the LISA (Laser Interferometric Space Antenna) and LISA Pathfinder missions are designed to operate in the presence of a very low frequency acceleration noise (at the mHz level), while the Pioneer anomalous acceleration is a strong constant bias in the Doppler frequency data.

In addition, currently available accelerometers are a few orders of magnitude less sensitive than is needed for a test [23, 252, 255, 393, 396]. To enable a clean test of the anomaly there is also a requirement to have an escape hyperbolic trajectory. This makes a number of other currently proposed missions less able to directly test the anomalous acceleration.

A number of alternative ground-based verifications of the anomaly have also been considered; for example, using VLBI astrometric observations. However, the trajectories of Pioneers, with small proper motions in the sky, make it presently impossible to use VLBI in accurately isolating an anomalous sunward acceleration of the size of a_P .

6.8 A mission to explore the Pioneer anomaly

The apparent inability to explain the anomalous behavior of the Pioneers with conventional physics has contributed to growing discussion about its origin. A number of researchers emphasized the need for a new experiment to explore the detected signal. As a result, [393] advocated for a program to study the Pioneer anomaly. This program effectively includes three phases:

- i) Analysis of the entire set of existing Pioneer data, obtained from launch to the last useful data received from Pioneer 10 in April 2002. This data provides critical new information about the anomaly [384, 393]. If the anomaly is confirmed,
- ii) Development of an instrument, to be carried on another deep space mission, to provide an independent confirmation for the anomaly. If further confirmed,
- iii) Development of a dedicated deep-space experiment to explore the Pioneer anomaly with an accuracy for acceleration resolution at the level of 10^{-12} m/s² in the extremely low frequency (or nearly DC) range.

Significant progress was accomplished concerning the first and second phases [252, 307, 384, 396]. Work on the third phase was also initiated [47, 94, 313, 384, 393]. Mission studies conducted in 2004–2005 [94] have identified two options: i) an experiment on a major mission to deep space capable of reaching acceleration sensitivity similar to that demonstrated by the Pioneers and ii) a dedicated mission to explore the Pioneer anomaly that offers full characterization of the anomaly. Below we discuss both of these proposals.

6.8.1 A Pioneer instrument package

A way to confirm independently the anomaly is to fly an instrumental package on a mission heading to the outer regions of the solar system. The primary goal is to provide an independent experimental confirmation of the anomaly. One can conceive of an instrument placed on a major mission to deep space. The instrument must be able to compensate for systematic effects to an accuracy below the level of 10^{-10} m/s². Another concept is a simple autonomous probe that could be jettisoned from the main vehicle, such as the proposed Interstellar Probe²⁷, presumably further out than at least the orbit of Jupiter or Saturn. The probe would then be navigated from the ground yielding a navigational accuracy below the level of 10^{-10} m/s². The data collected could provide an independent experimental verification of the anomaly's existence.

Dittus et al. [94] emphasized that the option of an instrument on a major mission to deep space would have a major impact on spacecraft and mission designs with limited improvement in measuring a_P . Nevertheless, a highly-accurate accelerometer has been proposed as part of the Gravity Advanced Package, which is a fundamental physics experiment that is being considered

²⁷see <http://interstellar.jpl.nasa.gov/interstellar/probe/> for details.

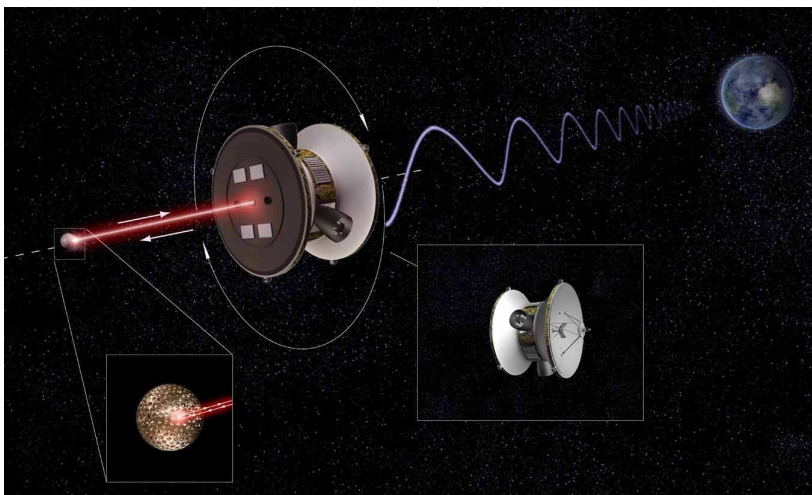


Figure 6.1: A drawing for the measurement concept chosen of the Deep Space Gravity Probe (from [94], drawing courtesy of Alexandre D. Szames). The formation-flying approach relies on actively controlled spacecraft and a set of passive test-masses. The main objective is to accurately determine the heliocentric motion of the test-mass by utilizing the 2-step tracking needed for common-mode noise rejection purposes. The trajectory of the spacecraft will be determined using standard methods of radiometric tracking, while the motion of the test mass relative to the spacecraft will be established by laser ranging technology. The test mass is at an environmentally quiet distance from the craft, ≥ 250 m. With occasional maneuvers to maintain formation, the concept establishes a flexible craft to test mass formation.

by the ESA for the future Jupiter Ganymede Orbiter Mission²⁸. At the same time, it is clear that to explore the anomaly one needs to travel beyond the orbit of Jupiter. Furthermore, an acceleration sensitivity at the level of $\sim 10^{-12}$ m/s² would be preferable, which can be done only with a dedicated mission, as discussed in Section 6.8.2 below.

6.8.2 A dedicated mission concept

The available knowledge of the Pioneer anomaly lead to the following science objectives for a dedicated mission to explore the Pioneer anomaly: i) investigate the origin of the anomaly with an improvement by a factor of 1,000; ii) improve spatial, temporal, and directional resolution; iii) identify and measure all possible disturbing and competing effects; iv) test Newtonian gravity potential at large distances; v) discriminate amongst candidate theories explaining a_P , and vi) study the deep-space environment in the outer solar system.

A viable concept would utilize a spacecraft pair capable of flying in a flexible formation (see Figure 6.1). The main craft would have a precision star-tracker and an accelerometer and would be capable of precise navigation, with disturbances, to a level less than $\sim 10^{-10}$ m/s² in the low-frequency acceleration regime. Mounted on the front would be a container holding a probe – a spherical test mass covered with corner cubes. Once the configuration is on its solar system escape trajectory and will undergo no further navigation maneuvers, and is at a heliocentric distance of ~ 5 –20 AU, the test mass would be released from the primary craft. The probe will be passively

²⁸See presentation by B. Christophe, “Gravity Advanced Package, a fundamental physics experiment for Jupiter Ganymede Orbiter Mission”, at the recent *Gravitation and Fundamental Physics in Space*, the GPhyS “Kick-Off” Colloquium, Les Houches, 20–22 October, 2009, at <http://gphys.obspm.fr/LesHouches2009/Program.html>.

laser-ranged from the primary craft with the latter having enough capabilities to maneuver with respect to the probe, if needed. The distance from the Earth to the primary would be determined with either standard radiometric methods operating at Ka-band or with optical communication. Note that any dynamical noise at the primary would be a common mode contribution to the Earth-primary and primary-probe distances. This design satisfies the primary objective, which would be accomplished by the two-staged accurate navigation of the probe with sensitivity down to the 10^{-12} m/s² level in the DC of extremely low frequency bandwidth.

Since the small forces affecting the motion of a craft in four possible directions all have entirely different characteristics (i.e., sunward, earthward, along the velocity vector or along the spin-axis [252, 393]), it is clear that an antenna with a highly directional radiation pattern along with star sensors will create even better conditions for resolving the true direction of the anomaly when compared to standard navigation techniques. On a craft with these additional capabilities, all on-board systematics will become a common mode factor contributing to all the attitude sensors and antennas. The combination of all the attitude measurements will enable one to clearly separate the effects of the on-board systematics referenced to the direction towards the Sun.

To enable fast orbital transfer to distances greater than 20 AU, hyperbolic escape trajectories enabled by solar sail propulsion technology were considered as an attractive candidate. Among other options is a standard chemical rocket and nuclear electric propulsion, as was successfully demonstrated recently [252]. The proposed combination of a formation-flying system aided by solar sail propulsion for fast trajectory transfer, leads to a technology combination that will benefit many missions in the future [390, 392].

Two missions were recently proposed to explore the Pioneer anomaly in a dedicated space experiment. The Solar System Odyssey mission will use modern-day high-precision experimental techniques to test the laws of fundamental physics, which determine dynamics in the solar system [70]. The mission design is similar to the one proposed for the Deep Space Gravity Probe (DSGP) [94]. Also, the proposed SAGAS (Search for Anomalous Gravitation using Atomic Sensors) mission [425] aims at flying highly sensitive atomic sensors (optical clock, cold atom accelerometer, optical link) on a solar system escape trajectory. SAGAS has numerous science objectives in solar system exploration and fundamental physics, including an accurate test of the Pioneer anomaly.

The extraordinary nature of the Pioneer anomalous acceleration led to serious questions concerning the possible origin of the effect. Answering these questions requires further in-depth analysis. This is especially true before any serious discussion of a dedicated experiment can take place. In fact, prior to the development of any dedicated mission to investigate the Pioneer anomaly, it is absolutely essential to analyze the complete Pioneer Doppler data in order to rule out, as much as possible, any engineering cause. This study is on-going and will be reviewed in Section 7.

7 Current Status of the Study of the Pioneer Anomaly

With the publication of the JPL’s definitive 2002 study of the Pioneer anomaly [18] the efforts to study the discovered effect have intensified. After some hesitation there was an agreement among the researchers that a thorough investigation of the anomaly is needed. The main question remained: What is the nature of the Pioneer anomaly? Is this a manifestation of new physics? Or a representation of some unmodeled conventional physics mechanism? Furthermore, it became clear that before the Pioneer anomaly can be fully accepted as a novel physical effect, the issue of the on-board heat redistribution must be fully addressed.

Ultimately, the search for the origin of the Pioneer anomaly came down to one principal question: “Is it the heat or not the heat?” Multiple community efforts are now guided by this question. In addition to the teams from JPL and The Aerospace Corporation, several independent teams and researchers have confirmed the existence of the anomalous acceleration in the Pioneer Doppler data; the new analyses also studied temporal behavior of the anomaly, establishing limits on the temporal change of anomalous acceleration. As a result of these extensive multi-year efforts, our understanding of the Pioneer anomaly improved significantly (see Section 7.1).

Meanwhile, a team at JPL along with C.B. Markwardt at the NASA Goddard Space Flight Center have been working on the recovery of a much extended radiometric Doppler data set, covering a significantly longer time period for both spacecraft than previously available data (Section 3.3). At the same time, thanks mainly to the efforts of L.R. Kellogg at the NASA Ames Research Center, a near complete record of telemetry from Pioneer 10 and 11 (Section 3.5) has been recovered, as well as significant quantities of original project documentation (Section 2.1.3). This made it possible to construct a detailed thermal model of the spacecraft, investigating the extent to which heat generated on-board and radiated away anisotropically may contribute to the anomalous acceleration (Section 7.4).

As of early 2010, some of these efforts are finished, such as the recovery of the Doppler data, while others, notably, the construction of a comprehensive thermal model, are still under way. This new effort to investigate the Pioneer anomalous acceleration, when completed, will for the first time use all available Doppler data to establish the acceleration profile of the two spacecraft, and it will also accurately account for any acceleration of on-board thermal origin.

In this section, we review these recent and on-going efforts and summarize our current knowledge of the Pioneer anomaly.

7.1 Independent verifications

By now several studies of the Pioneer 10 and 11 radiometric Doppler data have demonstrated that the anomaly is unambiguously present in the trajectory solutions for both spacecraft. These studies were performed with six independent (and different!) navigational computer programs (see [15, 18, 171, 185, 266, 382]), namely:

- The most detailed analysis of the Pioneer anomaly to date, the 2002 study by JPL [18] (which is discussed in depth in Section 5), used various versions of the JPL’s Orbit Determination Program (ODP), developed between 1980–2005 [15, 18],
- The Aerospace Corporation’s Compact High Accuracy Satellite Motion Program (CHASMP) code, extended for deep space navigation [15, 18],
- Code written at the Goddard Space Flight Center (GSFC) by C.B. Markwardt [185] that was used to analyze Pioneer 10 data for the period 1987–1994 obtained from the National Space Science Data Center (NSSDC)²⁹,

²⁹The National Space Science Data Center (NSSDC), see details at <http://nssdc.gsfc.nasa.gov/>

- The HELIOSAT orbit determination program that was co-developed at the Institute for Theoretical Astrophysics, University of Oslo, Norway, was recently used by one of the code's authors, Ø. Olsen [266], to analyze the set of the Pioneer 10 data set identical to the one used in the JPL's 2002 study,
- An orbit determination code that was independently developed by V.T. Toth [382] for the purposes of studying the Pioneer anomaly, and finally
- A dedicated software package called ODYSSEY that has been developed by Groupe Anomalie Pioneer (GAP)³⁰ for the purposes of investigating the Pioneer anomaly [171].

These recent independent analyses of the Pioneer 10 and 11 radiometric Doppler data confirmed the existence of the Pioneer anomaly at the level reported by the JPL's 2002 study and they also provided new knowledge of the effect. Below we review these analyses in some detail.

7.1.1 Independent verification by Markwardt

Shortly after publication of the 2002 JPL result, Markwardt [185] published an independent analysis that was unique in the sense that it utilized a separately obtained data set. Rather than using data in the form of JPL-supplied Orbit Determination Files, Markwardt obtained Pioneer 10 tracking data from the National Space Science Data Center (NSSDC) archive. This data was in the Archival Tracking Data File (ATDF) format, which Markwardt processed using tools developed for the purposes of this specific study [183, 184].

The Pioneer 10 data used in Markwardt's investigation spanned the years 1987 through 1994, and his result, $a_{P10} = (7.70 \pm 0.02) \times 10^{-10} \text{ m/s}^2$ (see Figure 7.1), is consistent with the JPL result. Markwardt was also the first to investigate explicitly the possible presence of a jerk (i.e., the rate of change of acceleration³¹, defined as $j \equiv \dot{a} = da/dt$) term, and found that a term $|j_{P10}| < 0.18 \times 10^{-10} \text{ m/s}^2/\text{year}$ is consistent with the data. Based on the studied Pioneer 10 data set, Markwardt found that the anomaly is nearly constant with time, with a characteristic variation time scale of over 70 yr, which is still too short to rule out on-board thermal radiation effects.

7.1.2 Analysis by Olsen using HELIOSAT

Olsen [266] focused on the constancy of the anomalous acceleration using the HELIOSAT orbit determination program that was independently developed by him at the University of Oslo, Norway. Analysis confirmed the acceleration at the levels reported by [18] for the same segments of Pioneer 10 and 11 data that were used by JPL (see Table 7.1). The study found that systematic variations in the anomalous acceleration are consistent with solar coronal mass ejections and that the Doppler data alone cannot distinguish between constant acceleration and slowly decreasing acceleration. Specifically, the study concluded that heat dissipation cannot be excluded as a source of the anomaly.

7.1.3 Independent analysis by Toth

Toth [382] also studied the anomalous acceleration using independently developed orbit determination software, and confirmed that the introduction of a constant acceleration term significantly

³⁰Groupe Anomalie Pioneer (GAP), a French collaboration on Pioneer Anomaly supported by The Centre National d'Etudes Spatiales (CNES), France, which includes researchers from LKB, ONERA, OCA, IOTA and SYRTE laboratories, see details at <http://www.lkb.ens.fr/~GAP-?lang=fr>

³¹See definition of the jerk term at [http://en.wikipedia.org/wiki/Jerk_\(physics\)](http://en.wikipedia.org/wiki/Jerk_(physics)).

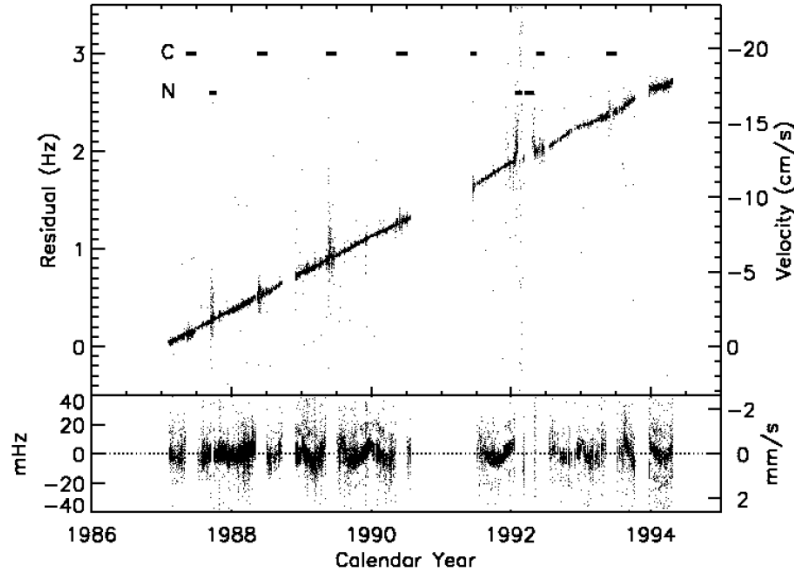


Figure 7.1: Results of Markwardt’s analysis [185] show Doppler residuals as a function of time of the best fit model. The top panel shows the residuals after setting $a_P = 0$, and demonstrates the linear increase with time. The top panel shows all of the data, including segments that were filtered out because of interference due to the solar corona (designated by a horizontal bar with “C”) or due to general noise (designated “N”). The bottom panel shows the filtered residuals, including the best fit value of the anomalous acceleration. The equivalent spacecraft velocity is also shown.

Table 7.1: The Pioneer anomalous acceleration in units of 10^{-10} m/s^2 . This table compares the results from JPL’s ODP and the Aerospace Corporation’s CHASMP codes from [18] (see Table 5.1) to results obtained using the HELIOSAT program developed by Olsen [266].

Software	Pioneer 10 (I)	Pioneer 10 (II)	Pioneer 10 (III)	Pioneer 11
ODP/Sigma	8.00 ± 0.01	8.66 ± 0.01	7.84 ± 0.01	8.44 ± 0.04
CHASMP	8.22 ± 0.02	8.89 ± 0.01	7.92 ± 0.01	8.69 ± 0.03
HELIOSAT	7.85 ± 0.02	8.78 ± 0.01	7.75 ± 0.01	8.10 ± 0.01

improves the post-fit residuals (Figure 7.2). Toth determined the anomalous accelerations of Pioneers 10 and 11 as $a_{P10} = (9.03 \pm 0.86) \times 10^{-10} \text{ m/s}^2$ and $a_{P11} = (8.21 \pm 1.07) \times 10^{-10} \text{ m/s}^2$ correspondingly, where the error terms were taken from [18] (excluding terms related to thermal modeling, which is the subject of on-going effort). Studying the temporal behavior of the anomalous acceleration, he was able to find a best fit for the acceleration and jerk terms of both spacecraft: $a_{P10} = (10.96 \pm 0.89) \times 10^{-10} \text{ m/s}^2$ and $j_{P10} = (-0.21 \pm 0.04) \times 10^{-10} \text{ m/s}^2/\text{year}$ (Pioneer 10) and $a_{P11} = (9.40 \pm 1.12) \times 10^{-10} \text{ m/s}^2$ and $j_{P11} = (-0.34 \pm 0.12) \times 10^{-10} \text{ m/s}^2/\text{year}$ (Pioneer 11). Toth’s study demonstrated that a moderate jerk term is consistent with the Doppler data and, therefore, an anomalous acceleration that is a slowly changing function of time cannot be excluded at present.

Toth’s orbit determination software also has the capability to utilize telemetry data. In particular, the code can be used to estimate the thermal recoil force as a function of the heat generated on-board, or conversely, to fit thermal recoil force coefficients to radiometric Doppler measure-

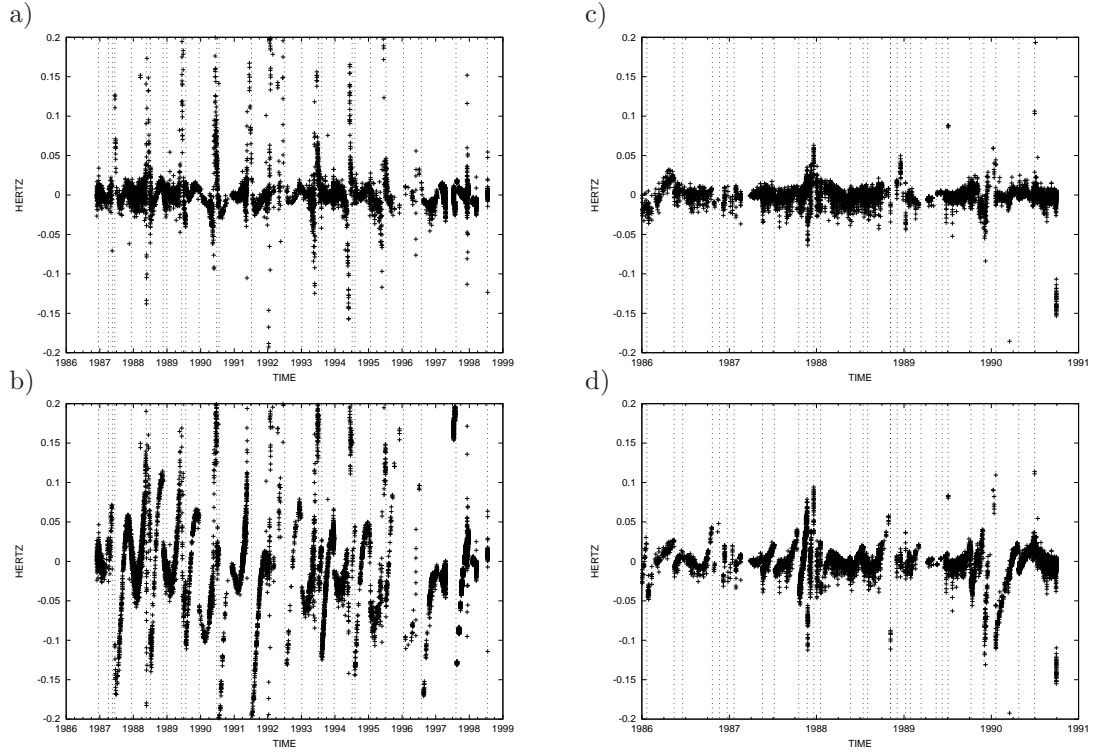


Figure 7.2: Results of Toth's analysis [382]: a) best-fit residuals for Pioneer 10; b) best-fit residuals for Pioneer 10 with no anomalous acceleration term; c–d) same as a–b, for Pioneer 11.

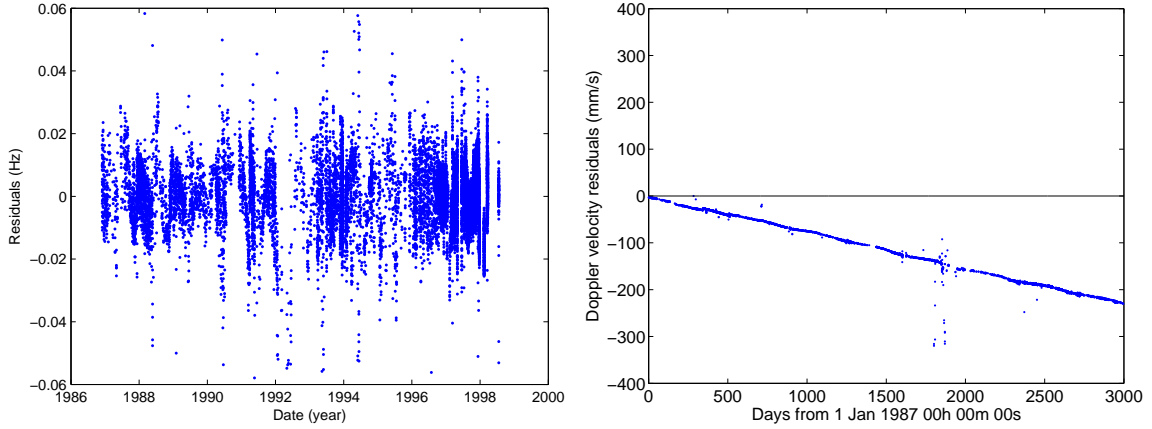


Figure 7.3: Best-fit Pioneer 10 residuals using the ODYSSEY orbit determination program [171]. Left: residuals after a best-fit constant acceleration of $a_P = (8.40 \pm 0.01) \times 10^{-10} \text{ m/s}^2$. Right: reconstruction of the anomalous acceleration contribution.

ments, as discussed in Section 7.4.4.

7.1.4 Analysis by Levy et al. using ODYSSEY

Levy et al. [171] also performed an analysis of the Pioneer data using the independently developed orbit determination program ODYSSEY. The team confirmed the presence of an acceleration signal consistent with that found in other studies: for Pioneer 10, they obtained an anomalous acceleration of $a_P = (8.40 \pm 0.01) \times 10^{-10} \text{ m/s}^2$ (see Figure 7.3). Their study shows the presence in the residual of periodic terms with periods consistent with half a sidereal day, one sidereal day, and half a year, and they investigate the possibility that these variations may be due to perturbations of unknown origin that modify the propagation of the signal.

In view of all these studies, the existence of the Pioneer anomaly in the Pioneer 10 and 11 radiometric Doppler data is established beyond doubt. Furthermore, the analyses [171, 185, 266, 382] brought new knowledge about the effect, especially insofar as the temporal behavior of the anomaly is concerned. As a result, the anomalous acceleration can no longer be characterized as having a constant magnitude. Instead, the effect clearly shows temporal decrease – perhaps consistent with the decay of the radioactive fuel on board – the conjecture that needs further investigation. This recently-gained knowledge serves as a guide for new study of the effect (discussed in Section 7.3); it also points out the unresolved questions that we summarize below.

7.2 Unresolved questions

Although JPL’s 2002 study [18] offered a very comprehensive review of the Pioneer anomaly, in some cases it left some questions unanswered. In other cases, the report’s conclusions were put into question, either by independent verifications or by the analysis of subsequently recovered data and spacecraft documentation.

Specifically, the following open questions are important for understanding the physical nature of the Pioneer anomaly and are a subject of on-going investigation:

- *Direction:* The true direction of the anomalous acceleration is yet unclear. Within the typical angular uncertainty of Doppler navigation in the S-band and a spacecraft HGA pointing accuracy of 3° (set within 10 dB antenna gain bandwidth), a_P behaves as a constant acceleration of the craft pointing in the innermost region of the solar system. Is it possible to determine, on the basis of available data, if the anomalous acceleration points towards the Sun, the Earth, the spin-axis direction, or the direction of the spacecraft’s motion?
- *Constancy:* The earlier analysis concluded that both temporal and spatial variations of the anomaly’s magnitude are of order 10% for each craft, while formal errors are significantly smaller. But what is the true temporal behavior of the anomaly? Is it really possible to exclude on-board heat (which decays with time) as its source?
- *Distance:* It is unclear how far out the anomaly extends, but the Pioneer 10 data supports its presence at distances up to ~ 70 AU from the Sun. The Pioneer 11 data shows the presence of the anomaly as close in as ~ 20 AU. What is the true range of the anomaly, does it extend beyond these limits?
- *Onset:* Early data suggests that the anomalous acceleration may not have been present when the spacecraft were much nearer to the Sun. Can this be confirmed using the extended Doppler data set?
- *Annual/diurnal terms:* Even after a best fit analysis is completed, the resulting residual is not completely random: both annual and diurnal variations are clearly visible [18, 171, 391]. Is it possible to pinpoint the source of these variations?

- *Pioneer spin anomaly*: The Pioneer 10 spacecraft exhibited anomalous spin behavior, and corresponding anomalous behavior in its fuel system. Similar issues exist with the spin of Pioneer 11. Does this spin anomaly have any bearing on the anomalous acceleration?
- *The thermal recoil force*: Since the publication of the 2002 study [18], it has become clear that the magnitude of the recoil force due to anisotropically emitted heat has been underestimated. To what extent is this heat responsible for the anomalous acceleration?

In the following subsections, we review these unresolved questions in detail, including information that has become available since 2002 as a result of the on-going efforts of several teams.

7.2.1 Direction

The direction of the anomalous acceleration vector has been the subject of many discussions. If this direction was precisely known, it would allow one to establish the possible cause(s) of the anomaly; at present, all causes must be considered.

The canonical value of $a_P = (8.74 \pm 1.33) \times 10^{-10} \text{ m/s}^2$ was developed using the *hypothesis* that the anomalous acceleration of the two spacecraft is Sun-pointing, and it finds that the hypothesis is consistent with the data. However, this does not exclude the possibility that equally good solutions can be obtained by postulating an hypothetical acceleration vector in some other direction.

Thus, we must consider at least four possible directions for the anomaly (see Figure 7.4), all indicating a different physical mechanism. Because these directions differ by at most a few degrees during the period of time from which Doppler data was studied, they cannot be distinguished easily. However, each of these four directions implies very different physics.

Specifically, if the acceleration was: i) in the direction *towards the Sun*, this would indicate a force, likely gravitational, originating from the Sun, likely signifying a need for gravity modification; ii) in the direction *towards the Earth*, this would indicate a time signal anomaly originating in the DSN hardware or introduced by the space flight-control methods; iii) in the direction *of the velocity vector*, this would indicate an inertial force or a drag force providing support for a media-dependent origin; or, finally, iv) in the *spin-axis direction*, this would indicate an on-board systematic, which is the most plausible explanation for the effect. As seen on the left of Figure 7.4, the corresponding directional signatures of these four directions are distinct and could be easily extracted from the data [252, 393, 399].

The navigation of the Pioneer spacecraft relied on an S-band radio-Doppler observable (no ranging capabilities!), which is not very accurate for the purposes of a 3-dimensional orbit reconstruction. To maintain communications with the Earth using the narrow beam of their HGA, an Earth-pointing attitude was necessary. During the flight through the inner solar system, this required frequent attitude correction maneuvers to re-orient the spin axis. At this time, the Sun-craft-Earth angle was relatively large, as was the angle between these and the direction of motion (Figure 7.4). Even so, the Pioneer data from distances up to 27 AU indicate an approximately sunward directional anomaly for both craft. However, at distances farther than 40 AU, both the Sun and the Earth were within the 3° of the antenna radiation pattern (set by 10 dbm range in the antenna gain), thus limiting accuracy in directional reconstruction.

Given the importance of the direction of the anomalous acceleration, it is perhaps surprising that this direction has not yet been established. This is due to the fact that the data that has been investigated to date is from the late cruise phase of the Pioneer 10 and 11 missions, when Pioneer 10 was over 40, and Pioneer 11 was over 22 AU from the Sun. From this distance, the Earth-spacecraft-Sun angle is less than 3° . The angle between the spacecraft spin axis and the Earth-spacecraft line is also small, as the spacecraft was always oriented towards the Earth in order to maintain continuous radio communication. Lastly, at these distances from the Sun the

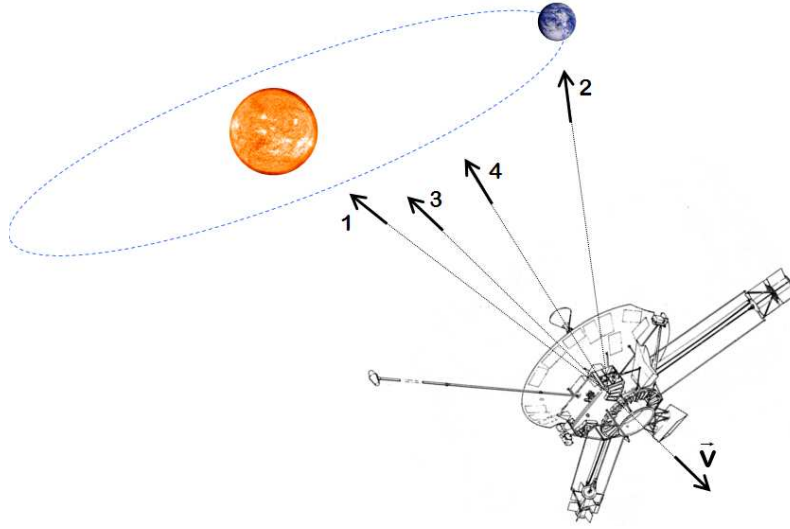


Figure 7.4: The four possible different directions for the Pioneer anomaly: (1) toward the Sun, (2) toward the Earth, (3) along the velocity vector, and (4) along the spin axis. These directions would offer different signal modulations [252, 393] that could be detected in the new study.

hyperbolic orbits of the spacecraft are nearly asymptotic, and the direction of motion corresponds closely with the Sun-spacecraft direction.

The discussion above indicates that the true direction of the Pioneer anomalous acceleration still remains poorly determined. Based on the Pioneer data analyzed to date, a more correct statement about the direction would be that the anomaly is directed towards the *inner* part of the solar system – the region that includes both the Sun and the Earth. This question will be re-examined with the extended data set that is now available for new investigation (see Section 3.3).

7.2.2 The magnitude and temporal behavior of the effect

The magnitude of the anomalous acceleration has been confirmed by several studies [171, 185, 266, 382], all of which show results that are consistent with JPL’s “canonical” value of $a_P = (8.74 \pm 1.33) \times 10^{-10} \text{ m/s}^2$. However, the constancy of the Pioneer anomalous acceleration remains a subject of serious debate.

For example, if the anomaly was of thermal origin, its magnitude would decay with time, consistent with the decreasing amount of heat generated on-board. Initially [18] it was assumed that the decay of a thermal recoil force would be consistent with the half-life of the ^{238}Pu fuel (87.74 years), but later it was realized [156, 236, 331] that other effects, such as regulation of the electric power on board, can mask at least some of this decay.

Meanwhile, Markwardt ([185]; see also Section 7.1.1) and later, Toth ([382], see Section 7.1.3) demonstrated that the Doppler data are, in fact, consistent with a change-of-acceleration (jerk) term for both spacecraft, and that the magnitude of this jerk term is consistent with the decay of the on-board thermal inventory.

7.2.3 Onset of the anomaly

Early Pioneer 10 and 11 data (before 1987) were never analyzed in detail, especially with regard to systematics. However, by about 1980 the Doppler navigational data had begun to indicate

the presence of an anomaly. At first this was considered to be only an interesting navigational curiosity. But even so, samples of data a few months long in duration were periodically examined by different analysts. By 1992 an interesting string of data-points had been obtained; they were gathered in a JPL memorandum [12], and are shown in Figure 5.1. (More details on this issue are in [15, 18, 394].)

For Pioneer 10, an approximately constant anomalous acceleration seems to exist in the data as close in as 27 AU from the Sun. For Pioneer 11, beginning just after Jupiter flyby, the early navigational data show a small value for the anomaly during the Jupiter-Saturn cruise phase in the interior of the solar system. But right at Saturn encounter, when the craft passed into an hyperbolic escape orbit, there was an apparent fast increase in the anomaly, whereafter it settled into the canonical value.

The data, therefore, indicate the possibility that there was an “onset” of the anomaly at around this time, as the anomalous acceleration component was much smaller prior to Saturn encounter. However, this is likely a premature conclusion. The observations shown in Figure 5.1 do not represent a systematic set of measurements obtained using a consistent, common editing strategy. The apparent onset of the anomaly that is seen in Figure 5.1 has been used to justify theoretical work that predicted a modification of gravity or other nongravitational forces that affect only objects at sufficient distance from the Sun, or objects in hyperbolic orbits. Yet it must be emphasized (as indeed, the authors of the 2002 study [18] emphasized in a footnote) that this early detection data cannot be viewed as a measurement; confirmation of the onset of the anomaly requires re-analysis of early Doppler data using a consistent editing strategy.

Other factors, such as the greater frequency of maneuvers, also put into question the extent to which one can rely on the apparent pattern represented by the first few data points in Figure 5.1. Also, during this time period, solar radiation pressure produced an acceleration that was several times larger than the anomaly. Scheffer [329, 331] pointed out that the onset that is seen in the data may, in fact, be an artifact of solar model calibration. If an anomalous sunward acceleration was present but not accounted for at the time the solar model coefficients were measured when the spacecraft were still near the Sun (i.e., if the anomalous acceleration was absorbed into estimates of solar model coefficients), later, as solar radiation decreased, one would observe an apparent onset as a result of this miscalibration.

7.2.4 Annual/diurnal terms

As indicated in Section 5.5.4, even after a best fit solution is obtained, the resulting residuals contain clearly discernible annual and diurnal signatures. These small, approximately sinusoidal contributions do not affect the determination of the (approximately constant) anomalous acceleration, as they are uncorrelated with it. However, the origin of these sinusoidal terms remains unknown.

The authors of [18, 391] expressed the belief that these terms are due to orbital mismodeling, notably mismodeling of the orbital inclination of the spacecraft to the ecliptic plane. Other possibilities also exist: for instance, the annual term may be related to mismodeling of the effects of solar plasma on the radio signal, whereas the diurnal term may be related to atmospheric effects on the signal.

7.2.5 Radio beam reaction force

Among the effects considered by the authors of [18], the radio beam reaction force produced the largest bias to the result (see Section 5.4.4). This bias is due to the fact that the spacecraft are continuously transmitting a $P_{\text{radio}} = \sim 8$ W highly collimated radio beam in the direction of the Earth, and as a result, experience a proportional recoil force, resulting in an acceleration of $a_{\text{radio}} = P_{\text{radio}}/mc \simeq -1.10 \times 10^{-10}$ m/s². As the force exerted by the radio beam necessarily points

away from the Earth and the Sun (as indicated by the negative sign in the preceding equation), the correction of the measured data increases the amount of the observed anomalous attractive force and makes the Pioneer effect larger.

Two open questions remain concerning the actual magnitude of the radio beam recoil force. First, according to the recovered flight telemetry, the radio beam reaction force might not have been constant. Flight telemetry indicates that during much of the mission, the radio beam was more powerful than the nominal 8 W, exceeding the nominal value by 1 W and more. Near the end of Pioneer 10's mission, however, the transmitter power may have decreased by as much as 3 W (see Figure 2.19). As this apparent decrease coincides with a drop in the main bus voltage on board (due to the depletion of the spacecraft's ^{238}Pu power supply), the decrease may be an artifact of a failing telemetry system (see also Section 2.4.5).

Second, Scheffer [331] argues that assuming a typical antenna design, as much as 10% of the power emitted by the high gain antenna (HGA) feed would have missed the parabolic dish altogether, and would have produced a reaction force in the opposite direction, at an approximately 45° angle. Although the HGA is discussed in detail in the recovered project documentation, no attempt has yet been made to establish more precise estimates on the efficiency with which the transmitter's power is converted into a recoil force.

7.2.6 The Pioneer spin anomaly

The spin rates of the Pioneer 10 and 11 spacecraft, nominally 4.8 revolutions per minute (rpm), were in fact changing with time. As we showed in Section 2.3.7, the two spacecraft exhibited markedly different behavior, with unique features.

Pioneer 10 was slowly spinning down, with three discernible phases in its spin history, described in detail in Section 2.3.7. The changes in Pioneer 10's spin rate approximately coincide with unexplained readings from its propulsion tank (see Section 2.3.6).

Meanwhile, Pioneer 11 was spinning up, although a detailed examination of its spin history reveals that spin-up events coincided with attitude correction maneuvers, and between maneuvers the spacecraft was spinning down, albeit at varying rates (see Section 2.3.7).

It is possible that a constant or near constant rate of spin change is of thermal origin: if thermal radiation is emitted by the spacecraft not just anisotropically but also asymmetrically with respect to the spacecraft's center-of-gravity, a torque acts on the spacecraft.

No convincing explanation has yet been offered for the anomalous change in the spin change rate during the history of Pioneer 10. The approximate coincidence of this change with the anomalous change in fuel tank pressure readings may be significant; on the other hand, it must be emphasized that this coincidence is only approximate, and may very well be accidental.

In contrast, the spin rate change of Pioneer 11 exhibits no dramatic changes, and appears to be a combination of three effects: A spindown that may be similar to that of Pioneer 10 and may be of thermal origin, instantaneous spinups that occur at each maneuver and may be a result of a small thruster misalignment, and a third effect that changes the spindown rate after each maneuver, and may be related to thruster leaks and outgassing.

It should be noted that these considerations are qualitative in nature, and no detailed study of the Pioneer 10 and 11 spin history has taken place to date. In particular, we do not know if the spin rate change is related to the anomalous acceleration of these spacecraft.

7.2.7 Thermal recoil forces

The effect of rejected thermal radiation was the second largest bias/uncertainty that has been the most critical systematic bias to quantify (see Section 4.4.3). If heat generated by the on-board power sources was asymmetrically reflected by the body of the craft, an acceleration along the spin axis could be produced causing the measured anomaly.

The Pioneer spacecraft were powered by SNAP-19 (Space Nuclear Ancillary Power) RTGs mounted on long extended booms (designed to protect the on-board electronics from heat and radiation impact) [15, 18, 19]. It was recognized early that, in principle, there was more than enough heat available on the craft to cause the anomaly (see Section 2.4). In addition to heat from the RTGs, additional waste heat was produced by electrical instrumentation, Radioisotope Heater Units (RHUs), and the propulsion system.

However, it was assumed that the spacecraft’s spin-stabilized attitude control, special design of the RTGs and the length of the RTG booms that resulted in a relatively small spacecraft surface available for the preferential heat rejection significantly minimized the amount of heat for the mechanism to work. These considerations led to an estimated acceleration not exceeding $a_{\text{hr}} = (-0.55 \pm 0.55) \times 10^{-10} \text{ m/s}^2$. This result is now being reconsidered, in view of on-going work on Pioneer thermal modeling, which suggests that the acceleration due to asymmetrically reflected heat from the RTGs may have been several times this value.

As the spacecraft is in an approximate thermal steady state, heat generated on board must be removed from the spacecraft [385]. In deep space, the only mechanism of heat removal is thermal radiation: the spacecraft can be said to be radiatively coupled to the cosmic background, which can be modeled by surrounding the spacecraft with a large, hollow spherical black body at the temperature of $\sim 2.7 \text{ K}$.

The spacecraft emits heat in the form of thermal photons, which also carry momentum p_γ , in accordance with the well known law of $p_\gamma = h\nu/c$, where ν is the photon’s frequency, h is Planck’s constant, and c is the velocity of light. This results in a recoil force in the direction opposite to that of the path of the photon. For a body that emits radiation in a spherically symmetric pattern, the net recoil force is zero. However, if the pattern of radiation is not symmetrical, the resulting anisotropy in the radiation pattern yields a net recoil force.

The magnitude of this recoil force is a subject of many factors, including the location and thermal power of heat sources, the geometry, physical configuration, and thermal properties of the spacecraft’s materials, and the radiometric properties of its external (radiating) surfaces.

The total thermal inventory on board the Pioneer spacecraft exceeded 2 kW throughout most of their mission durations. The spacecraft were in an approximate steady state: the amount of heat generated on-board was equal to the amount of heat radiated by the spacecraft.

The mass of the Pioneer spacecraft was approximately 250 kg. An acceleration of $8.74 \times 10^{-10} \text{ m/s}^2$ is equivalent to a force of $\sim 0.22 \mu\text{N}$ acting on a $\sim 250 \text{ kg}$ object. This is the amount of recoil force produced by a 65 W collimated beam of photons. In comparison with the available thermal inventory of 2500 W, a fore-aft anisotropy of less than 3% can account for the anomalous acceleration in its entirety. Given the complex shape of the Pioneer spacecraft, it is certainly conceivable that an anisotropy of this magnitude is present in the spacecrafts’ thermal radiation pattern.

The possibility that heat from the RTGs can be responsible for the Pioneer anomaly was first proposed by Katz [17, 156]. Murphy [16, 236] pointed out the potential significance of anisotropic rejection of electrically generated heat. Scheffer [329, 331] attempted to account for all possible sources of the thermal recoil force and estimated that the total recoil force is more than sufficient to produce an anomalous acceleration of the observed magnitude. Unfortunately, none of these studies benefited from detailed information about the spacecrafts’ design or from thermal and electrical telemetry. These data became available for study in 2005.

Key questions concerning the thermal recoil force that have been raised during the study of the Pioneer anomaly include [156, 236, 331]:

- How much heat from the RTGs is reflected by the spacecraft, notably the rear of its high-gain antenna, and in what direction?
- Was there a fore-aft asymmetry in the radiation pattern of the RTGs due to differential aging?

- How much electrical heat generated on-board was radiated through the spacecraft’s louver system?

A presently (2009) on-going effort is to build a comprehensive thermal model of the Pioneer spacecraft from design documentation. The model is to be validated by telemetry, and evaluated at different heliocentric distances at different times during the lifetime of the spacecraft. If successful, this effort will yield a high-accuracy estimate of the thermal recoil force, which can then be incorporated into future trajectory models.

7.3 An approach to finding the origin of the Pioneer anomaly

With the availability of the new Pioneer 10 and 11 radiometric Doppler data (see Section 3.3), a new study of the Pioneer anomaly became possible. This much extended set of Pioneer Doppler data is the primary source for the new ongoing investigation of the anomaly. In addition, the entire record of flight telemetry files received from Pioneer 10 and 11 is also available (see Section 3.5). Together with original project documentation (see Section 2.1.3) and newly developed software codes and trajectory analysis tools, this additional information is now used to reconstruct the engineering history of both spacecraft with the aim to establish the nature of the Pioneer anomaly. Below we review the current status of these efforts.

The primary objective of the new investigation is to determine the physical origin of the Pioneer anomaly and identify its properties. To achieve this goal, a study of the recently recovered radiometric Doppler and telemetry data has begun, focusing in particular on improving our understanding of the thermal behavior of the spacecraft and the extent to which radiated heat can be responsible for the acceleration anomaly.

The objectives of this new investigation of the Pioneer anomaly are sixfold:

- To analyze the early mission data; the goal would be to determine the true direction of the anomaly and thus, its origin;
- To study the physics of the planetary encounters; the goal would be to learn more about the onset of the anomaly (e.g., Pioneer 11’s Saturn flyby),
- To study the temporal evolution of a_P with the entire data set; the goal would be a better determination of the temporal behavior of the anomaly,
- To perform a comparative analysis of individual anomalous accelerations for the two Pioneers with the data taken from similar heliocentric distances, which could highlight properties of a_P , and
- To investigate the on-board systematics with recently recovered MDRs; the goal here would be to investigate the effect of on-board systematics on the solution for the Pioneer anomaly obtained with the Doppler data, and, finally
- To build a model of the thermal, electrical and dynamical behavior of the Pioneer vehicles and verify it with the actual data from the MDRs; the goal here would be to develop a model to be used to calibrate the Doppler anomaly with respect to the on-board sources of dynamical noise.

These objectives are not entirely independent of each other; by putting them on this list, we are identifying the main areas that are the focus of the on-going new investigation of the anomaly. Below we will discuss these objectives in more detail.

7.3.1 Analysis of the earlier trajectory phases

One objective of the new investigation is the study of the early parts of the trajectories of the Pioneers with the goal of determining the true direction of the Pioneer anomaly and possibly its origin [252, 393, 395]. The much longer data span is expected to improve the ability to determine the source of the acceleration. In particular, with data from much closer to the Earth and Sun, one should be able to better determine whether the acceleration is i) in the sunward direction, ii) in the Earth-pointing direction, iii) in the direction along the velocity vector, or iv) along the spin axis direction (see Section 7.2.1). Analysis of the earlier data is critical in helping to establish a precise 3-dimensional time history of the effect, and therefore to find out whether it is due to a systematic or new physics.

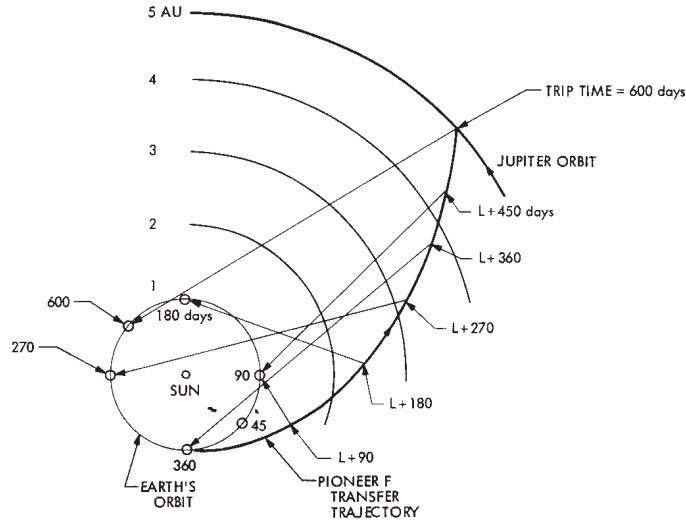


Figure 7.5: Proposed directions (along the spin and antenna axes) from the Pioneer F spacecraft (to become Pioneer 10) toward the Earth [341].

7.3.2 Study of the planetary encounters

An approximately constant anomalous acceleration seems to exist in the data of Pioneer 10 as close in as 27 AU from the Sun [15, 18, 261]. Navigational data collected for Pioneer 11, beginning just after Jupiter flyby, show a small value for the anomaly during the Jupiter-Saturn cruise phase in the interior of the solar system. However, right at Saturn encounter, when Pioneer 11 passed into a hyperbolic escape orbit, there was an apparent fast increase in the anomalous acceleration [18, 247, 395], but this has not yet been confirmed by rigorous analysis (see Section 7.2.3).

Doppler data covering Pioneer 11's encounter with Saturn are available. A successful study of the data surrounding the encounter [393] would lead to an improved understanding of the apparent onset of the anomalous acceleration. The encounters of both spacecraft with Jupiter may also be of interest (see [399]), although that close to the sun, much larger contributions to the acceleration noise are present.

While early data may improve our understanding of the direction of the anomaly, a difficult obstacle exists along the way towards this goal [18, 252]. Radiometric observables, notably Doppler, are sensitive in the line-of-sight direction, but are insensitive to small changes in the spacecraft's orbit in a direction that is perpendicular to the line-of-sight. The lack of a range observable on Pioneer 10 and 11 also reduces the accuracy with which the orbit can be determined in three

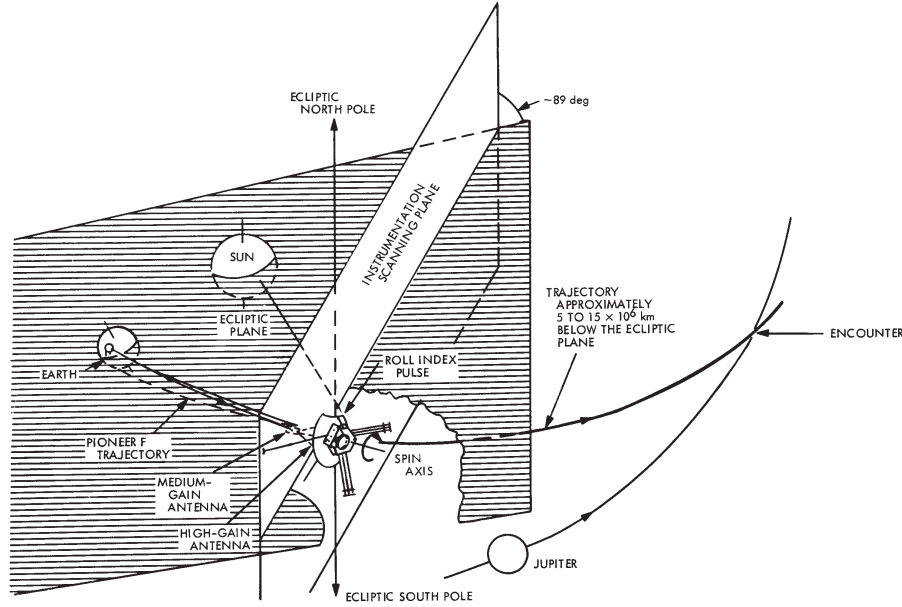


Figure 7.6: The earlier part of the Pioneer 10 trajectory before Jupiter encounter, the part of the trajectory when antenna articulation was largest [341].

dimensions. Nevertheless, these problems can be addressed and the on-going analysis should be able to yield the true direction of the anomaly and its origin [247, 393, 395].

7.3.3 Study of the temporal evolution of the anomaly

JPL's 2002 analysis [18] found that the anomalous acceleration is approximately constant. On the other hand, any explanation involving the on-board thermal inventory of the spacecraft must necessarily take into account this inventory's decay with time. It was on this basis that the authors of [18] rejected the hypothesis that the acceleration is due to collimated thermal emission.

While JPL's study of 11.5 years of Pioneer 10 data [18, 19] found no change in the anomalous acceleration, Markwardt [185], Olsen [266] and Toth [382] were not able to rule out this possibility. The now available extended data set, which includes over 20 years of usable Pioneer 10 data, may be sufficient to demonstrate unambiguously whether or not a jerk term is present in the signal, and if it is compatible with the temporal behavior of the on-board thermal inventory [383]. We note, however, the difficulty of the task of disentangling such a jerk term from the effects of solar radiation pressure.

7.3.4 Analysis of the individual trajectories for both Pioneers

The trajectories of Pioneer 10 and 11 were profoundly different. After its encounter with Jupiter, Pioneer 10 continued on a hyperbolic escape trajectory, leaving the solar system while remaining close to the plane of the ecliptic. Pioneer 11, in contrast, proceeded from Jupiter to Saturn along a trajectory that took it closer to the Sun, while outside the ecliptic plane. After its encounter with Saturn, Pioneer 11 also proceeded along a hyperbolic escape trajectory, but once again it was flying outside the plane of the ecliptic. In the end, the two spacecraft were flying out of the solar system in approximately opposite directions.

Nonetheless, the limited data set that was available previously precluded a meaningful comparison. The individual solutions for the two spacecraft were obtained from data segments that not only differed in length (11.5 and 3.75 years), but were also taken from different heliocentric distances (see Section 5.6).

From the recovered telemetry [399] we now also know that the actual thermal and electrical behavior of the two spacecraft was different [383, 384, 399]. These facts underline the importance of studying and comparing the behavior of both spacecraft, as this may help determine if the anomaly is of on-board origin or extravehicular in nature.

7.3.5 Investigation of on-board systematics

The availability of telemetry information makes it possible to conduct a detailed investigation of the on-board systematic forces as a source of the anomalous acceleration.

Previously, all known mechanisms of on-board systematic forces were examined [15, 17, 16, 18, 156, 236, 331, 399] (see Table 5.2). Current efforts are designed to improve our understanding of the contribution of on-board heat – notably, heat from the RTGs reflecting off the spacecraft, and electrical heat generated within the spacecraft – to the anomalous acceleration. The available telemetry also helps refine estimates of the radio beam reaction force. (Other effects, such as the differential emissivity of the RTGs, helium expulsion from the RTGs, propulsive gas leaks, were also analyzed [384, 399] but were found to be insignificant.)

As pointed out in [19], any thermal explanation should clarify why either the radioactive decay (if the heat is directly from the RTGs/RHUs) or electrical power decay (if the heat is from the instrument compartment) is not seen. One reason could be that previous analyses used only a limited data set of only 11.5 years when the thermal signature was hard to disentangle from the Doppler residuals or the fact that the actual data on the performance of the thermal and electrical systems was not complete or unavailable at the time the analyses were performed.

The present situation is very different. Not only do we have a much longer Doppler data segment for both spacecraft, we also have the actual telemetry data on the thermal and electric power subsystems for both Pioneers for the entire lengths of their missions. The electrical power profile of the spacecraft can be reconstructed with good accuracy using electrical telemetry measurements (see Section 2, and also [399]). The telemetry also contains measurements from a large number of on-board temperature sensors.

This information made it possible to construct a detailed thermal model of the Pioneer spacecraft (see Figures 7.7 and 7.8). As of early 2010, this work is near completion, and its results are being readied for publication.

7.4 The thermal recoil force

It has been long recognized [15, 18, 399] that anisotropically emitted thermal radiation can contribute to the acceleration of the Pioneer 10 and 11 spacecraft, and that the available thermal inventory on board (in excess of 2 kW), if directed, is more than sufficient to provide the necessary acceleration (requiring only ~ 65 W of collimated electromagnetic radiation.)

Nonetheless, in 2002, having only limited thermal data and relevant spacecraft information at hand, the authors of [18] estimated the contribution of the thermal recoil force as $(-0.55 \pm 0.73) \times 10^{-10}$ m/s² (the estimate is based on the values reported for the RTG heat reflected off the craft and nonisotropic radiative cooling of the spacecraft, items 2b) and 2d) in Table 5.2 correspondingly), i.e., only about 6% of the anomalous acceleration.

Since 2002, it has become clear that this figure is in need of a revision. A quantitative estimate was first offered by Scheffer in 2003 [331], who calculated a total of 52 W of directed thermal radiation (not including his estimate on asymmetrical radiation from the RTGs), or about 80% of

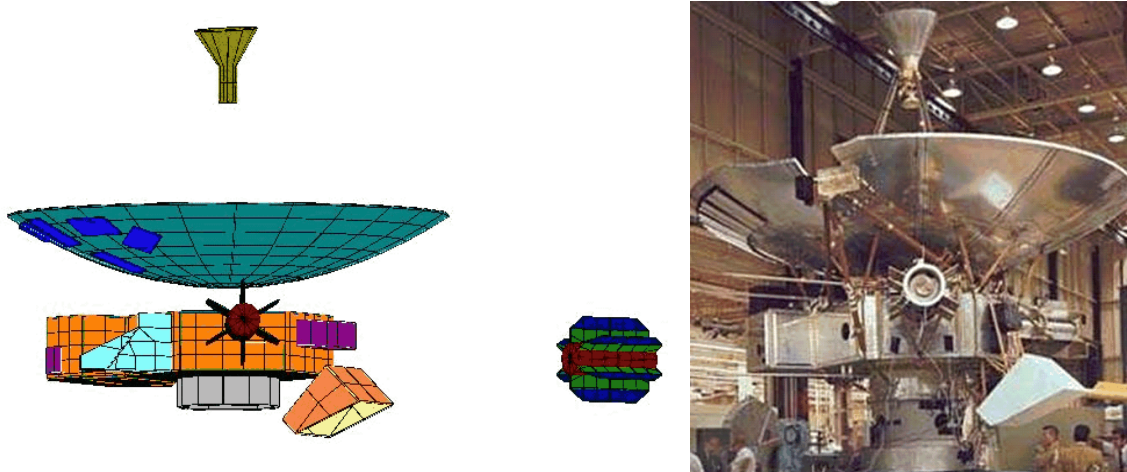


Figure 7.7: A geometric model (left) of the Pioneer spacecraft, used for finite element analysis, and a photograph (right) of Pioneer 10 prior to launch. The geometric model accurately incorporates details such as the Medium Gain Antenna (MGA), the Asteroid-Meteoroid Detector, and the star sensor shade. Note that in the geometric model, the RTGs are shown in the extended position; in the photograph, the RTGs are stowed. From [163, 164].

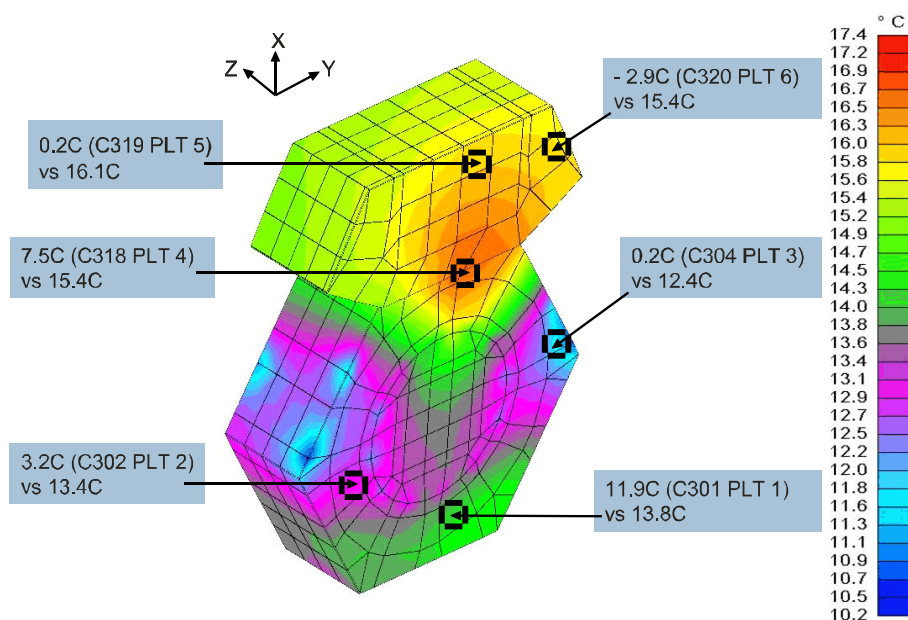


Figure 7.8: A “work-in-progress” temperature map of the outer surface of the Pioneer 10 spacecraft body, comparing temperatures calculated via a numerical finite element method vs. temperatures measured by platform temperature (PLT) sensors and telemetered. While agreement between calculated and telemetered temperatures is expected to improve as the model is being developed, discrepancies between these values illustrate the difficulties of creating a reliable temperature map using numerical methods. (From [163, 164]).

the thrust required to account fully for the anomalous acceleration. In 2007, Toth [381] presented an argument for expressing the combined recoil force due to electrical and RTG heat as a linear combination of the RTG thermal power and electrical power on board; his coefficients (0.012 for the RTGs, 0.36 for electrical heat) yield a figure of ~ 55 W of directed thermal radiation in the mid-1980s, which, after accounting for the heat from the RHUs (4 W) and the antenna beam (-7 W) as Scheffer did, translates into a result that is similar to Scheffer's.

Benefiting from the extensive discussions of the topic of thermal recoil force during the meetings of the Pioneer Explorer Collaboration at ISSI³² [163, 164, 401, 332, 333, 381], several researchers tried to model effects of this force on a Pioneer-like spacecraft using various computer tools. In 2008, Bertolami et al. [43] made an attempt to develop a methodology using point-like Lambertian sources to estimate the thermal recoil force on the Pioneer spacecraft, and obtained an acceleration estimate that corresponds to $\sim 67\%$ of the Pioneer anomaly, or ~ 45 W of directed thermal radiation. In addition, in 2009, Rievers et al. [315, 316] used finite element modeling and ray tracing algorithms to compute an acceleration that corresponds to ~ 48 W of directed heat in the mid-1980s.

These recent results support claims that the contribution of the thermal recoil forces to the Pioneer anomaly was previously (e.g., [18]) underestimated. However, the estimates above used only rough values for on-board thermal and electrical power and are valid only for a particular point in Pioneers' missions. As such, these estimates can provide only an overall magnitude of the effect and say little on its temporal behavior. On the other hand, the now available telemetry and recovered spacecraft design documentation [399] makes it possible to develop a comprehensive thermal model capable of estimating thermal recoil force throughout the entire mission of both Pioneers. Interim results show that this model is in good agreement with redundant telemetry observations [162, 163, 164]. Therefore, the development of a comprehensive, reliable estimate of the thermal recoil force is now within reach.

Below, we discuss the basic principles of modeling the thermal recoil force, as well as the application of these principles to the case of the Pioneer 10 and 11 spacecraft.

7.4.1 General formalism

While heat transfer textbooks provide all necessary details about thermal radiation as a mechanism for energy transfer, momentum transfer is rarely covered in any detail. This is perhaps not surprising: the momentum of a photon with energy E is $p = E/c$, and thus, the recoil force associated with a collimated beam of electromagnetic radiation with power P is $F = P/c$. For each watt of radiated power, the corresponding recoil force is only ~ 3.33 nN. Such tiny forces rarely, if ever, need to be taken into account in terrestrial applications. This is not so in the case of space applications [27, 97, 173, 322, 406, 428], in particular in the case of Pioneer 10 and 11: the observed anomalous acceleration corresponds to a force of less than 220 nN, which can be produced easily by a modest amount (~ 65 W) of electromagnetic radiation.

A formal treatment of the thermal recoil force must establish a relationship between heat sources within the radiating object and the electromagnetic field outside the object [385]. This can be accomplished in stages, first by describing heat conduction inside the object using Fourier's law [157, 172, 200]:

$$\mathbf{q} = -k\nabla T, \quad (7.1)$$

where \mathbf{q} is the heat flux (measured in units of power over area), T is the temperature, and k is the heat conduction coefficient, a tensorial quantity in the general case, but just a number for

³²The Pioneer Explorer Collaboration at the International Space Science Institute (ISSI), Bern, Switzerland, see details <http://www.issibern.ch/teams/Pioneer/>

homogeneous and isotropic materials. Heat flux also obeys the energy conservation equation

$$\nabla \cdot \mathbf{q} = b - C_h \rho \frac{\partial T}{\partial t}, \quad (7.2)$$

where b is the volumetric heat release (measured in units of power density), C_h is the material's specific heat, and ρ is its density. For discrete sources, $b(\mathbf{x}, t) = \sum_{i=1}^n B_i(t) \delta^3(\mathbf{x} - \mathbf{x}_i)$, where B_i is the thermal power of the i -th source, \mathbf{x}_i is its location, and δ denotes Dirac's delta function.

At a radiating surface,

$$q = \mathbf{q} \cdot \mathbf{a}, \quad (7.3)$$

where \mathbf{a} is the unit normal of the radiating surface element, and q is the surface element's radiant intensity. The radiant intensity, or energy flux, of a radiating surface is related to its temperature by the Stefan–Boltzmann law:

$$q(\mathbf{x}, t) = \sigma \epsilon(\mathbf{x}, t, T) T^4(\mathbf{x}, t), \quad (7.4)$$

where $\sigma \simeq 5.67 \times 10^{-8} \text{ Wm}^{-2} \text{ K}^{-4}$ is the Stefan–Boltzmann constant, while the dimensionless coefficient $0 \leq \epsilon \leq 1$ is a physical characteristic of the emitting surface. This coefficient can vary not only as a function of location and time, but also as a function of temperature. Equation (7.4) can be used to calculate the radiative coupling between facing surfaces of the object, and between the object and its environment (e.g., the deep sky, which can be modeled as a blackbody with temperature $T_{\text{sky}} \simeq 2.7 \text{ K}$). Together with internal boundary conditions (i.e., the power and distribution of internal heat sources, represented by b above) the problem becomes fully solvable: values of \mathbf{q} inside the object, and q on its boundary surface can be computed [385].

Outside the radiating object, the electromagnetic field is described by the stress-energy-momentum tensor

$$T^{\mu\nu} = \begin{pmatrix} c^{-2}u & \mathbf{p} \\ \mathbf{p} & \mathbb{P} \end{pmatrix}, \quad (7.5)$$

where u is the energy density of the radiation field, \mathbf{p} is its momentum density, and \mathbb{P} is the radiation pressure tensor. The stress-energy-momentum tensor obeys the conservation equation $\nabla_\mu T^{\mu\nu} = 0$, where ∇_μ is the covariant derivative with respect to the coordinate x^μ . This allows one to develop an expression for the recoil force \mathbf{F} acting on a radiating surface A in the form

$$\mathbf{F}(t) = - \int \mathbb{P}(\mathbf{x}, t) \cdot d\mathbf{A}, \quad (7.6)$$

which, for an isotropic (Lambertian) emitter yields the well-known law

$$\mathbf{F}(t) = - \frac{2}{3} \frac{1}{c} \int q(\mathbf{x}, t) d\mathbf{A}. \quad (7.7)$$

If the geometry of the emitter's exterior (represented by A) and the radiant intensity q along the exterior surface are known, the recoil force can be computed [385].

The Pioneer 10 and 11 spacecraft have two heat sources that contribute significant amounts to the thermal recoil force - the RTGs and the on-board electrical equipment. The case is further simplified by the fact that the Pioneer 10 and 11 spacecraft are spinning, as it allows a force computation in only one dimension (see Section 4.4).

7.4.2 Contribution of the heat from the RTGs

Although each of the spacecraft has four RTGs, their temporal behavior is identical (characterized by the half-life of the ^{238}Pu fuel and the decaying efficiency of the thermocouples). The placement of the RTGs is symmetrical. Consequently, the set of four RTGs can be treated as a single heat source,

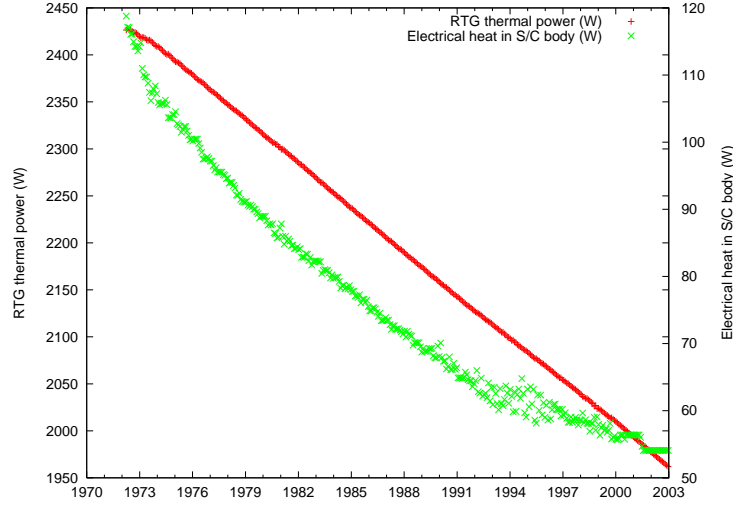


Figure 7.9: Heat generated by RTGs (red, approximately straight line, scale on left) and electrical equipment (green, scale on right) in Pioneer 10 over the lifetime of the spacecraft.

the power of which we denote as $B_{\text{rtg}}(t)$. The amount of ^{238}Pu fuel on board is well known from pre-launch test data, and the physics of the fuel's radioactive decay is well understood [383, 384, 399]; therefore, the total power of the RTGs, $P_{\text{rtg}}(t)$ is known:

$$P_{\text{rtg}}(t) = 2^{-(t-t_0)/T} P_{\text{rtg}}(t_0), \quad (7.8)$$

where t_0 is the time when the power $P_{\text{rtg}}(t_0)$ was measured, and $T \simeq 87.74$ years is the half-life of the radioactive fuel.

The amount of power $P_{\text{elec}}(t)$ removed from the RTGs in the form of electrical power is measured directly by telemetry and is available for the entire mission durations. Therefore, $B_{\text{rtg}}(t)$ is given as:

$$B_{\text{rtg}}(t) = P_{\text{rtg}}(t) - P_{\text{elec}}(t). \quad (7.9)$$

The value of $B_{\text{rtg}}(t)$ can be computed with good accuracy (Figure 7.9). The initial power $P_{\text{rtg}}(t_0) \simeq 650$ W per RTG was reported with a measurement accuracy of 1 W for each RTG; the month, though not the exact date, of t_0 is known. Therefore, $P_{\text{rtg}}(t)$ can be calculated with an accuracy of 0.2% or better. Currents and voltages from each RTG are found in the flight telemetry data stream, represented by 6-bit values. The combined error due mainly to the limited resolution of this data set amounts to an uncertainty of ~ 1 W per RTG. When all these independent error sources are combined, the resulting figure is an uncertainty of $\sigma_{\text{rtg}} = 2.1$ W; the total power of the four RTGs combined is ~ 2600 W at the beginning of the Pioneer 10 and 11 missions [385].

7.4.3 Effects of the electrical heat

Electrical power on board the Pioneer spacecraft was ~ 160 W at the beginning of mission [384], slowly decreasing to ~ 60 W at the time when the last transmission was received from Pioneer 10. Some of this power was radiated into space directly by a shunt radiator plate, some power was consumed by instruments mounted external to the spacecraft body, and some power was radiated away in the form of radio waves; however, most electrical power was converted into heat inside the spacecraft body. This heat escaped the spacecraft body through three possible routes: a passive

thermal louver system, other leaks and openings, and the spacecraft walls that were covered by multilayer thermal insulation blankets. While the distribution of heat sources inside the spacecraft body was highly inhomogeneous, there is little temporal variation in the distribution of heat inside the spacecraft body, and the exterior temperatures of the multilayer insulation remain linear functions of the total electrical heat. This allows us to treat all electrical heat generated inside the spacecraft body as another single heat source:

$$B_{\text{elec}}(t) = \text{known from telemetry.} \quad (7.10)$$

Therefore, the value of $B_{\text{elec}}(t)$ is available from telemetry (Figure 7.9). Uncertainties in the estimate of B_{elec} are due to several factors. First, telemetry is again limited in resolution to 6-bit data words. Second, the power consumption of specific instruments is not known from telemetry, only their nominal power consumption values are known from documentation. Third, there are uncertainties due to insufficient documentation. When these sources of error are combined, the result is an uncertainty of $\sigma_{\text{elec}} = 1.8 \text{ W}$ in the electrical heat output of the spacecraft body [385].

7.4.4 The thermal recoil force

In addition to heat from the RTGs and electrically generated heat, there are other mechanisms producing heat on board the Pioneer spacecraft. First, there are 11 radioisotope heater units (RHUs) on board, each of which generated 1 W of heat at launch, using ^{238}Pu fuel with a half-life of 87.74 years. Second, the propulsion system, when used, can also generate substantial amounts of heat.

Nonetheless, these heat sources can be ignored. The total amount of heat generated by the RHUs is not only small, most of the RHUs themselves are mounted near the edge of the high-gain antenna (see Figure 2.8), and a significant proportion of their heat is expected to be emitted in a direction perpendicular to the spin axis. As to the propulsion system, while it can generate substantial quantities of heat, these events are transient in nature and are completely masked by uncertainties in the maneuvers themselves, which are responsible for this heat generation. These arguments can lead to the conclusion that insofar as the anomalous acceleration is concerned, only the heat from the RTGs and electrical equipment contribute noticeably.

As discussed in Subsection 7.4.1 above, knowledge of the physical properties (thermal properties and geometry) of the spacecraft and its internal heat sources is sufficient to compute heat, and thus momentum, transfer between the spacecraft and the sky. This can be accomplished using direct calculational methods, such as industry standard finite element thermal-mechanical modeling software. The availability of redundant telemetry (in particular, the simultaneous availability of electrical and thermal measurements) makes it possible to develop a more robust thermal model and also establish reasonable limits on its accuracy. Such a model has recently been developed at JPL [161] and is yielding valuable results. The results of this analysis will be published when available (see also Figures 7.7 and 7.8).

It is also possible to conduct a simplified analysis of the Pioneer spacecraft. First, taking into consideration the spacecraft's spin means that the thermal recoil force only needs to be calculated in the spin axis direction (see Section 4.4). Second, it has been argued in [385] that for these spacecraft, the total recoil force can be accurately modeled as a quantity that is proportional to some linear combination of the thermal power of the two dominant heat sources, the RTGs and electrical equipment. Thus, one may write

$$\mathbf{F} = \frac{1}{c}(\xi_{\text{rtg}}B_{\text{rtg}} + \xi_{\text{elec}}B_{\text{elec}})\mathbf{s}, \quad (7.11)$$

where ξ_{rtg} and ξ_{elec} are efficiency factors associated with RTG thermal power B_{rtg} and electrical power B_{elec} , while \mathbf{s} is a unit vector in the spin axis direction.

The factors ξ_{rtg} and ξ_{elec} can be computed, in principle, from the geometry and thermal properties of the spacecraft. However, there also exists another possible approach [385]: after incorporating the force model Equation (7.11) into the orbital equations of motion, orbit determination software can solve for these parameters, fitting their values, along with the spacecraft’s initial state vector, maneuvers, and other parameters, to radiometric Doppler observations [385]. While this approach seems promising, its success depends on the extent to which orbit determination code can disentangle the thermal recoil force, solar pressure, and a possible anomalous contribution from one another based on radiometric Doppler data alone.

A further complication arises from the fact that although late in their mission, the physical and thermal configuration of the Pioneer spacecraft were constant in time, this was not always the case. Earlier in their mission, when the spacecraft were closer to the Sun, their internal temperatures were regulated by a thermal louver system located on the aft side (i.e., the side opposite the high-gain antenna; see Figure 2.10). When these louvers were partially open (see Figure 2.11), the effective thermal emissivity of the aft side was significantly higher, and varied as a function of internal temperatures (see Figures 2.12 and 2.13). While this effect is difficult to model analytically, it can be incorporated into a finite element thermal model accurately.

These recent studies and on-going investigations made it clear that the figure published in 2002 [18] is likely an underestimation of the thermal recoil force; far from being insignificant, the thermal recoil force represents a substantial fraction of the force required to generate the anomalous acceleration seen in Pioneer data, and may, in fact, account for all of it. This possibility clearly demands a thorough, in-depth analysis of the thermal environment on-board the Pioneers. Meanwhile, all the needed thermal and power data exist in the form of on-board telemetry [383, 384, 399]. All the tools needed to analyze resulted thermal recoil forces are now built and tested [161, 163, 164, 315, 316, 382, 385, 397]. The analysis now approaches its most exciting part.

If the anomaly, even in part, is of thermal origin, its magnitude must decrease with time as the on-board fuel inventory decreases (see Figure 7.9, for example). Therefore, a thermal model will necessarily predict a decreasing trend in the anomaly. To what extent will this trend contradict the previously reported “constancy” of the effect? Or will it support trends already seen as the jerk terms reported by independent verifications (Section 7.1)? To that extent we emphasize that the primary data set for the new investigation of the Pioneer anomalous acceleration is the much extended set of radiometric Doppler tracking data available for both spacecraft (Section 3.3). It is clear that if the anomaly was found in the navigational data, it must be re-evaluated using data of the same nature. This is why the new set of Doppler data that recently became available, in conjunction with the newly built tools to evaluate thermal recoil forces discussed above, is now being used to evaluate the long-term temporal behavior, direction and other important properties of the Pioneer anomaly (Section 7.2).

Finally, after a period of tedious preparatory work conducted during 2002–2009, the study of the Pioneer anomalous acceleration enters its final stages; the results of this work will be reported.

8 Conclusions

The Pioneer anomaly entered the phenomenology of modern physics at a time when researchers have mounted significant efforts to investigate two other observational anomalies: the flat rotation curves of spiral galaxies and the accelerated expansion of the universe. Although the true origin of the anomalous acceleration of the Pioneer 10 and 11 spacecraft is yet to be reported, its existence has already helped us deepen our understanding of gravity. Unlike the other two anomalies, the Pioneer anomaly is “local” in character, taking place within our own solar system, involving a spacecraft of our own making. As a result, the Pioneer anomaly has led to increasing interest in space-based fundamental physics research focusing on solar system tests of gravity. This renewed interest is, perhaps, the most significant contribution of the Pioneer effect to modern physics to date.

The presence of the unexpected acceleration signal in the Pioneer radiometric Doppler data has led to a re-evaluation of theoretical frameworks used to test gravity in the solar system. It has also motivated the development of new physical mechanisms to explain the effect. The anomaly has necessitated a re-analysis of many physical concepts, resulting in studies of the behavior of gravitationally bound systems in an expanding universe, investigations of gravity modification mechanisms, and efforts to detect the anomaly with other spacecraft, planets, and other bodies in the solar system. The anomaly has also motivated the development of new methods to improve the accuracy of spacecraft navigation, including methods of accounting for the effect of thermal recoil forces.

In this review we describe the Pioneer 10 and 11 spacecraft. We provide a significant amount of information on the design, operations and behavior of the two Pioneers during their entire missions. This includes information from original project documentation and descriptions of various data formats and techniques that were used for acquisition of the Pioneer data. We describe the radiometric Doppler data and techniques for data preparation and analysis. We also discussed the Pioneer telemetry data and its value for the anomaly investigation. We review the observational techniques and physical models that were used for precision tracking of the Pioneer spacecraft. We summarize the current knowledge of the physical properties of the Pioneer anomaly and review various mechanisms proposed for its explanation.

October 5, 2009 marked the eleventh anniversary of the first announcement of the Pioneer anomaly [15] (see also [18, 391]). In the decade that followed, the existence of the anomalous acceleration in the radiometric Doppler data received from the Pioneer 10 and 11 spacecraft was confirmed by several independent researchers [171, 185, 266, 382]. Thus, the existence and approximate magnitude of the anomaly can be considered established fact. However, the direction of the acceleration remains unclear: the four principal directions (sunward, earthward, along the spin axis, or along the velocity vector) fall within a few degrees of each other and based on available data, cannot be distinguished easily. The temporal behavior of the anomaly has been put into question by studies [185, 382] that demonstrate the presence of a jerk term. Meanwhile, other studies (see [163, 164, 401, 332, 333, 381], followed by [43, 315, 316]), indicate that the magnitude of acceleration due to thermal recoil forces of on-board origin may be significantly larger than previously estimated. As a result, the question of the origin of the Pioneer anomaly remains open, but hopefully not for long.

A comprehensive investigation of the anomaly has recently begun. The new study relies on the much-extended set of radiometric Doppler data for both spacecraft in conjunction with the entire record of the Pioneer 10 and 11 spacecraft telemetry files and large archive of project documentation. This unique information has already led to the development of new software tools capturing all aspects of the in-flight behavior of the Pioneer vehicles throughout their missions. These efforts may soon reveal the origin of the anomaly. Our review provides the necessary background for the new results to appear in the near future. Such an anticipated development

makes the study of the Pioneer anomaly a good subject for *Living Reviews*.

9 Acknowledgements

We would like to express our gratitude to our many colleagues who have either collaborated with us on this manuscript or given us their wisdom. First among the many people who have helped us with suggestions, comments, and constructive criticisms, we must thank Craig B. Markwardt of GSFC, whose enthusiastic contribution to the Pioneer Doppler data recovery efforts was matched by the thoroughness with which he reviewed and commented on this manuscript. We also thank John D. Anderson, Hansjörg Dittus, Claus Lämmerzahl, Agnès Levy, John Moffat, and Serge Reynaud, for their encouraging comments and suggestions on this manuscript.

We specifically thank Sami Asmar, Curt J. Cutler, William M. Folkner, Timothy P. McElrath, Robert A. Jacobson, Michael M. Watkins, and James G. Williams of JPL, who provided us with encouragement and valuable comments while this manuscript was in preparation. We also thank Jordan Ellis, Gene L. Goltz, and Neil A. Mottinger of JPL for their help in obtaining, understanding and conditioning of the Pioneer Doppler data.

We are grateful to Gary Kinsella of JPL and Siu-Chun Lee and Daniel S. Lok of Applied Sciences Laboratory who benefited us with their insightful comments and suggestions regarding the thermal modeling of Pioneer spacecraft. Louis K. Scheffer of Cadence Design Systems contributed with useful observations on the thermal modeling, design and analysis.

Invaluable information on the history, spacecraft design and mission operations of the Pioneers 10 and 11, as well as the structure of their telemetry data, came from Lawrence Lasher, Larry Kellogg and David Lozier formerly of the NASA Ames Research Center.

It is our special pleasure to thank the members of the Pioneer Explorer Collaboration (POC) that conducted an extensive Pioneer anomaly investigation at the ISSI for many fruitful discussions of various aspects of the study of the anomaly. In particular, in addition to our colleagues on the POC already mentioned above, our wholehearted thanks are going to Orfeu Bertolami, Francois Bondu, Bruno Christophe, Jean-Michel Courty, Denis Defrere, Jonathan Fitt, Frederico Francisco, Bernard Foulon, Paolo Gill, Stefanie Grotjan, Eva Hackmann, Ulrich Johann, Meike List, Clovis J. De Matos, Gilles Mètris, Laura Mulin, Øystein Olsen, Jorge Paramos, Sergei Podgrebenko, Andreas Rathke, Benny Rievers, Wolfgang Seboldt, Stephan Theil, Paolo Tortora, Pierre Touboul, Patrick Vrancken, Peter Wolf and many others.

Our gratitude goes to Michael H. Salamon of NASA and Hans Mark of University of Texas in Austin who have kindly provided us with encouragement, stimulating conversations, and support during various phases of our work.

We also thank The Planetary Society for support and, in particular, Louis D. Freidman, Charlene M. Anderson, and Bruce Betts for their interest, stimulating conversations and encouragement.

This work was partially performed at the International Space Science Institute (ISSI), Bern, Switzerland, when both of us visited ISSI as part of an International Team program. In this respect we thank Roger M. Bonnet, Vittorio Manno, Brigitte Schutte, and Saliba F. Saliba of ISSI for their hospitality and support.

Finally, we would like to thank *Living Reviews in Relativity* and especially Bernard F. Schutz and Clifford M. Will for the rewarding opportunity to prepare this manuscript.

The work described here, in part, was carried out at the Jet Propulsion Laboratory, California Institute of Technology, under a contract with the National Aeronautics and Space Administration.

Appendices

Appendix A Pioneer Spacecraft Geometry

Only scarce documentation is available about the exact geometry of the Pioneer 10 and 11 spacecraft. A sketch of the major components of the spacecraft (our reconstruction) with approximate dimensions is shown below.

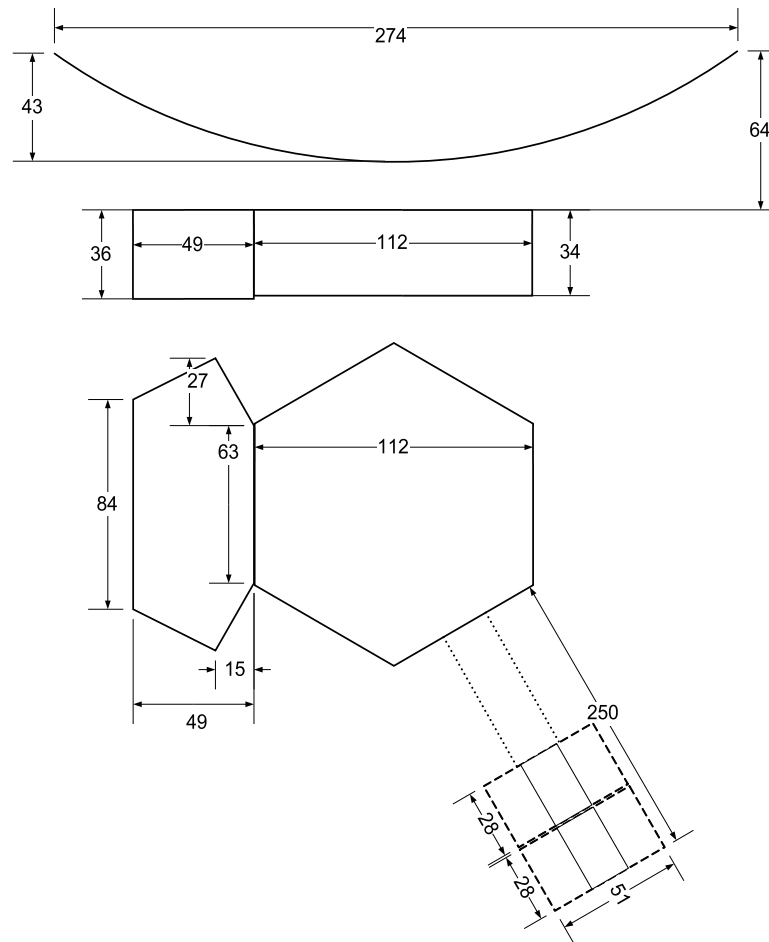


Figure Appendix A.1: Side view (above) and top view (below) of the high gain antenna, spacecraft body, and one RTG, with the boom length not to scale. Approximate measurements are in centimeters. For more accurate dimensions of the RTGs, consult Figure 2.5.

Appendix B Format of the Orbit Data Files (ODF)

The following table contains a concise but complete description of the structure of Orbit Data Files (ODFs). Records appear in ODFs in the order indicated. We offer this table to illustrate what information is available in the form of radio-metric Doppler measurements [91].

ODF File Label Group Header			
0	Primary Key = 101	Secondary Key = 0	Logical Record Length = 1
96	Group Start Packet Number = 0		0
192		0	
ODF File Label Group Data			
0	System ID in ASCII		Program ID in ASCII
96	Program ID (cont.)	Spacecraft ID	File Creation Date (YYMMDD)
192	File Creation Time (hhmmss)	File Reference Date (19500101)	File Reference Time (000000)
ODF Identifier Group Header			
0	Primary Key = 107	Secondary Key = 0	Logical Record Length = 1
96	Group Start Packet Number = 2		0
192		0	
ODF Identifier Group Data			
0		"TIMETAG"	"OBSR"
96	VBL"		"FREQ. AN"
192		CILLARY-DATA"	
ODF Orbit Data Group Header			
0	Primary Key = 109	Secondary Key = 0	Logical Record Length = 1
96	Group Start Packet Number = 4		0
192		0	
ODF Orbit Data Group Data			
0	0	Record Time Tag Integer Part (s)	
	32	Record Time Tag Fractional Part (ns)	
	42	Receiving Station Downlink Delay (ns)	
	64	Observable Integer Part (signed)	
	96	Observable Fractional Part (10 ⁻⁹ , signed)	
	128	Format ID = 2	
	131	Receiving Station ID	
	138	Transmitting Station ID	
	145	Network ID (0 = DSN Block V, 1 = Other, 2 = OTS, 3 = NSP)	
	147	Data Type (1x = x-way Doppler)	
	153	Downlink Band ID (1 = S-band)	
	155	Uplink Band ID (1 = S-band)	
	157	Exciter Band ID (1 = S-band)	
	159	Data Validity Indicator (0 = good)	
	160	Second Receiving Station ID	
	167	Spacecraft ID	
	177	Receiver/Exciter Independent Flag	
	178	Reference Frequency (mHz)	
192	224	Train Axis Angle (mdeg, OTS Doppler)	
	244	Compression Time (0.01 s)	
	266	Transmitting Station Uplink Delay (ns)	
ODF Ramp Groups Header			
0	Primary Key = 2030	Secondary Key = 0	Logical Record Length = 1
96	Group Start Packet Number		0
192		0	
ODF Ramp Groups Data			
0	Start Time Integer Part (s)	Start Time Fract. Part (ns)	Rate Integer Part (signed, Hz/s)
96	Rate Fract. Part (nHz/s)	Start Freq. GHz Part	Station ID
192	Start Frequency Fract. Part (nHz)	End Time Integer Part (s)	End Time Fract. Part (ns)
ODF Clock Offsets Group Header			
0	Primary Key = 2040	Secondary Key = 0	Logical Record Length = 1
96	Group Start Packet Number		0
192		0	
ODF Clock Offsets Group Data			
0	Start Time Integer Part (s)	Start Time Fract. Part (ns)	Offset Integer Part (s, signed)
96	Offset Fract. Part (ns)	Primary Station ID	Secondary Station ID
192	0 (spare)	0 (reserved for End Time)	
ODF Data Summary Group Header			
0	Primary Key = 105	Secondary Key = 0	Logical Record Length = 1
96	Group Start Packet Number		0
192		0	
ODF Data Summary Group Data			
0	1st Sample Time Integer Part (s)	1st Sample Time Fract. Part (ns)	Receiving Station ID
96	Doppler Channel Number	Downlink Band ID	Data Type ID
192	Number of Samples	Last Sample Time Integer Part (s)	Last Sample Time Fract. Part (ns)
ODF End-Of-File Group Header			
0	Primary Key = 1	Secondary Key = 0	Logical Record Length = 0
96	Group Start Packet Number		0
192		0	

Appendix C Master Data Records

All information received by the DSN from the Pioneer 10 and 11 spacecraft was stored in the form of Master Data Records, which were structured as shown in the table below. As the structure demonstrates, in addition to the 6-bit data words (see Appendix D) encoded in the data frames, the MDRs also contain information about the receiving DSN station [403, 95, 275, 142, 143, 310].

0	TIME TAG			
32	SC/ID	TIME COR FLAG	DAY OF YEAR	
64	UDT	DDT	SYNC COND CODE	DQI
96	# BIT ERRORS PN	YEAR DIGIT	SNR	
128	DSS	LOCK STATUS BITS	CONFIGURATION INDICATORS	
160	SPCL DATA TYPE	GDD	# OF DATA BITS IN RECORD	
192	# AGC SAMP AVER	HSD ERR CON BITS	RATE OF DATA TRANSMISSION	
224	AVERAGE AGC OVER DATA IN RECORD			
256	FORMAT	SPARE	NUMBER OF FRAMES	
288	0			
320	DATA FRAMES			
.				
.				
.				
1087				
1088	MS CLOCK LSB (FRAME 2 OF 4)		MS CLOCK LSB (FRAME 3 OF 4)	
1120	MS CLOCK LSB (FRAME 4 OF 4)		DDA I/P ERRORS (1)	DDA
1152	COMPUTATIONS (1)	DDA STATUS (1)	SPARE	GROUND RECEIVER AGC
1184	DDA I/P ERRORS (2)	DDA COMPUTATIONS (2)		DDA STATUS (2)
1216	SPARE		DATA I/P ERRORS (3)	DDA
1248	COMPUTATIONS (3)	DDA STATUS (2)	SPARE	
1280	DDA I/P ERRORS (4)	DDA COMPUTATIONS (4)		DDA STATUS (4)
1312	SCF 1	SCF 2	SCF 3	SCF 4

Appendix D Selected Engineering and Science Instrument Telemetry Words

In the following table, we list selected engineering and science instrument telemetry words (Formats C and E). Analog sensor readings have word type 'A'; word type 'B' is for bit fields, while 'D' represents digital values (e.g., counters). This list illustrates the redundant information that is available from telemetry, describing the thermal and electrical state of the spacecraft.

Word	Bit	Definition	Type
C ₁₀₄		Extended subcommutator ID.	B
C ₁₀₅		RTG 2 current (0–11 A)	A
C ₁₀₆		Battery voltage (0–15 V)	A
C ₁₀₇		DC bus voltage (26–30 V)	A
C ₁₀₈	1	JPL/HVM power	B
	2	ARC/PA power	
	3	UC/CPI power	
	4	UI/GTT power	
	5	GSFC/CRT power	
C ₁₀₉		Battery charge current (0–0.3 A)	A
C ₁₁₀		RTG 1 voltage (0–6 V)	A
C ₁₁₁		Receiver A AGC CONSCAN –4 to +4 dB	A
C ₁₁₃		RTG 4 voltage (0–6 V)	A
C ₁₁₄		RTG 3 current (0–11 A)	A
C ₁₁₅		Battery temperature (–20 to 120° F)	A
C ₁₁₇		TRF +5 V output CDU Bus A (0–6 V)	A
C ₁₁₈		TRF +5 V output CDU Bus B (0–6 V)	A
C ₁₁₉		DC bus voltage (0–30 V)	A
C ₁₂₁		Receiver B AGC CONSCAN –4 to +4 dB	A
C ₁₂₂		Shunt bus current (0–3 A)	A
C ₁₂₃		RTG 4 current (0–11 A)	A
C ₁₂₄	1	UCSD/TRD power	B
	2	USC/UV power	
	3	UA/IPP power	
	4	CIT/IR power	
	5	GE/AMD power	
	6	LaRC/MD power	
C ₁₂₅		RTG 2 voltage (0–6 V)	A
C ₁₂₆		Battery discharge current (0–10 A)	A
C ₁₂₇		RTG 1 current (0–11 A)	A
C ₁₂₈	1	Battery charge (0=auto, 1=float)	B
	2	Battery discharge (0=enabled)	
C ₁₂₉		DC bus current (0–6 A)	A
C ₁₃₀		Nitrogen tank temperature (° F)	A
C ₁₃₁		RTG 3 voltage (0–6 V)	A
C ₂₀₁		RTG 1 fin root temperature (160–360° F)	A
C ₂₀₂		RTG 2 fin root temperature (160–360° F)	A
C ₂₀₃		RTG 3 fin root temperature (160–360° F)	A
C ₂₀₄		RTG 4 fin root temperature (160–360° F)	A
C ₂₀₅		TWT A temperature (40–125° F)	A
C ₂₀₆		Driver a temperature (20–110° F)	A
C ₂₀₇		TWT A converter temperature (40–125° F)	A
C ₂₀₈		TWT A cathode current (24–30 mA)	A
C ₂₀₉		Shunt bus current (0–3 A)	A
C ₂₁₀		Propellant supply pressure (0–600 PSIA)	A

Word	Bit	Definition	Type
C ₂₁₁		TWT A helix current (0–10 mA)	A
C ₂₁₂		Receiver A loop stress (–100 to 100 kHz)	A
C ₂₁₃		Receiver B signal strength (–149 to –63 dBm)	A
C ₂₁₄		TWT B RF output power (26–40.4 dBm)	A
C ₂₁₅		TWT B cathode current (24–30 mA)	A
C ₂₁₆		TWT B helix current (0–10 mA)	A
C ₂₁₇		RTG 4 hot junction temperature (880–1200° F)	A
C ₂₁₈		RTG 3 hot junction temperature (880–1200° F)	A
C ₂₁₉		RTG 2 hot junction temperature (880–1200° F)	A
C ₂₂₀		RTG 1 hot junction temperature (880–1200° F)	A
C ₂₂₁		TWT B converter temperature (40–125° F)	A
C ₂₂₂		Receiver A VCO temperature (20–110° F)	A
C ₂₂₃		Driver B temperature (20–110° F)	A
C ₂₂₄		TWT A reference voltage (0–28 V)	A
C ₂₂₅		+Y PSA line temperature (° F)	A
C ₂₂₆		–Y PSA line temperature (° F)	A
C ₂₂₇		Receiver B VCO temperature (20–110° F)	A
C ₂₂₈		TWT B temperature (40–125° F)	A
C ₂₂₉		Receiver B loop stress (–100 to 100 kHz)	A
C ₂₃₀		TWT B reference voltage (0–28 V)	A
C ₂₃₁		TWT A RF output power (26–40.4 dBm)	A
C ₂₃₂		Receiver A signal strength (–149 to –63 dBm)	A
C ₃₀₁		Platform temperature 1 (0–140° F)	A
C ₃₀₂		Platform temperature 2 (0–140° F)	A
C ₃₀₃		SRA temperature (–10 to 95° F)	A
C ₃₀₄		Platform temperature 3 (0–140° F)	A
C ₃₀₈	1	Receiver A signal present	B
	2	Receiver B signal present	
	3	Receiver A oscillator enabled	
	4	Receiver B oscillator enabled	
	5	Spin thruster B pulse count	
	6	Spin thruster A pulse count	
C ₃₀₉		Velocity thruster cluster 1 temperature (40–200° F)	A
C ₃₁₀		Spin thruster cluster temperature (40–200° F)	A
C ₃₁₁		VPT 1 temperature (400–1800° F)	A
C ₃₁₂		VPT 2 temperature (400–1800° F)	A
C ₃₁₆	1	CONSCAN power	D
	2	CONSCAN threshold (1=above)	
	4	Receiver switch status (1=A/B=Hi/Med)	
	5	Transmitter switch status (1=A/B=Med/Hi)	
	6	Antenna feed switch status (1=offset)	
C ₃₁₇		SSA temperature (–30 to 194° F)	A
C ₃₁₈		Platform temperature 4 (0–140° F)	A
C ₃₁₉		Platform temperature 5 (0–140° F)	A
C ₃₂₀		Platform temperature 6 (0–140° F)	A
C ₃₂₁		Velocity thruster 2 (1B) pulse count	D
C ₃₂₂		Velocity thruster 4 (2A) pulse count	D
C ₃₂₄	1	Command memory status (0=processing, 1=standby)	B
C ₃₂₅		VPT 4 temperature (400–1800° F)	A
C ₃₂₆		Velocity thruster cluster 2 temperature (40–200° F)	A
C ₃₂₇		Propellant supply temperature (40–160°)	A
C ₃₂₈		VPT 3 temperature (400–1800° F)	A
C ₃₂₉		Velocity thruster 1 (1A) pulse count	D

Word	Bit	Definition	Type
C ₃₃₀		Velocity thruster 3 (2B) pulse count	D
C ₄₀₃	1	Precession pair (1=VPT 1&4)	D
	2-4	Pulse length bits 1-3	
	5	Δv pair (1=VPT 1&3)	
	6	Spin control direction (0=up)	
C ₄₀₄	1-5	Star time gate bits 0-4	D
	6	Δv /SCT mode enabled	
C ₄₀₅		Spin period MSB	D
C ₄₀₆		Spin period	D
C ₄₀₇		Spin period LSB	D
C ₄₀₈	1-5	Roll pulse/index pulse phase error bits 4-0	D
	6	Phase error sign (1=roll pulse before index pulse)	
C ₄₀₉	1	VPT 1 firing status	B
	2	VPT 2 firing status	
	3	VPT 4 firing status	
	4	VPT 3 firing status	
	5	SCT 1 firing status	
	6	SCT 2 firing status	
C ₄₁₀	1	Despin on/off	D
	2	CONSCAN enabled	
C ₄₂₁	1-2	Star count bits 0-2	D
	4	CEA power status DSL A	
	5	CEA power status DSL B	
	6	CEA power status PSE	
E ₁₀₁		ARC/PA detectors temperature	A
E ₁₀₂		ARC/PA electronics temperature	A
E ₁₀₉		USC/UV electronics temperature	A
E ₁₁₀		UC/CPI electronics temperature	A
E ₁₁₇		CIT/IR low range temperature	A
E ₁₁₈		GE/AMD preamp temperature	A
E ₁₂₅		GSFC/CRT electronics temperature	A
E ₁₂₈		GSFC/CRT detector temperature	A
E ₂₀₁		CIT/IR high range temperature	A
E ₂₀₉		UCSD/TRD electronics temperature	A
E ₂₂₁		UI/GTT electronics temperature	A

References

- [1] Abelson, R.D., Balint, T.S., Marshall, K.E., Noravian, H., Randolph, J.E., Satter, C.M., Schmidt, G.R., and Shirley, J.H., *Enabling Exploration with Small Radioisotope Power Systems*, (JPL, Pasadena, CA, 2004). Related online version (cited on 3 June 2010): <http://hdl.handle.net/2014/40856>.
- [2] Abramovici, A., and Vager, Z., “Test of Newton’s second law at small accelerations”, *Phys. Rev. D*, **34**, 3240–3241, (1986). [DOI].
- [3] Acker, R.M., “Pioneer F/G Feed Movement Mechanism”, in Herzl, G.G., ed., *6th Aerospace Mechanisms Symposium*, NASA Ames Research Center, Moffett Field, CA, September 9–10, 1971, NASA Technical Memorandum, vol. NASA TM X-2557, pp. 21–26, (NASA, Washington, DC, 1972). Related online version (cited on 26 May 2010): <http://hdl.handle.net/2060/19720018727>.
- [4] Acton, C.H., “Ancillary data services of NASA’s Navigation and Ancillary Information Facility”, *Planetary and Space Science*, **44**, 65–70, (1996). [ADS].
- [5] Adamski, T.P., *Pioneer Mission Support*, DSN Progress Report, 42-35, (JPL, Pasadena, CA, 1976). Related online version (cited on 19 May 2010): http://ipnpr.jpl.nasa.gov/progress_report2/42-35/35title.htm.
- [6] Adamski, T.P., *Pioneer Mission Support*, DSN Progress Report, 42-37, (JPL, Pasadena, CA, 1977). Related online version (cited on 19 May 2010): http://ipnpr.jpl.nasa.gov/progress_report2/42-37/37title.htm.
- [7] Adamski, T.P., *Pioneer Mission Support*, DSN Progress Report, 42-39, (JPL, Pasadena, CA, 1977). Related online version (cited on 19 May 2010): http://ipnpr.jpl.nasa.gov/progress_report2/42-39/39title.htm.
- [8] Adamski, T.P., *Pioneer Mission Support*, DSN Progress Report, 42-41, (JPL, Pasadena, CA, 1977). Related online version (cited on 19 May 2010): http://ipnpr.jpl.nasa.gov/progress_report2/42-41/41title.htm.
- [9] Adamski, T.P., *Pioneer Mission Support*, DSN Progress Report, 42-44, (JPL, Pasadena, CA, 1978). Related online version (cited on 19 May 2010): http://ipnpr.jpl.nasa.gov/progress_report2/42-44/44title.htm.
- [10] Amendola, L., Charmousis, C., and Davis, S.C., “Mimicking general relativity in the Solar System”, *Phys. Rev. D*, **78**, 084009, (2008). [DOI], [ADS], [arXiv:0801.4339].
- [11] Anderson, J.D., “Lectures on physical and technical problems posed by precision radio tracking”, in Bertotti, B., ed., *Experimental Gravitation*, Proceedings of the International School of Physics ‘Enrico Fermi’, Course LVI, July 17–29, 1972, Varenna, Italy, pp. 163–199, (Academic Press, New York, 1974).
- [12] Anderson, J.D., *Quarterly Report to NASA/Ames Research Center: Celestial Mechanics Experiment, Pioneer 10/11*, JPL Interoffice Memorandum, (JPL, Pasadena, CA, 1992). Also see the later quarterly report for the period 1 Oct. 1992 to 31 Dec. 1992, dated 17 Dec. 1992, Letter of Agreement ARC/PP017.
- [13] Anderson, J.D., Campbell, J.K., Ekelund, J.E., Ellis, J., and Jordan, J.F., “Anomalous Orbital-Energy Changes Observed during Spacecraft Flybys of Earth”, *Phys. Rev. Lett.*, **100**, 091102, (2008). [DOI].

- [14] Anderson, J.D., Campbell, J.K., and Nieto, M.M., “The energy transfer process in planetary flybys”, *New Astronomy*, **12**, 383–397, (2007). [DOI], [ADS], [astro-ph/0608087].
- [15] Anderson, J.D., Laing, P.A., Lau, E.L., Liu, A.S., Nieto, M.M., and Turyshev, S.G., “Indication, from Pioneer 10/11, Galileo, and Ulysses Data, of an Apparent Anomalous, Weak, Long-Range Acceleration”, *Phys. Rev. Lett.*, **81**, 2858–2861, (1998). [ADS], [gr-qc/9808081].
- [16] Anderson, J.D., Laing, P.A., Lau, E.L., Liu, A.S., Nieto, M.M., and Turyshev, S.G., “Anderson et al. Reply”, *Phys. Rev. Lett.*, **83**, 1891, (1999). [ADS], [gr-qc/9906113].
- [17] Anderson, J.D., Laing, P.A., Lau, E.L., Liu, A.S., Nieto, M.M., and Turyshev, S.G., “Anderson et al. Reply”, *Phys. Rev. Lett.*, **83**, 1893, (1999). [ADS], [gr-qc/9906112].
- [18] Anderson, J.D., Laing, P.A., Lau, E.L., Liu, A.S., Nieto, M.M., and Turyshev, S.G., “Study of the anomalous acceleration of Pioneer 10 and 11”, *Phys. Rev. D*, **65**(8), 082004, (2002). [ADS], [gr-qc/0104064].
- [19] Anderson, J.D., Laing, P.A., Lau, E.L., Nieto, M.M., and Turyshev, S.G., “The search for a standard explanation of the Pioneer anomaly”, *Mod. Phys. Lett. A*, **17**, 875–886, (2002). [DOI], [arXiv:gr-qc/0107022].
- [20] Anderson, J.D., Levy, G.S., and Renzetti, N.A., “Application of the Deep Space Network (DSN) to the testing of general relativity”, in Kovalevsky, J., and Brumberg, V.A., eds., *Relativity in Celestial Mechanics and Astrometry*, p. 329. Kluwer Academic, (1986).
- [21] Anderson, J.D., and Mashhoon, B., “Pioneer anomaly and the helicity-rotation coupling”, *Phys. Lett. A*, **315**, 199–202, (2003). [ADS], [gr-qc/0306024].
- [22] Anderson, J.D., Turyshev, S., and Nieto, M.M., “Effect of the Pioneer Anomaly on Long-Period Comet Orbits”, *Bulletin of the Amer. Astron. Soc.*, **34**, 1172, (2002). [ADS].
- [23] Anderson, J.D., Turyshev, S.G., and Nieto, M.M., “A Mission to Test the Pioneer Anomaly”, *Int. J. Mod. Phys. D*, **11**, 1545–1551, (2002). [DOI], [ADS], [gr-qc/0205059].
- [24] Anderson, J.L., “Multiparticle Dynamics in an Expanding Universe”, *Phys. Rev. Lett.*, **75**, 3602–3604, (1995). [DOI].
- [25] Antoniadis, I., Dimopoulos, S., and Dvali, G. R., “Millimeter range forces in superstring theories with weak-scale compactification”, *Nucl. Phys. B*, **516**, 70–82, (1998). [hep-ph/9710204].
- [26] Antreasian, P.G., and Guinn, J.R., *Investigations into the Unexpected Delta-V Increases During the Earth Gravity Assists of Galileo and NEAR*, AIAA 98-4287, (1998). Related online version (cited on 26 May 2010): <http://hdl.handle.net/2014/20322>.
- [27] Antreasian, P.G., and Rosborough, G.W., “Prediction of Radiant Energy Forces on the TOPEX/POSEIDON Spacecraft”, *Journal of Spacecraft and Rockets*, **29**(1), 81–92, (1992).
- [28] Arkani-Hamed, N., Dimopoulos, S., and Dvali, G. R., “The hierarchy problem and new dimensions at a millimeter”, *Phys. Lett. B*, **429**, 263–272, (1998). [hep-ph/9803315].
- [29] Arkani-Hamed, N., Dimopoulos, S., and Dvali, G. R., “Phenomenology, astrophysics and cosmology of theories with sub-millimeter dimensions and TeV scale quantum gravity”, *Phys. Rev. D*, **59**, 086004, (1999). [hep-ph/9807344].

- [30] Asmar, S.W., Armstrong, J.W., Iess, L., and Tortora, P., “Spacecraft Doppler tracking: Noise budget and accuracy achievable in precision radio science observations”, *Radio Science*, **40**, (2005). [DOI].
- [31] *Atomic Power In Space: A History*, DOE/NE/32117-H1, (U.S. Department of Energy, Washington, DC, 1987). Related online version (cited on 3 June 2010): <http://www.fas.org/nuke/space/>.
- [32] Backman, D.E., Dasgupta, A., and Stencel, R.E., “Model of a Kuiper Belt Small Grain Population and Resulting Far-Infrared Emission”, *Astrophys. J. Lett.*, **450**, L35, (1995). [DOI], [ADS].
- [33] Bekenstein, J., and Milgrom, M., “Does the missing mass problem signal the breakdown of Newtonian gravity?”, *Astrophys. J.*, **286**, 7–14, (1984). [DOI], [ADS].
- [34] Bekenstein, J.D., “Relativistic gravitation theory for the MOND paradigm”, *Phys. Rev. D*, **70**, 083509, (2004). [astro-ph/0403694].
- [35] Belayev, W.B., “Cosmological model in 5D, stationarity, yes or no”, arXiv e-print, (1999). [ADS], [gr-qc/9903016].
- [36] Belayev, W.B., and Tsipenyuk, D. Y., “Gravi-electromagnetism in five dimensions and moving bodies in galaxy area”, *Spacetime and Substance*, **22**, 49, (2004). [arXiv:gr-qc/0409056].
- [37] Berman, A.L., *Effects of the Pioneer 10 Antenna Polarization and Spacecraft Rotation as Seen in the Radio Metric Data*, JPL Technical Report 32-1526, vol. IX, (1972). Related online version (cited on 3 June 2010): http://ipnpr.jpl.nasa.gov/progress_report2/IX/IXtitle.htm.
- [38] Berman, A.L., *Tracking Operations During the Pioneer 10 Encounter*, DSN Progress Report, 42-20, (JPL, Pasadena, CA, 1974). Related online version (cited on 19 May 2010): http://ipnpr.jpl.nasa.gov/progress_report2/42-20/20title.htm.
- [39] Berman, A.L., and Schlaifer, R.S., *Tracking Operations During the Pioneer 11 Jupiter Encounter*, DSN Progress Report, 42-27, (JPL, Pasadena, CA, 1975). Related online version (cited on 19 May 2010): http://ipnpr.jpl.nasa.gov/progress_report2/42-27/27title.htm.
- [40] Berman, A.L., Wackley, J.A., and Rockwell, S.T., *The 1976 Helios and Pioneer Solar Conjunctions—Continuing Corroboration of the Link Between Doppler Noise and Integrated Signal Path Electron Density*, DSN Progress Report, 42-36, (JPL, Pasadena, CA, 1976). Related online version (cited on 19 May 2010): http://ipnpr.jpl.nasa.gov/progress_report2/42-36/36title.htm.
- [41] Berman, A.L., Wackley, J.A., Rockwell, S.T., and Yee, J.G., *The Pioneer 11 1976 Solar Conjunction: A Unique Opportunity to Explore the Heliographic Latitudinal Variations of the Solar Corona*, DSN Progress Report, 42-35, (JPL, Pasadena, CA, 1976). Related online version (cited on 19 May 2010): http://ipnpr.jpl.nasa.gov/progress_report2/42-35/35title.htm.
- [42] Bertolami, O., Böhmer, C.G., Harko, T., and Lobo, F.S.N., “Extra force in $f(R)$ modified theories of gravity”, *Phys. Rev. D*, **75**, 104016, (2007). [DOI], [ADS], [arXiv:0704.1733].
- [43] Bertolami, O., Francisco, F., Gil, P.J.S., and Páramos, J., “Thermal analysis of the Pioneer anomaly: A method to estimate radiative momentum transfer”, *Phys. Rev. D*, **78**, 103001, (2008). [DOI], [ADS], [arXiv:0807.0041].

- [44] Bertolami, O., and García-Bellido, J., “Astrophysical and cosmological constraints on a scale-dependent gravitational coupling.”, *Int. J. Mod. Phys. D*, **5**, 363–373, (1996). [DOI], [ADS], [astro-ph/9502010].
- [45] Bertolami, O., and Páramos, J., “The Pioneer anomaly in the context of the braneworld scenario”, *Class. Quantum Grav.*, **21**, 3309–3321, (2004). [DOI], [ADS], [gr-qc/0310101].
- [46] Bertolami, O., and Páramos, J., “Astrophysical constraints on scalar field models”, *Phys. Rev. D*, **71**, 023521, (2005). [DOI], [ADS], [astro-ph/0408216].
- [47] Bertolami, O., and Páramos, J., “A Mission to Test the Pioneer Anomaly: Estimating the Main Systematic Effects”, *Int. J. Mod. Phys. D*, **16**, 1611–1623, (2007). [DOI], [ADS], [gr-qc/0702149].
- [48] Bertolami, O., and Vieira, P., “Pioneer anomaly and the Kuiper Belt mass distribution”, *Class. Quantum Grav.*, **23**, 4625–4635, (2006). [DOI], [ADS], [astro-ph/0506330].
- [49] Bertotti, B., Iess, L., and Tortora, P., “A test of general relativity using radio links with the Cassini spacecraft”, *Nature*, **425**, 374–376, (2003). [DOI], [ADS].
- [50] Bierman, G.J., and Nead, M.W., *A Parameter Estimation Subroutine Package*, JPL Publication, 77-26 Revision 1, (JPL, Pasadena, CA).
- [51] Bini, D., Cherubini, C., and Mashhoon, B., “Vacuum C metric and the gravitational Stark effect”, *Phys. Rev. D*, **70**, 044020, (2004). [DOI], [ADS], [gr-qc/0401071].
- [52] Brans, C., and Dicke, R. H., “Mach’s Principle and a Relativistic Theory of Gravitation”, *Phys. Rev.*, **124**, 925–935, (1961). [DOI].
- [53] Broadway, N.J., *Radiation Effects Design Handbook: Section 2. Thermal-Control Coatings*, NASA Contractor Report, CR-1786, (1971).
- [54] Brownstein, J.R., and Moffat, J.W., “Gravitational solution to the Pioneer 10/11 anomaly”, *Class. Quantum Grav.*, **23**, 3427–3436, (2006). [DOI], [ADS], [gr-qc/0511026].
- [55] Brumberg, V. A., *Relativistic Celestial Mechanics*, (Nauka, Moscow, 1972). In Russian.
- [56] Brumberg, V. A., *Essential Relativistic Celestial Mechanics*, (Hilger, Bristol, 1991).
- [57] Bruneton, J.-P., and Esposito-Farese, G., “Field-theoretical formulations of MOND-like gravity”, *Phys. Rev. D*, **76**, 124012, (2007). [DOI], [arXiv:0705.4043 [gr-qc]].
- [58] Bryan, A.I., *DSN System Testing: A Report on the DSN Pioneer G Compatibility Program*, JPL Technical Report 32-1526, vol. XV, (1973). Related online version (cited on 3 June 2010): http://ipnpr.jpl.nasa.gov/progress_report2/XV/XVtitle.htm.
- [59] Cadoni, M., “An Einstein-Like Theory of Gravity with a Non-Newtonian Weak-Field Limit”, *Gen. Relativ. Gravit.*, **36**, 2681–2688, (2004). [DOI], [ADS], [gr-qc/0312054].
- [60] Calchi Novati, S., Capozziello, S., and Lambiase, G., “Newtonian Limit of Induced Gravity”, *Grav. Cosm.*, **6**, 173–180, (2000). [ADS], [astro-ph/0005104].
- [61] Capozziello, S., De Laurentis, M., and Faraoni, V., “A bird’s eye view of $f(R)$ -gravity”, arXiv e-print, (2009). [arXiv:0909.4672 [gr-qc]].

- [62] Capozziello, S., de Martino, S., de Siena, S., and Illuminati, F., “Non-Newtonian Gravity, Fluctuative Hypothesis and the Sizes of Astrophysical Structures”, *Mod. Phys. Lett. A*, **16**, 693–706, (2001). [DOI], [ADS], [gr-qc/0104052].
- [63] Capozziello, S., and Lambiase, G., “Neutrino oscillations in Brans–Dicke theory of gravity”, *Mod. Phys. Lett. A*, **14**, 2193, (1999). [DOI], [arXiv:gr-qc/9910026].
- [64] Capozziello, S., Stabile, A., and Troisi, A., “The Newtonian Limit of $f(R)$ gravity”, *Phys. Rev. D*, **76**, 104019, (2007). [DOI], [arXiv:0708.0723 [gr-qc]].
- [65] Carrera, M., and Giulini, D., “On the influence of global cosmological expansion on the dynamics and kinematics of local systems”, arXiv e-print, (2008). [arXiv:0810.2712 [gr-qc]].
- [66] Chafin, R., and Pancino, M., *Pioneer F & G Telemetry and Command Processor Core Dump Program*, JPL Technical Report 32-1526, vol. XVI, (1973). Related online version (cited on 3 June 2010):
http://ipnpr.jpl.nasa.gov/progress_report2/XVI/XVItitle.htm.
- [67] Chao, C.C., *QVLBI Doppler Demonstrations Conducted During Pioneer 11 Encounter and Solar Conjunctions*, DSN Progress Report, 42-31, (JPL, Pasadena, CA, 1976). Related online version (cited on 19 May 2010):
http://ipnpr.jpl.nasa.gov/progress_report2/42-31/31title.htm.
- [68] Chao, C.C., Ondrasik, V.J., and Siegel, H.L., *A Demonstration of Differenced Dual-Station One-Way Doppler Conducted with Pioneer 11*, DSN Progress Report, 42-45, (JPL, Pasadena, CA, 1978). Related online version (cited on 19 May 2010):
http://ipnpr.jpl.nasa.gov/progress_report2/42-45/45title.htm.
- [69] Chiba, T., “ $1/R$ gravity and scalar-tensor gravity”, *Phys. Lett. B*, **575**, 1–3, (2003). [astro-ph/0307338].
- [70] Christophe, B., Andersen, P.H., Anderson, J.D., Asmar, S., B  rio, P., Bertolami, O., Bingham, R., Bondu, F., Bouyer, P., Bremer, S., Courty, J.-M., Dittus, H., Foulon, B., Gil, P., Johann, U., Jordan, J.F., Kent, B., L  mmerzahl, C., L  vy, A., M  tris, G., Olsen, O., P  ramos, J., Prestage, J.D., Progrebenko, S.V., Rasel, E., Rathke, A., Reynaud, S., Rievers, B., Samain, E., Sumner, T.J., Theil, S., Touboul, P., Turyshev, S., Vrancken, P., Wolf, P., and Yu, N., “Odyssey: a Solar System Mission”, *Exper. Astron.*, **23**, 529–547, (2009). [DOI], [arXiv:0711.2007 [gr-qc]].
- [71] Clausen, O.W., and Kirkpatrick, J.P., “Thermal tests of an improved louver system for spacecraft thermal control”, conference paper, (1969).
- [72] Coffin, R.C., Johnson, D.E., and Kuhnle, P.F., “Frequency and timing system for the consolidated DSN and STDN tracking network”, in *Proceedings of the Twelfth Annual Precise Time and Time Interval (PTTI) Applications and Planning Meeting*, 2–4 December 1980, Greenbelt, Maryland, USA, NASA Conference Publication, vol. 2175, pp. 591–614. NASA, (1981). [ADS]. Related online version (cited on 26 May 2010):
<http://hdl.handle.net/2060/19810018929>.
- [73] Consoli, M., and Siringo, F., “Newtonian gravity from Higgs condensates”, arXiv e-print, (1999). [ADS], [hep-ph/9910372].
- [74] Cooperstock, F.I., Faraoni, V., and Vollick, D. N., “The influence of the cosmological expansion on local systems”, *Astrophys. J.*, **503**, 61, (1998). [DOI], [arXiv:astro-ph/9803097].

- [75] Crompton, T.R., *Battery Reference Book*, (Newnes, Oxford; Boston, 2000), 3rd edition.
- [76] Curkendall, D.W., and McReynolds, S.R., “A Simplified Approach for Determining the Information Content of Radio Tracking Data”, *J. Spacecraft*, **6**(5), 520–525, (1969).
- [77] Dabrowski, M.P., Denkiewicz, T., and Blaschke, D.B., “The conformal status of $\omega = -3/2$ Brans-Dicke cosmology”, *Ann. Phys. (Berlin)*, **16**, 237–257, (2007). [DOI], [ADS], [hep-th/0507068].
- [78] Damour, T., and Krauss, L.M., “A New Solar System Dark Matter Population of Weakly Interacting Massive Particles”, *Phys. Rev. Lett.*, **81**, 5726–5729, (1998). [DOI], [ADS], [astro-ph/9806165].
- [79] Damour, T., and Nordtvedt, K., “General relativity as a cosmological attractor of tensor scalar theories”, *Phys. Rev. Lett.*, **70**, 2217–2219, (1993).
- [80] Damour, T., and Nordtvedt, K., “Tensor - scalar cosmological models and their relaxation toward general relativity”, *Phys. Rev. D*, **48**, 3436–3450, (1993).
- [81] Damour, T., Soffel, M., and Xu, C., “General-relativistic celestial mechanics. I. Method and definition of reference systems”, *Phys. Rev. D*, **43**, 3273–3307, (1991). [ADS].
- [82] Damour, T., Soffel, M., and Xu, C., “General-relativistic celestial mechanics. II. Translational equations of motion”, *Phys. Rev. D*, **45**, 1017–1044, (1992). [ADS].
- [83] Damour, T., Soffel, M., and Xu, C., “General-relativistic celestial mechanics. III. Rotational equations of motion”, *Phys. Rev. D*, **47**, 3124–3135, (1993). [ADS].
- [84] Damour, T., Soffel, M., and Xu, C., “General-relativistic celestial mechanics. IV. Theory of satellite motion”, *Phys. Rev. D*, **49**, 618–635, (1994). [ADS].
- [85] de Bernardis, P., Ade, P.A.R., Bock, J.J., Bond, J.R., Borrill, J., Boscaleri, A., Coble, K., Crill, B.P., De Gasperis, G., Farese, P.C., Ferreira, P.G., Ganga, K., Giacometti, M., Hivon, E., Hristov, V.V., Iacoangeli, A., Jaffe, A., Lange, A.E., Martinis, L., Masi, S., Mason, P.V., Mauskopf, P.D., Melchiorri, A., Miglio, L., Montroy, T., Netterfield, C.B., Pascale, E., Piacentini, F., Pogosyan, D., Prunet, S., Rao, S., Romeo, G., Ruhl, J.E., Scaramuzzi, F., Sforza, D., and Vittorio, N., “A flat Universe from high-resolution maps of the cosmic microwave background radiation”, *Nature*, **404**, 955–959, (2000). [DOI].
- [86] de Diego, J.A., Núñez, D., and Zavala, J., “Pioneer Anomaly? Gravitational Pull due to the Kuiper Belt”, *Int. J. Mod. Phys. D*, **15**, 533–544, (2006). [DOI], [ADS], [astro-ph/0503368].
- [87] de Groot, N.F., and Bahadori, H.R., *Historical Data on Characteristics of Radio Systems Used for United States Deep-Space Communications*, TDA Progress Report, 42-61, (JPL, Pasadena, CA, 1981). Related online version (cited on 19 May 2010): http://ipnpr.jpl.nasa.gov/progress_report/42-61/61title.htm.
- [88] *Deep Space Mission System (DSMS) Services Catalog, Version 7.5, by Wallace S. Tai. DSMS No. 820-100.*, JPL Document #D-19002, (JPL, Pasadena, CA, 2003).
- [89] *Deep Space Network, Flight Project Interface Design Book*, Document 810-5, (JPL, Pasadena, CA).

- [90] *Deep Space Network System Requirements Detailed Interface Design*, Document DSN820-13, (JPL, Pasadena, CA, 1991). JPL Document 820-13, Rev. A. See *DSN Tracking System Interfaces, Archival Tracking Data File Interface, TRK-2-25*. An example of an ATDF for the Ulysses mission (part of SFOC-NAV-2-25) may be found at <http://www.igpp.ucla.edu/pds3/ULY.5101/DATA/ATDF/2040040A.LBL>.
- [91] *Deep Space Network System Requirements Detailed Interface Design*, Document DSN820-13, (JPL, Pasadena, CA, 1991). JPL Document 820-13, Rev. A. See chapter on *DSN Tracking System Interfaces, Orbit Data File Interface, TRK-2-18*. An example of an ODF for the NEAR mission (part of SFOC-NAV-TRK-2-18) may be found at http://pdssbn.astro.umd.edu/data3/NEAR/nreros_2001/erosfb/odf/8357357c.lbl.
- [92] Diemand, J., Kuhlen, M., and Madau, P., “Formation and Evolution of Galaxy Dark Matter Halos and Their Substructure”, *Astrophys. J.*, **667**, 859–877, (2007). [DOI], [ADS], [astro-ph/0703337].
- [93] Dimopoulos, S., and Giudice, G. F., “Macroscopic Forces from Supersymmetry”, *Phys. Lett. B*, **379**, 105–114, (1996). [hep-ph/9602350].
- [94] Dittus, H., Turyshv, S.G., Lämmerzahl, C., Theil, S., Foerstner, R., Johann, U., Ertmer, W., Rasel, E., Dachwald, B., Seboldt, W., Hehl, F.W., Kiefer, C., Blome, H.-J., Kunz, J., Giulini, D., Bingham, R., Kent, B., Sumner, T.J., Bertolami, O., Páramos, J., Rosales, J.L., Christophe, B., Foulon, B., Touboul, P., Bouyer, P., Reynaud, S., Brillet, A., Bondu, F., Samain, E., de Matos, C.J., Erd, C., Grenouilleau, J.C., Izzo, D., Rathke, A., Anderson, J.D., Asmar, S.W., Lau, E.L., Nieto, M.M., and Mashoon, B., “A mission to explore the Pioneer anomaly”, *ESA Spec. Publ.*, **588**, 3–10, (2005). [ADS], [gr-qc/0506139].
- [95] *Documentation*, BFEC/ARC-166A, (Bendix Field Engineering Corporation). Documentation fragment recovered by L.R. Kellogg.
- [96] *DSN Telecommunications Link Design Handbook*, 810-005 Rev. E, (JPL, Pasadena, CA, 2010)URL: <http://deepspace.jpl.nasa.gov/dsndocs/810-005/>.
- [97] Duha, J., Afonso, G.B., and Ferreira, L.D.D., “Thermal re-emission effects on GPS satellites”, *J. Geod.*, **80**, 665–674, (2006).
- [98] Dvali, G., Gabadadze, G., Kolanovic, M., and Nitti, F., “Scales of gravity”, *Phys. Rev. D*, **65**, 024031, (2002). [hep-th/0106058].
- [99] Dvali, G., Gruzinov, A., and Zaldarriaga, M., “The accelerated universe and the Moon”, *Phys. Rev. D*, **68**, 024012, (2003). [hep-ph/0212069].
- [100] Dyal, P., *Pioneer 10 and 11 Deep Space Missions*, NASA Technical Memorandum, 102269, (1990).
- [101] Earman, J., and Janssen, M., “Einstein’s Explanation of the Motion of Mercury’s Perihelion”, in Earman, J., Janssen, M., and Norton, J.D., eds., *The Attraction of Gravitation: New Studies in the History of General Relativity*, Einstein Studies, vol. 5, pp. 129–172, (Birkhäuser, Boston; Basel, 1993). [Google Books].
- [102] Eddington, A.S., *The Mathematical Theory of Relativity*, (Cambridge University Press, Cambridge, 1957).

- [103] Edwards, D.K., and Hall, W.M., *Far-Infrared Reflectance of Spacecraft Coatings*, NASA Technical Report, No. 32-873, (1966).
- [104] Einstein, A., “Die Feldgleichungen der Gravitation”, *Sitzungsber. Preuss. Akad. Wiss.*, **1915**, 844–847, (1915) Related online version:
http://einstein-annalen.mpiwg-berlin.mpg.de/related_texts/sitzungsberichte/6E3MAXK4.
- [105] Einstein, A., “Die Grundlage der allgemeinen Relativitätstheorie”, *Ann. Phys. (Leipzig)*, **49**, 769–822, (1916). [DOI] Related online version:
<http://www.alberteinstein.info/gallery/gtext3.html>.
- [106] Einstein, A., Infeld, L., and Hoffmann, B., “The gravitational equations and the problem of motion”, *Ann. Math.*, **39**, 65–100, (1938).
- [107] Einstein, A., and Straus, E.G., “The Influence of the Expansion of Space on the Gravitation Fields Surrounding the Individual Stars”, *Rev. Mod. Phys.*, **17**, 120–124, (1945). [DOI].
- [108] Estabrook, F.B., “Post-Newtonian n -body Equations of the Brans-Dicke Theory”, *Astrophys. J.*, **158**, 81, (1969). [DOI], [ADS].
- [109] Estefan, J.A., and Sovers, O.J., *A Comparative Survey of Current and Proposed Tropospheric Refraction-Delay Models for DSN Radio Metric Data Calibration*, JPL Publication, 94-24, (1994).
- [110] Evans, D., ed., *Pioneer Mission to Jupiter – Special Issue*, The Astrogram, vol. XIV, (Ames Research Center, Moffat Field, CA, 1972). Related online version (cited on 25 May 2010):
<http://history.arc.nasa.gov/astrogram.htm>.
- [111] Exirifard, Q., “A new evidence against the covariant resolution of the Pioneers’ anomaly”, *Class. Quantum Grav.*, **26**, 025001, (2009). [ADS], [arXiv:0708.0662 [hep-th]].
- [112] Falin, B.W., *DSN frequency and timing system, Mark 4-85*, TDA Progress Report, 42-82, (1985). Related online version (cited on 19 May 2010):
http://ipnpr.jpl.nasa.gov/progress_report/42-82/82title.htm.
- [113] Ferreira, P.C., “A Locally Anisotropic Metric for Matter in an Expanding Universe: I. The Ansatz and the Modified Newton Law”, arXiv e-print, (2009). [arXiv:0907.0847 [astro-ph.CO]].
- [114] Fienga, A., Laskar, J., Kuchynka, P., Le Poncin-Lafitte, C., Manche, H., and Gastineau, M., “Gravity tests with INPOP planetary ephemerides”, in Klioner, S.A., Seidelmann, P.K., and Soffel, M.H., eds., *Relativity in Fundamental Astronomy: Dynamics, Reference Frames, and Data Analysis*, Proceedings IAU Symposium No. 261, 22 April–1 May 2009, Virginia Beach, VA, USA, Proc. IAU, vol. 261, pp. 159–169. Cambridge University Press, (2010). [DOI], [ADS].
- [115] Fimmel, R.O., Swindell, W., and Burgess, E., *Pioneer Odyssey: First into the Outer Solar System*, NASA Special Publication, vol. SP-349/396, (NASA, Washington, DC, 1977), rev. edition Related online version:
<http://history.nasa.gov/SP-349/sp349.htm>.
- [116] Fimmel, R.O., Van Allen, J.A., and Burgess, E., *Pioneer: First to Jupiter, Saturn, and Beyond*, NASA Publications, vol. SP-446, (NASA, Washington, DC, 1980). Related online version (cited on 26 May 2010):
<http://hdl.handle.net/2060/19810007410>.

- [117] Folkner, W.M., *DSN Station Locations and Uncertainties*, TDA Progress Report, 42-128, (Pasadena, CA, 1997).
- [118] Folkner, W.M., “Relativistic aspects of the JPL planetary ephemeris”, in Klioner, S.A., Seidelmann, P.K., and Soffel, M.H., eds., *Relativity in Fundamental Astronomy: Dynamics, Reference Frames, and Data Analysis*, Proceedings IAU Symposium No. 261, 22 April – 1 May 2009, Virginia Beach, VA, USA, Proc. IAU, vol. 261, pp. 155–158, (Cambridge University Press, Cambridge, 2010). [DOI], [ADS].
- [119] Foot, R., and Volkas, R.R., “A mirror world explanation for the Pioneer spacecraft anomalies?”, *Phys. Lett. B*, **517**, 13–17, (2001). [hep-ph/0108051].
- [120] Frauenholz, R.B., “Maneuver Reconstruction Techniques for Open-Loop Spin-Stabilized Spacecraft”, *J. Guidance*, **5**(3), 270–277, (1980).
- [121] Frauenholz, R.B., and Brady, W.F., “Maneuver Sequence Design for the Post-Jupiter Leg of the Pioneer Saturn Mission”, *J. Spacecraft*, **14**(7), 395–400, (1977).
- [122] Frauenholz, R.B., and Farless, D.L., “Maneuver Strategies for the Extended Pioneer 11 Jupiter/Saturn Mission”, AIAA Mechanics and Control of Flight Conference, Anaheim, CA, August 5–9, 1974, conference paper, (1974).
- [123] Frauenholz, R.B., and Farless, D.L., “Earth-Line Maneuver Strategies for the Extended Pioneer 11 Jupiter/Saturn Mission”, *J. Spacecraft*, **12**(5), 271–279, (1975).
- [124] Furlong, R.R., and Wahlquist, E.J., “U.S. space missions using radioisotope power systems”, *Nuclear News*, 26–34, (April 1999).
- [125] Galbreath, E.A., *Brouwer-Lyddane Orbit Generator Routine*, NASA Technical Memorandum, TM X-65361, (Greenbelt, MD, 1970). Related online version (cited on 3 June 2010): <http://hdl.handle.net/2060/19700033083>.
- [126] Gautreau, R., “Imbedding a Schwarzschild mass into cosmology”, *Phys. Rev. D*, **29**, 198–206, (1984). [DOI].
- [127] Gelb, A., ed., *Applied Optimal Estimation*, (MIT Press, Cambridge, 1974). [Google Books].
- [128] Gor’kavyi, N.N., Ozernoy, L.M., and Taidakova, T., “The Large Scale Structures in the Solar System: II. Resonant Dust Belts Associated With the Orbits of Four Giant Planets”, arXiv e-print, (1998). [ADS], [astro-ph/9812480].
- [129] Gundlach, J.H., Schlamming, S., Spitzer, C.D., Choi, K.-Y., Woodahl, B.A., Coy, J.J., and Fischbach, E., “Laboratory Test of Newton’s Second Law for Small Accelerations”, *Phys. Rev. Lett.*, **98**, 150801, (2007). [DOI].
- [130] Hackmann, E., and Lämmerzahl, C., “Complete Analytic Solution of the Geodesic Equation in Schwarzschild-(Anti-)de Sitter Spacetimes”, *Phys. Rev. Lett.*, **100**, 171101, (2008). [DOI].
- [131] Hackmann, E., and Lämmerzahl, C., “Geodesic equation in Schwarzschild-(anti-)de Sitter space-times: Analytical solutions and applications”, *Phys. Rev. D*, **78**, 024035, (2008). [DOI].
- [132] Hall, C.F., and Mickelwatt, A.B., “Development of the interplanetary Pioneer spacecraft”, Systems Engineering I (Unmanned) Session at the XVIIIth IAF Congress in Belgrade, Yugoslavia, conference paper, (1967).

- [133] Henninger, J.H., *Solar Absorptance and Thermal Emittance of Some Common Spacecraft Thermal-Control Coatings*, NASA Reference Publication, 1121, (1984).
- [134] Hesprich, G.V., *Pioneer F/G appendage deployment*, (TRW Systems Space Vehicles Division, Redondo Beach, CA). Related online version (cited on 19 May 2010): <http://hdl.handle.net/2060/19710069136>.
- [135] *Hexadecimal Dump of MDR Records*, ATSC/ARC-223, (AlliedSignal Technical Services Corporation).
- [136] Hinedi, S., *A Functional Description of the Advanced Receiver*, TDA Progress Report, 42-100, (JPL, Pasadena, CA, 1990). Related online version (cited on 19 May 2010): http://ipnpr.jpl.nasa.gov/progress_report/42-100/100title.htm.
- [137] Ho, C., and Morabito, D., *DSMS Telecommunications Link Design Handbook 106, Rev. A*, (2005).
- [138] Hoffmann, A.H., *Pioneer F and G Mission Support Area*, JPL Technical Report 32-1526, vol. V, (1971). Related online version (cited on 3 June 2010): http://ipnpr.jpl.nasa.gov/progress_report2/V/Vtitle.htm.
- [139] Hurd, W.J., Brown, D.H., Vilnrotter, V.A., and Wiggins, J.D., *Telemetry SNR Improvement Using the DSN Advanced Receiver With Results for Pioneer 10*, TDA Progress Report, 42-93, (JPL, Pasadena, CA, 1988). Related online version (cited on 19 May 2010): http://ipnpr.jpl.nasa.gov/progress_report/42-93/93title.htm.
- [140] *IEEE Standard for Binary Floating-Point Arithmetic*, ANSI/IEEE Std 754-1985, (IEEE, 1985). [DOI].
- [141] Imbriale, W.A., *Large Antennas of the Deep Space Network*, (Wiley, Hoboken, NJ, 2003). [DOI].
- [142] *Interface Change Authorization: HSD Formats Pioneer 10-11*, ICA84, (1978).
- [143] *Interface Change Authorization: Telemetry System 1200-bit Data Interfaces, Pioneer 10-11*, ICA155, (1982).
- [144] Iorio, L., “Dynamical determination of the mass of the Kuiper Belt from motions of the inner planets of the Solar system”, *Mon. Not. R. Astron. Soc.*, **375**, 1311–1314, (2007). [DOI], [ADS], [gr-qc/0609023].
- [145] Iorio, L., and Giudice, G., “What do the orbital motions of the outer planets of the Solar System tell us about the Pioneer anomaly?”, *New Astronomy*, **11**, 600–607, (2006). [DOI], [ADS], [gr-qc/0601055].
- [146] Ivanov, M.A., “Possible Manifestations of the Graviton Background”, *Gen. Relativ. Gravit.*, **33**, 479–490, (2001). [ADS], [astro-ph/0005084].
- [147] Jaekel, M.-T., and Reynaud, S., “Gravity Tests in the Solar System and the Pioneer Anomaly”, *Mod. Phys. Lett. A*, **20**, 1047–1055, (2005). [DOI], [ADS], [gr-qc/0410148].
- [148] Jaekel, M.-T., and Reynaud, S., “Post-Einsteinian tests of linearized gravitation”, *Class. Quantum Grav.*, **22**, 2135–2158, (2005). [gr-qc/0502007].
- [149] Jaekel, M.-T., and Reynaud, S., “Post-Einsteinian tests of gravitation”, *Class. Quantum Grav.*, **23**, 777–798, (2006). [DOI], [ADS], [gr-qc/0510068].

- [150] Jaekel, M.-T., and Reynaud, S., “Radar ranging and Doppler tracking in post-Einsteinian metric theories of gravity”, *Class. Quantum Grav.*, **23**, 7561–7579, (2006). [DOI], [ADS], [gr-qc/0610155].
- [151] Jaekel, M.-T., and Reynaud, S., “Gravity tests and the Pioneer anomaly”, in Dittus, H., Lämmerzahl, C., and Turyshchev, S.G., eds., *Lasers, Clocks and Drag-Free Control: Exploration of Relativistic Gravity in Space*, Astrophysics and Space Science Library, vol. 193–208, p. 75. Springer, (2008). [ADS].
- [152] Johnston, D.W.H., *Pioneer Mission Support*, DSN Progress Report, 42-46, (JPL, Pasadena, CA, 1978).
- [153] JPL, *Pioneer 10 Doppler Tracking Data*, 72-012A-09A, (1982).
- [154] *Jupiter*, (Ames Research Center, Moffett Field, CA, 1974).
- [155] Kagramanova, V., Kunz, J., and Lämmerzahl, C., “Solar system effects in Schwarzschild–de Sitter spacetime”, *Phys. Lett. B*, **634**, 465–470, (2006). [DOI], [arXiv:gr-qc/0602002].
- [156] Katz, J.I., “Comment on ‘Indication, from Pioneer 10/11, Galileo, and Ulysses Data, of an Apparent Anomalous, Weak, Long-Range Acceleration’”, *Phys. Rev. Lett.*, **83**, 1892, (1999). [ADS], [gr-qc/9809070].
- [157] Kaviany, M., *Principles of Heat Transfer*, (Wiley, New York, 2001).
- [158] Keihm, S.J., *Water Vapor Radiometer Measurements of the Tropospheric Delay Fluctuations at Goldstone Over a Full Year*, TDA Progress Report, 42-122, (1995).
- [159] Kellogg, L.R., “Pioneer 10 MDR interpretation”, personal communication, (2003).
- [160] Kerr, A.W., Hauck, J.C., and Mashhoon, B., “Standard Clocks, Orbital Precession and the Cosmological Constant”, *Class. Quantum Grav.*, **20**, 2727, (2003). [DOI], [arXiv:gr-qc/0301057].
- [161] Kinsella, G., “Pioneer 10 Thermal Analysis”, personal communication, (2007).
- [162] Kinsella, G., Lee, S.-C., and Lok, D., “Pioneer anomaly thermal analysis status”, personal communication, (2007–2009).
- [163] Kinsella, G., Lee, S.-C., Lok, D.S., and Turyshchev, S.G., “Pioneer thermal modelling: An Overview of Recent Activities and the Current Status”, Second Pioneer Explorer Collaboration meeting at ISSI, Bern, Switzerland, February 19–23, 2007, conference paper, (2007).
- [164] Kinsella, G., Lee, S.-C., Lok, D.S., and Turyshchev, S.G., “Thermal Engineering Status for the Pioneer 10 Anomaly Meeting”, Third Pioneer Explorer Collaboration meeting at ISSI, Bern, Switzerland, February 18–22, 2008, conference paper, (2008).
- [165] Konopliv, A.S., Yoder, C.F., Standish, E.M., Yuan, D.-N., and Sjogren, W.L., “A global solution for the Mars static and seasonal gravity, Mars orientation, Phobos and Deimos masses, and Mars ephemeris”, *Icarus*, **182**, 23–50, (2006). [DOI], [ADS].
- [166] Kowalski-Glikman, J., and Smolin, L., “Triply special relativity”, *Phys. Rev. D*, **70**, 065020, (2004). [DOI], [arXiv:hep-th/0406276].
- [167] Lachièze-Rey, M., “Cosmology in the solar system: the Pioneer effect is not cosmological”, *Class. Quantum Grav.*, **24**, 2735–2741, (2007). [DOI], [ADS], [gr-qc/0701021].

- [168] Lämmerzahl, C., “The Pioneer Anomaly and the Solar System in the Expanding Universe”, Workshop ‘Intertwining Theory and Observational Evidence in Contemporary Cosmology’, Wuppertal University, Germany, February 12–14, 2009, conference paper, (2009). Related online version (cited on 20 May 2010):
http://www.izwt.uni-wuppertal.de/files/Laemmerzahl_Pioneer_anomaly.pdf.
- [169] Lämmerzahl, C., Preuss, O., and Dittus, H., “Is the Physics Within the Solar System Really Understood?”, in Dittus, H., Lämmerzahl, C., and Turyshev, S.G., eds., *Lasers, Clocks and Drag-Free Control: Exploration of Relativistic Gravity in Space*, Astrophysics and Space Science Library, vol. 349, pp. 75–104, (Springer, Berlin; New York, 2008). [ADS], [gr-qc/0604052], [Google Books].
- [170] Landgraf, M., Liou, J.-C., Zook, H.A., and Grün, E., “Origins of Solar System Dust beyond Jupiter”, *Astrophys. J.*, **123**, 2857–2861, (2002). [DOI], [ADS], [astro-ph/0201291].
- [171] Levy, A., Christophe, B., Berio, P., Metris, G., Courty, J.-M., and Reynaud, S., “Pioneer Doppler data analysis: study of periodic anomalies”, *Adv. Space Res.*, **43**, 1538–1544, (2009). [DOI], [arXiv:0809.2682 [gr-qc]].
- [172] Lienhard IV, J.H., and Lienhard V, J.H., *A Heat Transfer Textbook*, (Phlogiston Press, Cambridge, 2002), 3rd edition. Related online version (cited on 26 May 2010):
<http://web.mit.edu/lienhard/www/ahtt.html>.
- [173] Lisman, S., *Cassini Non-Gravitational Force and Torque Estimates, Final Guidance Analysis Book Documentation*, JPL Interoffice Memorandum, 3456-94-004, (1994).
- [174] Liu, A., and Pease, G., “Preliminary Estimates of Range Measurements to a Spacecraft by Means of Ground Digitally Controlled Oscillators”, AIAA Mechanics and Control of Flight Conference, Anaheim, CA, August 5–9, 1974, conference paper, (1974).
- [175] Liu, A., and Pease, G., “Spacecraft Ranging from a Ground Digitally Controlled Oscillator”, *J. Spacecraft*, **12**(9), 528–532, (1974).
- [176] Liu, A.S., *Range Measurements to Pioneer 10 Using the Digitally Controlled Oscillator*, JPL Technical Report 32-1526, vol. XIX, (1974). Related online version (cited on 3 June 2010):
http://ipnpr.jpl.nasa.gov/progress_report2/XIX/XIXtitle.htm.
- [177] Liu, A.S., *Three Tropocentric Range Measurements to Pioneer 10 Near Jupiter Encounter and a Preliminary Estimate of an Earth Barycenter to Jupiter Barycenter Distance*, DSN Progress Report, 42-21, (JPL, Pasadena, CA, 1974). Related online version (cited on 19 May 2010):
http://ipnpr.jpl.nasa.gov/progress_report2/42-21/21title.htm.
- [178] Longuski, J.M., Todd, R.E., and König, W.W., “Survey of Nongravitational Forces and Space Environmental Torques: Applied to the Galileo”, *J. Guidance, Control, and Dynamics*, **15**, 545, (1992).
- [179] Mäkelä, J., “Pioneer Effect: An Interesting Numerical Coincidence”, arXiv e-print, (2007). [ADS], [arXiv:0710.5460 [gr-qc]].
- [180] Malhotra, R., “The Origin of Pluto’s Orbit: Implications for the Solar System Beyond Neptune”, *Astron. J.*, **110**, 420, (1995). [DOI], [ADS], [astro-ph/9504036].
- [181] Mann, I., and Kimura, H., “Interstellar dust properties derived from mass density, mass distribution, and flux rates in the heliosphere”, *J. Geophys. Research*, **105**, 10,317–10,328, (2000). [DOI], [ADS].

- [182] Mansouri, R., Naseri, F., and Khorrami, M., “Effective time variation of G in a model universe with variable space dimension”, *Phys. Lett. A*, **259**, 194–200, (1999). [DOI], [ADS], [gr-qc/9905052].
- [183] Markwardt, C.B., “Markwardt IDL Library”, print. URL (cited on 9 February 2008): <http://cow.physics.wisc.edu/~craigm/idl/idl.html>.
- [184] Markwardt, C.B., “Notes on ATDF Doppler Tracking Data”, print. URL (cited on 9 February 2008): <http://lheawww.gsfc.nasa.gov/users/craigm/atdf/>.
- [185] Markwardt, C.B., “Independent Confirmation of the Pioneer 10 Anomalous Acceleration”, arXiv e-print, (2002). [ADS], [gr-qc/0208046].
- [186] Marmet, P., “Anomalous Acceleration of Pioneer 10 and 11: Dust Density in the Kuiper Belt”, in Duffy, M.C., Gladyshev, V.O., and Morozov, A.N., eds., *Physical Interpretations of Relativity (PIRT 2003)*, Moscow, 30 June–3 July, 2003, pp. 334–337, (Bauman Moscow State Technical University, Moscow, 2003). Related online version (cited on 19 May 2010): <http://www.newtonphysics.on.ca/anomalous/>.
- [187] Mashhoon, B., “Modification of the Doppler effect due to the helicity-rotation coupling”, *Phys. Lett. A*, **306**, 66–72, (2002). [DOI], [ADS], [gr-qc/0209079].
- [188] Massa, C., “Variable cosmological ‘constant’ and motion of a test particle in a cloud of dust”, *Astrophys. Space Sci.*, **317**, 139–141, (2008). [DOI].
- [189] Matsakis, D.N., Taylor, J.H., and Eubanks, T.M., “A statistic for describing pulsar and clock stabilities”, *Astron. Astrophys.*, **326**, 924–928, (1997). [ADS].
- [190] Mbelek, J.P., “General relativity and quintessence explain the Pioneer anomaly”, arXiv e-print, (2004). [ADS], [gr-qc/0407023].
- [191] Mbelek, J.P., Mosquera Cuesta, H.J., Novello, M., and Salim, J.M., “Nonlinear electrodynamics and the Pioneer 10/11 spacecraft anomaly”, *Europhys. Lett.*, **77**, 19001, (2007). [DOI], [ADS], [astro-ph/0608538].
- [192] McCulloch, M.E., “Modelling the Pioneer anomaly as modified inertia”, *Mon. Not. R. Astron. Soc.*, **376**, 338–342, (2007). [DOI], [ADS], [astro-ph/0612599].
- [193] McVittie, G.C., “Expansion of the universe, The problem of η bodies and the”, *Mon. Not. R. Astron. Soc.*, **91**, 274, (1931). [ADS].
- [194] McVittie, G.C., “The mass-particle in an expanding universe”, *Mon. Not. R. Astron. Soc.*, **93**, 325–339, (1933). [ADS].
- [195] Melbourne, W.G., *Radio Occultations Using Earth Satellites: A Wave Theory Treatment*, vol. 6, (JPL, Pasadena, 2004). URL (cited on 20 May 2010): http://descanso.jpl.nasa.gov/Monograph/series6_chapter.cfm.
- [196] Mendes, V.B., and Langley, R.B., “A Comprehensive Analysis of Mapping Functions Used in Modeling Tropospheric Propagation Delay in Space Geodetic Data”, in *Proceedings of KIS94*, International Symposium on Kinematic Systems in Geodesy, Geomatics and Navigation, Banff, Canada, August 30–September 2, 1994, pp. 87–98, (The University of Calgary, Calgary, 1994).

- [197] Merrill, R., Snoddy, W., and Schocken, K., *The Results of Emittance Measurements Made in Relation to the Thermal Design of Explorer Spacecraft*, NASA Technical Note, D-1116, (1962).
- [198] Meshishnek, M.J., Hemminger, C.S., and Gyetvay, S.R., *Space Environmental Exposure of IITRI White Thermal Control Paints*, A634203, (The Aerospace Corporation, El Segundo, CA, 1995).
- [199] Meyer, F., Bamler, R., Jakowski, N., and Fritz, T., “The Potential of Broadband L-Band SAR Systems for Small Scale Ionospheric TEC Mapping”, in *Proceedings of Fringe 2005 Workshop ‘Advances in SAR Interferometry from ENVISAT and ERS Missions’*, Frascati, Italy, 28–2 December 2005. ESA, (2005)URL: <http://earth.esa.int/fringe05/proceedings/>.
- [200] Mihalas, D., and Weibel-Mihalas, B., *Foundations of Radiation Hydrodynamics*, (Dover, Mineola, NY, 1999).
- [201] Milani, A., Nobili, A.M., and Farinella, P., *Non-Gravitational Perturbations and Satellite Geodesy*, (Adam Hilger, Bristol, 1987).
- [202] Milgrom, M., “A modification of the Newtonian dynamics as a possible alternative to the hidden mass hypothesis”, *Astrophys. J.*, **270**, 365–370, (1983). [DOI], [ADS].
- [203] Milgrom, M., “A modification of the Newtonian dynamics: Implications for galaxies”, *Astrophys. J.*, **270**, 371–389, (1983). [DOI], [ADS].
- [204] Milgrom, M., “MOND – a Pedagogical Review”, *Acta Phys. Pol. B*, **32**, 3613, (2001). [astro-ph/0112069].
- [205] Milgrom, M., “MOND as modified inertia”, in Mamon, G.A., Combes, F., Deffayet, C., and Fort, B., eds., *EAS Publications Series*, EAS Publications Series, vol. 20, pp. 217–224, (2006). [DOI], [ADS], [arXiv:astro-ph/0510117].
- [206] Miller, R.B., *Pioneer 10 and 11 Mission Support*, JPL Technical Report 32-1526, vol. XV, (1973). Related online version (cited on 3 June 2010): http://ipnpr.jpl.nasa.gov/progress_report2/XV/XVtitle.htm.
- [207] Miller, R.B., *Pioneer 10 and 11 Mission Support*, JPL Technical Report 32-1526, vol. XVI, (1973). Related online version (cited on 3 June 2010): http://ipnpr.jpl.nasa.gov/progress_report2/XVI/XVItitle.htm.
- [208] Miller, R.B., *Pioneer 10 and 11 Mission Support*, JPL Technical Report 32-1526, vol. XVII, (1973). Related online version (cited on 3 June 2010): http://ipnpr.jpl.nasa.gov/progress_report2/XVII/XVIItitle.htm.
- [209] Miller, R.B., *Pioneer 10 and 11 Mission Support*, JPL Technical Report 32-1526, vol. XVIII, (1973). Related online version (cited on 3 June 2010): http://ipnpr.jpl.nasa.gov/progress_report2/XVIII/XVIIItitle.htm.
- [210] Miller, R.B., *Pioneer 10 and 11 Mission Support*, JPL Technical Report 32-1526, vol. XIX, (1974). Related online version (cited on 3 June 2010): http://ipnpr.jpl.nasa.gov/progress_report2/XIX/XIXtitle.htm.
- [211] Miller, R.B., *Pioneer 10 and 11 Mission Support*, DSN Progress Report, 42-21, (JPL, Pasadena, CA, 1974). Related online version (cited on 19 May 2010): http://ipnpr.jpl.nasa.gov/progress_report2/42-21/21title.htm.

- [212] Miller, R.B., *Pioneer 10 and 11 Mission Support*, DSN Progress Report, 42-22, (JPL, Pasadena, CA, 1974). Related online version (cited on 19 May 2010): http://ipnpr.jpl.nasa.gov/progress_report2/42-22/22title.htm.
- [213] Miller, R.B., *Pioneer 10 and 11 Mission Support*, DSN Progress Report, 42-24, (JPL, Pasadena, CA, 1974). Related online version (cited on 19 May 2010): http://ipnpr.jpl.nasa.gov/progress_report2/42-24/24title.htm.
- [214] Miller, R.B., *Pioneer 11 Mission Support*, DSN Progress Report, 42-26, (JPL, Pasadena, CA, 1975). Related online version (cited on 19 May 2010): http://ipnpr.jpl.nasa.gov/progress_report2/42-26/26title.htm.
- [215] Miller, R.B., *Pioneer Mission Support*, DSN Progress Report, 42-30, (JPL, Pasadena, CA, 1975). Related online version (cited on 19 May 2010): http://ipnpr.jpl.nasa.gov/progress_report2/42-30/30title.htm.
- [216] Miller, R.B., *Pioneer 10 and 11 Mission Support*, DSN Progress Report, 42-33, (JPL, Pasadena, CA, 1976). Related online version (cited on 19 May 2010): http://ipnpr.jpl.nasa.gov/progress_report2/42-33/33title.htm.
- [217] Miller, R.B., *Pioneer 10 and 11 Mission Support*, DSN Progress Report, (JPL, Pasadena, CA, 1978). Related online version (cited on 19 May 2010): http://ipnpr.jpl.nasa.gov/progress_report2/42-47/47title.htm.
- [218] Miller, R.B., *Pioneer 11 Saturn Encounter Mission Support*, DSN Progress Report, 42-52, (JPL, Pasadena, CA, 1979). Related online version (cited on 19 May 2010): http://ipnpr.jpl.nasa.gov/progress_report2/42-52/52title.htm.
- [219] Miller, R.B., *Pioneer 11 Saturn Encounter Mission Support*, DSN Progress Report, 42-54, (JPL, Pasadena, CA, 1979). Related online version (cited on 19 May 2010): http://ipnpr.jpl.nasa.gov/progress_report2/42-54/54title.htm.
- [220] Minguzzi, E., “Possible relation between galactic flat rotational curves and the Pioneers’ anomalous acceleration”, *New Astronomy*, **12**, 142–145, (2006). [DOI], [ADS], [astro-ph/0603790].
- [221] Misner, C.W., Thorne, K.S., and Wheeler, J.A., *Gravitation*, (W.H. Freeman, San Francisco, 1973).
- [222] Modanese, G., “Effect of a scale-dependent cosmological term on the motion of small test particles in a Schwarzschild background”, *Nuclear Phys. B*, **556**, 397–408, (1999). [DOI], [ADS], [gr-qc/9903085].
- [223] Moffat, J. W., “Modified Gravitational Theory and the Pioneer 10 and 11 Spacecraft Anomalous Acceleration”, arXiv e-print, (2004). [gr-qc/0405076].
- [224] Moffat, J.W., “Scalar–tensor–vector gravity theory”, *J. Cosmol. Astropart. Phys.*, **2006**(03), 004, (2006). [DOI], [ADS], [gr-qc/0506021].
- [225] Moffat, J.W., and Toth, V. T., “Fundamental parameter-free solutions in Modified Gravity”, *Class. Quantum Grav.*, **26**, 085002, (2009). [DOI], [arXiv:0712.1796 [gr-qc]].
- [226] Montenbruck, O., and Gill, B., *Satellite Orbits: Models, Methods and Applications*, (Springer, Berlin; New York, 2005), 3rd edition.

- [227] Morabito, D.D., and Asmar, S.W., *Radio-Science Performance Analysis Software*, TDA Progress Report, 42-120, (1995).
- [228] Moyer, T.D., *Mathematical Formulation of the Double Precision Orbit Determination Program (DPODP)*, JPL Technical Report, 32-1527, (JPL, 1971)Related online version: <http://hdl.handle.net/2060/19710017134>.
- [229] Moyer, T.D., “Transformation from Proper Time on Earth to Coordinate Time in Solar System Barycentric Space-Time Frame of Reference - Part I”, *Celestial Mechanics*, **23**, 33–56, (1981). [ADS].
- [230] Moyer, T.D., “Transformation from Proper Time on Earth to Coordinate Time in Solar System Barycentric Space-Time Frame of Reference - Part II”, *Celestial Mechanics*, **23**, 57–68, (1981). [DOI], [ADS].
- [231] Moyer, T.D., *Formulation for Observed and Computed Values of Deep Space Network Data Types for Navigation*, JPL Deep-Space Communications and Navigation Series, (John Wiley & Sons, Inc., Hoboken, NJ, 2003).
- [232] Mudgway, D.J., *Uplink-Downlink: A History of the Deep Space Network*, vol. SP-2001-4227, (NASA, 2001).
- [233] Muhleman, D.O., and Anderson, J.D., “Solar Wind Electron Densities From Viking Dual-Frequency Radio Measurements”, *Astrophys. J.*, **247**, 1093–1101, (1981).
- [234] Muhleman, D.O., Esposito, P.B., and Anderson, J.D., “The electron density profile of the outer corona and the interplanetary medium from Mariner-6 and Mariner-7 time-delay measurements”, *Astrophys. J.*, **211**, 943–957, (1977).
- [235] Munyaneza, F., and Viollier, R.D., “Heavy neutrino dark matter in the solar system”, arXiv e-print, (1999). [ADS], [astro-ph/9910566].
- [236] Murphy, E.M., “Prosaic Explanation for the Anomalous Accelerations Seen in Distant Spacecraft”, *Phys. Rev. Lett.*, **83**, 1890, (1999). [ADS], [gr-qc/9810015].
- [237] Natarajan, A., and Sikivie, P., “Robustness of discrete flows and caustics in cold dark matter cosmology”, *Phys. Rev. D*, **72**, 083513, (2005). [DOI], [ADS], [astro-ph/0508049].
- [238] *National Launch Vehicle Summary*, (Aeronautics and Astronautics Coordinating Board, 1972).
- [239] Navarro, J.F., Frenk, C.S., and White, S.D.M., “A Universal Density Profile from Hierarchical Clustering”, *Astrophys. J.*, **490**, 493, (1997). [DOI], [ADS], [astro-ph/9611107].
- [240] Nevarez, R.E., *Pioneer 10 Through 12 Support*, TDA Progress Report, 42-58, (JPL, Pasadena, CA, 1980). Related online version (cited on 19 May 2010): http://ipnpr.jpl.nasa.gov/progress_report/42-58/58title.htm.
- [241] Nevarez, R.E., *Pioneer 10 and 11 Mission Support*, TDA Progress Report, 42-61, (JPL, Pasadena, CA, 1981). Related online version (cited on 19 May 2010): http://ipnpr.jpl.nasa.gov/progress_report/42-61/61title.htm.
- [242] Nevarez, R.E., *Pioneers 6 Through 12 Mission Support*, TDA Progress Report, 42-63, (JPL, Pasadena, CA, 1981). Related online version (cited on 19 May 2010): http://ipnpr.jpl.nasa.gov/progress_report/42-63/63title.htm.

- [243] Nevarez, R.E., *Pioneers 6 Through 12 Mission Support*, TDA Progress Report, 42-65, (JPL, Pasadena, CA, 1981). Related online version (cited on 19 May 2010): http://ipnpr.jpl.nasa.gov/progress_report/42-65/65title.htm.
- [244] Newhall, X.X., Standish, E.M., and Williams, J.G., “DE 102: A numerically integrated ephemeris of the Moon and planets spanning forty-four centuries”, *Astron. Astrophys.*, **125**, 150, (1983).
- [245] Nieto, M.M., “Analytic gravitational-force calculations for models of the Kuiper Belt, with application to the Pioneer anomaly”, *Phys. Rev. D*, **72**, 083004, (2005). [DOI], [ADS], [astro-ph/0506281].
- [246] Nieto, M.M., “New Horizons and the onset of the Pioneer anomaly”, *Phys. Lett. B*, **659**, 483–485, (2008). [DOI], [ADS], [arXiv:0710.5135].
- [247] Nieto, M.M., and Anderson, J.D., “Using early data to illuminate the Pioneer anomaly”, *Class. Quantum Grav.*, **22**, 5343–5354, (2005). [DOI], [ADS], [gr-qc/0507052].
- [248] Nieto, M.M., and Anderson, J.D., “Search for a Solution of the Pioneer Anomaly”, *Contemp. Phys.*, **48**, 41–54, (2007). [DOI], [arXiv:0709.3866 [gr-qc]].
- [249] Nieto, M.M., and Anderson, J.D., “Seeking a solution of the Pioneer Anomaly”, arXiv e-print, (2007). [ADS], [arXiv:0709.1917 [gr-qc]].
- [250] Nieto, M.M., and Anderson, J.D., “Earth Flyby Anomalies”, *Phys. Today*, **62N10**, 76–77, (2009). [arXiv:0910.1321 [gr-qc]].
- [251] Nieto, M.M., Anderson, J.D., Laing, P.A., Lau, E.L., and Turyshev, S.G., “The Anomalous Trajectories of the Pioneer Spacecraft”, arXiv e-print, (2001). [ADS], [hep-ph/0110373].
- [252] Nieto, M.M., and Turyshev, S.G., “Finding the origin of the Pioneer anomaly”, *Class. Quantum Grav.*, **21**, 4005–4023, (2004). [DOI], [ADS], [gr-qc/0308017].
- [253] Nieto, M.M., and Turyshev, S.G., “Measuring the Interplanetary Medium with a Solar Sail”, *Int. J. Mod. Phys. D*, **13**, 899–906, (2004). [DOI], [arXiv:astro-ph/0308108].
- [254] Nieto, M.M., Turyshev, S.G., and Anderson, J.D., “Directly measured limit on the interplanetary matter density from Pioneer 10 and 11”, *Phys. Lett. B*, **613**, 11–19, (2005). [DOI], [ADS], [astro-ph/0501626].
- [255] Nieto, M.M., Turyshev, S.G., and Anderson, J.D., “The Pioneer Anomaly: The Data, its Meaning, and a Future Test”, in Macias, A., Lämmerzahl, C., and Nunez, D., eds., *Gravitation and Cosmology*, AIP Conf. Proc., vol. 758, pp. 113–128, (American Institute of Physics, Melville, NJ, 2005). [DOI], [ADS].
- [256] Nordtvedt, K., “Equivalence Principle for Massive Bodies. I. Phenomenology”, *Phys. Rev.*, **169**, 1014–1016, (1968). [DOI], [ADS].
- [257] Nordtvedt, K., “Equivalence Principle for Massive Bodies. II. Theory”, *Phys. Rev.*, **169**, 1017–1025, (1968). [DOI].
- [258] Nordtvedt, K., “Equivalence principle for massive bodies including rotational energy and radiation pressure”, *Phys. Rev.*, **180**, 1293–1298, (1969). [ADS].
- [259] Nordtvedt, K.J., and Will, C.M., “Conservation Laws and Preferred Frames in Relativistic Gravity. II. Experimental Evidence to Rule Out Preferred-Frame Theories of Gravity”, *Astrophys. J.*, **177**, 775, (1972). [ADS].

- [260] Nottale, L., “The Pioneer anomalous acceleration: a measurement of the cosmological constant at the scale of the solar system”, arXiv e-print, (2003). [arXiv:gr-qc/0307042].
- [261] Null, G.W., “Gravity field of Jupiter and its satellite from Pioneer 10 and Pioneer 11 tracking data”, *Astron. J.*, **81**, 1153–1161, (1976). [ADS].
- [262] Null, G.W., Lau, E.L., Biller, E.D., and Anderson, J.D., “Saturn gravity results obtained from Pioneer 11 tracking data and Earth-based Saturn satellite data”, *Astron. J.*, **86**, 456, (1981).
- [263] Nyambuya, G.G., “On a Possible Gravitational Origin of the Pioneer Anomaly”, arXiv e-print, (2008). [arXiv:0803.1370 [physics.gen-ph]].
- [264] Office of Space Science and Applications, *The Pioneer Mission to Jupiter*, SP-268, (NASA, Washington, DC, 1971). Related online version (cited on 27 May 2010): <http://hdl.handle.net/2060/19710022890>.
- [265] Oliveira, F.J., “Is the Pioneer Anomaly a Counter Example to the Dark Matter Hypothesis?”, *Int. J. Theor. Phys.*, **46**, 3193–3200, (2007). [DOI], [ADS], [gr-qc/0610029].
- [266] Olsen, Ø., “The constancy of the Pioneer anomalous acceleration”, *Astron. Astrophys.*, **463**, 393–397, (2007). [DOI], [ADS].
- [267] O’Reilly, B.D., and Chao, C.C., *An Evaluation of QVLBI OD Analysis of Pioneer 10 Encounter Data in the Presence of Unmodeled Satellite Accelerations*, DSN Progress Report, 42-22, (JPL, Pasadena, CA, 1974). Related online version (cited on 19 May 2010): http://ipnpr.jpl.nasa.gov/progress_report2/42-22/22title.htm.
- [268] Ostvang, D., “An explanation of the ‘Pioneer effect’ based on quasi- metric relativity”, *Class. Quantum Grav.*, **19**, 4131–4140, (2002). [DOI], [arXiv:gr-qc/9910054].
- [269] Page, G.L., Dixon, D.S., and Wallin, J.F., “Can Minor Planets Be Used to Assess Gravity in the Outer Solar System?”, *Astrophys. J.*, **642**, 606–614, (2006). [DOI], [ADS], [astro-ph/0504367].
- [270] Page, G.L., Wallin, J.F., and Dixon, D.S., “Minor Planets as a Probe of the Gravitational Field in the Outer Solar System”, *Bull. Am. Astron. Soc.*, **37**, 1414, (2005). [ADS].
- [271] Peacock, J.A., Cole, S., Norberg, P., Baugh, C.M., Bland-Hawthorn, J., Bridges, T., Cannon, R.D., Colless, M., Collins, C., Couch, W., Dalton, G., Deeley, K., Proprius, R.D., Driver, S.P., Efstathiou, G., Ellis, R.S., Frenk, C.S., Glazebrook, K., Jackson, C., Lahav, O., Lewis, I., Lumsden, S., Maddox, S., Percival, W.J., Peterson, B.A., Price, I., Sutherland, W., and Taylor, K., “A measurement of the cosmological mass density from clustering in the 2dF galaxy redshift survey”, *Nature*, **410**, 169–173, (2001). [astro-ph/0103143].
- [272] Perlmutter, S., Aldering, G., della Valle, M., Deustua, S., Ellis, R.S., Fabbro, S., Fruchter, A., Goldhaber, G., Groom, D.E., Hook, I.M., Kim, A.G., Kim, M.Y., Knop, R.A., Lidman, C., McMahon, R.G., Nugent, P., Pain, R., Panagia, N., Pennypacker, C.R., Ruiz-Lapuente, P., Schaefer, B., and Walton, N., “Discovery of a supernova explosion at half the age of the universe”, *Nature*, **391**, 51, (1998). [DOI], [ADS], [astro-ph/9712212].
- [273] Pham, T.T., Simon, M.K., Peng, T.K., Brockman, M.H., Kent, S.S., and Weller, R., *A Carrier-Arraying Demonstration at Goldstone for Receiving Pioneer 11 Signals*, TDA Progress Report, 42-106, (JPL, Pasadena, CA, 1991). Related online version (cited on 19 May 2010): http://ipnpr.jpl.nasa.gov/progress_report/42-106/106title.htm.

- [274] “Pioneer 10 Sequence of Events”, unknown format, (1972). Documentation fragment recovered by Kellogg, L.R.
- [275] *Pioneer 10 Sigma 5 On-line Data Processing System (SOLDPS)*, BFEC/ARC-061, (Bendix Field Engineering Corporation, 1975).
- [276] *Pioneer 11: First to Saturn*, (BENDIX Field Engineering Corporation, Sunnyvale, CA, 1979).
- [277] *Pioneer 6-11 Project: Network Operations Plan*, DSN Doc. No. 616-55 Rev.-C. Issue date: Feb. 18, 1994, JPL Doc. # D-10579 Rev. C, (JPL, Pasadena, CA, 1994).
- [278] *Pioneer F & G Spacecraft/RTG Reentry Breakup Study*, 12356-6001-R0-00, (NASA, 1970). Related online version (cited on 27 May 2010):
<http://hdl.handle.net/2060/19800072741>.
- [279] *Pioneer F/G Thermal Control Subsystem Design Review Number 3*, (1971).
- [280] *Pioneer: First to Jupiter, Saturn and Beyond. Bibliography*, (Ames Research Center, Moffett Field, CA, 1980).
- [281] *Pioneer H Jupiter Swingby Out-of-the-Ecliptic Mission Study: Final Report*, NASA-TM-108108, (Ames Research Center, Moffett Field, CA, 1971). Related online version (cited on 3 June 2010):
<http://hdl.handle.net/2060/19930073120>.
- [282] “Pioneer Missions Pioneer 10/11 PSG Meeting”, (June 1990).
- [283] “Pioneer Missions Pioneer 10/11 PSG Meeting”, (June 1993).
- [284] “Pioneer Missions Pioneer 10/11 PSG Meeting”, (March 1994).
- [285] “Pioneer Missions Pioneer 10/11 PSG Meeting”, (December 1994).
- [286] “Pioneer Missions Pioneer PSG Meeting”, (June 1996).
- [287] “Pioneer Missions PSG Meeting”, (June 1988).
- [288] “Pioneer Missions Quarterly Review”, (May 1987).
- [289] *Pioneer Program Pioneer F/G: EGSE Computer Programming Specifications for Scientific Instruments*, PC-260, (Ames Research Center, 1972).
- [290] *Pioneer Program Pioneer F/G: GOE/DSN Interface*, PC-224, (Ames Research Center, 1971).
- [291] *Pioneer Program Pioneer F/G: On-line Ground Data System Software Specification*, PC-261, (Ames Research Center, 1970).
- [292] *Pioneer Program Pioneer F/G: Spacecraft Operational Characteristics*, PC-202, (Ames Research Center, Moffett Field, CA, 1971).
- [293] *Pioneer Program Pioneer F/G: Spacecraft Scientific Instruments*, PC-220, (Ames Research Center, Moffett Field, CA, 1970).
- [294] *Pioneer Program Pioneer F/G Spacecraft/RTG Interface*, PC-223, (Ames Research Center, Moffett Field, CA).
- [295] *Pioneer Project Flights F and G Final Report*, PFG. 100.151, (1973).

- [296] “Pioneer Project PSG”, (December 1995).
- [297] *Pioneer Saturn Encounter*, (Ames Research Center, Moffett Field, CA, 1979).
- [298] *Pioneer to Jupiter: A History*, (TRW Corporation, 1973).
- [299] “Pioneer/Jupiter Newsletter”, (1972–1974).
- [300] “Pioneer/Jupiter Status Bulletin”, (1973–1974).
- [301] Plamondon, J.A., *Analysis Of Movable Louvers For Temperature Control*, JPL Technical Report, No. 32-555, (1964).
- [302] Press, W.H., and Spergel, D.N., “Capture by the sun of a galactic population of weakly interacting, massive particles”, *Astrophys. J.*, **296**, 679–684, (1985). [DOI], [ADS].
- [303] Rañada, A. F., “The Pioneer riddle, the quantum vacuum and the variation of the light velocity”, *Europhys. Lett.*, **63**, 653–659, (2003). [DOI], [ADS], [gr-qc/0211052].
- [304] Rañada, A. F., “The Pioneer anomaly as acceleration of the clocks”, *Found. Phys.*, **34**, 1955–1971, (2005). [DOI], [arXiv:gr-qc/0410084].
- [305] Rañada, A.F., and Tiemblo, A., “Time, Clocks and Parametric Invariance”, *Foundations of Physics*, **38**, 458–469, (2008). [DOI], [ADS].
- [306] Randall, L., and Sundrum, R., “Large Mass Hierarchy from a Small Extra Dimension”, *Phys. Rev. Lett.*, **83**, 3370–3373, (1999). [DOI].
- [307] Rathke, A., “Testing for the Pioneer anomaly on a Pluto exploration mission”, arXiv e-print, (2004). [astro-ph/0409373].
- [308] Rathke, A., and Izzo, D., “Options for a Nondedicated Mission to Test the Pioneer Anomaly”, *J. Spacecraft and Rockets*, **43**, 806–821, (2006). [DOI], [ADS], [astro-ph/0504634].
- [309] Reid, M.S., and Gardner, R.A., *System Noise Temperature Calibrations of the Research and Development Systems at DSS 14*, JPL Technical Report 32-1526, vol. XIX, (Pasadena, CA, 1974). Related online version (cited on 3 June 2010):
http://ipnpr.jpl.nasa.gov/progress_report2/XIX/XIXtitle.htm.
- [310] *Release Change Description: DSN 1200-bit & 4800-bit Data Block Header Formats*, RCD 020, (1992).
- [311] Renzetti, N.A., ed., *TDA Progress Report*, TDA Progress Report, (JPL, Pasadena, CA, 1981).
- [312] Renzetti, N.A., Stelzried, C.T., Noreen, G.K., Slobin, S.D., Petty, S.M., Trowbridge, D.L., Donnelly, H., Kinman, P.W., Armstrong, J.W., Burow, N.A., Tam, M.K., Layland, J.W., and Berman, A.L., *The Deep Space Network – A Radio Communications Instrument for Deep Space Exploration*, 82-104, (JPL, 1983). [ADS]. Related online version (cited on 19 May 2010):
<http://hdl.handle.net/2060/19830028031>.
- [313] Reynaud, S., and Jaekel, M.-T., “Long range gravity tests and the Pioneer anomaly”, *Int. J. Mod. Phys. D*, **16**, 2091–2105, (2007). [DOI], [arXiv:gr-qc/0610160].

- [314] Riess, A.G., Filippenko, A.V., Challis, P., Clocchiatti, A., Diercks, A., Garnavich, P.M., Gilliland, R.L., Hogan, C.J., Jha, S., Kirshner, R., Leibundgut, B., Phillips, M., Reiss, D., Schmidt, B.P., Schommer, R.A., Smith, R.C., Spyromilio, J., Stubbs, C., Suntzeff, N.B., and Tonry, J., “Observational Evidence from Supernovae for an Accelerating Universe and a Cosmological Constant”, *Astron. J.*, **116**, 1009–1038, (1998).
- [315] Rievers, B., Bremer, S., List, M., Lämmerzahl, C., and Dittus, H., “Thermal dissipation force modeling with preliminary results for Pioneer 10/11”, *Acta Astronautica*, **66**(3–4), 467–476, (2010). [DOI].
- [316] Rievers, B., Lämmerzahl, C., List, M., Bremer, S., and Dittus, H., “New powerful thermal modelling for high-precision gravity missions with application to Pioneer 10/11”, *New J. Phys.*, **11**, 113032, (2009). [DOI]. URL (cited on 19 May 2010): <http://stacks.iop.org/1367-2630/11/i=11/a=113032>.
- [317] Rockwell, G.M., *Pioneer 11 Saturn Encounter Support*, DSN Progress Report, 42-53, (JPL, Pasadena, CA, 1979). Related online version (cited on 19 May 2010): http://ipnpr.jpl.nasa.gov/progress_report2/42-53/53title.htm.
- [318] Rockwell, G.M., *Pioneer Mission Support*, DSN Progress Report, 42-55, (JPL, Pasadena, CA, 1980). Related online version (cited on 19 May 2010): http://ipnpr.jpl.nasa.gov/progress_report2/42-55/55title.htm.
- [319] Rosales, J. L., “The Pioneer’s Anomalous Doppler Drift as a Berry Phase”, arXiv e-print, (2004). [arXiv:gr-qc/0401014].
- [320] Rosales, J.L., “The Pioneer Anomaly: the measure of a topological phase defect of light in cosmology”, in Favata, F., Sanz-Forcada, J., Giménez, A., and Battrick, B., eds., *39th ESLAB Symposium on Trends in Space Science and Cosmic Vision 2020*, 19–21 April 2005, Noordwijk, The Netherlands, ESA Special Publications, vol. SP-588, p. 263, (2005). [ADS].
- [321] Rosales, J.L., and Sánchez-Gómez, J.-L., “A possible cosmological origin of the indicated anomalous acceleration in Pioneer 10/11 orbital data analysis”, arXiv e-print, (1998). [arXiv:gr-qc/9810085v2].
- [322] Rosborough, G.W., and Antreasian, P.G., “Radiation force modeling for the Topex/Poseidon spacecraft”, in *AIAA/AAS Astrodynamics Conference, Portland, OR, August 20–22, 1990, Technical Papers, Part 1*, (AIAA, Washington, DC, 1990).
- [323] Rubakov, V.A., and Tinyakov, P.G., “Infrared-modified gravities and massive gravitons”, *Usp. Fiz. Nauk*, **178**(8), 785–822, (2008). [arXiv:0802.4379 [hep-th]].
- [324] Saffari, R., and Rahvar, S., “ $f(R)$ gravity: From the Pioneer anomaly to cosmic acceleration”, *Phys. Rev. D*, **77**, 104028, (2008). [DOI], [ADS], [arXiv:0708.1482].
- [325] Sanders, R. H., “Modified Gravity Without Dark Matter”, in Papantonopoulos, L., ed., *The Invisible Universe: Dark Matter and Dark Energy*, Lecture Notes in Physics, vol. 720, p. 375, (Springer, Berlin; New York, 2007). [ADS].
- [326] Sanders, R.H., “Anti-gravity and galaxy rotation curves”, *Astron. Astrophys.*, **136**, L21–L23, (1984). [ADS].
- [327] Sanders, R.H., “Solar system constraints on multifield theories of modified dynamics”, *Mon. Not. R. Astron. Soc.*, **370**, 1519–1528, (2006). [DOI], [ADS], [astro-ph/0602161].

- [328] Schär, S., *Mapping and Predicting the Earth's Ionosphere Using the Global Positioning System*, Ph.D. Thesis, (University of Bern, Bern, 1999).
- [329] Scheffer, L.K., “A Conventional Physics Explanation for the Anomalous Acceleration of Pioneer 10/11”, arXiv e-print, (2001). [ADS], [gr-qc/0108054].
- [330] Scheffer, L.K., “Support for a prosaic explanation for the anomalous acceleration of Pioneer 10 and 11”, arXiv e-print, (2001). [arXiv:gr-qc/0106010].
- [331] Scheffer, L.K., “Conventional forces can explain the anomalous acceleration of Pioneer 10”, *Phys. Rev. D*, **67**, 084021, (2003). [ADS], [gr-qc/0107092].
- [332] Scheffer, L.K., “Pioneer Thermal Questions”, First Pioneer Explorer Collaboration meeting at ISSI, Bern, Switzerland, November 7–11, 2005, conference paper, (2005).
- [333] Scheffer, L.K., “The Spin of Pioneer 10/11, with implications for the Pioneer Anomaly”, conference paper, (2008). Third Pioneer Explorer Collaboration meeting at ISSI, Bern, Switzerland, February 18–22, 2008.
- [334] Schüller, T., *On Ground-Based GPS Tropospheric Delay Estimation*, Ph.D. Thesis, (Universität der Bundeswehr, Munich, 2001).
- [335] Seidelmann, P.K., ed., *Explanatory Supplement to the Astronomical Almanac*, (University Science Books, Mill Valley, CA, 1992).
- [336] Sereno, M., and Jetzer, P., “Solar and stellar system tests of the cosmological constant”, *Phys. Rev. D*, **73**, 063004, (2006). [DOI], [ADS], [astro-ph/0602438].
- [337] Sidharth, B.G., “Effects of varying G ”, *Nuovo Cimento B*, **115**, 151–154, (2000). [ADS], [astro-ph/9904088].
- [338] Siegmeth, A.J., *Pioneer Mission Support*, JPL Technical Report 32-1526, (1971). Related online version (cited on 3 June 2010):
http://ipnpr.jpl.nasa.gov/progress_report2/V/Vtitle.htm.
- [339] Siegmeth, A.J., *Pioneer Mission Support*, JPL Technical Report 32-1526, vol. III, (1971). Related online version (cited on 3 June 2010):
http://ipnpr.jpl.nasa.gov/progress_report2/III/IIItitle.htm.
- [340] Siegmeth, A.J., *Pioneer Mission Support*, JPL Technical Report 32-1526, vol. IV, (1971). Related online version (cited on 3 June 2010):
http://ipnpr.jpl.nasa.gov/progress_report2/IV/IVtitle.htm.
- [341] Siegmeth, A.J., *Pioneer Mission Support*, JPL Technical Report 32-1526, vol. II, (1971). Related online version (cited on 3 June 2010):
http://ipnpr.jpl.nasa.gov/progress_report2/II/IItitle.htm.
- [342] Siegmeth, A.J., *Pioneer Mission Support*, JPL Technical Report 32-1526, vol. VI, (1971). Related online version (cited on 3 June 2010):
http://ipnpr.jpl.nasa.gov/progress_report2/VI/VItitle.htm.
- [343] Siegmeth, A.J., *Pioneer 10 and G Mission Support*, JPL Technical Report 32-1526, vol. XI, (1972). Related online version (cited on 3 June 2010):
http://ipnpr.jpl.nasa.gov/progress_report2/XI/XItitle.htm.

- [344] Siegmeth, A.J., *Pioneer 10 and G Mission Support*, JPL Technical Report 32-1526, vol. X, (1972). Related online version (cited on 3 June 2010):
http://ipnpr.jpl.nasa.gov/progress_report2/X/Xtitle.htm.
- [345] Siegmeth, A.J., *Pioneer 6-9 Mission Support*, JPL Technical Report 32-1526, vol. X, (1972). Related online version (cited on 3 June 2010):
http://ipnpr.jpl.nasa.gov/progress_report2/X/Xtitle.htm.
- [346] Siegmeth, A.J., *Pioneer 6-9 Mission Support*, JPL Technical Report 32-1526, vol. XI, (1972). Related online version (cited on 3 June 2010):
http://ipnpr.jpl.nasa.gov/progress_report2/XI/XItitle.htm.
- [347] Siegmeth, A.J., *Pioneer Mission Support*, JPL Technical Report 32-1526, vol. VII, (1972). Related online version (cited on 3 June 2010):
http://ipnpr.jpl.nasa.gov/progress_report2/VII/VIItitle.htm.
- [348] Siegmeth, A.J., *Pioneer Mission Support*, JPL Technical Report 32-1526, vol. VIII, (1972). Related online version (cited on 3 June 2010):
http://ipnpr.jpl.nasa.gov/progress_report2/VIII/VIIItitle.htm.
- [349] Siegmeth, A.J., *Pioneer Mission Support*, JPL Technical Report 32-1526, vol. IX, (1972). Related online version (cited on 3 June 2010):
http://ipnpr.jpl.nasa.gov/progress_report2/IX/IXtitle.htm.
- [350] Sikivie, P., “Caustic rings of dark matter”, *Phys. Lett. B*, **432**, 139–144, (1998). [DOI], [ADS], [astro-ph/9705038].
- [351] Simon, H.S., *Mariner Mars 1971/Pioneer 10 Multi-Mission Level Modeling Runs Using the SFOF Mark IIIA Central Processing System Model*, JPL Technical Report 32-1526, vol. IX, (1972). Related online version (cited on 3 June 2010):
http://ipnpr.jpl.nasa.gov/progress_report2/IX/IXtitle.htm.
- [352] Simon, M.K., *Bandwidth-Efficient Digital Modulation with Application to Deep-Space Communications*, Deep Space Communications and Navigation Series, vol. 3, (JPL, Pasadena, 2001). URL (cited on 20 May 2010):
http://descanso.jpl.nasa.gov/Monograph/series3_chapter.cfm.
- [353] Smith, M.A., and Dyer, J.W., “Long term prediction of roll phase for an undisturbed spinning spacecraft”, Reno, NV, January 12–15, 1987, conference paper, (1987).
- [354] *SNAP 19 Pioneer F & G Final Report*, Teledyne report IESD 2873-172, Technical report no. DOE/ET/13512-T1; DE85017964, gov. doc. #E 1.9, (Teledyne Isotopes Energy Systems Division, 1973).
- [355] Sotiriou, T.P., and Faraoni, V., “ $f(R)$ Theories Of Gravity”, arXiv e-print, (2008). [arXiv:0805.1726 [gr-qc]].
- [356] Sovers, O.J., Fanselow, J.L., and Jacobs, C.S., “Astrometry and geodesy with radio interferometry: experiments, models, results”, *Rev. Mod. Phys.*, **70**, 1393–1454, (1998). [DOI], [ADS], [astro-ph/9712238].
- [357] Sovers, O.J., and Jacobs, C.S., “Observation Model and Parameter Partial for the JPL VLBI Parameter Estimation Software ‘MODEST’-1996 (Rev. 6)” (83–39), (1996).
- [358] *Space Pioneers: And Where They Are Now*, EP-264, (Ames Research Center, Moffett Field, CA, 1987).

- [359] Spergel, D.N., Bean, R., Doré, O., Nolta, M.R., Bennett, C.L., Dunkley, J., Hinshaw, G., Jarosik, N., Komatsu, E., Page, L., Peiris, H.V., Verde, L., Halpern, M., Hill, R.S., Kogut, A., Limon, M., Meyer, S.S., Odegard, N., Tucker, G.S., Weiland, J.L., Wollack, E., and Wright, E.L., “Wilkinson Microwave Anisotropy Probe (WMAP) three year results: Implications for cosmology”, *Astrophys. J. Suppl.*, **170**, 377, (2007). [DOI], [arXiv:astro-ph/0603449].
- [360] Spradlin, G.L., *DSN Tracking System Mark III-1979*, DSN Progress Report, 42-56, (1980). Related online version (cited on 19 May 2010):
http://ipnpr.jpl.nasa.gov/progress_report2/42-56/56title.htm.
- [361] Standish, E.M., “Planetary and Lunar Ephemerides: testing alternate gravitational theories”, in Macias, A., Lämmerzahl, C., and Camacho, A., eds., *Recent Developments in Gravitation and Cosmology*, AIP Conf. Proc., vol. 977, pp. 254–263, (American Institute of Physics, Melville, NJ, 2008). [DOI], [ADS].
- [362] Standish, E.M., “Testing alternate gravitational theories”, in Klioner, S.A., Seidelmann, P.K., and Soffel, M.H., eds., *Relativity in Fundamental Astronomy: Dynamics, Reference Frames, and Data Analysis*, Proceedings IAU Symposium No. 261, 22 April–1 May 2009, Virginia Beach, VA, USA, Proc. IAU, vol. 261, pp. 179–182. Cambridge University Press, (2010). [DOI], [ADS].
- [363] Standish, E.M., Newhall, X.X., Williams, J.G., and Yeomans, D.K., “Orbital Ephemerides of the Sun, Moon, and Planets”, Explanatory Supplement to the Astronomical Almanac, pp. 279–323, (University Science Books, Mill Valley, 1992).
- [364] Standish, E.M., and Williams, J.G., “Orbital Ephemerides of the Sun, Moon, and Planets”, unknown status, (2007). Related online version (cited on 19 May 2010):
<http://iau-comm4.jpl.nasa.gov/XSChap8.pdf>.
- [365] Standish Jr, E.M., “Conversion of positions and proper motions from B1950.0 to the IAU system at J2000.0”, *Astron. Astrophys.*, **115**, 20–22, (1982). [ADS].
- [366] Stein, C.K., *DSN System Testing: A Critical Review of the Pioneer 10 Test Program*, JPL Technical Report 32-1526, vol. X, (1972). Related online version (cited on 3 June 2010):
http://ipnpr.jpl.nasa.gov/progress_report2/X/Xtitle.htm.
- [367] Stern, S.A., “Signatures of collisions in the Kuiper Disk”, *Astron. Astrophys.*, **310**, 999–1010, (1996). [ADS].
- [368] Stimpson, L.D., and Jaworski, W., “Effects of Overlaps, Stitches, and Patches on Multilayer Insulation”, AIAA 7th Thermophysics Conference, conference paper, (1972).
- [369] Stochl, R.J., *Basic performance of a multilayer insulation system containing 20 to 160 layers*, NASA Technical Notes, NASA TN D-7659, (1974). Related online version (cited on 25 May 2010):
<http://hdl.handle.net/2060/19740014296>.
- [370] *Study of Pioneer Missions to Jupiter, Final Report, Volume 1*, 11339-6003-R0-00, (NASA, Redondo Beach, CA, 1968). Related online version (cited on 26 May 2010):
<http://hdl.handle.net/2060/19690010484>.
- [371] Sundrum, R., “Towards an effective particle-string resolution of the cosmological constant problem”, *JHEP*, **07**, 001, (1999). [hep-ph/9708329].

- [372] Sutton, G.P., *Rocket Propulsion Elements: An Introduction to the Engineering of Rockets*, (Wiley, New York, 1992), 6th edition.
- [373] Tangen, K., “Could the Pioneer anomaly have a gravitational origin?”, *Phys. Rev. D*, **76**, 042005, (2007). [DOI], [ADS], [gr-qc/0602089].
- [374] *Telemetry Calibration Data for Pioneer F*, BFEC/ARC-037, (BENDIX Field Engineering Corporation, 1972).
- [375] Teplitz, V.L., Stern, S.A., Anderson, J.D., Rosenbaum, D., Scalise, R.J., and Wentzler, P., “Infrared Kuiper Belt Constraints”, *Astrophys. J.*, **516**, 425–435, (1999). [DOI], [ADS], [astro-ph/9807207].
- [376] Teren, F., *Analysis of broken plane trajectories for the Pioneer-F mission*, NASA Technical Memorandum, TM X-2024, (1970).
- [377] *The Need for Space Flight Opportunities in Fundamental Physics*, EPS Position Paper, (2005).
- [378] Thorne, K.S., and Will, C.M., “Theoretical Frameworks for Testing Relativistic Gravity. I. Foundations”, *Astrophys. J.*, **163**, 595, (1971). [ADS].
- [379] Thornton, C.L., and Border, J.S., *Radiometric Tracking Techniques for Deep-Space Navigation*, Deep Space Communications and Navigation Series, vol. 1, (JPL, Pasadena, 2000). URL (cited on 20 May 2010): http://descanso.jpl.nasa.gov/Monograph/series1_section.cfm.
- [380] Tortora, P., Graziani, A., and Melloni, S., “Doppler analysis capabilities in Bologna”, Second Pioneer Explorer Collaboration meeting at ISSI, Bern, Switzerland, February 19–23, 2007, conference paper, (2007).
- [381] Toth, V.T., “Pioneer spacecraft thermal analysis”, Second Pioneer Explorer Collaboration meeting at ISSI, Bern, Switzerland, February 19–23, 2007, conference paper, (2007).
- [382] Toth, V.T., “Independent analysis of the orbits of Pioneer 10 and 11”, *Int. J. Mod. Phys. D*, **18**, 717, (2009). [DOI], [arXiv: 0901.3466 [physics.space-ph]].
- [383] Toth, V.T., and Turyshev, S.G., “The Pioneer anomaly: seeking an explanation in newly recovered data”, *Can. J. Phys.*, **84**, 1063–1087, (2006). [ADS], [gr-qc/0603016].
- [384] Toth, V.T., and Turyshev, S.G., “Pioneer Anomaly: Evaluating Newly Recovered Data”, in Macías, A., Lämmerzahl, C., and Camacho, A., eds., *Recent Development in Gravitation and Cosmology*, 3rd Mexican Meeting on Mathematical and Experimental Physics, Mexico City, Mexico, 10–14 September 2007, AIP Conf. Proc., vol. 977, pp. 264–283, (American Institute of Physics, Melville, NJ, 2008). [DOI], [ADS], [arXiv:0710.2656 [gr-qc]].
- [385] Toth, V.T., and Turyshev, S.G., “Thermal recoil force, telemetry, and the Pioneer anomaly”, *Phys. Rev. D*, **79**, 043011, (2009). [DOI].
- [386] Trencovski, K., “Time dependent gravitational potential in the universe and some consequences”, *Gen. Relativ. Gravit.*, **37**, 507, (2005). [DOI].
- [387] *Troposphere Model*, IERS Technical Note, No. 32, (IERS, 1999).
- [388] Turyshev, S.G., *Relativistic Navigation: A Theoretical Foundation*, NASA JPL Publication, 96-13, (JPL, Pasadena, CA, 1996). [gr-qc/9606063].

- [389] Turyshev, S.G., “Experimental Tests of General Relativity”, *Annu. Rev. Nucl. Part. Sci.*, **58**, 207–248, (2008). [arXiv:0806.1731 [gr-qc]].
- [390] Turyshev, S.G., “Experimental Tests of General Relativity: Recent Progress and Future Directions”, *Usp. Fiz. Nauk*, **179**, 3–34, (2009). [DOI], [arXiv:0809.3730 [gr-qc]].
- [391] Turyshev, S.G., Anderson, J.D., Laing, P.A., Lau, E.L., Liu, A.S., and Nieto, M.M., “The Apparent Anomalous, Weak, Long-Range Acceleration of Pioneer 10 and 11”, in Dumarchez, J., and Trần Than Vân, J., eds., *Gravitational Waves and Experimental Gravity*, Proceedings of the XXXIVth Rencontres de Moriond, Les Arcs, France, January 23–30, 1999, pp. 481–486, (World Publishers, Hanoi, Vietnam, 2000). [ADS], [gr-qc/9903024].
- [392] Turyshev, S.G., Israelsson, U.E., Shao, M., N.Y., Kusenko, A., Wright, E.L., Franci, C.W., Everitt, Kasevich, M., Lipa, J.A., Mester, J.C., Reasenberg, R.D., Walsworth, R.L., Ashby, N., Gould, H., and Paik, H.J., “Space-based research in fundamental physics and quantum technologies”, *Int. J. Mod. Phys. D*, **16**, 1879–1925, (2007). [arXiv:0711.0150 [gr-qc]].
- [393] Turyshev, S.G., Nieto, M.M., and Anderson, J.D., “A Route to Understanding of the Pioneer Anomaly”, in Chen, P., Bloom, E., Madejski, G., and Petrosian, V., eds., *Proceedings of the 22nd Texas Symposium on Relativistic Astrophysics*, Stanford, CA, December 13–17 2004, vol. econf C041213. Stanford University, (2004). [ADS], [gr-qc/0503021] Related online version: <http://www.slac.stanford.edu/econf/C041213/>.
- [394] Turyshev, S.G., Nieto, M.M., and Anderson, J.D., “Study of the Pioneer anomaly: a problem set”, *Am. J. Phys.*, **73**, 1033–1044, (2005). [DOI], [arXiv:physics/0502123].
- [395] Turyshev, S.G., Nieto, M.M., and Anderson, J.D., “The Pioneer anomaly and its implications”, in Mamon, G.A., Combes, F., Deffayet, C., and Fort, B., eds., *Mass Profiles and Shapes of Cosmological Structures*, 21st IAP Colloquium, Institut d’Astrophysique de Paris, France, July 4–9, 2005, EAS Publications Series, vol. 20, pp. 243–250, (2006). [DOI], [arXiv:gr-qc/0510081].
- [396] Turyshev, S.G., Nieto, M.M., and Anderson, J.D., “Lessons learned from the Pioneers 10/11 for a mission to test the Pioneer anomaly”, *Adv. Space Res.*, **39**, 291–296, (2007). [DOI], [ADS], [gr-qc/0409117].
- [397] Turyshev, S.G., and Toth, V.T., “Physics Engineering in the Study of the Pioneer Anomaly”, arXiv e-print, (2007). [ADS], [arXiv:0710.0191 [physics.space-ph]].
- [398] Turyshev, S.G., and Toth, V.T., “The Puzzle of the Flyby Anomaly”, *Space Science Reviews*, (2009). [DOI], [arXiv:0907.4184 [gr-qc]].
- [399] Turyshev, S.G., Toth, V.T., Kellogg, L.R., Lau, E.L., and Lee, K.J., “The study of the Pioneer anomaly: New data and objectives for new investigation”, *Int. J. Mod. Phys. D*, **15**, 1–56, (2006). [DOI], [ADS], [gr-qc/0512121].
- [400] Turyshev, S.G., Williams, J.G., Nordtvedt, K., Shao, M., and Murphy, T.W., “35 Years of Testing Relativistic Gravity: Where Do We Go from Here?”, in Karshenboim, S.G., and Peik, E., eds., *Astrophysics, Clocks and Fundamental Constants*, Lecture Notes in Physics, vol. 648, pp. 311–330, (Springer, Berlin; New York, 2004). [ADS], [gr-qc/0311039].
- [401] Turyshev, S.G. et al., *Proposal in Response to the ISSI Call for International Teams: Investigation of the Pioneer Anomaly at the ISSI*, (ISSI, Bern, 2005). Related online version (cited on 20 January 2010): <http://www.issibern.ch/teams/Pioneer/>.

- [402] *Type 66 File Format (Appendix B)*. Documentation fragment recovered by L.R. Kellogg.
- [403] *User's Guide for the VAXMDR Program*, ATSC/ARC-221, (AlliedSignal Technical Services Corporation, 1995).
- [404] Van Allen, J.A., *Geometrical Relationships of Pioneer 11 to Uranus and Voyager 2 in 1985-86*, (Dept. of Physics and Astronomy, University of Iowa, 1984). 84-07-12.
- [405] Van Allen, J.A., "Gravitational assist in celestial mechanics—a tutorial", *Amer. J. Phys.*, **71**, 448–451, (2003). [DOI], [ADS].
- [406] Vigue, Y., Schutz, B.E., and Abusali, P.A.M., "Thermal Force Modeling for Global Positioning System Satellites Using the Finite Element Method", *Journal of Spacecraft and Rockets*, **31**(5), 855–859, (1994).
- [407] Vilnrotter, V.A., Hurd, W.J., and Brown, D.H., *Optimized Tracking of RF Carriers With Phase Noise, Including Pioneer 10 Results*, TDA Progress Report, 42-91, (JPL, Pasadena, CA, 1987). Related online version (cited on 19 May 2010): http://ipnpr.jpl.nasa.gov/progress_report/42-91/91title.htm.
- [408] Wallin, J.F., Dixon, D.S., and Page, G.L., "Testing Gravity in the Outer Solar System: Results from Trans-Neptunian Objects", *Astrophys. J.*, **666**, 1296–1302, (2007). [DOI], [ADS], [arXiv:0705.3408].
- [409] Watola, D.A., *Adaptive Low-Bandwidth Tracking of Galileo and Pioneer 10 Carriers*, TDA Progress Report, 42-111, (JPL, Pasadena, CA, 1992). Related online version (cited on 19 May 2010): http://ipnpr.jpl.nasa.gov/progress_report/42-111/111title.htm.
- [410] Weeks, C.J., and Bowers, M.J., "Analytical Models of Doppler Data Signatures", *J. Guidance, Control, and Dynamics*, **18**(6), 1287–1291, (1995).
- [411] Wex, N., "Strong Gravity Clock Experiments", in Lämmerzahl, C., Everitt, C.W.F., and Hehl, F.W., eds., *Gyros, Clocks, Interferometers...: Testing Relativistic Gravity in Space*, Lecture Notes in Physics, vol. 562, pp. 381–399, (Springer, Berlin; New York, 2001). [DOI].
- [412] Wilkes, D.R., *Thermal Control Surfaces Experiment*, NASA/CR-1999-209008, (Marshall Space Flight Center, Huntsville, AL, 1999). Related online version (cited on 3 June 2010): <http://hdl.handle.net/2060/19990021250>.
- [413] Will, C.M., "Relativistic Gravity in the Solar System. I. Effect of an Anisotropic Gravitational Mass on the Earth-Moon Distance", *Astrophys. J.*, **165**, 409, (1971). [ADS].
- [414] Will, C.M., "Relativistic Gravity in the Solar System. II. Anisotropy in the Newtonian Gravitational Constant", *Astrophys. J.*, **169**, 141, (1971). [ADS].
- [415] Will, C.M., "Theoretical Frameworks for Testing Relativistic Gravity. II. Parametrized Post-Newtonian Hydrodynamics, and the Nordtvedt Effect", *Astrophys. J.*, **163**, 611, (1971). [ADS].
- [416] Will, C.M., "Theoretical Frameworks for Testing Relativistic Gravity. III. Conservation Laws, Lorentz Invariance, and Values of the PPN Parameters", *Astrophys. J.*, **169**, 125, (1971). [ADS].
- [417] Will, C.M., "Relativistic Gravity in the Solar System. III. Experimental Disproof of a Class of Linear Theories of Gravitation", *Astrophys. J.*, **185**, 31–42, (1973). [ADS].

- [418] Will, C.M., *Theory and Experiment in Gravitational Physics*, (Cambridge University Press, 1993), rev. edition.
- [419] Will, C.M., “The Confrontation between General Relativity and Experiment”, *Living Rev. Relativity*, **9**, lrr-2006-3, (2006). [gr-qc/0510072]. URL (cited on 20 January 2010): <http://www.livingreviews.org/lrr-2006-3>.
- [420] Will, C.M., and Nordtvedt, K.J., “Conservation Laws and Preferred Frames in Relativistic Gravity. I. Preferred-Frame Theories and an Extended PPN Formalism”, *Astrophys. J.*, **177**, 757, (1972). [DOI], [ADS].
- [421] Williams, J.G., Turyshev, S.G., and Boggs, D. H., “Progress in Lunar Laser Ranging Tests of Relativistic Gravity”, *Phys. Rev. Lett.*, **93**, 261101, (2004). [DOI], [arXiv:gr-qc/0411113].
- [422] Williams, J.G., Turyshev, S.G., and Murphy, T.W., “Improving LLR Tests of Gravitational Theory”, *Int. J. Mod. Phys. D*, **13**, 567–582, (2004). [gr-qc/0311021].
- [423] Wilson, T.L., and Blome, H-J., “The Pioneer Anomaly and a Rotating Gödel Universe”, *Adv. Space Res.*, **44**, 1345–1353, (2009). [DOI], [arXiv:0908.4067 [gr-qc]].
- [424] Wiltshire, D.L., “Cosmic clocks, cosmic variance and cosmic averages”, *New J. Phys.*, **9**, 377, (2007). [DOI], [ADS], [gr-qc/0702082].
- [425] Wolf, P., Bordé, C.J., Clairon, A., Duchayne, L., Landragin, A., Lemonde, P., Santarelli, G., Ertmer, W., Rasel, E., Cataliotti, F.S., Inguscio, M., Tino, G.M., Gill, P., Klein, H., Reynaud, S., Salomon, C., Peik, E., Bertolami, O., Gil, P., Páramos, J., Jentsch, C., Johann, U., Rathke, A., Bouyer, P., Cacciapuoti, L., Izzo, D., De Natale, P., Christophe, B., Touboul, P., Turyshev, S.G., Anderson, J.D., Tobar, M.E., Schmidt-Kaler, F., Vigué, J., Madej, A., Marmet, L., Angonin, M., Delva, P., Tournenc, P., Metris, G., Müller, H., Walsworth, R., Lu, Z.H., Wang, L., Bongs, K., Toncelli, A., Tonelli, M., Dittus, H., Lämmerzahl, C., Galzerano, G., Laporta, P., Laskar, J., Fienga, A., Roques, F., and Sengstock, K., “Quantum Physics Exploring Gravity in the Outer Solar System: The Sagas Project”, *Exper. Astron.*, **23**, 651–687, (2009). [DOI], [ADS], [arXiv:0711.0304 [gr-qc]].
- [426] Wong, S.K., and Lubeley, A.J., “Orbit Determination Strategy and Results for the Pioneer 10 Jupiter Mission”, AIAA Mechanics and Control of Flight Conference, Anaheim, CA, August 5–9, 1974, conference paper, (1974).
- [427] Wood, J., and Moreau, W., “Solutions of conformal gravity with dynamical mass generation in the solar system”, arXiv e-print, (2001). [gr-qc/0102056].
- [428] Ziebart, M., Adhya, S., Sibthorpe, A., Edwards, S., and Cross, P., “Combined radiation pressure and thermal modelling of complex satellites: Algorithms and on-orbit tests”, *Adv. Space Res.*, **36**, 424–430, (2005).